Universidade de Aveiro
Ano 2023

LÚCIA ISABEL FERREIRA SANTOS

Plataformas celulares com resposta a campos magnéticos com aplicação em engenharia de tecidos

Magnetic responsive cell-based platforms for tissue engineering applications

Universidade de Aveiro
Ano 2023

LÚCIA ISABEL FERREIRA SANTOS

Plataformas celulares com resposta a campos magnéticos com aplicação em engenharia de tecidos

Magnetic responsive cell-based platforms for tissue engineering applications

Tese apresentada à Universidade de Aveiro para cumprimento dos requisitos necessários à obtenção do grau de Doutor em Biotecnologia, realizada sob a orientação científica do Doutor João Filipe Colardelle da Luz Mano, Professor Catedrático do Departamento de Química da Universidade de Aveiro e da Doutora Ana Sofia Matias da Silva, Investigadora Doutorada.

Modalidade alternativa à apresentação de Tese, nos termos do artigo 63.º e 64.º do Regulamento de Estudos da Universidade de Aveiro.

Financial support by the Portuguese Foundation for Science and Technology (FCT) with doctoral grant SFRH/BD/141523/2018 and individual contract 2021.02196.CEECIND is acknowledged. This thesis was also supported by national funds (OE) through FCT in the scope of the projects “PROMENADE”(PTDC/BTM-MAT/29830/2017), POCI-01-0145-FEDER-029830), and when appropriate also supported by the Programa Operacional Competitividade e Internacionalização in the component FEDER. This work was also within the scope of the project CICECO-Aveiro Institute of Materials, UIDB/50011/2020, UIDP/50011/2020 & LA/P/0006/2020, financed by national funds through the FCT/MEC (PIDDAC).

“Listening is one of the loudest forms of kindness”

o júri

Presidente	Doutor Vasco Afonso da Silva Branco Professor catedrático da Universidade de Aveiro
Vogais	Doutor João Filipe Colardelle da Luz Mano (Orientador/Supervisor) Professor catedrático da Universidade de Aveiro
	Doutora Maria Manuela Estima Gomes Professor associada com agregação da Universidade do Minho
	Doutor Frederico Castelo Alves Ferreira Professor associado da Universidade de Lisboa
	Doutor Alireza Dolatshahi-Pirouz Professor associado da Trchnical University of Denmark
	Doutora Elvin Karana Professora associada da Delft Unversity of Technology

Acknowledgement

A decisão de ingressar num doutoramento acarreta não só uma grande disponibilidade a nível profissional como emocional. Um doutoramento com sucesso só é possível quando temos bons pilares fora e dentro do laboratório. Então esta página é na verdade uma das mais importantes deste documento.

Em primeiro lugar, queria agradecer aos meus orientadores pela supervisão e por disponibilizarem todas as condições necessárias à realização do mesmo. Ao professor João Mano, que mesmo com um grupo de 70 pessoas, sabe exatamente o trabalho dos alunos. E à "chefinha" Sofia, por na verdade 6 anos de partilha e aprendizagem. Como "filha da ciência" mais velha, espero que estejas orgulhosa!

Além disso, agradeço também o acolhimento pelo professor Håvard Haugen da Universidade de Oslo, e à professora Isabel Henriques pelo apoio prestado nos ensaios *in vivo*, na Universidade de Vila Real.

Mas sabemos que só trabalhando em grupo se consegue resultados! Obrigada a todo o grupo Compass pela oportunidade de aprender. Um especial obrigada à minha compincha Maria, aos meus comparsas Marta e Pedro e ao meu técnico preferido Doutor Paulo.

Mas o que a maioria não teve foi a minha sorte em ter o grupo de amigos a fazer doutoramento na mesma universidade. Obrigada "les memes" por estes 10 anos! Fica ainda mais difícil este fim. Por todas as horas de almoço, aquela pergunta do "alguém já fez isto", "alguém tem este reagente". Meninos, nós tínhamos o monopólio de vários departamentos! ahah

E também a todos os amigos que mesmo sem saberem o que é "engenharia de tecidos", tiveram sempre aquela palavra amiga. Um especial obrigada à Catarina, que me ouve dizer "não vou conseguir" há 10 anos, à Joana que me perdoa todas as não idas a casa, e ao Daniel não só pelos gráficos em Python ahah mas por se calhar ser das pessoas que mais acredita no meu valor.

Ao meu pai, que todas as semanas tentou saber exatamente o que estava a fazer e à minha mãe, por todas as sopinhas e bolinhos de cenoura, porque para ela uma boa comida soluciona qualquer problema!

palavras-chave folhas de tecido, campo magnético, mecanotransdução, células estaminais, engenharia de tecidos

O principal objetivo da engenharia de tecidos consiste no desenvolvimento de substitutos biológicos para reparar ou substituir tecidos danificados. No entanto, o fabrico de tecidos funcionais continua ilusório, dificultando a sua translação para a prática clínica. Durante o design de tecidos *in vitro*, todas as características funcionais e morfológicas devem ser recapituladas. Para resolver este desafio, a abordagem "*scaffold-free*" emergiu como uma estratégia poderosa no fabrico de tecidos, com uma deposição de matriz extracelular aprimorada, essencial para o desenvolvimento da arquitetura natural dos tecidos. No entanto, as abordagens tradicionais ainda falham na engenharia de tecidos com alto grau de complexidade, como visto em conformações estratificadas e hierárquicas, bem como com desempenho mecânico adequado. Assim, este projeto de doutoramento pretendeu desenvolver substitutos de tecidos aprimorados, mimetizando aspetos funcionais chave do microambiente nativo. Utilizando células magnetizadas como unidade base, propomos o fabrico de folhas de tecidos magnéticas por engenharia de tecidos baseada em força magnética. O caracter magnético permitiu o controlo preciso sobre o posicionamento das células e consequentemente, uma construção extremamente guiada dos tecidos. Seguindo essa estratégia, foram fabricados macrotecidos coesos e robustos com comportamento mecânico aprimorado, contornando uma das principais limitações da abordagem "*scaffold-free*", que inclui o desenvolvimento de construções de tecidos mecanicamente fracos. Relativamente à arquitetura dos tecidos nativos, foram fabricados tecidos magnéticos com geometrias complexas, atestando a versatilidade desta abordagem. Outro problema é a inadequada difusão de nutrientes e oxigénio, levando à morte celular prematura. Para ultrapassar este obstáculo, projetamos folhas tecidulares em multicamada pré-vascularizadas, exibindo uma estrutura vascular humana preservada e a capacidade de integrar a vasculatura do hospedeiro. Nesta tese, pequenas unidades de tecidos à microescala foram também desenhadas através da combinação da engenharia de tecidos baseada em força magnética e uma plataforma de alto rendimento. Estes microtecidos podem atuar ainda como blocos de construção para a fabricação de construções de tecidos heterotípicos maiores ou como plataformas *in vitro* para *screening* de doenças e fármacos. Finalmente, explorando o caracter magnético dos nossos tecidos vivos aprimorados, avaliamos o papel do campo magnético na modulação do comportamento celular dos tecidos produzidos *in vitro*. Depois de estimulados magneticamente, a diferenciação osteogénica dos tecidos magnetizados foi incitada, abrindo novas possibilidades para estratégias avançadas na regeneração do osso. Utilizando um modelo vivo de ratinho, podemos estimular a integração do tecido e diferenciação osteogénica do implante. Usando células magnetizadas como unidades de construção, prevemos o fabrico de tecidos complexos e multifuncionais com relevância clínica. O caracter magnético dos tecidos poderá potenciar a translação, permitindo a orientação remota e local (*in situ*) do implante na função do tecido esperado, garantindo também uma adequada monitorização ao longo do tempo.

keywords cell sheet, magnetic field, mechanotransduction, stem cells, tissue engineering

abstract

The major goal of tissue engineering consists on the development of biological substitutes to repair or replace damaged tissues. However, the fabrication of clinically relevant tissue replacements is still illusory, hampering their transactional to clinical practices. During the design of tissues *in vitro*, all the functional and morphological features must be recapitulated. To address this challenge, scaffold-free approaches have emerged as powerful strategies for the fabrication of tissue constructs with enhanced deposition of extracellular matrix, essential for the natural development of the tissue architecture. Nevertheless, the traditional approaches still fail on engineering tissues with high level of complexity, as seen in stratified and hierarchical conformations, as well with adequate mechanical performance. Therefore, this PhD proposal aimed to develop improved tissue substitutes that closely mimic key functional aspects of the native microenvironment. By using magnetized cells as basic living units, we propose the fabrication of magnetic membranes of cells through magnetic force-based tissue engineering (Mag-TE). The magnetic character of the created tissues allowed a precise control over cells' positioning and, consequently, an extremely guided-assembling of the tissues. Following this strategy, cohesive and robust macrotissues with enhanced mechanical behavior were fabricated, circumventing one of the major limitations of scaffold-free approaches which includes the development of mechanically weak tissue constructs. Concerning the architecture of the native tissues, magnetic living substitutes with intricate geometries were developed, attesting the versatility of this approach. Another problematic regarding the development of tissue substitutes is the lack of adequate diffusion of nutrients and oxygen, which may lead to premature cell death. To overcome this obstacle, we engineered pre-vascularized multilayered cell sheets, exhibiting preserved human vascular structures and the ability to integrate the host vasculature. In this thesis, small tissue units at the microscale were also designed through the combination of Mag-TE and a high-throughput platform. These microtissues could further act as living building blocks for the fabrication of larger heterotypic tissue constructs or as *in vitro* platforms for disease modelling and drug screening. Finally, by exploring the magnetic character of our improved living tissues, we evaluated the role of magnetic field on modulating the cell fate of tissues produced *in vitro*. Upon magnetic stimulation, we triggered the osteogenic differentiation of the magnetized tissues, opening new possibilities for advanced strategies in bone regeneration. Using an *in vivo* mice model, we were also able to stimulate tissue integration and the osteogenic differentiation of the implant *in situ*.

By using magnetized cells as building materials, we envisaged the fabrication of complex multiscale and multifunctional tissues with clinical relevance. The magnetic features of the designed tissues could accelerate the translation of Mag-TE to the clinical practices, allowing the remote and *in situ* guiding of implants into the expected tissue function, while guarantying a feasible monitoring and tracking along the time.

TABLE OF CONTENTS

List of Abbreviations and Acronyms

A	
ALP	Alkaline phosphatase
ASCs	Adipose stem cells
APTES	Aminopropyl)triethoxysilane
B	
bFGF	Basic fibroblast growth factor
BMP-2	Bone morphogenetic protein-2
BMSCs	Bone mesenchymal stem cells
BSA	Bovine serum albumin
C	
Ca	Calcium
CAM	Chick chorioallantoic membrane
CEC	Competent Ethics Committee
CSs	Cell sheets
CSLM	Confocal laser scanning microscopy
D	
DAPI	4’,6-diamidino-2-phenylindole
DEA	Diethanolamine
DGAV	Direção-Geral da Alimentação e Veterinária
DiD	1,1'-dioctadecyl-3,3,3',3'-tetramethylindodicarbocyanine, 4-chlorobenzenesulfonate salt
DiO	3,3’-dioctadecyloxacarbocyanine perchlorate
E	
ECM	Extracellular matrix
ECs	Endothelial cells
EDTA	Ethylenediaminetetraacetic
EDS	Energy dispersive X-ray spectroscopy
ERK1/2	Extracellular signal-regulated kinases
F	
FAK	Focal adhesion kinase
FBS	Fetal bovine serum
FN	Fibronectin
G	
GADPH	Glyceraldehyde 3-phosphate dehydrogenase
H	
HA	Hyaluronic acid
hASCs	Human adipose stem cells
HGF	Hepatocyte growth factor
H&E	Haematoxylin and Eosin
HuNu	Human nuclei
HUVECs	Human umbilical
I	
ICP-OES	Inductively Coupled Plasma Optical Emission Spectrometry
IL-6	Interleukin 6
IPSCs	Induced pluripotent stem cells
L	
LAM	Methacrylated laminarin
M	
MADK	Mitogen-activated protein kinase
Mag-TE	Magnetic tissue engineering
MC3T3	Pre-osteoblast cell line
MNPs	Magnetic nanoparticles
MicroCT	Microtomography
MPI	Magnetic particle imaging

MPI	Magnetic particle imaging
MSCs	Mesenchymal stem cells
MRI	Magnetic resonance imaging
MTS	3-(4,5-dimethylthiazol-2-yl)-5-(3-carboxymethoxyphenyl)-2-(4- sulphofenyl)-2H-tetrazolium)

N

NanoCT	Nanotomography
NMR	Nuclear magnetic resonance
NPh	p-nitrophenol

P

P	Phosphate
PBS	Phosphate buffer saline
PEMF	Pulsed magnetic field
PI	Propidium iodide
PLMA	Methacrylated platelet lysates
PNIPAAm	Poly(N-isopropylacrylamide)
PPARG	Peroxisome proliferator-activated receptor gamma
PVA	Polyvinyl alcohol

Q

qPCR	Quantitative reverse Transcription polymerase chain reaction

R

rEMS	Repetitive electromagnetic stimulation
RhodB	Rhodamine B isothiocyanate
RMF	Rotating magnetic field
RT	Room temperature
RUNX2	Runt-related transcription factor 2

S

SEM	Scanning Electron Microscopy

T

TE	Tissue engineering

U

UTS	Ultimate tensile strength
UV	Ultraviolet

V

VEGF	Vascular endothelial growth factor
VWF	Von Willebrand factor

List of Figures

Section 1: Introduction

Chapter II – Magnetic tissue engineering

Section 2: Materials & Methods

Chapter III - Experimental methodologies and materials

Section 3: Results & Discussion

Chapter IV - Complex-shaped magnetic 3D cell-based structures for tissue engineering

Chapter V - Multi-layer pre-vascularized magnetic cell sheets for bone regeneration

Figure V.S4: Live-dead assay of homotypic CSs. Live-dead fluorescence assay at day 7, 14 and 21 of culture in basal and osteogenic medium. Living cells were stained by calcein (green) and dead cells by propidium iodide (red).

Figure V.S5: Osteopontin staining of homotypic CS. Immunofluorescence of ASCs (green), osteopontin (red) and cell nucleus- DAPI (blue) in 3D homotypic CS cultured for 7, 14 and 21 days in basal and osteogenic media**.**

Figure V.S6: Immunostaining of CS with VWF(green)/FN(red); collagen IV(green)/CD31(red) and VWF(green)/CD31(red) demonstrating the presence of capillary-like structures (white arrows). DAPI stains the cells' nuclei.

Figure V.S7: Number of junctions and total number of vessels.

Figure V.S8: Immunostaining of CAM + bFGF (positive control) and CAM with implanted CS. VWF (in green) labels both human and chick endothelial cells, DAPI (in blue) stains all nuclei, and HuNu (in pink) stains the human nuclei.

Chapter VI - Freestanding magnetic microtissues for tissue engineering Applications

Figure VI.2: Fabrication of freestanding microtissues composed by hASCs, via Mag-TE.

Figure VI.3: Morphological analysis of the freestanding magnetic cell-based microtissues with circle and square geometry.

Figure VI.4: Cell viability, proliferation and metabolic activity. Morphometric characterization of the freestanding microtissues.

Figure VI.4: Freestanding magnetic microtissues ability to fill defects using LAM and PLMA hydrogels as *in vitro* tissue models, in static and dynamic conditions.

Figure VI.5: Evaluation of the microtissues invasion and their secretory profile in LAM and PLMA hydrogels for both static and dynamic conditions.

Figure VI.S1: Flow cytometry analysis of surface markers expression of hASCs.

Figure VI.S2: Magnetic microtissues prior and after the magnetic harvesting.

Figure VI.S3: Characterization of the fabricated microtissues. SEM micrographs of the freestanding microtissues after 7 days of culture, revealing a high cell dense structure.

Figure VI.S4: Live-dead fluorescence assay of the freestanding magnetic microtissues after 1, 3 and 7 days of culture. Living cells were stained with calcein (green) and dead cells with propidium iodide (red).

Figure VI.S5: Confocal images of magnetic microtissues after 7 days of culture, showing the living cells (calcein, in green) and the dead cells (PI, in red).

Figure VII.S10: H&E staining of paraffin-embedded magnetized tissues under control and dynamic conditions, 4 and 6 weeks post implantation.

Figure VII.S11: Analysis of the mineral deposition within the magnetic implant by EDS. The hydroxyapatite nodules can be identified in yellow, by the overlapping of calcium (in red) and phosphorus (in green)

List of Tables

Section 1: Introduction

Chapter II – Magnetic tissue engineering

Section 3: Materials & Methods

Chapter III - Experimental methodologies and materials

List of Publications

A – Publications resulting from work performed during the PhD thesis

A1 – International peer-reviewed journals

1. Lúcia F. Santos, Maria C. Mendes, Isabel Dias, Carlos Viegas, Carlos O. Amorim, João S. Amaral, Håvard J. Haugen, A. Sofia Silva, João F. Mano. " A novel therapeutic strategy for in situ bone regeneration powered by magnetic stimulation". *In preparation*.
2. Lúcia F. Santos, A. Sofia Silva, João F. Mano. "Magnetic Tissue Engineering". *Submitted*.
3. Lúcia F. Santos, Sónia G. Patrício, A. Sofia Silva, João F. Mano. **2022** "Freestanding magnetic microtissues for tissue engineering applications". *Advanced Healthcare Materials*, 11, 2101532.
4. Lúcia F. Santos, A. Sofia Silva, João F. Mano. **2020** "Complex-shaped magnetic 3D cell-based structures for tissue engineering". *Acta Biomaterialia*, 118, 18-31.
5. A. Sofia Silva[1], Lúcia F. Santos[1], Maria C. Mendes, João F. Mano. **2020** "Multi-layer pre-vascularized magnetic cell sheets for bone regeneration". *Biomaterials*, 231, 119664. ([1] The authors contributed equal to the work).

A2 – International and national conferences

A2.1 – Oral communications

1. A. Sofia Silva, Lúcia F. Santos, Clara R. Correia, João F. Mano. **2018** "Multi-layer vascularized cell sheets for tissue regeneration". *World TERMIS*.
2. Lúcia F. Santos, A. Sofia Silva, João F. Mano. **2019** "Development of versatile stratified 3D tissues through magnetic cell sheet technology". *European Society of Biomaterials*.
3. A. Sofia Silva, Lúcia F. Santos, João F. Mano. **2019** "Multi-layer vascularized magnetic cell sheets for bone regeneration". *European Society of Biomaterials*.
4. Lúcia F. Santos; Sónia G. Patrício, A. Sofia Silva, Joao F. Mano. **2021** "Freestanding magnetic microtissues for tissue engineering applications". *European Society for Biomaterials*.
5. Lúcia F. Santos; Sónia G. Patrício, A. Sofia Silva, Joao F. Mano. **2023** "Freestanding magnetic microtissues for TE engineering applications". *TERMIS*.

A2.1 – Poster communications

1. Lúcia F. Santos, A. Sofia Silva, João F. Mano. **2022** "Magnetic stimulation of cell-based tissue constructs for advanced strategies on bone regeneration". *Jornadas CICECO*.

2. Lúcia F. Santos; Sónia G. Patrício, A. Sofia Silva, Joao F. Mano. **2021** "Living tissue stamps". *Jornadas CICECO*.
3. Lúcia F. Santos, A. Sofia Silva, João F. Mano. **2020** "Freestanding magnetic microtissues". World Biomaterials Congress (WBC).
4. Lúcia F. Santos; Sónia G. Patrício, A. Sofia Silva, Joao F. Mano. **2020** "Freestanding magnetic microtissues for tissue engineering applications". *Jornadas do CICECO*.
5. A. Sofia Silva, Lúcia F. Santos, João F. Mano. **2019** "Multi-layer vascularized cell sheets for tissue regeneration". *Jornadas CICECO*.
6. Maria C. Mendes, Lúcia F. Santos, A. Sofia Silva, João F. Mano. **2019** "Versatile stratified 3D tissues through magnetic cell sheet engineering". *Jornadas CICECO*.
7. A. Sofia Silva, Lúcia F. Santos, Clara R. Correia, João F. Mano. **2018** "Magnetic-responsive double-step heterotypic layer cell sheets using internalizable magnetite nanoparticles: new prospects for bone regeneration". *6th Portuguese Young Chemists Meeting*.

B – Publications in international peer-reviewed journals resulting from collaborative work performed during the present PhD thesis

1. Katia R. Amaral, Lúcia F. Santos, Edgar J. Castanheira, Maria C. Mendes, Dora C.S. Costa, João M. M. Rodrigues, Joana Marto, A. Sofia Silva, and João F. Mano. "Biomimetic drug load patches for wound healing". *Submitted*.
2. Isabel M. Bjørge, Bárbara M. de Sousa, Sónia G. Patrício, Ana Sofia Silva, Liebert P. Nogueira, Lúcia F. Santos, Sandra I. Vieira, Håvard J. Haugen, Clara R. Correia, João F. Mano. **2022** "Bioengineered Hierarchical Bonelike Compartmentalized Microconstructs Using Nanogrooved Microdiscs." *ACS Applied Materials & Interfaces*, 14.17, 19116-19128.

C – Book chapters resulting from collaborative work performed during the present PhD thesis

1. Lúcia F. Santos, A. Sofia Silva, João F. Mano. **2022** "Natural-based biomaterials for drug delivery wound healing patches". *Natural Polymers in Wound Healing and Repair*, 51-73. Elsevier.
2. A. Sofia Silva, Lúcia F. Santos, Mariana B. Oliveira, João F. Mano. **2021** "Cell-based Soft Biomaterials". *Soft Matter for Biomedical Applications*, 720-749. Royal Society of Chemistry.

1

Introduction

Chapter I

Thesis Motivation

Chapter II

Magnetic Tissue Engineering

Chapter I - Thesis Motivation

Despite of the incredible efforts of tissue engineering (TE) in integrating cell biology principles with material science, the translation to clinical practice still represents a major challenge.[1] The lack of suitable mechanical, chemical, and biological properties, all in one biomaterial, as well as the inability to generate large and vascularized tissues with the architectural complexity of native tissues is restricting its application.

Over the past decades, natural and synthetic biomaterials have been serving as scaffolds for biologically active components (cells) in order to define an artificial *in vivo* milieu with complex and dynamic interactions, mimicking their natural cellular microenvironment and consequently, leading to tissue formation.[2],[3] Howbeit, the limited diffusion of oxygen and nutrients, the use of isolated cell suspensions that deprive cells of their endogenous extracellular matrix (ECM), and even the potential inflammatory response upon scaffold degradation, may hamper tissue reconstruction.[4]

Although biomaterials have played a central role in the production of tissues *in vitro*, several works have evidenced the primordial role of cells as the local tissue builders, and strategies have been focusing on minimizing the amount of biomaterials to aid the regenerative process.[4] At the extreme of such minimalistic-engineering approaches, scaffold-free TE has emerged as a powerful strategy using multicellular building blocks, including spheroids, tissue strands and cell sheets (CSs), to fabricate larger cohesive tissue constructs and produce ECM, essential for naturally developing their tissue architecture. Particularly, CS technology permits the engineering of cell-dense like tissues by keeping the natural networks of tissues without breaking them through the harvesting of entire sheet-like cells, guarantying the maintenance of cell–cell and cell–ECM interactions.[5] This approach has already been implicated in the production of several types of tissues such as heart, liver, bladder, bone, cornea and esophagus.[6]

Thermo-responsive methodologies have been widely explored for CS engineering, allowing the recovery of CSs in a non-invasive manner, typically through the use of poly(N-isopropylacrylamide) thermo-responsive substrates. Nevertheless, the high cost, the low mechanical performance of the tissues and the cellular abnormalities linked to physiological changes within cell microenvironment are still limiting this strategy.[7] Moreover, traditional CS engineering still fails to create larger and heterogeneous 3D tissue constructs. Until now, stratified and heterotypic CSs were fabricated through

the individual stacking of formerly built CS monolayers in a time-consuming manner, which could limit the establishment of cell-cell interactions and hinder the spatial positioning control of the target cells.[8] To circumvent those issues, magnetic-force based TE (Mag-TE) has been explored to produce CSs by combining magnetic force with CS technology, enabling an easier manipulation of those cells by a magnetic field.[9],[10] Interestingly, Mag-TE has been implied on the fabrication of complex tissues that are not easily achieved by conventional cell culture or co-culture methods such as 2D and 3D cell layers, tubular structures and 3D ordered assemblies consisting of several cell types. Full description of the Mag-TE achievements in the last years can be accessed in **Chapter II**, where a review of the Mag-TE strategies is given in detail. Encouraged by the huge potential of Mag-TE, the main goal of this thesis consisted of the fabrication of functional magnetic tissues using magnetized cells as building unit materials. Along with this thesis, important aspects of the *in vivo* environment were recapitulated in order to obtain completely clinically relevant tissues. All the materials and methods described throughout this thesis are depicted in **Chapter III**. The specific techniques and materials used in the following experimental works are better detailed along the following chapters.

Firstly, tissue engineered constructs should resemble the *in vivo* structural and mechanical properties of the native tissues to assure their functionality and integration within the host.[11] Still, for cell-based materials, the major problematic remains on the difficulty in recapitulating the mechanical properties of the native tissues. Considering this, **Chapter IV** describes the fabrication of magnetic tissues with improved mechanical behaviour. The robustness of the tissues was evaluated along the time and by varying the cell density. Most importantly, this chapter shows that by making use of a universal approach that only relies on the geometries of the substrate and the magnet, together with a particular cell density, tissues with distinct and well-defined geometries and sizes can be produced. Of course, the versatility of this strategy was assured by the enhanced mechanical performance of the biological materials.

Envisioning the replacement of tissues and organs, the fabrication of functional substitutes depends on a rapid and sufficient vascularization in the tissue-engineered constructs, which is a pre-requisite for optimal cell survival and perfect tissue integration *in vivo.*[6] To solve this issue, recent studies have been focused on pre-vascularization strategies, reducing the time required to vascularize the implant when compared with approaches that depend on the scaffold design and delivery of angiogenic factors.[12],[13] Additionally, CS engineering is known to provide an excellent microenvironment for vascularization since this technology allows the maintenance of cell matrix integrity, crucial for angiogenesis.[14] In this

sense, **Chapter V** displays a simple, one-pot and time-saving strategy to produce complex, hierarchical and vascularized 3D cellular constructs by Mag-TE. For this, magnetically labelled adipose stem cells (ASCs) and human umbilical vein endothelial cells (HUVECs) were organized in a triple sheet conformation with HUVECs in between two sheets of ASCs. The synergetic effect of HUVECs and ASCs not only prompted the osteogenesis but also led to the recruitment of blood vessels, showing the ability to migrate and integrate within the chick vasculature.

Another recurrent limitation in TE is the lack of satisfactory morphological and functional features of the tissue engineered constructs. During the design of tissues, the engineered structures should preferentially recapitulate aspects of the tissue architecture from the microscopic to macroscopic dimension levels, consistent with the hierarchical organization of biological systems. In tissues, such complex hierarchy is formed by heterogeneous building blocks that are responsible for regulating their functionality.[15] By mimicking such native microstructural functional units with microarchitectural features, modular TE aims to create more biomimetic engineered tissues, providing more guidance on the cellular level to direct tissue morphogenesis.[16] Then, these small tissue units can be used as building blocks to engineer larger and heterogenous tissues. In this sense, small tissues at the microscale have been designed aiming to mimic the functional units of native tissues. After the successful fabrication of robust tissues at macroscale, **Chapter VI** reports the production of freestanding magnetic microtissues with well-defined size and design, acting as building blocks for the construction of complex and hierarchical tissues. Microtissues with distinct architectures namely circle, square and fiber-like shape were fabricated only by changing the geometry of the patterned superhydrophobic high-throughput surfaces. The combination of Mag-TE and such high-throughput platform permitted the fabrication of robust tissues at microscale with preserved geometry and integrity along the time. Besides the huge contribute of MNPs to tissue design, such nanosystems have also been used as nano-instructive tools for diagnosis and therapeutics, that once incorporated within cells or biomaterials led to the activation of several mechano-signaling pathways to control cell behavior. Concisely, these nanomagnetic systems can act as mechanostimulation platforms to apply controlled forces directly to single cells and multicellular biological tissues to precisely regulate cellular functions.[17] The mechanical stresses are implicated on a set of physiological processes namely cell and tissue growth, production of tissue matrix and differentiation of stem cells. Mechanotransduction is the well-known pathway, in which cells convert physical stimulus into biochemical activities. Therefore, the field of Mag-TE has been focused not only on the fabrication of tissue substitutes but also on

controlling the cell behavior under the presence of the magnetic field. Until now, this concept was only explored in 2D cell culture conformation or using targeted cells from the pre-determined tissue. Hence, **Chapter VII** illustrates the power of the magnetic field on the construction of improved and differentiated tissues. Recently, several works reported the influence of pulsed magnetic field in both cell proliferation and differentiation.[18] Here, the osteogenic differentiation of tissues composed by human ASCs (hASCs) was induced by applying a cyclic magnetic field (CMF). This behaviour was demonstrated for both *in vitro* and *in vivo* scenarios, highlighting the potential of Mag-TE for clinical practices. Interestingly, the integration of the cell construct within the host was accelerated by the presence of the CMF. Altogether, this chapter proposes a new therapeutic strategy for *in situ* tissue regeneration, triggering the bone tissue formation.

Ultimately, **Chapter VIII** briefly revises all the investigation work developed throughout this thesis, while evaluating the accomplishment of the major goals of this PhD: i) The fabrication of magnetic tissues using magnetized cells as building living units with enhanced robustness and adequate mechanical behavior; ii) The creation of hierarchical tissues with high complexity; iii) The development of pre-vascularized tissues for bone TE; and iv) The *in vitro* and *in vivo* evaluation of the effect of a remote magnetic field in triggering the osteogenic differentiation of magnetic tissues composed of stem cells. Future expectations and forthcoming works that can arise from this thesis are also given in this chapter.

References

1. Oliveira, S. M., Reis, R. L. & Mano, J. F. Towards the design of 3D multiscale instructive tissue engineering constructs: Current approaches and trends. *Biotechnology Advances* **33,** 842–855 (2015).
2. Liu, X. & Ma, P. X. Polymeric scaffolds for bone tissue engineering. *Ann Biomed Eng* **32,** 477–486 (2004).
3. O'Brien, F. J. Biomaterials & scaffolds for tissue engineering. *Materials Today* **14,** 88–95 (2011).
4. Correia, C. R., Bjørge, I. M., Nadine, S. & Mano, J. F. Minimalist Tissue Engineering Approaches Using Low Material-Based Bioengineered Systems. *Adv Healthc Mater* 2002110 (2021). doi:10.1002/adhm.202002110
5. da Silva, R. M. P., Mano, J. F. & Reis, R. L. Smart thermoresponsive coatings and surfaces for tissue engineering: switching cell-material boundaries. *Trends in Biotechnology* **25,** 577–583 (2007).
6. Moschouris, K., Firoozi, N. & Kang, Y. The application of cell sheet engineering in the vascularization of tissue regeneration. *Regenerative Med* **11,** 559–570 (2016).

7. Kim, I. Y. *et al.* Thermoreversible behavior of κ-carrageenan and its apatite-forming ability in simulated body fluid. *Materials Science and Engineering: C* **31,** 1472–1476 (2011).
8. Ito, A., Jitsunobu, H., Kawabe, Y. & Kamihira, M. Construction of Heterotypic Cell Sheets by Magnetic Force-Based 3-D Coculture of HepG2 and NIH3T3 Cells. *J Biosci Bioeng* **104,** 371–378 (2007).
9. Castro, E. & Mano, J. F. Magnetic Force-Based Tissue Engineering and Regenerative Medicine. *J Biomed Nanotechnol* **9,** 1129–1136 (2013).
10. Ito, A. *et al.* Tissue Engineering Using Magnetite Nanoparticles and Magnetic Force: Heterotypic Layers of Cocultured Hepatocytes and Endothelial Cells. *Tissue Eng* **10,** 833–840 (2004).
11. Courtney, T., Sacks, M. S., Stankus, J., Guan, J. & Wagner, W. R. Design and analysis of tissue engineering scaffolds that mimic soft tissue mechanical anisotropy. *Biomaterials* **27,** 3631–3638 (2006).
12. Ren, L., Kang, Y., Browne, C., Bishop, J. & Yang, Y. Fabrication, vascularization and osteogenic properties of a novel synthetic biomimetic induced membrane for the treatment of large bone defects Liling. *Bone* **64,** 173–182 (2015).
13. Pirraco, P. *et al.* Endothelial cells enhance the in vivo bone-forming ability of osteogenic cell sheets. **94,** 663–673 (2014).
14. Silva, A. S., Santos, L. F., Mendes, M. C. & Mano, J. F. Multi-layer pre-vascularized magnetic cell sheets for bone regeneration. *Biomaterials* **231,** 119664 (2020).
15. Guven, S. *et al.* Multiscale assembly for tissue engineering and regenerative medicine. *Trends Biotechnol* **33,** 269–279 (2015).
16. Gaspar, V. M. *et al.* Advanced Bottom-Up Engineering of Living Architectures. *Advanced Materials* **32,** 1903975 (2020).
17. Gil, S. & Mano, J. F. Magnetic composite biomaterials for tissue engineering. *Biomater Sci* **2,** 812–818 (2014).
18. Mert, T. *et al.* Pulsed Magnetic Field EnhancesTherapeutic Efficiency of Mesenchymal Stem Cells in Chronic Neuropathic Pain Model. *Bioelectromagnetics* **38,** 255–264 (2017).

Chapter II - Magnetic Tissue Engineering[1]

Abstract

A long-sought goal in tissue engineering (TE) is the fabrication of biological substitutes to repair, replace, or enhance tissue and organ-level functions. Howbeit, the clinical translation of TE is hindered by several challenges which include the lack of suitable mechanical, chemical and biological properties, all in one biomaterial, as well as the inability to generate large, vascularized tissues with the architectural complexity of native tissues. Over the past decade, a new generation of "smart" materials has revolutionized the conventional medical field, transforming TE in a more accurate and sophisticated conception. At the forefront of innovation, magnetic nanoparticles (MNPs) have been extensively investigated owing to their promising potentials in biomedical applications, by taking advantage of its inherent properties such as rapid and biocompatible response to magnetic field remotely. Hence, aspiring the creation of functional tissue replacements, magnetic force-based TE (Mag-TE) arose as an alternative to conventional TE strategies, allowing for the fabrication and monitoring of tissues produced *in vitro*. This review addresses the recent works encompassing the use of MNPs for TE, emphasizing the in vitro, in vivo and clinical applications. Future perspectives of Mag-TE in the field of TE and regenerative medicine are also disclosed.

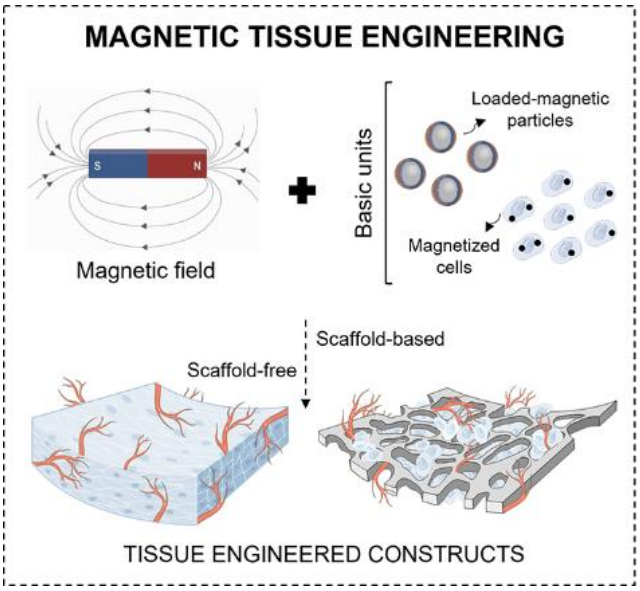

[1]Baseed on the publication: Lúcia F. Santos, A. Sofia Silva, João F. Mano. Magnetic tissue engineering. *Submitted.*

1. Introduction

Concerning the complexity of native tissues, the huge challenge of TE remains on the fabrication of completely functional tissues *in vitro* that closely mimic the *in vivo* environment.[1] Classically, cells are cultured on tissue culture polystyrene dishes and harvested through the proteolytic action of trypsin or by chelating the Ca^{2+} and Mg^{2+} ions with ethylenediaminetetraacetic acid (EDTA) to disrupt cell-cell junctions with a substrate. Nevertheless, the interaction of cells with components of the extracellular matrix (ECM) like proteins and integrins are crucial for the development and maintenance of tissues.[2] The introduction of stimuli-responsive materials has allowed the development of new methodologies to reverse cells' attachment/detachment, avoiding damages on cells' membranes and ECM, caused by nonspecific proteases.[3] In the last decades, magnetic-responsive systems have been explored in TE and regenerative medicine, achieving prosperous outcomes in drug delivery, cell therapy and/or *in vivo* monitoring. Particularly, magnetically labelled cells have been developed either to fabricate tissue replacements with a fine control over the cell positioning, or to support tissue regeneration.[4],[5] In fact, MNPs-labelled cells can be magnetically directed to a specific location to prompt the repair of a tissue or to restore its function.[6] The magnetic character of such tissues' substitutes can also provide information about the correct positioning and function of cells and materials over time, by monitoring the bioengineered materials. Several preclinical *in vitro* and *in vivo* studies have revealed the successful magnetic-based cell therapy and TE and its monitoring by MRI for regeneration or replacement of diseased or injured tissue.[7] Nonetheless, the clinical trials involving the application of a magnetic field are still restricted to monitoring purposes. This review highlights the recent advances of magnetic responsive systems for regenerative medicine, including monitoring TE, magnetic cell guidance, and tissue regeneration **(Figure II.1)**.

2. Tissue Engineering: different approaches to create and repair tissues

TE aims at restoring the functionality of damaged tissues and/or organs resulting from trauma, aging, or disease.[8] The development of structures that mimic the intricate architecture and complexity of native organs and tissues is crucial to guaranty the proper function of the engineered tissues. Traditional TE strategies employ a "top-down" approach, in which cells are seeded onto a scaffold with biocompatible and biodegradable properties.[9] Herein, the cells are expected to populate the scaffold and create their own ECM and appropriate microarchitecture. Mechanical stimulation, perfusion or the incorporation of biomolecules like

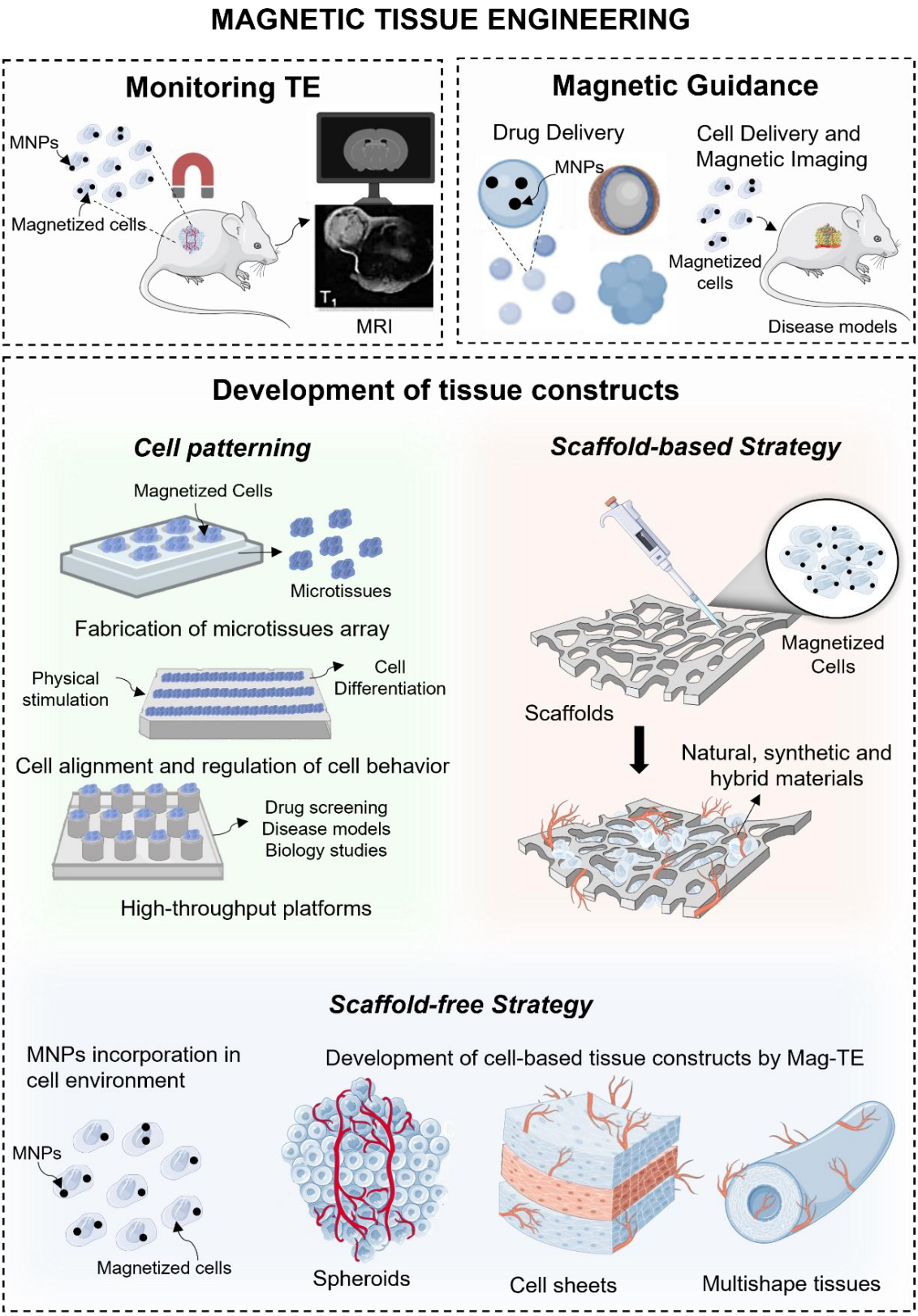

Figure II.1: Schematic illustration of the different approaches for magnetic tissue engineering (TE), including monitoring TE, magnetic guidance and development of tissues constructs by cell patterning, scaffold-based and scaffold-free strategies.

growth factors and signaling molecules have been employed to support the formation of these structures.[10] Commonly used techniques to fabricate top-down scaffolds include freeze-drying,[11] solvent-casting,[12] electrospinning[13] and supercritical fluids.[14] Thin or avascular tissues including skin, bladder and cartilage have been successfully engineered via "top-down" approaches.[15] Nevertheless, the fabrication of larger and complex tissue-like constructs remains a challenge. In fact, top-down approaches often present difficulties in recreating the sophisticated microstructural features of tissues which leads to non-functional constructs. Inspired by the building blocks that compose the complex hierarchy of tissues and that regulate the their entire function, "bottom-up" approaches have also been explored in the fabrication and assembly of microscale tissue building blocks with a specific microarchitecture to engineer larger tissue constructs.[16] Herein, several features such as shape and composition of individual blocks can be easily controlled, enabling the development of versatile tissue structures.[17] Cell-encapsulating microscale hydrogels (microgels), self-assembled cell aggregation, generation of CSs, and direct printing of cells are some of the strategies that have been recently used to fabricate these tissue building blocks.[18]

3. Tissue engineering via external stimulus

The new generation of "smart" biomaterials is at the forefront of innovation in the medical field, revolutionizing the conventional fields of TE, drug delivery or the manufacture of medical devices. Such class of biomaterials can be designed to adapt their chemical and mechanical properties in response to external signals and/or the surrounding environment.[19] Temperature, pH, redox-state, light and magnetic field are the most promising stimulus that are explored in the field of "smart" biomedicine (**Figure II.2**). The specificity of stimuli response, and ability to respond to endogenous cues inherently present in living systems, provide possibilities to transform the conventional field of TE into a more accurate and sophisticated conception. Nevertheless, the translation of these new materials to clinic practice remains a challenge. Thermo-responsive polymers are highly explored in biomedical field, permitting the fabrication of CSs, *in situ* drug delivery and 3D printing under physiological conditions.[20] Particularly, poly(N-isopropylacrylamide) (PNIPAm) has been implicated on the fabrication of thermo-responsive surfaces for TE purposes, acting as substrate for thermo-responsive cell culture dishes. In contrast to traditional strategies, thermo-responsive surfaces allow the recovery of unharmed and interconnected CSs without destroying the cell junctions,[21] by simply decreasing the temperature below the lower critical solution temperature, which trigger the cell detachment.[22] However, such substrates are mainly limited due to their high cost and low

mechanical strength of the resulting CSs, as well as, by the cellular abnormalities linked to physiological changes within cell microenvironment.[23]

Responsive systems that take advantage of the different pHs within the human body to induce a more targeted response are also well explored in the literature. Such pH-responsive systems are being widely explored as drug delivery platforms including anticancer agents due to the acidic extracellular pH of tumor cells, or for oral drug administration by the pH changes along the gastrointestinal tract.[24] Concerning TE applications, cell-based tissue constructs were successfully obtained by the detachment of a CS only by decreasing the pH of the cell culture.[25]

Notwithstanding, the changes in the pH might be detrimental for more sensitive cells and, consequently, this type of system is weakly explored for TE purposes. Electrical stimulation is a recent tool in TE and regenerative medicine, acting in the morphology, orientation, migration, and phenotype of several cell types. In fact, these systems showed promising results in wound healing and bone regeneration in both animal experiments and clinical treatments.[20] Regarding the fabrication of tissues *in vitro*, polyelectrolyte-modified surfaces have been used for CS fabrication, based on the mechanism of absorption and desorption of oppositely charged surfaces. Through the aid of a positive potential, the surface monolayer desorbs, and cells lose their attachment points and CSs can be harvested.[26] The recurrent charge accumulation during the application of an electric field affects the cell behavior and can induce a non-homogenous distribution of the cells, constraining their application for TE applications.[27]

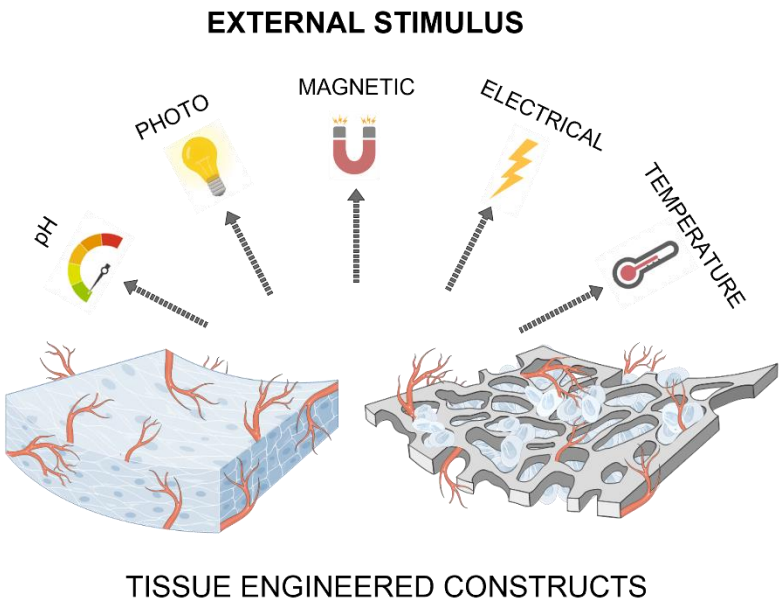

Figure II.2: External stimuli are being explored for the construction of functional tissues namely pH, photo, magnetic, electrical and temperature.

Light-responsive smart biomaterials are also an attractive strategy for TE, being involved in the fabrication of complex scaffolds, control of cellular behavior, release of key factors and tissue regeneration. The light stimulus offers some advantages over other strategies, as it can be imposed instantly and delivered in exact amounts, providing spatial and temporal control with less invasive techniques.[28],[29] In regenerative medicine, light-responsive composite coatings have already shown promising results, allowing the control of the cell attachment/detachment based on the wettability changes.[30] This concept inspired the fabrication of CSs, where a completely cell-based membrane can be recovered after UV irradiation at the cell safe wavelength of 365nm, by using a coated-surface as substrate.[31] Several biosynthetic soft tissues have also been engineered through photopolymerization.[32] Briefly, the prepolymer is injected into the damage site enabling the tissue reconstruction *in situ* after light exposure.[33] Nevertheless, several concerns have been highlighted by the scientific community regarding the use photopolymerization in TE. The energy of the polymerizing light, heat and the radical species produced during the polymerization, as well as the toxicity of photo-initiators and monomers could be a source of damage for the surrounding tissues and/or for the entrapped molecules.[34]

4. Magnetic tissue engineering

The remarkable features of magnetic responsive materials have prompted their application in the biomedical field and more specifically in TE. One of the major concerns among the scientific community relies on the biocompatibility and long-term stability of materials like MNPs.[35] It is notable that MNPs are highly compatible, as the iron cell homeostasis is well controlled by uptake, excretion and storage and the iron excess is efficiently cleared from the body. In fact, *in vivo* assays (rat models) revealed that these iron-based particles do not cause oxidative stress or long-term changes in the levels of liver enzymes, which are indicators of biosafety.[36] Of course, the safety of these materials depends on several parameters such as particle size, shape, functionalization and concentration. Regulatory guidelines should be discussed to prompt the clinical application of these propitious materials. Concerning their application in biological organisms, MNPs offer the advantage to not retain any remnant magnetization upon removal of the magnetic field, which prevents aggregation and enables them to redisperse rapidly after withdrawing the magnetic field. Beyond this, they have many advantages in terms of tissue penetration and invasiveness since biological tissues have a lower absorption capacity for magnetic fields than for other types of stimuli, like electric fields, making it possible to remotely activate an event at a relevant distance from the magnet.[37]

Hence, the power of MNPs has been emphasized in the biomedical field – see **Figure II.1**. Starting with more conventional strategies, MNPs allow the use of a minimally invasive methodology to perform cell separation, drug and cell targeting, and the delivery of small molecules. Withal, MNPs had also demonstrated a crucial role on monitoring through MRI, and on the treatment of challenging diseases like cancer, by making use of magnetic hyperthermia. More advanced strategies are now employing MNPs for the engineering of functional tissues substitutes.[38] The major achievements in fabrication of magnetized tissues are displayed in the next sections, highlighting the key approaches for tissue development and potential applications.

4.1. Monitoring tissue engineering processes

In regenerative medicine, replacement tissues can be produced *à priori* and then transplanted, or be assembled *de novo* at the injury site. In both scenarios, the implanted tissue constructs must be followed and monitored over time to evaluate the tissue development and functionality. Hence, the development of suitable methodologies for tissue monitoring is undeniably critical to instigate the application of tissues' substitutes. Aiming a proper tissue regeneration, the structure, composition, and strength of the developing tissues must be investigated along the process.[39] Conventionally, optical and fluorescence microscopy are used to monitor tissue growth, but even more advanced techniques like multi-photon have a limited depth of field. Although techniques such as micro computed tomography (micro-CT) could solve the tissue penetration problematics, this method uses ionizing radiation and requires dense tissue to provide contrast.[40] In fact, the exposure to ionizing radiation, even at low frequency, poses a significant health hazard. The mechanisms behind this include induction of reactive oxygen species, gene expression alteration and DNA damage through both epigenetic and genetic processes.[41] MRI, on the other hand, offers a promising alternative imaging modality, as it uses non-ionizing radiation and a paramagnetic agent i.e., MNPs, showing promising results for *in vivo* imaging due to its optimal tissue penetration and 3D spatial resolution. MRI is a very sensitive method that allows the visualization of structural and functional changes, even in biological organisms. During the regeneration process, as tissue develops, dies, or regenerates, the local environment of the tissue, namely water content (the source of the MR signal), changes. These fluctuations are reflected in MR images through local variations in the amount of tissue water and its nuclear magnetic resonance (NMR) relaxation times.[42] Cartilage, bone, pancreas, tendon, ligament, heart, brain, kidney and liver are the main engineered tissues already assessed by MRI. Until now, the diffusion of oxygen and nutrients, cellular metabolism and ECM formation are the key parameters usually analyzed by MRI in the

engineered tissues. Nevertheless, depending on the targeted tissue, other important features must also be investigated. For example, constructs aiming for cartilage regeneration require mechanical strength, viscoelastic properties and synthesis of collagen II and proteoglycans, while bone involves the bone matrix synthesis, mineralization, angiogenesis, and mechanical strength.[42] Thus, MRI represents nowadays, the most feasible monitoring methodology, permitting the scanning of any kind of tissue and the analyzes of a huge set of parameters in different scenarios such as diagnosis, patient treatment and tissue regeneration. Overall, the magnetic field opened new tools for *in vivo* imaging, overcoming the main problems of conventional methodologies.

4.2. Magnetic-guidance

Conventional drug delivery is mainly limited by the difficulty to overcome the natural physiological barriers and their lack of tissue/cell specificity.[43] By combining electro-magnetic devices and MNPs, magnetic-guidance systems are being established with huge relevance for TE, enabling simultaneously, the guidance and tracking of drugs, cells and/or biomolecules.

As stated in the previous section, MRI is considered the most efficient method for feedback control of targeted biomolecules, enabling a precise real-time tracking of magnetic nano/microdevices. Targeted drug delivery applications may take advantages of this monitoring strategy as molecules can be magnetically guided toward specific tissues, enabling their tracking inside the body.[44]

Still, as the MRI image reflects signals from blood, muscles, and tissues to depict the body/organ anatomy, its application for drug delivery monitoring may be compromised by the background signal from the host tissue. To overcome this issue, magnetic particle imaging (MPI) arose as a novel emerging noninvasive and radiation-free imaging modality that can quantify MNPs tracers. This strategy allows the creation of fully 3D images of the injected tracer particles without exhibiting the background of soft tissues, thus overcoming the challenges of MRI.[45] Of note, MPI scanners can achieve fast and high-sensitivity with millimeter-scale resolutions, and it has high potential to revolutionize the biomedical imaging field.

Focusing on sustained release of bioactive compounds, Li and co-workers showed that a controlled release of drugs can be achieved by applying a low frequency oscillating magnetic field, remotely. Such conduct was demonstrated in magnetic hydrogels containing dextran and insulin. The remote release of the drugs was achieved due to temperature changes in the magnetic hydrogel, composed by a thermo-responsive polymer, in the presence of a magnetic field.[46] When the temperature is increased above the LCST, a fraction of the magnetic hydrogels collapses, resulting in the release of the encapsulated drugs. Using magnetic hydrogels, the presence of an alternating magnetic field

leads to significant differences in the swelling ratio. When turned to the "on" state, the swelling ratio of the magnetic hydrogel reduced, but it raised and almost recovered to the original state when was switched to the "off" state.[44] This phenomenon is attributed to the change of porosity or pore size of the magnetic hydrogel under the switching "on-off" mode. This strategy was already explored in neuromodulation by combining the genetic targeting of a magnetoreceptor with remote magnetic stimulation, in a non-invasive manner.[45] The magnetogenetic control of neuronal activity might be dependent on the direction of the magnetic field and exhibits on-response and off-response patterns for the external magnetic field applied. Comparing to conventional methodologies like optogenetics (a method that allows the activation or inhibition of light sensitive ion channels, commonly used for the spatial and temporal manipulation of neurons), magnetogenetics (a technique that involves the use of magnetic field to remotely control cell activity) offers several advantages including non-invasiveness, deep penetration, long-term continuous dosing, unlimited accessibility, and spatial uniformity.

Directing to cell therapy, simple approaches like the injection of magnetized cells have been explored, promoting the accumulation of cells at the target site. For example, Polyak and colleagues revealed that the re-endothelization of a carotid artery was attained in the left ventricular cavity of rats by the injection of aortic endothelial cells, previously magnetized.[47] Still, a more sophisticated system based in an on-off remote system has also been engineered.[48] Xia and colleagues employed this system for the controlled release of stem cells using composite scaffolds. Different release profiles were obtained by changing the strength and frequency of the external magnetic field, and the number of magnetic cycles. Later, Wang and co-workers indicated that the release rate of both hydrophobic and hydrophilic drugs could be increased through the application of an alternating magnetic field.[49]

In contrast to conventional approaches, magnetic-guided methodologies enable a finer, targeted, and efficient procedure. Drugs, biomolecules, or cells can all be tracked and guided in an extremely precise manner.

4.3. Development of tissue-like constructs

4.3.1. Cell-patterning

By merging magnetic forces with micropatterning technologies, magnetic force-based cell patterning platforms have been developed for TE purposes. Regarding the high accuracy of these platforms, single cell arrays can be developed for studying the individual cell behavior and morphological alterations with potential application in cell diagnosis and studies in cell-cell

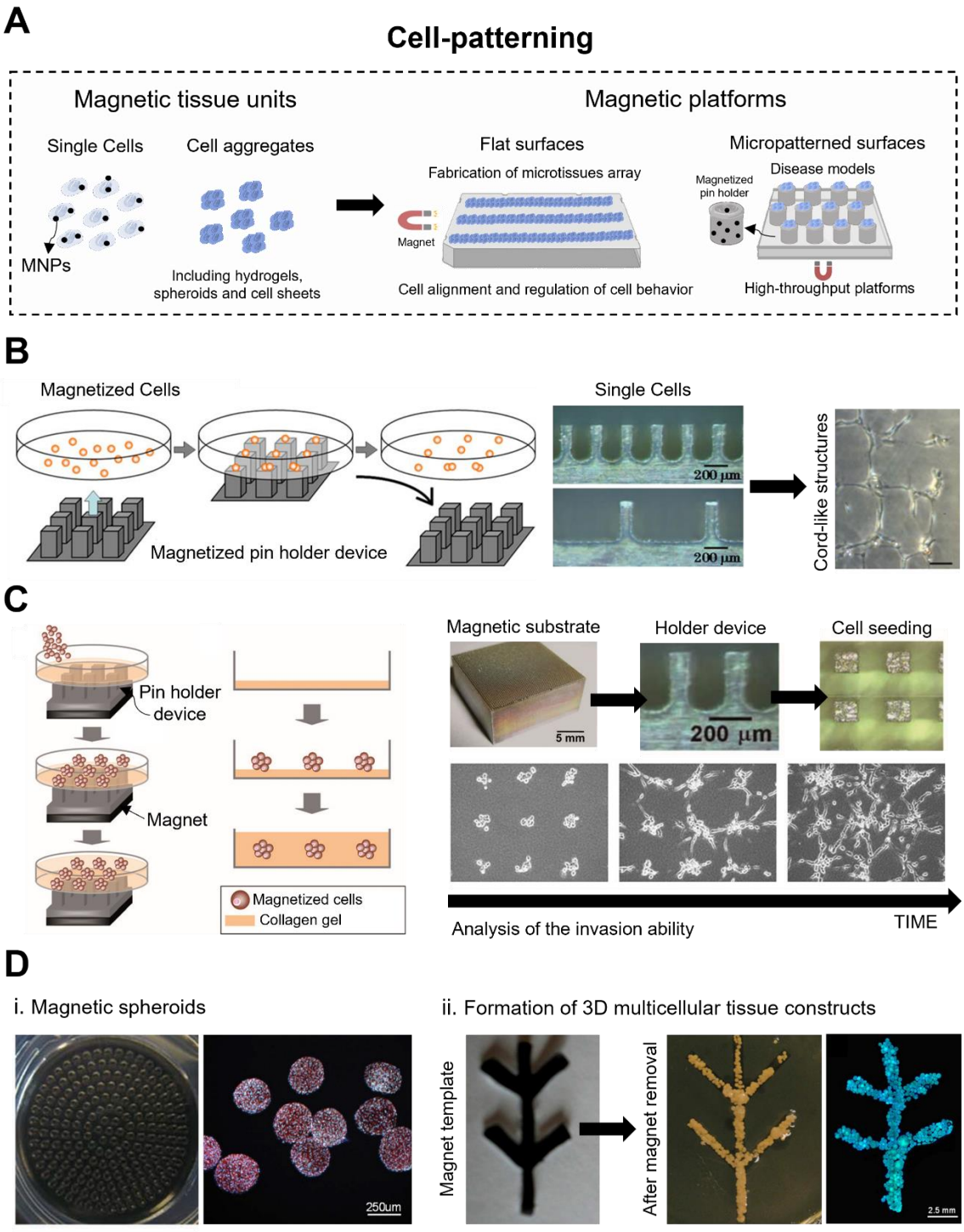

Figure II.3: Cell patterning strategy for Mag-TE. **A.** Representation of the magnetic patterned platforms for TE, using magnetic units such as magnetized cells or cell aggregates; **B.** The patterning of single cells was achieved by a magnetized pin holder device, promoting the formation of cord-like structures, crucial during angiogenesis; **C.** Similar devices was used to investigate the invasive capacity of BALB/3T3 cells, used as cancer model; **D.** 3D tissue constructs were also fabricated using this strategy, where magnetic spheroids formed *à priori* were guided to a prefabricated magnetic template. At the end, the spheroids fused and a 3D tissue with the template' geometry was formed. Reproduced with permission.[50] Copyright 2009, Wiley. Reproduced with permission.[52] Copyright 2009, Royal Society of Chemistry. Reproduced with permission.[53] Copyright 2014, Wiley.

interactions.[50] Devices composed by spaced micropillars are one of the most explored configurations for creating arrays of single adherent cells - see **Figure II.3A**. For instance, a magnetic holder device with an array of pillars was fabricated by Ino and co-workers, acting as substrate to magnetically attract the magnetized cells. This magnetic device was used to investigate the cell function and behaviour during angiogenesis- see **Figure II.3B**. For the purpose, magnetic-labelled cells were re-arranged in accordance with the micropatterned device, promoting the formation of cell clusters in adjacent spots and therefore, the creation of branched-like structures. Cell-cell interactions have proven to be crucial during the angiogenesis step.

More ambitious systems were also proposed, including the fabrication 3D magnetic patterning systems.[51] Goranov and colleagues developed a 3D magnetic scaffold for the fabrication of vascularized tissues. The proposed scaffold was composed by separate arrangements of vascular and osteoprogenitor cells, established on opposite side of the scaffold fibers, showing promising features on the development of materials with angiogenic potential.[52]

Such 3D arrays were also explored by Okochi and colleagues to analyze the invasive capacity of BALB/3T3 cells, used as a cancer model cell line (**Figure II.3C**). The 3D cell patterning was performed using an external magnetic force and a pin holder, which enabled the assembly of the magnetically labelled cells on a collagen gel-coated surface. The developed 3D cell culture array system may be useful to assess the effects of pharmacologic and/or microenvironmental influences on tumor cell invasion.[50] A similar approach was employed by Whatley and colleagues for the fabrication of 3D cell-based structures, using endothelial cell spheroids as basic units. After the MNPs' cellular uptake and the formation of the magnetized spheroids, they were then guided to the prefabricated magnetic template through the attractive magnetic forces between the magnetized spheroids and the magnetic template.[53] The magnetic spheroids started to fuse along the time and at the end, by removing the template, 3D multicellular tissue constructs were obtained (**Figure II.3D**). Such strategy allowed the patterning of cell spheroids in accordance with desirable magnetic patterns, therefore holding promise for scalable fabrication of tissue structures with high complexity. Stratified tissues' structures were also designed by combining cell patterning with magnetic force. Akiyama and colleagues described the fabrication of multi-layered CSs using a magnetic concentrator device. Briefly, a cell layer of C2C12 cells (a myoblast cell line) was formed and then, a line patterning of human umbilical vein endothelial cells (HUVECs) was created on the top of the previously formed cell monolayer.[54]

Magnetic patterning platforms also arose as a promising strategy for the fabrication of tissue constructs with complex architecture, where the tissue design relies only on the configuration of

the micropatterned platform.[54]–[56] The 3D arrangements were controlled by a magnetic concentrator and the magnetization of the material, allowing fot the fabrication of fine and distinct biomaterials such as cell aggregates, fibers, spheroids and CSs.

4.3.2. Scaffold-based tissue engineering strategy

Conventional scaffold-based approaches rely on the use of "templates" that support the attachment and proliferation of living cells to form a 3D tissue.[57] The possibility to use specially designed materials prompted the use of scaffolds in TE over the last decades. The ideal scaffold should possess a repertoire of cues - chemical, biochemical and biophysical - able to control and promote specific events at the cellular and tissue level.[58] 3D scaffolds are expected to protect cells from the damage associated with external factors, while granting a biomimetic environment for cells, with the delivery of growth and differentiation factors that leads to tissue formation.[59] Materials of natural,[60] synthetic,[61] semi-synthetic and hybrid origins[62] have been employed for the fabrication of scaffolds for TE purposes (**Figure II.4A**). Despite many advantages offered by materials from natural sources, their application has been delimited by their possible immunogenicity, purification issues or even the difficulties in controlling the material properties and performance. Conversely, synthetic materials are easily reproducible and programmable but their insufficient biological recognition also limits their application as tissue regeneration matrices.[63] Alternatively, hybrid materials combine the performance and properties of the synthetic materials with biomolecular cues, capable of directly interacting with cells.[64] Scaffolds must recapitulate the ECM of native tissues guiding the adhesion, migration and proliferation of living cells.[65] Several ECM signals such as fibronectin (FN), laminin and integrin molecules, which are key regulators of cell adhesion and migration, have been conjugated with scaffolds to create synthetic ECM analogues.[66] Nevertheless, the use of scaffolds in TE is still associated with some constrains. In porous 3D scaffolds, cell distribution tends to be inhomogeneous, and the initial density is low, especially in case of larger constructs.[67] To overcome this problematic, researchers have engineering hydrogels in the presence of cells that not only enable their homogenous distribution and but also lead to higher cellular densities.[68] Hydrogel microcapsules are one of the most explored microscale hydrogels, being focus on cell encapsulation strategies. Such approach allows the transplantation of non-autologous cells that are protected from the host's immune system due to their encapsulation in a semi-permeable hydrogel membrane.[69] It allows the diffusion of nutrients and cellular metabolic products while excluding antibodies and immune cells.

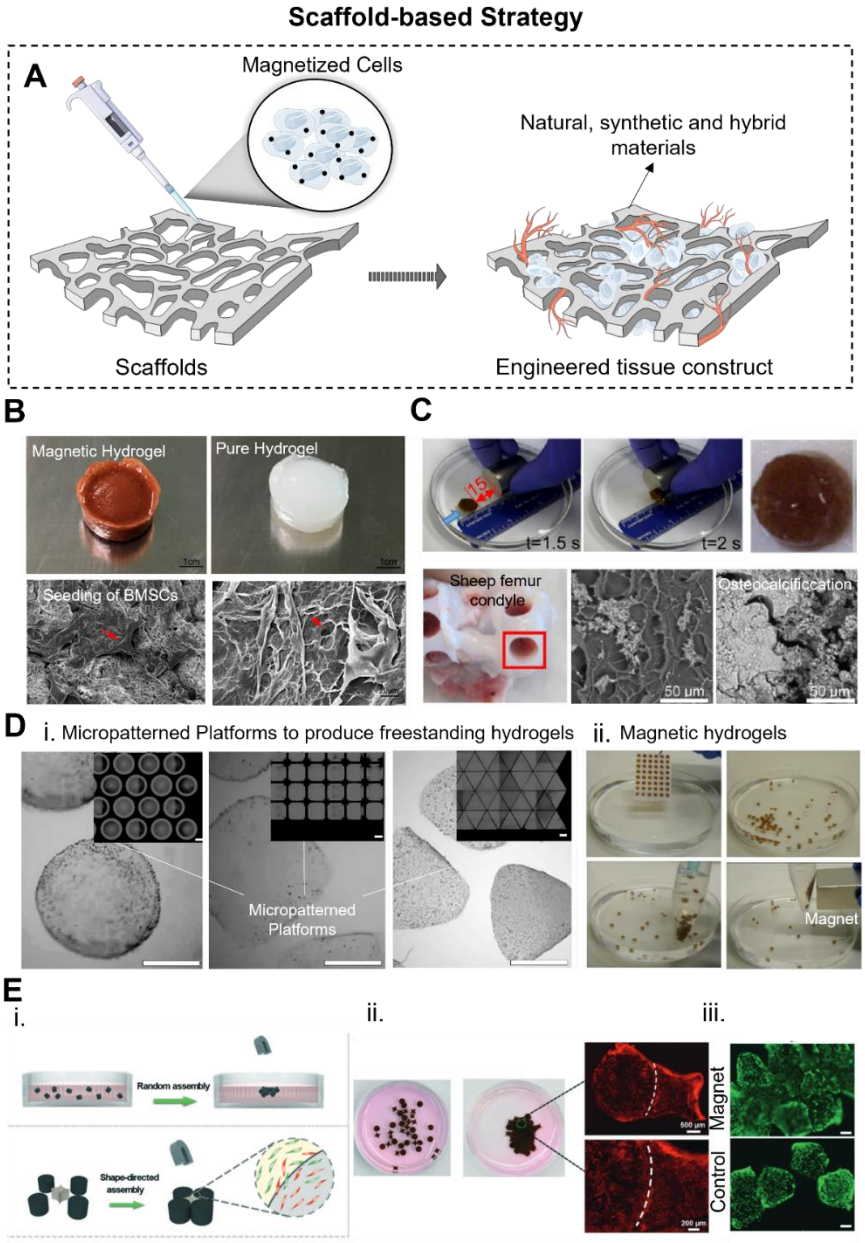

Figure II.4: Fabrication of magnetic tissues by scaffold-based approach. **A.** Schematic illustration of the scaffold-based strategy, where magnetized cells are seeded or encapsulated in scaffolds composed by natural, synthetic or hybrid materials; **B.** General view of hydrogels composites – Fe_2O_3/hyaluronic acid/polyvinyl alcohol (on top). SEM images of porous hydrogels, where BMSCs can adhered and aggregated in the pores. In control, small number of cells adhered to the porous surface (on bottom); **C.** Micrographs of a hybrid hydrogel containing collagen type II, hyaluronic acid, polyethylene glycol and magnetic nanoparticles (on top). These materials were explored for cartilage TE, where the collagen was extracted from sheep femur condyle with potential calcification (on bottom); **D.** Micropatterned platform for the high throughput fabrication of microtissues with complex geometry (on left); these magnetic hydrogels can be used to produce larger structures by magnetic-guided assembling (on right); **E.** i) Construction of macro-scale tissues by random or shape-directed assembly of magnetic microcryogels under magnetic force; ii) Photographs of circle and clover magnetic microcryogels and their accurate assembling. Even at macroscale, the tissue constructs remained viable (live/dead images in Figure 4Biii). Reproduced with permission.[55] Copyright 2016, Wiley. Reproduced with permission.[76] Copyright 2018, American Chemical Society. Reproduced with permission.[77] Copyright 2015, American Chemical Society. Reproduced with permission.[81] Copyright 2014, Royal Society of Chemistry.

Multi-shaped complex structures with clinical relevance have been engineered by the assembly of those cell encapsulation systems, in accordance with the concept of modular TE.[70]

Concerning the sophisticated arrangements of native tissues, nano- and micro-structured materials are being incorporated into the hydrogel network to mimic its non-homogenous structure.[71] Due to the remote actuation of MNPs, such materials have been increasingly explored in biomedical field, including the manipulation of MNPs distribution within the 3D space of hydrogels' networks, allowing a controlled design of anisotropic magnetically responsive scaffolding materials. Such smart hydrogels were introduced in the biomedical field for several applications including drug delivery, bioseparation, biosensor and TE. In addition, this magneto/mechanical stimulus can be harnessed to control the growth, migration, proliferation, and differentiation of cells encapsulated within magnetic hydrogels toward targeted lineages, allowing the production of cell-laden constructs with specific ordered features, re-creating the architectures of native tissues. Such behavior is mainly attributed to the physical, biochemical, and mechanical alterations of the milieu surrounding the cells and tissues in response to external magnetic stimuli.[72]

Largely, magnetic hydrogels have been showing promising results in recreating the native structure of neural, heart, skin, cartilage and bone tissue.[46] For instance, N-isopropylacrylamide-methacrylic acid (NIPAAM-MAA) hydrogels were combined with Fe_3O_4 nanoparticles and curcumin to reduce the doxorubicin-induced cardiac toxicity and hold the cardioprotective capability.[73]By conjugating the ferrogel scaffolds and alginate, the regeneration of muscle tissues was also reported. Through the magnetic stimulation (5 min at 1 Hz every 12 h), the biomaterial was mechanically activated, and the regeneration of the injured muscle tissue was promoted.[74]

Huang and colleagues have also demonstrated the capability of polyethylene glycol (PEG) magnetic hydrogels to induce fibroblasts alignment, which is crucial for wound healing.[75] The presence of the magnetic field in collagen hydrogels containing MNPs triggered the alignment of collagen fibers. Neurons within a 3D aligned magnetic hydrogel complex exhibited good cell viability and more elongations as well as directionality in comparison with those of without fiber alignment, indicating that 3D aligned magnetic hydrogels open a promising possibility for directional neuronal regeneration.

Nevertheless, the major achievements of magnetic TE have been focused on the engineering of cartilage and bone tissue. Huang and colleagues developed a magnetic nanocomposite hydrogel composed by polyvinyl alcohol (PVA), hyaluronic acid (HA) and Fe_2O_3 MNPs for cartilage TE.[76] The hydrogel regulated the differentiation of bone mesenchymal stem cells (BMSCs) – **Figure II.4B**. Moreover, the introduction of the magnetic nanoparticles increased the mechanical performance

of the hydrogel and promoted the formation of microporous structures on the hydrogel surface that favored both cell adhesion and proliferation (**Figure II.4C**).[77] Regarding the cartilage tissue, scaffolds composed by MNPs, collagen II, HA and PEG showed similar microstructure and chemistry to hyaline cartilage, while assuring the biocompatibility of the proposed device.[78] Such behavior was also verified using other materials including hydrogels composed by fibrin-agarose, MNPs and hyaline chondrocytes. The resulted artificial tissues combined a stronger and stable mechanical response with the introduction of the MNPs with promising *in vitro* cytocompatibility and correct deposition of collagen type II.

Magnetic hydrogel composites were also developed for bone TE. Farzaneh and co-workers proposed a polyacrylic acid hydrogel with cobalt ferrite nanoparticles ($CoFe_2O_4$) as magnetic agents.[79] The synergetic effect between the magnetic scaffold and the external magnetic field prompted the osteogenic differentiation of human dental pulp stem cells (hDPSCs) by increasing the alkaline phosphatase (ALP) activity and mineral deposition, being a promising alternative to chemical stimulants. Henstock and colleagues also showed that collagen hydrogels encapsulating MNPs, bone morphogenetic protein-2 (BMP-2) and human mesenchymal stem cells (MSCs) can stimulate the mineralization of the artificial tissues. [80]

Magnetic hydrogels were also designed at microscale, resembling functional tissue living units. The manipulation of microtissues, such as regular medium exchange, can pose a relative challenge to the microtissues' integrity (**Figure II.4D and II.4E**). To overcome this issue, Liu and co-workers proposed the fabrication of on-chip of magnetic hydrogels at microscale, more specifically, microcryogels (**Figure II.4E**).[81] The magnetic microcryogels lead to convenient manipulation of the microtissues, eliminating potential cell loss during medium exchange, guaranteeing microtissue integrity during long-term culture and allowing magnetic purification of the desired functional units.

4.3.3. Scaffold-free tissue engineering strategy

Regardless of the incredible efforts in the engineering of hydrogels for TE applications, several concerns including scaffold choice, immunogenicity, degradation rate, toxicity of degradation products, host inflammatory responses, fibrous tissue formation and mechanical mismatch with the surrounding tissue can all affect the performance of the engineered tissue construct, compromising the biological function.[70] In addition, scaffolds are also usually associated with reduced cell-to-cell connection, as well as incorrect deposition and alignment of ECM that compromises the target function of the fabricated tissues.[82],[83] Moreover, the complex, well-organized and hierarchical architecture of tissues and organs may not be fulfilled by scaffold-based

approaches. Flat tissues, tubular structures, hallow, nanotubular, viscous organs and complex solid organs exhibit unique features that truly challenge conventional TE.[84] Thus, materials science, matrix biology and TE have been increasingly combined to generate a new class of biomimetic materials to closely mimic critical aspects of natural tissues regarding its physical and chemical properties. Aspiring the creation of completely functional tissues, scaffold-free TE has emerged as powerful strategy to recapitulate the native tissues, by exploiting cells' own abilities to synthesize the entire tissue matrix without the use of exogenous scaffolds (**Figure II.5A**).[85],[86] Scaffold-free TE enables the formation of complex tissues with 3D architectures and intensive cell-cell interactions, while guaranteeing the correct deposition of ECM. Due to the high cell density of the engineered tissues, such methodology facilitates the rapid tissue formation and accelerates the tissue maturation.[82]

Regarding the heterogeneity of almost all tissues and organs, it is also critical the establishment of a heterogeneous cell culture system to recreate native tissue/organ-like 3D constructs.[87] Monoculture and heterotypic tissues, pre-vascularization, specific and complex tissue assemblies are some of the diverse topics that have been intensely investigated in TE. The recent advances in the development of cell-based tissue constructs are explored in the following sections, highlighting the current methodologies and major outcomes. Although scaffold-free approaches foresee that the final biological product ready for implantation should be scaffoldless, some of the scaffold-free strategies may accommodate biomaterials with specific cell function other than serving as anchor for the tissue to grow. As so, the list of scaffold-free systems herein discussed will be categorized as cell-based biomaterial approaches since biomaterials may be used to prompt and help to orchestrate specific functions of natural tissues.

4.3.3.1. Spheroids and multishape microtissues

The greatest part of mammalians' native tissues displays 3D and highly compact organotypic cellular organization.[88],[89] Owing to their architectural and organizational resemblance with native tissue structures concerning cell-cell and cell-ECM contacts, the role of multicellular aggregates as providers of closer-to-physiological moieties with regenerative ability has been widely explored. The remarkable ability of cells to self-organize *in vitro* into multicellular spheroids has driven not only the fabrication of regenerative units, but also the use of these structures - ranging from stem cells aggregates to specialized organoid structures - as models to study human development and disease *in vitro* with improved predictability when compared to traditional cellular monolayers.[89] In general, the use of multicellular aggregates as regenerative devices has been mostly focused on

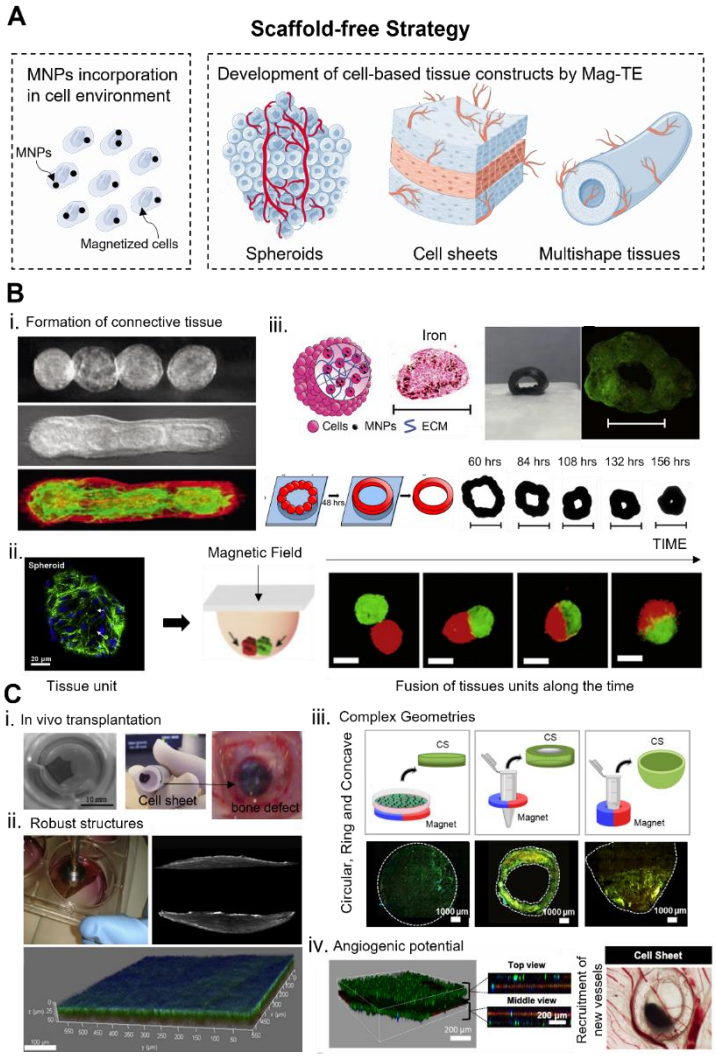

Figure II.5: Fabrication of cell-based tissue constructs by scaffold-free approaches. **A.** Illustrative image of scaffold-free TE strategy, where magnetized cells are used as building block for the fabrication of cell-based tissue constructs namely spheroids, cell sheets and multi-shape tissues; **B.** Production of magnetic spheroids by Mag-TE. ii) Sequential steps of tissue fusion of vascular tissue spheroids placed in collagen type I hydrogel; i) By using magnetic spheroids as tissue unit and in the presence of a magnetic pin, the fusion of spheroids into a single tissue construct was accelerated and the union of the spheroids was achieved after 24h; iii) Magnetoferritin NPs in magnetic cellular spheroids. Magnetic-labelled spheroids were assembled onto a ring magnet. The presence of a strong magnet was crucial for the spheroid fusion in the desired shape. In the presence of a weak magnet, the inner diameter contraction was visualized; **C.** Fabrication of sheets of cells by Mag-TE. iv) The transplantation of MSC sheet (single layer) to a cranial bone of nude rats using an electromagnet (on bottom); ii) Simple magnetic harvesting process that allows the recovery of robust tissue structures with high cohesiveness; i) By changing the magnet shape and cell density, cell sheets with different geometries can be designed; iii). More hierarchical and stratified tissue structures were also developed by Mag-TE. The recruitment of new vessels was attested by a CAM assay, even in the presence of structures with higher complexity. Reproduced with permission.[90] Copyright 2013, Elsevier. Reproduced with permission.[93] Copyright 2014, Elsevier. Reproduced with permission.[96] Copyright 2014, Elsevier. Reproduced with permission.[110] Copyright 2020, Elsevier. Reproduced with permission.[114] Copyright 2007, Wiley. Reproduced with permission.[119] Copyright 2017, Elsevier. Reproduced with permission.[120] Copyright 2020, Elsevier.

two possible regenerative roadways, which are not necessarily independent: i) the use of aggregated cells as secretory vehicles of pro-angiogenic, trophic and immunomodulatory molecules, with high local retention efficacy when compared to the direct injection of suspensions of cells into defects (**Figure II.5Bii**),[90] and/or (ii) the administration of healthy *in vitro*-prepared tissue precursors or mimetics into the injured site.[91]

Several methodologies have been employed for the fabrication of multicellular aggregates. Starting with well-defined approaches, such as hanging drops, the cells spontaneously aggregate at the bottom of droplets placed in culture plate lids turned upside down.[92] Regarding this concept, magnetic cellular spheroids can be engineering by hanging drops only by the previous labelling of the cells with MNPs. The final spheroids can be easily magnetically manipulated and separated without the need of centrifugation. Additionally, Kim and colleagues have also reported a simple and efficient spheroid generation method based on a magnetic pin-array system to concentrate previously magnetized cells in a focal direction. For this, the system only comprised external magnets and magnetically induced iron pins to generate a concentrated magnetic field for attracting cells in a focused direction. This strategy allowed the generation of size-controlled spheroids in a reproducible manner. Furthermore, spheroids with a versatile design, including random mixed, core–shell, and fused spheroids were successfully produced by this methodology (**Figure II.5Bi**).[93]

Microfluidic devices also appeared as new tool for the high-throughput production of multicellular spheroids with precise size control. Yoon and colleagues proposed a droplet-based microfluidic system that can encapsulate both cells and MNPs within alginate beads to mimic the function of a multicellular tumor spheroid. At the end, the magnetic spheroids could be collected and easily transferred to the target.[94]

As alternative to the traditional iron oxide MNPs – herein referred as MNPs, magnetiferritin nanoparticles were also explored for the fabrication of magnetic spheroids. Stated as a biological alternative to MNPs, these particles could avoid the requirement of complex surface modifications to reduce the adverse effects on cells.[95]

In previous works, the spheroids magnetism relied on the previously internalization of magnetic particles within the cells. [92],[93] Still, non-conventional approaches have also been investigated, such as the Janus structure of magnetic cellular spheroids proposed by Mattix and co-workers. These structures possess two domains: one composed of cells and the other of MNPs and ECM components to form a Janus magnetic cellular spheroid (**Figure II.5Biii**).[96] Cellular spheroids with

cells and MNPs apart were successfully produced, allowing the fabrication of tissues with several cellular and extracellular composition and contents.

One major problematic in tissue constructs with high cell density relies on the need of correct perfusion of essential nutrients and oxygen for tissue survival. By applying a magnetic field, microvascular tissue constructs can be engineered, where an aligned vascular network is promoted by the presence of the magnetic field. Particularly, Morin and colleagues showed the formation of aligned sprouting of endothelial cells in magnetic spheroids, a crucial step in the generation of aligned microvascular networks.[97]

Despite of the incredible outcomes of spheroids in the engineering of tissue constructs *in vitro*, their application for disease modeling and drug screening has also been highly recognized. Due to their superior complexity comparing to conventional 2D models, spheroid models have showed an important role for cancer treatment. Perez and co-workers demonstrated that by simply promoting the magnetic aggregation of cells with internalized MNPs, magnetic spheroids with high sphericity can be obtained. Using a carcinoma cell line as a proof-of-concept, such structures were explored in terms of cell proliferation, invasion capacity and how the spheroid maturation impacts on cell invasion, and penetrability of drugs such as doxorubicin, all important parameters in therapeutic screening.[98] These tissue models were also investigated to recreate the *in vivo* environment of neural tissue. Using magnetic-labelled spinal cord cells, magnetic spheroids were engineering with high fidelity of size and shape only by imposing an external magnetic field.[99]

Advanced strategies, including the robotic-assisted assembly are currently being used for the fabrication of uniform-sized spheroids by the assembling of magnetized cells. Whatley and co-workers showed that 3D cell-based structures can be produced by using MNPs as a patterning agent to direct the attachment and self-assembly of MNPs-loaded endothelial cell spheroids, on a prefabricated magnetic template.[100]

4.3.3.2. Cell sheet engineering

Regarding the fabrication of tissues *in vitro*, CSs have been also explored as basic tissue units to engineer complex and hierarchical constructs. CS technology arose as a reliable alternative to conventional and limiting harvesting strategies that make use of proteolytic enzymes, such as trypsin chelating agents like ethylenediaminetetraacetic acid, that affect cell integrity and disrupt crucial intercellular junctions and cell surfaces proteins.[21],[101] Such methodology allows the creation of cell-dense like tissues with uniform cell distribution that can be harvested as a whole, preserving their ECM.[102] Then, upon *in vivo* transplantation, tissues contrived by CS engineering

are able to adhere to the surface of the host tissue without suture and form a cell-like dense structure,[103] enabling the maintenance of cell-cell interactions that lead to a proper tissue regeneration.[104] Moreover, because its composition is similar to natural tissues, it also avoids the limitations associated with scaffold degradation and the possible inflammatory responses and limited passive diffusion (e.g. insufficient delivery of oxygen and essential nutrients and removal of metabolic waste) that may compromise tissue formation.[105],[106] The mechanism of preparation, harvesting/manipulation and transplantation of CSs was firstly reported by Okano in the 90s.[100],[107] It mainly consisted on the use of thermo-responsive culture dishes that enable the reversible cell adhesion and detachment by changes in the hydrophobicity state of the surface.[106] By simply lowering the culture temperature below 32°C for 30 min, intact CS monolayers could be collected and transplanted into the host tissue. In this context, CS technology has been applied to several types of tissues such as heart, liver, bladder, bone, cornea and esophagus,[102] with the two latter having achieved successful clinical outcomes.[108] Such substrates are essentially limited by their high cost and low mechanical strength, as well as by the cellular abnormalities linked to physiological changes within the cellular microenvironment.[23] Additionally, traditional CS engineering may represent a challenge for the development of larger 3D tissue-like constructs due to their high complexity. In fact, stratified and heterotypic CSs have been previously produced through the individual stacking of formerly built CS monolayers in a time-consuming methodology that may limit the establishment of cell-cell interactions and hinder the spatial positioning control of the target cells.[104]

To address this challenge, magnetic harvesting systems were proposed for the first time by Ito and co-workers with the ambition to produce in a faster approach, heterotypic and stratified CSs with aided spatial manipulation.[109],[110] Initially, magnetized cells were obtained by the incorporation of magnetic cationic liposomes with a positive surface charge and the successfully particles internalization was demonstrated for distinct cell types namely rat hepatocytes, human aortic endothelial cells and human retinal pigment epithelium cell line. The magnetized cells were easily manipulated with the aid of neodymium magnets, resulting in cell accumulation towards the source of the magnet.[6],[111] By using magnetically labelled keratinocytes, Ito and colleagues demonstrated the ability to produce stratified CSs with 10-layered conformation. When the magnet was removed, the sheets were detached from the bottom of the plates and then, by placing the magnet on top the CS, the sheets could be harvested.[112] Then, this concept was explored by the same group to engineer heterotypic multi-layered CSs, composed by human hepatoblastoma HepG2 cells and mouse NIH3T3 fibroblasts. The results revealed major ECM components like fibronectin and

collagen type I, crucial to the development of robust tissues akin to native organisms.[104] Following the same methodology, tissue constructs with complex shapes like tubular structures were also produced. Briefly, when a cylindrical magnet was rolled onto the cell sheet, the cell sheet was attracted to the magnet and formed a tube around it. Upon magnet removal, a tubular structure was obtained.[113]

Magnetic layered CSs composed MSCs were also successfully fabricated. The ability of these tissues to differentiate into specific linages namely osteogenic, adipogenic and chondrogenic, was investigated after 21 days of culture with each induction medium (**Figure II.5Ci**).[114] In fact, when the MCSs sheets were transplanted into a bone defect in nude rats, new bone surrounded by osteoblast-like cells was formed in the defect area.

Another major limitation in TE is the formation of blood vessels in implanted tissues. In this sense, angiogenic CSs were also engineered by a similar approach, where vascular endothelial growth factor (VEGF) was labelled with magnetic cationic liposomes developed by Ito's group. After the implantation of the tissue grafts in nude mice, the authors visualized the vascularization of the tissue construct, a thick structure with a high cell density.[115] Notably, even without the presence of VEGF, MSCs sheets revealed higher angiogenesis when compared to the injection of isolated MSCs.[116] The introduction of RGD domains in magnetic cationic liposomes facilitated cell growth, CS construction and CS harvesting using solely magnetic force.[117]

Recently, Gil and co-workers have also demonstrated, in a proof-of-concept study, the ability to create magnetic CSs by making use of rod and sphere shapes of amino-functionalized iron oxide nanoparticles.[118] The functionalization of nanoparticles' surface could be useful for TE applications, including the immobilization of cell differentiation agents to control stem cell fate and antibodies for the attachment of biomaterials to other cells or specific proteins.

This technology has been applied in monoculture CSs such as keratinocytes, cardiomyocytes, hepatocytes, endothelial cells, MSCs and retinal pigmental cells.[28] Mag-TE has also been implied in the production of complex tissues that are not easily achieved by conventional cell culture or co-culture methods such as 2D and 3D cell layers, tubular structures and 3D ordered assemblies consisting of several cell types.[6],[109] Gonçalves et al, has reported the successfully fabrication of magnetically responsive tenogenic patches based on Mag-TE by using commercially available chitosan-coated MNPs and the subpopulation tenomodulin positive (TNMD+) hASCs (**Figure II.5Cii**).[119] In addition, Lu and colleagues have developed magnetic CSs using magnetic nanoparticles coated with nanoscale graphene oxide. Such particles were easily uptake by cells like dental pulp stem cells, preosteoblasts cell line (MC3T3-E1), bone marrow-derived MSCs,

chondrocytes and HUVECs. The authors also demonstrated the ability in creating multilayered CSs with precise control of CS shape and structure.

Howbeit, the fabrication of complex-shaped 3D-like constructs using living-based materials is hampered through the difficulty in recapitulating the mechanical properties of the native tissues. At the macroscale, magnetic CSs with versatile shapes and enhanced mechanical performance were fabricated using MC3T3-E1, through a universal approach that relies on the design of the substrate, cell density and magnetic force (**Figure II.5Ciii**).[120] Such magnetic CSs exhibited a Young's modulus similar to those encountered in the soft tissues.

More recently, Mag-TE has also shown remarkable outcomes in the fabrication of hierarchical 3D cohesive bone-like vascularized tissue in a simple, one-pot, cost-effective and time-saving manner, enabling the construction and manipulation aided by a magnetic force. In fact, such 3D construct revealed to be effective in stimulating *in vitro* the osteogenic differentiation of hASCs while triggering the recruitment of blood vessels with empowering pre-angiogenic potential (**Figure II.5Civ**). [110]

Upon implantation, the fate and distribution of transplanted CSs is crucial to evaluate the regeneration process. In Mag-TE, the presence of MNPs not only allows the engineering of complex hierarchal tissues, but also provides a non-invasive manner to track the implanted tissue along the time. Zhou and co-workers demonstrated that MNPs were feasible for *in vivo* labelling of CSs with a tracking time up to 12 weeks, using MRI scanning.[121] Another group also corroborated these findings, showing that the healing capacity of CSs-derived bone marrow-derived MSCs in a digestive fistula model (mice) can be accessed by MRI. This imaging tool granted the assessment of CS's integration into the host tissue, the inflammation and healing status and the vascularization.[22]

Resuming, the regenerative potential of magnetic CSs has been investigated in tissues like skeletal and cardiac muscle,[113],[122] bone and even on angiogenesis,[115],[123],[124] emphasizing the ability of this technology over artificial synthetic scaffolding materials for a wide range of tissues.

4.3.4. Cell behavior under magnetic stimulation

The role of external stimuli on cellular behavior, namely mechanical stimulation, has been widely investigated in last years. The mechanical stresses are implicated on a set of physiological processes namely cell and tissue growth, production of tissue matrix and differentiation of stem cells. Mechanotransduction is the well-known pathway, in which cells convert physical stimulus into biochemical activities. MNPs have been used as nano-instructive tools for diagnosis and therapeutics, that when incorporated in cells or biomaterials led to mechanoresponsive systems to

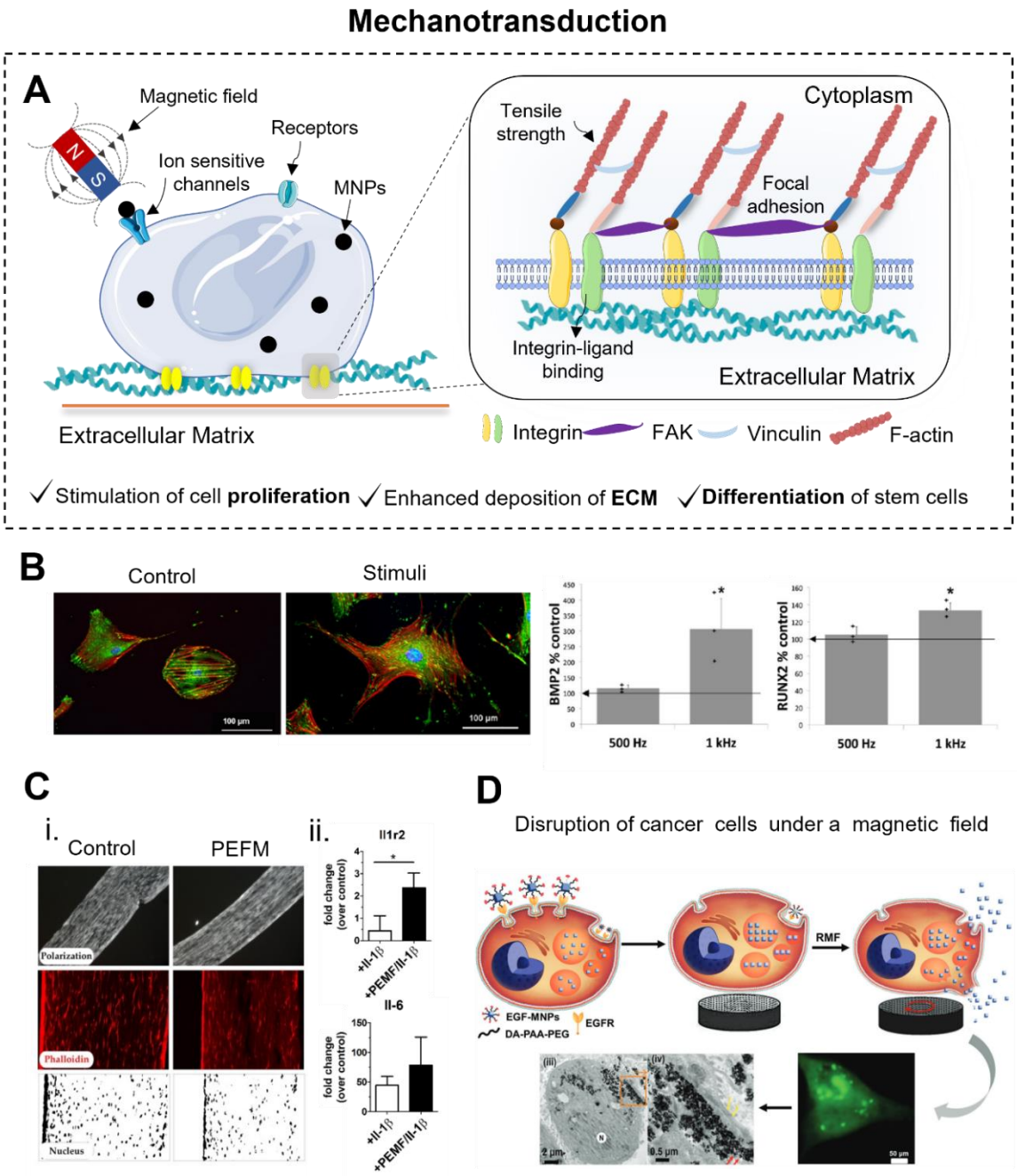

Figure II.6: The role of magnetic field on cell behaviour. **A.** Illustrative scenario of mechanotransduction pathways after mechanical stimulation of cells. **B.** In the presence of the magnetic stimuli, MSCs showed an increased gene expression of BMP-2 and RUNX2. Moreover, the cell morphology also changed with more adhesion domains and elongated shape. **C.** The presence of a pulsed magnetic field (PEMF) also shown a positive effect on typical cell alignment in tendon within cell-based constructs. Moreover, PEMF also influenced the expression of cytokines, including pro-inflammatory factors that could guide the healing process. **D.** The magnetic field was also implicated in cancer treatment. The breakage of lysosomes via magnetic-mechanical destruction induces cancer cell death. Reproduced with permission.[126] Copyright 2018, Wiley. Reproduced with permission.[131] Copyright 2013, American Chemical Society. Reproduced with permission.[134] Copyright 2019, MDPI.

control cell behavior. Concisely, these nanomagnetic systems can act as mechanostimulation platforms to apply controlled forces directly to single cells and multicellular biological tissues to precisely regulate cellular functions.[125] [37] The presence of a magnetic field generates mechanical forces on the cell membrane, which are converted on mechanotranduction signals inside the cell. Then, the tensile strength is delivered to actin cytoskeleton on cell membrane, promoting the integrin-ligand binding formation and maturation of focal adhesions. All these processes lead to the activation of several mechanosensitive and signaling proteins, which could stimulate the cell adhesion, proliferation or differentiation (**Figure II.6A**). Cells can be guided to specific biological events by regulating the mechanical forces produced by the magnetic field. [126]

This concept was demonstrated using osteoblasts with MNPs adhered on cell surface. Upon magnetic stimulation, the magnetized cells led to an enhanced regeneration of bone matrix. Later, this concept was extended to scaffold-based approaches, whereby providing an external magnetic field, supermagnetic scaffolds can supply the necessary cues for stimulating cell behavior.[127],[128] For example, hydroxyapatite scaffolds encapsulating pre-osteoblast cells showed an increased cell adhesion, proliferation and differentiation after the incorporation of MNPs.[129] However, the mechanism by which cell behavior is influenced is not fully disclosed.

By using periodontal ligament stem cells, Rampino and colleagues investigated the effect of a time-dependent magnetic field on their biological performance.[130] Briefly, in the presence of magnetic stimulation, the MAPK cascade (p-ERK1/2) is activated, promoting cell proliferation. Prominent effects on cell differentiation were substantiated on cells' metabolic profile, where magnetic stimulus induced osteogenesis in a time-dependent manner.[130] Considering the bone physiology, this tissue requires a dynamic mechanical stimulation to maintain its functionally. However, most part of the therapeutic approaches fail in this topic, focusing only on biochemical and structural aspects, neglecting the pivotal role on shear stress during bone formation. Thus, one valuable solution could be the application of a dynamic magnetic environment. Henstock and colleagues combined magnetic-labelled human MSCs (positive for TREK1 mechanosensitive ion channel) with BMP-2 and then, the cells were seeded into a collagen hydrogel scaffold and delivered into either the chick femur.[80] The nanoparticle-receptor complex was stimulated using a vertically oscillating external field, promoting calcium deposition and consequently the biomineralization of the tissue construct. The positive effect of magnetic field was also demonstrated in cell-based tissue constructs, where the presence of MNPs stimulated specific biochemical responses, involving the deposition of ECM and cell differentiation. Kikukar and co-workers also described that the magnetic field could influence the magnetized cells in terms of cell morphology, leading to changes in cell

signaling and gene expression. Using MSCs, the authors verified that by increasing the magnetic field, the expression of osteogenic factors, such as RUNX2 and BMP-2, is improved. Regarding the cell morphology, the authors corroborated the presence of more adhesion domains and an elongated shape (**Figure II.6B**).[131]

Recently, the influence of pulsed magnetic field (PEMF) in cell behavior was also investigated. Several works reported that PEMF stimulated specific biochemical responses.[132],[133] For instance, PEMF has shown great impact in the inflammatory process, influencing the release and expression of cytokines and therefore, creating synergistic actions to guide the healing process.

Such behavior was observed in tendon TE, where MNPs and PEMF prompted the typical cell alignment in tendon within cell-based constructs. Cellular organization is an important aspect for proper healing, while disorganized architectures may favor degenerative conditions mediated by pro-inflammatory niches (**Figure II.6C**).[134]

PEMF was also implicated in the proliferation and differentiation of bone marrow stem cells, encouraging the osteogenic differentiation process by several Ca^{2+} related mechanisms. The PEMF effect is primarily associated to early enhancement of intracellular calcium concentration, which is proposed as a reliable hallmark of the osteogenic developmental stage.[135]

The pulsed magnetic stimulation has also revealed important outcomes in neural TE by supporting the neural stem cells proliferation. *In vivo* assays showed that by increasing the number of pulses per day, the proliferation of neural stem cells was drastically higher by modulating cell cycle progression. In fact, the therapeutic effects of repetitive magnetic stimulation have been implicated for the treatment of depression, avoiding the decreased number of neural cells, and enhancing the neurogenesis. Neurogenesis is believed to be a potential therapeutic method for central nerve system diseases.[136]

Aiming the treatment of neural lesions, magnetic stimulation has been explored for the differentiation of induced pluripotent stem cells (iPSCs) into neuron cells. By comparing three magnetic stimuli, namely high frequency, low frequency, and intermittent theta-burst stimulation, the authors saw that low frequency and intermittent theta-burst stimulation can promote the generation of mature neurons from human iPSCs. Nevertheless, the mechanism of cell response to different magnetic stimulation is not completely clarified and could be a limitation in the therapeutic effect of neural stem cells.[137]

Mechanotransduction strategies were also reported for cancer treatment since the oscillation of MNPs can induced the rupture of cancer cells membrane. As illustrated in **Figure II.6D**, MNPs modified with epidermal growth factor (EGF) peptide were selectively accumulated in the cancer

cell lysosomes via endocytosis.[126] Under a rotating magnetic field, the aggregated MNPs exerted mechanical force to lysosomes, resulting in local mechanical membrane damage and consequently, cell death.

Generally, MNPs provide a unique approach to direct mechanotranduction in cells, easily translated to clinical practices. In large part of the tissue defects, the implanted materials tend to rapidly fail since the cells do not receive the stimulatory loading required for the integration and development of the tissue matrix.[138] MNPs, by simply tailoring the size, coating or even the magnetism of the particle, can be rigorously directed to mechanotransduction pathways. By this avenue, the mechanical properties of the biomaterial, a common weakness during the implantation, will not constrain the biological mechanism of mechanotransduction.

This approach has several advantages as it offers a level of drug-free control over differentiation and is amenable to be enclosed in several cell culturing methodologies for cell therapy purposes.

5. Assembling of the building blocks into complex tissues/organoids

Regardless of the relevance and recognized potential of cellular microaggregates as regenerative single units, recent trends have highlighted their role as interesting components to integrate larger scale tissues prepared *in vitro*. Those mechanisms may be crucial to promote the effective regeneration of large defects. Extra structural cohesion must be produced by cells, through their own secreted ECM.[139] Based on this knowledge, larger-scale constructs can be engineering by combining pre-assembled clusters, namely scaffolds, CSs, spheroids and multicellular aggregates. In this case, the cellular crosstalk occurs naturally, being essential to engineer cell-heterogeneous tissues where the intercellular communication is crucial. Currently, there are three main strategies to assemble these units into complex structures namely self-assembly, guided-assembly and direct assembly.[140] Considering the inherent magnetic force of the tissue building blocks fabricated by Mag-TE, large tissue constructs and/or tissues with increase complexity can be assembled by magnetic guided-assembly strategy. Comparing to the conventional methodologies, the magnetism also facilitates the *in vitro* tissues manipulation, allowing their recovery or media change with minimal tissue disruption.[141]

With the assistance of external magnetic forces, accelerated assembly of shape-controlled magnetic microtissues can be achieved, resulting in macro-scale tissue constructs by random or directed assembly. For example, magnetic microcryogels were designed by Liu and co-workers in circle- and clover-shaped inspired by the ‘lock-and-key’ design to direct the microtissue assembly. The tissue constructs were quickly agglomerated forming a connection between neighboring

microtissues after 5 days (**Figure II.3B**).[81] The individual microtissue building blocks were merged with each other and the whole assembly became inseparable at day 10. Conversely, in the absence of the magnet, scattered magnetic microtissue building blocks were observed with minimum connections at day 10, even when the microtissue building blocks were seeded at high density to guarantee proximity.

Ho and colleagues also showed that by using spheroids as tissue units, large tissue constructs could be formed by the fusion of patterned spheroids in the presence of a magnetic field.[92] Envisioning the fabrication of more advanced and sophisticated tissues *in vitro*, MNPs were also used by Whatley and co-workers to direct the attachment of magnetic spheroids on a prefabricated magnetic template for the formation of 3D cell-based structures. A magnetic-directed technique allows quick patterning of cell spheroids in accordance with desirable magnetic patterns, therefore owing promising potential for the fabrication of scalable and convoluted 3D multicellular tissue structures.[100] Complex geometries were also produced, including tissue rings, where a single homogenous tissue was formed without the presence of individual cellular spheroids. As stated in the section 5.3.1 – *Cell patterning*, this methodology allows the high-throughput fabrication of small tissue units. Hence, complex tissue constructs were engineered by combining cell patterning with scaffold approaches and CS engineering. Freestanding tissue building blocks were also designed with distinct geometries and sizes using a microarray composed by a superhydrophobic surface with wettable domains, resembling the functional units of living structures to recreate tissues' architecture (**Figure II.3E**).[55][56] This concept has already shown remarkable results in the fabrication of magnetic hydrogel and CSs, in accordance with the methodologies described in previous sections. Considering the strong deposition of ECM in CSs, such microfabrication-platforms allowed the fabrication of robust tissues with conserved architecture, a common issue in scaffold-free approaches.[56] By simply using cells as building units and such microfabrication-platform, the fabrication of complex multiscale and multifunctional tissues with clinical relevance is envisaged, including for therapies or disease models.

Thermo-responsive surfaces with nanotopography were also applied for the fabrication of CSs, combining the nanotopography to support cellular, with the magnetic nanoparticles that facilitate the magnetic levitation of the CSs.[142]The fabrication of these microphysiological systems, frequently referred as organs-on-chips or *in vitro* organ constructs is mostly achieved by manual processes with high user dependency, making reproducibility more challenging.[143] In this sense, automated processes are required in microphysiological model technologies for widespread industry adoption. Bioprinting has arose as a promising alternative for the manual procedures,

allowing a more controlled position of the tissue constructs. The magnetic character of the magnetically labeled spheroids allows its motion over short distances with the aid of the magnetic force. By combining external magnetic spheroids and bioprinting technology, complex aggregated tissue constructs can be engineered by the positioning and assembly of multiple spheroids, used as bioinks.[99] This concept was demonstrated for neural TE, where the magnetic forces enabled the precise control of spheroids position in a hydrogel template. This approach enabled the fabrication of neural constructs mimicking the hierarchical organization of the central nervous system with cell populations that project axons toward distant populations.

6. Clinical Trials

Cell-based therapies have been clinically applied in last decades mostly based on the direct injection of single cell suspensions. Nevertheless, TE is nowadays considered an excellency strategy for regenerative therapies, with 63 ongoing clinical trials focusing on collagen matrices and sheets of cells.[144] Regarding the clinical trials in TE, there are only six studies involving the use of the magnetic field. The safety concerns regarding the use of MNPs and magnetic field on TE have been hampering their translation to clinical practice. The mechanism behind MNPs degradation in *in vivo* environment still poorly explored, leading to an apprehensive use of MNPs in biomedicine. Therefore, the MNPs toxicity profile and the degradation along time must be extensively investigated to clarify all the benefits and injuries of Mag-TE. By changing several features of MNPs such as shape, size, structure, and surface, it is possibly to identify the most suitable design of MNPs for specified applications. In fact, several studies suggest that the surface modification can significantly increase the biosafety of MNPs.[145] Other preliminary studies also indicate that besides the physical modifications of MNPs along the time and its degradation at atomic scale, no toxic effects were observed in living organisms. According to Wilhelm and colleagues, cells could timely orchestrate the redistribution of a nanoparticle from a dense assembly in early endosomes to a more dispersed and exposed state into lysosomal compartments.[146] This mechanism might be activated to retard the release of free cytotoxic iron ions only to the lysosome, where ferritin proteins can store the released iron in a safe form. Nevertheless, the exact mechanism is still not completely identified. Additionally, these studies must be also performed in complex living organisms. **Table II.1** displays the selected information regarding the ongoing studies encompassing the use of magnetic field.

The main outcomes of magnetic field in clinical practices rely on MRI for monitoring purposes. For instance, the determination of fluid status in dialysis patients is a major clinical problem. Normally,

the fluid management of dialysis patients is solely based on body weight differences. Patients can suffer from either hypotension, if too much fluid is eliminated by dialysis, or from fluid-overload symptom. By using a mobile non-invasive NMR-MOUSE setup (a nuclear magnetic resonance spectroscopy measurement), the study pretended to develop a methodology to measure the hydration status of the skin, therefore monitoring the fluids' levels in patients during the dialysis.[147]

MRI was also useful to determine predictive factors in arterial embolization of uterine leiomyoma, by a pelvic magnetic resonance. This study followed symptomatic premenopausal women with uterine leiomyoma who underwent uterine artery embolization (UAE). Treatment was accompanied by MRI of both the volume of the entire uterus and the leiomyomas one month before and six months after UAE.[148] The radiological dimensions and volume of the leiomyoma and the uterus were both evaluated, and the number of leiomyoma fibroids and their location in the myometrium was classified.

PEMF has been approved by FDA for the treatment of non-union fractures, neurogenic bladder, and musculoskeletal pains. PEMF demonstrated a positive effect on the reduction of neuropathic pain from carpal tunnel syndrome. Substantial evidence exists that time-varying magnetic fields produce biological effects by safely inducing extremely low-frequency electrical currents within the tissues. Data showed that by directing PEMF to the carpal tunnel region, neuropathic pain was significantly reduced.[44]

The role of PEMF has also been explored for the reduction of post-operative pain due to the modulation of inflammation in patients with bone bruise on the knee. In this study, PEMF is being investigated to reduce the size of the bone bruise area, improving the level of knee function and the amount of anti-inflammatory drugs used in the aforementioned patients in the postoperative period, compared to a control group.[149]

Static magnetic fields are also being considered for biomedical applications. An ongoing study is focused in determine the effects of static magnetic fields produced by a small magnet on peripheral pulses and skin blood flow. A specific neodymium magnet and sham device will be placed on specific sites near the ulnar and medial arteries, and the effect of such placement on peripheral pulses will be assessed via Photoplethysmography (PPG) on fingers and on skin blood flow via laser Doppler perfusion will be determined.[150]

By combining stem cells with electromagnetic stimulation, the magnetism can also act for the treatment of several conditions. Sildenafil is a vasoactive drug used in erectile dysfunction that normally decreases optic nerve head blood flow and promotes neuroinflammation and could lead to permanent vision loss. Wharton's jelly derived mesenchymal stem cells (WJ-MSC) can increase

mitochondrial ATP synthesis with paracrine effects and suppress neuroinflammation with immunomodulatory effects. Repetitive electromagnetic stimulation (rEMS) can rearrange ion channel balances and axoplasmic flow. The combination of WJ-MSC and rEMS was then explored for the therapy of toxic optic neuropathies.[151]

Table II.1: Clinical trials involving the application of magnetic field in TE field.

Clinical Trial	Condition	Treatment	Phase	Status
Dermal Profile Analysis Using the NMR-MOUSE	Hypotension During Dialysis Disturbance; Balance, Fluid	Dermal nuclear magnetic resonance (NMR)-profile measurement	-	Terminated[147]
Predictive Factors of Pelvic Magnetic Resonance in the Response of Arterial Embolization of Uterine Leiomyoma	Uterine Leiomyoma	Magnetic Resonance Image	-	Completed[148]
Short and Long Term Exposure to Unique, Time-Varying Pulsed Electro-Magnetic Fields in Refractory Carpal Tunnel Syndrome	Refractory Carpal Tunnel Syndrome Neuropathic Pain Neuromodulation	Reduction of pain scores by magnetic energy	Phase 4	Completed[44]
Evaluation of the Effect of Biophysical Stimulation With Pulsed Electromagnetic Fields on Intraspongious Bone Edema in Anterior Cruciate Ligament Reconstruction	ACL Injury Pain	Specific pulsed electromagnetic fields	-	Recruiting[149]
Assessing Impacts of Static Magnetic Fields on Peripheral Pulses and Skin Blood Flow	Peripheral Arterial Disease Arterial Stiffness	Magnet and sham	-	Recruiting[150]
Therapy of Toxic Optic Neuropathy Via Combination of Stem Cells With Electromagnetic Stimulation	Toxic optic neuropathies	Stem Cells With Electromagnetic Stimulation	Phase 3	Completed[151]

7. Conclusions

The advances in TE during the last decades have enabled the fabrication of tissues with structural and compositional accuracy. However, functional recapitulation of their native counterparts poses a major challenge toward TE clinical translation. Emerging approaches that address this challenge include the new generation of "smart" materials due to its precise and selective response under external signals or the surrounding environment. Among them, tremendous progress has been achieved using MNPs, with ones being included in cells and scaffolds, and/or acting as magnetic carriers of drugs and biomolecules. Hence, functional 3D tissues can be fabricated by Mag-TE, using these magnetized units as building blocks. Other competences, such as the influence on cell behavior, can also be supported by Mag-TE, affecting the adhesion, proliferation and differentiation of the cells. Smart drug delivery systems can also be developed, controlling the release of drugs and growth factors by a remote magnetic field. Concerning the *in vivo* implantation, the tissues produced *in vitro* can be easily transplanted and fixed in the injury site by the action of an external magnetic field.

Scaffold-free Mag-TE strategy has showed remarkable outcomes in the fabrication of functional tissue constructs. Due to the high initial cell density in this approach, the time for tissue formation is dramatically reduced and the proliferation and migration of cells are not crucial parameters. Moreover, the strong deposition of ECM in these constructs assures the development of very cohesive structures, enabling the creation of cell-based assemblies with complex architectures, mimicking the native tissue environment. Generally, small tissue building blocks such as CSs, spheroids and tissue strands, are engineered and then, by bottom-up strategy, complex tissues and organoids are obtained by controlled assembly of heterogeneous building blocks consisting of different cell types. Howbeit, concerns like the immobilization time necessary for the initial fusion of these building blocks or the inferior mechanical properties are restricting its application. Such problematic is disclosed by scaffold-based strategies, where scaffolds act as cell protectors during the tissue formation. Moreover, the mechanical behavior of the tissues can be easily adjusted by changing the scaffolds' constituents. Nevertheless, the superior mechanical properties of these materials can have dramatic effects on cell adhesion, migration and spreading, leading to non-homogenous structures, and compromising the tissue function.

Pondering an ideal scenario for TE, we envisage the fusion of scaffold-based and scaffold-free approaches, usually seen as rivals, into a synergetic TE strategy.

Briefly, the integration of different technologies and materials into one operational strategy, together with the ability to modulate the materials' properties (either chemically, physically or in terms of biodegradability), will permit the development of elevated living structures through bottom-up approaches, enabling the construction of complex functional tissues with relevant physiological architecture for clinical applications.

Additionally, we believe that a rapid clinical acceptance is strongly correlated with the ability to define a universal strategy whereby only modulating the scaffolds' properties, one could be further extended to several cell and tissue types without considerable modifications in the assembly process. In this regard, it is anticipated that such synergy will accelerate the in situ tissue assembly benefiting from the development of improved living materials designed to meet the patient needs. Further association of this concept with the magnetic field could provide additional control over the tissue formation with tunable tissue size, shape, and architecture, contributing to the development of functional tissues that more closely recapitulate the native environment, as described throughout the literature. The intrinsic magnetism also offers the advantage of easy manipulation, transplantation, and monitoring of the tissues along the time, prompting its application to the clinical practice.

This new concept might represent an optimal solution capable of addressing a wide range of current TE challenges, offering numerous opportunities for overcome their individual bottlenecks and develop new solutions based on their added value. Yet, the application of MNPs needs further translational studies to attest the MNPs' efficacy and advantages, in order to elevate their potential on TE and regenerative medicine. Hence, to further advance this big idea it is essential to have the corporation of biologists, materials scientists, engineers, products designers, and medical doctors to further push the boundaries of what can be accomplished in the field and help to develop relevant clinical solutions.

Acknowledgements

We acknowledge the project CICECO-Aveiro Institute of Materials, UIDB/50011/2020 & UIDP/50011/2020, financed by national funds through the FCT/MEC and when appropriate co-financed by FEDER under the PT2020 Partnership. The authors also acknowledge financial support by FCT through a Ph.D. grant (SFRH/BD/141523/2018, Lúcia F. Santos) and through the individual contract (CEECIND/2020.04344, A. Sofia. Silva).

References

1. Gumbiner, B. M. Cell adhesion: the molecular basis of tissue architecture and morphogenesis. *Cell* **84,** 345–57 (1996).

2. da Silva, R. M. P., Mano, J. F. & Reis, R. L. Smart thermoresponsive coatings and surfaces for tissue engineering: switching cell-material boundaries. *Trends Biotechnol* **25,** 577–583 (2007).
3. Stuart, M. A. C. *et al.* Emerging applications of stimuli-responsive polymer materials. *Nat Mater* **9,** 101–113 (2010).
4. Dobson, J. Remote control of cellular behaviour with magnetic nanoparticles. *Nat Nanotechnol* **3,** 139–143 (2008).
5. Pankhurst, Q. A., Connolly, J., Jones, S. K. & Dobson, J. Applications of magnetic nanoparticles in biomedicine. *J Phys D Appl Phys* **36,** R167–R181 (2003).
6. Ito, A. *et al.* Tissue Engineering Using Magnetite Nanoparticles and Magnetic Force: Heterotypic Layers of Cocultured Hepatocytes and Endothelial Cells. *Tissue Eng* **10,** 833–840 (2004).
7. Berry, C. C. & Curtis, A. S. G. Functionalisation of magnetic nanoparticles for applications in biomedicine. *J Phys D Appl Phys* **36,** R198–R206 (2003).
8. O'Brien, F. J. Biomaterials & scaffolds for tissue engineering. *Materials Today* **14,** 88–95 (2011).
9. Lu, T., Li, Y. & Chen, T. Techniques for fabrication and construction of three-dimensional scaffolds for tissue engineering. *International Journal of Nanomedicine* **8,** 337–350 (2013).
10. Chan, G. & Mooney, D. J. New materials for tissue engineering: towards greater control over the biological response. *Trends Biotechnol* **26,** 382–392 (2008).
11. Correia, C. R. *et al.* Chitosan scaffolds containing hyaluronic acid for cartilage tissue engineering. *Tissue Eng Part C Methods* **17,** 717–730 (2011).
12. Kong, J., Hwang, I.-W. & Lee, K. Top-Down Approach for Nanophase Reconstruction in Bulk Heterojunction Solar Cells. *Advanced Materials* **26,** 6275–6283 (2014).
13. Jayakumar, R., Prabaharan, M., Nair, S. v. & Tamura, H. Novel chitin and chitosan nanofibers in biomedical applications. *Biotechnology Advances* **28,** 142–150 (2010).
14. Santo, V. E. *et al.* Enhancement of osteogenic differentiation of human adipose derived stem cells by the controlled release of platelet lysates from hybrid scaffolds produced by supercritical fluid foaming. *Journal of Controlled Release* **162,** 19–27 (2012).
15. Bhowmick, S. *et al.* Biomimetic electrospun scaffolds from main extracellular matrix components for skin tissue engineering application – The role of chondroitin sulfate and sulfated hyaluronan. *Materials Science and Engineering C* **79,** 15–22 (2017).
16. Parmar, P. A. *et al.* Collagen-mimetic peptide-modifiable hydrogels for articular cartilage regeneration. *Biomaterials* **54,** 213–225 (2015).
17. Elbert, D. L. Bottom-up tissue engineering. *Curr Opin Biotechnol* **22,** 674–680 (2011).
18. Rivron, N. C. *et al.* Tissue assembly and organization: Developmental mechanisms in microfabricated tissues. *Biomaterials* **30,** 4851–4858 (2009).
19. Liu, J. S. & Gartner, Z. J. Directing the assembly of spatially organized multicomponent tissues from the bottom up. *Trends in Cell Biology* **22,** 683–691 (2012).
20. Doberenz, F., Zeng, K., Willems, C., Zhang, K. & Groth, T. Thermoresponsive polymers and their biomedical application in tissue engineering – a review. *J Mater Chem B* **8,** 607–628 (2020).
21. Yang, J. *et al.* Cell sheet engineering: Recreating tissues without biodegradable scaffolds. *Biomaterials* **26,** 6415–6422 (2005).

22. Rahmi, G. *et al.* Designing 3D Mesenchymal Stem Cell Sheets Merging Magnetic and Fluorescent Features: When Cell Sheet Technology Meets Image-Guided Cell Therapy. *Theranostics* **6,** 739 (2016).
23. Kim, I. Y. *et al.* Thermoreversible behavior of κ-carrageenan and its apatite-forming ability in simulated body fluid. *Materials Science and Engineering: C* **31,** 1472–1476 (2011).
24. Tang, H., Zhao, W., Yu, J., Li, Y. & Zhao, C. Recent development of pH-responsive polymers for cancer nanomedicine. *Molecules* **24,** 4 (2019).
25. Guillaume-Gentil, O. *et al.* PH-controlled recovery of placenta-derived mesenchymal stem cell sheets. *Biomaterials* **32,** 4376–4384 (2011).
26. Ryan, C. N. M., Doulgkeroglou, M. N. & Zeugolis, D. I. Electric field stimulation for tissue engineering applications. *BMC Biomedical Engineering* **3,** 1–9 (2021).
27. Koons, G. L., Diba, M. & Mikos, A. G. Materials design for bone-tissue engineering. *Nature Reviews Materials* **5,** 584–603 (2020).
28. Patel, N. G., Zhang, G., Patel, N. G. & Zhang, G. Responsive systems for cell sheet detachment Responsive systems for cell sheet detachment. *Organogenesis* **9,** 93–100 (2013).
29. Borges, J., Rodrigues, L. C., Reis, R. L. & Mano, J. F. Layer-by-Layer Assembly of Light-Responsive Polymeric Multilayer Systems. *Advanced Functional Materials* **24,** 5624-5648 (2014).
30. Municoy, S. *et al.* Stimuli-Responsive Materials for Tissue Engineering and Drug Delivery. *International Journal of Molecular Sciences* **21,** 4724 (2020).
31. Yu, L. *et al.* Photoregulating Antifouling and Bioadhesion Functional Coating Surface Based on Spiropyran. *Chemistry – A European Journal* **24,** 7742–7748 (2018).
32. Zhu, Y., Cheng, Z., Weng, W. & Cheng, K. A facile synthesis of polydopamine/TiO2 composite films for cell sheet harvest application. *Colloids Surf B Biointerfaces* **172,** 355–361 (2018).
33. Nguyen, K. T. & West, J. L. Photopolymerizable hydrogels for tissue engineering applications. *Biomaterials* **23,** 4307–4314 (2002).
34. Baroli, B. Photopolymerization of biomaterials: issues and potentialities in drug delivery, tissue engineering, and cell encapsulation applications. *Journal of Chemical Technology & Biotechnology* **81,** 491–499 (2006).
35. Williams, C. G., Malik, A. N., Kim, T. K., Manson, P. N. & Elisseeff, J. H. Variable cytocompatibility of six cell lines with photoinitiators used for polymerizing hydrogels and cell encapsulation. *Biomaterials* **26,** 1211–1218 (2005).
36. Corchero, J. L. & Villaverde, A. Biomedical applications of distally controlled magnetic nanoparticles. *Trends in Biotechnology* **27,** 468–476 (2009).
37. Gil, S. & Mano, J. F. Magnetic composite biomaterials for tissue engineering. *Biomater Sci* **2,** 812–818 (2014).
38. Lee, E. A. *et al.* Application of magnetic nanoparticle for controlled tissue assembly and tissue engineering. *Arch Pharm Res* **37,** 120–128 (2014).
39. Ito, A. & Kamihira, M. Tissue Engineering Using Magnetite Nanoparticles. *Prog Mol Biol Transl Sci* **104,** 355–395 (2011).
40. Xu, H., Othman, S. F. & Magin, R. L. Monitoring Tissue Engineering Using Magnetic Resonance Imaging. *J Biosci Bioeng* **106,** 515–527 (2008).

41. Belpomme, D., Hardell, L., Belyaev, I., Burgio, E. & Carpenter, D. O. Thermal and non-thermal health effects of low intensity non-ionizing radiation: An international perspective. *Environmental Pollution* **242,** 643–658 (2018).
42. Helmchen, F. & Denk, W. Deep tissue two-photon microscopy. *Nature Methods* **2,** 932–940 (2005).
43. Thévenot, J., Oliveira, H., Sandre, O. & Lecommandoux, S. Magnetic responsive polymer composite materials. *Chem. Soc. Rev* **42,** 7099 (2013).
44. ClinicalTrials.gov. Short and Long Term Exposure to Unique, Time-Varying Pulsed Electro-Magnetic Fields in Refractory Carpal Tunnel Syndrome . (2006). Available at: https://clinicaltrials.gov/ct2/show/NCT00277563?cond=Short+and+Long+Term+Exposure+to+Unique%2C+Time-Varying+Pulsed+Electro-Magnetic+Fields+in+Refractory+Carpal+Tunnel+Syndrome&draw=2&rank=1. (Accessed: 26th July 2022)
45. Zhang, X., Le, T. A. & Yoon, J. Development of a real time imaging-based guidance system of magnetic nanoparticles for targeted drug delivery. *J Magn Magn Mater* **427,** 345–351 (2017).
46. Li, Y. *et al.* Magnetic Hydrogels and Their Potential Biomedical Applications. *Adv Funct Mater* **23,** 660–672 (2013).
47. Polyak, B. *et al.* High field gradient targeting of magnetic nanoparticle-loaded endothelial cells to the surfaces of steel stents. *Proceedings of the National Academy of Sciences* **105,** 698–703 (2008).
48. Xia, Y. *et al.* Magnetic field and nano-scaffolds with stem cells to enhance bone regeneration. *Biomaterials* **183,** 151–170 (2018).
49. Wang, Y. *et al.* Tough Magnetic Chitosan Hydrogel Nanocomposites for Remotely Stimulated Drug Release. *Biomacromolecules* **19,** 3351–3360 (2018).
50. Ino, K., Okochi, M. & Honda, H. Application of magnetic force-based cell patterning for controlling cell–cell interactions in angiogenesis. *Biotechnol Bioeng* **102,** 882–890 (2009).
51. Goranov, V. *et al.* 3D Patterning of cells in Magnetic Scaffolds for Tissue Engineering. *Sci Rep* **10,** 2289 (2020).
52. Okochi, M. *et al.* Three-dimensional cell culture array using magnetic force-based cell patterning for analysis of invasive capacity of BALB/3T3/ v-src. *Lab Chip* **9,** 3378–3384 (2009).
53. Whatley, B. R., Li, X., Zhang, N. & Wen, X. Magnetic-directed patterning of cell spheroids. *Journal of biomedical materials research Part A* **102,** 1537-1547 (2013).
54. Akiyama, H., Ito, A., Kawabe, Y. & Kamihira, M. Fabrication of complex three-dimensional tissue architectures using a magnetic force-based cell patterning technique. *Biomedical microdevices* **11,** 713-721 (2009).
55. Neto, A. I. *et al.* Fabrication of Hydrogel Particles of Defined Shapes Using Superhydrophobic-Hydrophilic Micropatterns. *Advanced Materials* **28,** 7613–7619 (2016).
56. Santos, L. F., Patrício, S. G., Silva, A. S. & Mano, J. F. Freestanding Magnetic Microtissues for Tissue Engineering Applications. *Adv Healthc Mater* **11,** 2101532 (2022).
57. Kotecha, M., Magin, R. & Mao, J. Magnetic resonance imaging in tissue engineering. *John Wiley & Sons* (2017).

58. Hutmacher, D. W., Sittinger, M. & Risbud, M. v. Scaffold-based tissue engineering: Rationale for computer-aided design and solid free-form fabrication systems. *Trends in Biotechnology* **22,** 354–362 (2004).
59. Causa, F., Netti, P. A. & Ambrosio, L. A multi-functional scaffold for tissue regeneration: The need to engineer a tissue analogue. *Biomaterials* **28,** 5093–5099 (2007).
60. Hutmacher, D. W. & Cool, S. Concepts of scaffold-based tissue engineering—the rationale to use solid free-form fabrication techniques. *J Cell Mol Med* **11,** 654–669 (2007).
61. Baier Leach, J., Bivens, K. A., Patrick Jr., C. W. & Schmidt, C. E. Photocrosslinked hyaluronic acid hydrogels: Natural, biodegradable tissue engineering scaffolds. *Biotechnol Bioeng* **82,** 578–589 (2003).
62. Place, E. S., George, J. H., Williams, C. K. & Stevens, M. M. Synthetic polymer scaffolds for tissue engineering. *Chemical Society Reviews* **38,** 1139–1151 (2009).
63. Ruiz-Hitzky, E., Aranda, P., Darder, M. & Rytwo, G. Hybrid materials based on clays for environmental and biomedical applications. *J Mater Chem* **20,** 9306–9321 (2010).
64. Badylak, S. F. The extracellular matrix as a biologic scaffold material. *Biomaterials* **28,** 3587–3593 (2007).
65. Nelson, C. M. & Bissell, M. J. Of Extracellular Matrix, Scaffolds, and Signaling: Tissue Architecture Regulates Development, Homeostasis, and Cancer. *Annu Rev Cell Dev Biol* **22,** 287–309 (2006).
66. Khademhosseini, A. & Langer, R. Microengineered hydrogels for tissue engineering. *Biomaterials* **28,** 5087–5092 (2007).
67. Drury, J. L. & Mooney, D. J. Hydrogels for tissue engineering: Scaffold design variables and applications. *Biomaterials* **24,** 4337–4351 (2003).
68. Dang, T. T. *et al.* Microfabrication of homogenous, asymmetric cell-laden hydrogel capsules. *Biomaterials* **30,** 6896–6902 (2009).
69. Correia, C. R., Nadine, S. & Mano, J. F. Cell Encapsulation Systems Toward Modular Tissue Regeneration: From Immunoisolation to Multifunctional Devices. *Adv Funct Mater* **30,** 1908061 (2020).
70. Williams, D. F. On the mechanisms of biocompatibility. *Biomaterials* **29,** 2941–2953 (2008).
71. Pardo, A. *et al.* Magnetic Nanocomposite Hydrogels for Tissue Engineering: Design Concepts and Remote Actuation Strategies to Control Cell Fate. *ACS nano* **15,** 175-209 (2021).
72. Kilian Weiss, C. *et al.* Article 124 (2020) Recent Advances on Magnetic Sensitive Hydrogels in Tissue Engineering. *Front. Chem* **8,** 124 (2020).
73. Namdari, M. & Eatemadi, A. Cardioprotective effects of curcumin-loaded magnetic hydrogel nanocomposite (nanocurcumin) against doxorubicin-induced cardiac toxicity in rat cardiomyocyte cell lines. *Artif Cells Nanomed Biotechnol* **45,** 731–739 (2016).
74. Thompson, R. E. *et al.* Effect of hyaluronic acid hydrogels containing astrocyte-derived extracellular matrix and/or V2a interneurons on histologic outcomes following spinal cord injury. *Biomaterials* **162,** 208–223 (2018).
75. Liu, Z. *et al.* Recent Advances on Magnetic Sensitive Hydrogels in Tissue Engineering. *Front Chem* **8,** 124 (2020).
76. Huang, J. *et al.* Development of Magnetic Nanocomposite Hydrogel with Potential Cartilage Tissue Engineering. *ACS omega* **3,** 6182-6189. (2018).

77. Zhang, N., Lock, J., Sallee, A. & Liu, H. Magnetic Nanocomposite Hydrogel for Potential Cartilage Tissue Engineering: Synthesis, Characterization, and Cytocompatibility with Bone Marrow Derived Mesenchymal Stem Cells. *ACS Appl Mater Interfaces* **7,** 20987–20998 (2015).
78. Bonhome-Espinosa, A. B. *et al.* In vitro characterization of a novel magnetic fibrin-agarose hydrogel for cartilage tissue engineering. *J Mech Behav Biomed Mater* **104,** 103619 (2020).
79. Farzaneh, S. *et al.* Fabrication and characterization of cobalt ferrite magnetic hydrogel combined with static magnetic field as a potential bio-composite for bone tissue engineering. *J Drug Deliv Sci Technol* **64,** 102525 (2021).
80. Henstock, J. R. *et al.* Remotely Activated Mechanotransduction via Magnetic Nanoparticles Promotes Mineralization Synergistically With Bone Morphogenetic Protein 2: Applications for Injectable Cell Therapy. *Stem Cells Transl Med* **3,** 1363–1374 (2014).
81. Liu, W. *et al.* Magnetically controllable 3D microtissues based on magnetic microcryogels. *Lab Chip* **14,** 2614–2625 (2014).
82. Norotte, C., Marga, F. S., Niklason, L. E. & Forgacs, G. Scaffold-free vascular tissue engineering using bioprinting. *Biomaterials* **30,** 5910–5917 (2009).
83. Syed-Picard, F. N. *et al.* Scaffold-free tissue engineering of functional corneal stromal tissue. *J Tissue Eng Regen Med* **12,** 59–69 (2018).
84. Atala, A., Kurtis Kasper, F. & Mikos, A. G. Engineering complex tissues. *Sci Transl Med* **4,** 1–12 (2012).
85. DuRaine, G. D., Brown, W. E., Hu, J. C. & Athanasiou, K. A. Emergence of Scaffold-Free Approaches for Tissue Engineering Musculoskeletal Cartilages. *Ann Biomed Eng* **43,** 543–554 (2015).
86. Correia, C. R., Bjørge, I. M., Nadine, S. & Mano, J. F. Minimalist Tissue Engineering Approaches Using Low Material-Based Bioengineered Systems. *Adv Healthc Mater* **10,** 2002110 (2021).
87. Haraguchi, Y., Shimizu, T., Yamato, M. & Okano, T. Scaffold-free tissue engineering using cell sheet technology. *RSC Adv* **2,** 2184–2190 (2012).
88. Pampaloni, F., Reynaud, E. G. & Stelzer, E. H. K. The third dimension bridges the gap between cell culture and live tissue. *Nature Reviews Molecular Cell Biology* **8,** 839–845 (2007).
89. Fennema, E., Rivron, N., Rouwkema, J., van Blitterswijk, C. & de Boer, J. Spheroid culture as a tool for creating 3D complex tissues. *Trends in Biotechnology* **31,** 108–115 (2013).
90. Laschke, M. W. & Menger, M. D. Spheroids as vascularization units: From angiogenesis research to tissue engineering applications. *Biotechnology Advances* **35,** 782–791 (2017).
91. Wang, W. *et al.* 3D spheroid culture system on micropatterned substrates for improved differentiation efficiency of multipotent mesenchymal stem cells. *Biomaterials* **30,** 2705–2715 (2009).
92. Ho, V. H. B., Müller, K. H., Barcza, A., Chen, R. & Slater, N. K. H. Generation and manipulation of magnetic multicellular spheroids. *Biomaterials* **31,** 3095–3102 (2010).
93. Kim, J. A. *et al.* High-throughput generation of spheroids using magnetic nanoparticles for three-dimensional cell culture. *Biomaterials* **34,** 8555–8563 (2013).

94. Yoon, S., Kim, J. A., Lee, S. H., Kim, M. & Park, T. H. Droplet-based microfluidic system to form and separate multicellular spheroids using magnetic nanoparticles. *Lab Chip* **13,** 1522–1528 (2013).
95. Mattix, B. *et al.* Biological magnetic cellular spheroids as building blocks for tissue engineering. *Acta Biomater* **10,** 623–629 (2014).
96. Mattix, B. M. *et al.* Janus magnetic cellular spheroids for vascular tissue engineering. *Biomaterials* **35,** 949–960 (2014).
97. Morin, K. T. & Tranquillo, R. T. Guided sprouting from endothelial spheroids in fibrin gels aligned by magnetic fields and cell-induced gel compaction. *Biomaterials* **32,** 6111–6118 (2011).
98. Perez, J. E., Nagle, I. & Wilhelm, C. Magnetic molding of tumor spheroids: emerging model for cancer screening. *Biofabrication* **13,** 015018 (2020).
99. Bowser, D. A. & Moore, M. J. Biofabrication of neural microphysiological systems using magnetic spheroid bioprinting. *Biofabrication* **12,** 015002 (2019).
100. Whatley, B. R., Li, X., Zhang, N. & Wen, X. Magnetic-directed patterning of cell spheroids. *J Biomed Mater Res A* **102,** 1537–1547 (2014).
101. Yang, J. *et al.* Reconstruction of functional tissues with cell sheet engineering. *Biomaterials* **28,** 5033–5043 (2007).
102. Moschouris, K., Firoozi, N. & Kang, Y. The application of cell sheet engineering in the vascularization of tissue regeneration. *Regenerative Med* **11,** 559–570 (2016).
103. Sekine, W., Haraguchi, Y., Shimizu, T., Umezawa, A. & Okano, T. Thickness limitation and cell viability of multi-layered cell sheets and overcoming the diffusion limit by a porous-membrane culture insert. *Biochips & Tissue chips* **1,** 1–9 (2011).
104. Ito, A., Jitsunobu, H., Kawabe, Y. & Kamihira, M. Construction of Heterotypic Cell Sheets by Magnetic Force-Based 3-D Coculture of HepG2 and NIH3T3 Cells. *J Biosci Bioeng* **104,** 371–378 (2007).
105. LI, M., MA, J. U. N., GAO, Y. & YANG, L. E. I. Cell sheet technology: a promising strategy in regenerative medicine. *Cytotherapy* **21,** 3–16 (2019).
106. Matsuda, N., Shimizu, T., Yamato, M. & Okano, T. Tissue engineering based on cell sheet technology. *Advanced Materials* **19,** 3089–3099 (2007).
107. Yamato, M. & Okano, T. Cell sheet engineering. *Materials Today* **7,** 42–47 (2004).
108. Hong, S., Young, B. & Changmo, J. Multilayered Engineered Tissue Sheets for Vascularized Tissue Regeneration. *Tissue Eng Regen Med* **14,** 371–381 (2017).
109. Castro, E. & Mano, J. F. Magnetic Force-Based Tissue Engineering and Regenerative Medicine. *J Biomed Nanotechnol* **9,** 1129–1136 (2013).
110. Silva, A. S., Santos, L. F., Mendes, M. C. & Mano, J. F. Multi-layer pre-vascularized magnetic cell sheets for bone regeneration. *Biomaterials* **231,** 119664 (2020).
111. Ito, A. *et al.* Construction and delivery of tissue-engineered human retinal pigment epithelial cell sheets, using magnetite nanoparticles and magnetic force. *Tissue Eng* **11,** 489–496 (2005).
112. Ito, A. *et al.* Construction and Harvest of Multilayered Keratinocyte Sheets Using Magnetite Nanoparticles and Magnetic Force. *Tissue Eng* **10,** 873–880 (2004).
113. Ito, A. *et al.* Novel Methodology for Fabrication of Tissue-Engineered Tubular Constructs Using Magnetite Nanoparticles and Magnetic Force. *https://home.liebertpub.com/ten* **11,** 1553–1561 (2005).
114. Shimizu, K. *et al.* Bone tissue engineering with human mesenchymal stem cell sheets constructed using magnetite nanoparticles and magnetic force. *J Biomed Mater Res B Appl Biomater* **82B,** 471–480 (2007).

115. Akiyama, H., Ito, A., Kawabe, Y. & Kamihira, M. Biomaterials Genetically engineered angiogenic cell sheets using magnetic force-based gene delivery and tissue fabrication techniques. *Biomaterials* **31,** 1251–1259 (2010).
116. Ishii, M. *et al.* Enhanced angiogenesis by transplantation of mesenchymal stem cell sheet created by a novel magnetic tissue engineering method. *Arterioscler Thromb Vasc Biol* **31,** 2210–2215 (2011).
117. Ito, A., Ino, K., Kobayashi, T. & Honda, H. The effect of RGD peptide-conjugated magnetite cationic liposomes on cell growth and cell sheet harvesting. *Biomaterials* **26,** 6185–6193 (2005).
118. Gil, S., Correia, C. R. & Mano, J. F. Magnetically labeled cells with surface-modified Fe3O4 spherical and rod-shaped magnetic nanoparticles for tissue engineering applications. *Adv Healthc Mater* **4,** 883–891 (2015).
119. Gonçalves, A. I., Rodrigues, M. T. & Gomes, M. E. Tissue-engineered magnetic cell sheet patches for advanced strategies in tendon regeneration. *Acta Biomater* **63,** 110–122 (2017).
120. Santos, L. F., Sofia Silva, A. & Mano, J. F. Complex-shaped magnetic 3D cell-based structures for tissue engineering. *Acta Biomater* **118,** 18–31 (2020).
121. Zhou, S. *et al.* Labeling adipose derived stem cell sheet by ultrasmall super-paramagnetic Fe3O4 nanoparticles and magnetic resonance tracking in vivo. *Scientific Reports* **7,** 1–12 (2017).
122. Owaki, T., Shimizu, T., Yamato, M. & Okano, T. Cell sheet engineering for regenerative medicine: Current challenges and strategies. *Biotechnol J* **9,** 904–914 (2014).
123. Asakawa, N. *et al.* Pre-vascularization of in vitro three-dimensional tissues created by cell sheet engineering. *Biomaterials* **31,** 3903–3909 (2010).
124. Kito, T. *et al.* iPS cell sheets created by a novel magnetite tissue engineering method for reparative angiogenesis. *Sci Rep* **3,** 1418 (2013).
125. Matos, A. M., Gonçalves, A. I., el Haj, A. J. & Gomes, M. E. Magnetic biomaterials and nano-instructive tools as mediators of tendon mechanotransduction. *Nanoscale Adv* **2,** 140–148 (2020).
126. Wu, C. *et al.* Recent Advances in Magnetic-Nanomaterial-Based Mechanotransduction for Cell Fate Regulation. *Advanced Materials* **30,** 1705673. (2018).
127. Abdeen, A. A., Lee, J., Bharadwaj, N. A., Ewoldt, R. H. & Kilian, K. A. Temporal Modulation of Stem Cell Activity Using Magnetoactive Hydrogels. *Adv Healthc Mater* **5,** 2536–2544 (2016).
128. Filippi, M. *et al.* Magnetic nanocomposite hydrogels and static magnetic field stimulate the osteoblastic and vasculogenic profile of adipose-derived cells. *Biomaterials* **223,** 119468 (2019).
129. Zeng, X. B. *et al.* Magnetic responsive hydroxyapatite composite scaffolds construction for bone defect reparation. *Int J Nanomedicine* **7,** 3365–3378 (2012).
130. Rampino, A. *et al.* Impact of Magnetic Stimulation on Periodontal Ligament Stem Cells. *International Journal of Molecular Sciences* **23,** 188 (2021).
131. Nikukar, H. *et al.* Osteogenesis of Mesenchymal Stem Cells by Nanoscale Mechanotransduction. *ACS nano* **7,** 2758-2767. (2013).
132. Safavi, A. S., Sendera, A., Haghighipour, N. & Banas-Zabczyk, A. The Role of Low-Frequency Electromagnetic Fields on Mesenchymal Stem Cells Differentiation: A

Systematic Review. *Tissue Eng Regen Med* 1–14 (2022). doi:10.1007/S13770-022-00473-1/FIGURES/4

133. Mert, T. *et al.* Pulsed Magnetic Field EnhancesTherapeutic Efficiency of Mesenchymal Stem Cells in Chronic Neuropathic Pain Model. *Bioelectromagnetics* **38,** 255–264 (2017).
134. Gehwolf, R. *et al.* Global Responses of Il-1β-Primed 3D Tendon Constructs to Treatment with Pulsed Electromagnetic Fields. *Cells* **8,** 399 (2019).
135. Petecchia, L. *et al.* Electro-magnetic field promotes osteogenic differentiation of BM-hMSCs through a selective action on Ca 2+-related mechanisms. *Scientific reports* **5,** 1-13. (2015).
136. Liu, H. *et al.* Repetitive Magnetic Stimulation Promotes Neural Stem Cells Proliferation by Upregulating MiR-106b In Vitro. *J Huazhong Univ Sci Technol* **35,** 766-772 (2015).
137. Liu, G. *et al.* The effect of magnetic stimulation on differentiation of human induced pluripotent stem cells into neuron. *J Cell Biochem* **121,** 4130–4141 (2020).
138. Henstock, J. & Haj, A. el. Controlled mechanotransduction in therapeutic MSCs: Can remotely controlled magnetic nanoparticles regenerate bones? *Regenerative Med* **10,** 377–380 (2015).
139. Guven, S. *et al.* Multiscale assembly for tissue engineering and regenerative medicine. *Trends Biotechnol* **33,** 269–279 (2015).
140. Rahman, A., Majewski, P. W., Doerk, G., Black, C. T. & Yager, K. G. Non-native three-dimensional block copolymer morphologies. *Nat Commun* **7,** 1–8 (2016).
141. Guo, W. M., Loh, X. J., Tan, E. Y., Loo, J. S. C. & Ho, V. H. B. Development of a magnetic 3D spheroid platform with potential application for high-throughput drug screening. *Mol Pharm* **11,** 2182–2189 (2014).
142. Penland, N., Choi, E., Perla, M., Park, J. & Kim, D. H. Facile fabrication of tissue-engineered constructs using nanopatterned cell sheets and magnetic levitation. *Nanotechnology* **28,** 075103 (2017).
143. Leung, C. M. *et al.* A guide to the organ-on-a-chip. *Nature Reviews Methods Primers* **2,** 1–29 (2022).
144. ClinicalTrials.gov. Available at: https://clinicaltrials.gov/ct2/results?cond=tissue+engineering&term=&cntry=&state=&city=&dist=. (Accessed: 22nd January 2023)
145. Billings, C., Langley, M., Warrington, G., Mashali, F. & Johnson, J. A. Magnetic Particle Imaging: Current and Future Applications, Magnetic Nanoparticle Synthesis Methods and Safety Measures. *International Journal of Molecular Sciences 2021, Vol. 22, Page 7651* **22,** 7651 (2021).
146. Lartigue, L. *et al.* Biodegradation of iron oxide nanocubes: High-resolution in situ monitoring. *ACS Nano* **7,** 3939–3952 (2013).
147. ClinicalTrials.Gov. Dermal Profile Analysis Using the NMR-MOUSE. (2016). Available at: https://clinicaltrials.gov/ct2/show/NCT02934009?cond=Dermal+Profile+Analysis+Using+the+NMR-MOUSE&draw=2&rank=1. (Accessed: 26th July 2022)
148. ClinicalTrials.gov. Predictive Factors of Pelvic Magnetic Resonance in the Response of Arterial Embolization of Uterine Leiomyoma . (2011). Available at: https://clinicaltrials.gov/ct2/show/NCT01468402?cond=Predictive+Factors+of+Pelvic+Magnetic+Resonance+in+the+Response+of+Arterial+Embolization+of+Uterine+Leiomyoma&draw=2&rank=1. (Accessed: 26th July 2022)

149. ClinicalTrials.Gov. Effect of Biophysical Stimulation on Intraspongious Bone Edema in Anterior Cruciate Ligament Reconstruction . (2020). Available at: https://clinicaltrials.gov/ct2/show/NCT04255407?cond=Evaluation+of+the+Effect+of+Biophysical+Stimulation+With+Pulsed+Electromagnetic+Fields+on+Intraspongious+Bone+Edema+in+Anterior+Cruciate+Ligament+Reconstruction&draw=2&rank=1. (Accessed: 26th July 2022)
150. ClinicalTrials.Gov. Assessing Impacts of Static Magnetic Fields on Peripheral Pulses and Skin Blood Flow. (2020). Available at: https://clinicaltrials.gov/ct2/show/NCT04539704?cond=Assessing+Impacts+of+Static+Magnetic+Fields+on+Peripheral+Pulses+and+Skin+Blood+Flow&draw=2&rank=1. (Accessed: 26th July 2022)
151. ClinicalTrials.Gov. Therapy of Toxic Optic Neuropathy Via Combination of Stem Cells With Electromagnetic Stimulation. (2021). Available at: https://clinicaltrials.gov/ct2/show/NCT04877067?cond=Therapy+of+Toxic+Optic+Neuropathy+Via+Combination+of+Stem+Cells+With+Electromagnetic+Stimulation&draw=2&rank=1. (Accessed: 26th July 2022)

2

Materials & Methods

Chapter III

Experimental methodologies and materials

Chapter III - Experimental methodologies and materials

This chapter summarises the experimental methodologies applied in **Chapters III through VI**, as well as the reasons for their selection. In the experimental subsection of each chapter, the materials and corresponding commercial distributors can be found, as well as the experimental procedures and equipment suppliers.

1. Fabrication of cell sheets by magnetic tissue engineering

Scaffold-free TE has emerged as a powerful strategy using multicellular building blocks, including spheroids, tissue strands and CSs to fabricate larger cohesive tissue constructs and produce ECM, essential for naturally developing their tissue architecture.[1],[2] Particularly, CS engineering has been widely explored due to its ability to fabricate functional, complex and robust tissues.[3] Such approach allows to keep the natural networks of tissues without breaking them, through the harvesting of entire sheet-like cells, guarantying the maintenance of cell–cell and cell–ECM interactions. Conventional TE strategies face several obstacles to clinical translation, namely the lack of tissue substitutes with suitable mechanical behaviour, appropriate approaches to recapitulate physiological architectures, and the inefficient cell growth, cell stimulation and consequently, proper tissue response. At the forefront of nanotechnology, MNPs have shown promise in solving current TE challenges. In the last decades, MNPs have been increasingly investigated owing to their promising potentials in biomedical applications, including TE.[4],[5] Aspiring the creation of functional tissues replacements, magnetic tissue engineering (Mag-TE) arose as an alternative to conventional strategies, permitting the fabrication and monitoring of tissues produced *in vitro*. The intrinsic properties of MNPs empower their application for the engineering of tissue constructs with high control of size, architecture and extremely guided assembling based on the control of cells' positioning.

1.1. Production of supermagnetic iron oxide nanoparticles and its characterization

MNPs were synthesized based on the previously published procedure.[6] Briefly, magnetite (Fe_3O_4) nanoparticles - MNPs were synthesized by the co-precipitation reaction of ferrous ($FeCl_2{\cdot}4H_2O$) and ferric ($FeCl_3{\cdot}6H_2O$) salts in the presence of ammonium hydroxide (NH_4OH), at 60 °C and under a nitrogen atmosphere. Afterwards, MNPs' surface was modified with (3-aminopropyl)triethoxysilane (APTES) through a silanization reaction and then washed with deionized water and ethanol. Consequently, MNPs-APTES were conjugated with rhodamine B isothiocyanate (RodB) (MNPs-RodB). MNPs-APTES (previously freeze dried) were dispersed in

ethanol (5 mg/mL) and then RodB (2.5 mg/mL) was added and stirred overnight at RT. Lastly, MNPs-RodB were washed until no traces of RodB were detected by fluorescent microscopy and freeze dried. MNPs, MNPs-APTES and MNPs-RodB were visualized by TEM at 20kV, which were previously added dropwise to a carbon film copper grid. The images were analyzed by Image J software. The successful modification of the particles with APTES was confirmed by attenuated total reflectance (ATR-FTIR). The spectra were recorded at a 4 cm^{-1} resolution with a total of 256 scans in the spectral width of 4000–350 cm^{-1}.

The stability of RhodB-MNPs was investigated by scanning the fluorescence of RhodB on cell culture medium and (phosphate-buffered saline) PBS (pH=7.4). Briefly, the samples were immersed and subsequently stirred in a shaking water bath at 60 rpm and 37°C. After 1, 3, 7, 14 and 21 days, the fluorescence spectrum was peaked at an excitation wavelength of 556 nm and 627 nm of emission using a spectrofluorometer.

1.2. Cell sources

1.2.1. Cell lines

The commercially available pre-osteoblast cell line (MC3T3-E1) was used in **Chapter IV**. MC3T3 are derived from Mus musculus (mouse) calvaria, being widely used as model cell source in bone biology. In fact, MC3T3-E1 present similar behaviour to primary osteoblasts and are already anticipated to exhibit osteogenic markers.[7] In this sense, the osteogenic potential of MC3T3 was explored in **Chapter IV**.

1.2.2. Commercially available primary cells

Adipose-derived mesenchymal stem cells (ASCs) were purchased from commercial suppliers. ASCs were used in **Chapter IV and V** due to their numerous appealing features for TE, including self-renewal capacity, multilineage differentiation potential, and availability in large quantities with diminutive donor site morbidity or patient discomfort.[8]

1.2.3. Cells isolated from adipose tissue

Later, our group started to isolate human adipose-derived stem cells (hASCs) from adipose tissue. The advantage of employing isolated cells relies on the capacity to create personalized cell therapies, while avoiding the creation of more biological waste. Moreover, autologous cells are attractive for TE strategies because it avoids a graft-versus-host immune response. As so, hASCs were used in **Chapter VI and VII**. The collected tissues were obtained under a cooperation agreement between CICECO–Aveiro Institute of Materials, University of Aveiro and Hospital da

Luz (Aveiro, Portugal), after approval of the Competent Ethics Committee (CEC). The human tissues received were handled in accordance with the guidelines approved by the CEC. Informed consent was obtained from all subjects. Subcutaneous adipose tissue from liposuction procedures was used to isolate hASCs. Briefly, samples were transported in PBS supplemented with 10% (v/v) penicillin-streptomycin and kept at 4 °C. The lipoaspirates were washed with PBS and incubated with collagenase type II (0.05% w/v) for 45 min at 37 °C in a shaking water bath. The digested samples were filtered (200 µm) and centrifuged at 800 g for 10 min at 4 °C. The obtained stromal vascular fraction (SVF) was resuspended in erythrocyte lysis buffer at pH 7.4 containing ammonium chloride (155×10^{-3} m), potassium bicarbonate (5.7×10^{-3} m), and ethylenediaminetetraacetic acid (0.1 m, EDTA) in distilled water. After 10 min of incubation at room temperature (RT), the mixture was centrifuged at 300 g for 5 min. To isolate the hASCs the red blood cell-free SVF was resuspended in α-MEM medium (Invitrogen) supplemented with fetal bovine serum (10%, FBS, Invitrogen) and penicillin-streptomycin (1% v/v). Culture medium was changed 48 h after initial plating and then every 3–4 days.

1.2.4. Cells isolated from umbilical cord

The collected umbilical cord was obtained under a cooperation agreement between the Aveiro Institute of Materials, University of Aveiro and Hospital do Baixo Vouga (Aveiro, Portugal), after approval of the Competent Ethics Committee (CEC). The human tissues received were handled in accordance with the guidelines approved by the CEC. Informed consent was obtained from all subjects. HUVECs were isolated following well-established protocols in the group. The enzymatic mixture containing dispase II (Sigma-Aldrich) and collagenase type IV (Sigma-Aldrich) was used for the isolation of HUVECs from cord vein. Afterwards, the cord vein was filled with the enzyme cocktail and incubated at 37 °C for 20 min_2 at 37 °C. At the end of 4–6 h, the medium was changed to M199 containing 20% umbilical cord blood serum (UCBS), 2 mM l-glutamine, 5 ng/mL vascular endothelial growth factor, 10 µg/mL heparin, 100 U/mL penicillin and 100 µg/mL streptomycin.[9][10]

HUVECs were explored in **Chapter V** in combination with ASCs. Several works reported that the synergetic interaction of these cells' phenotypes boost both osteo- and angiogenesis in *in vitro* systems.[11] **In Chapter V,** HUVECs were used to attempt pre-vascularized tissues and promote the osteogenic differentiation of the ASCs.

1.3. Cellular uptake of MNPs

Aiming the production of magnetized cells, the co-location of MNPs was visualized for all cell phenotypes (**Chapters IV and V**). Firstly, cells were seeded at density of 2.4×10^6 cells/cm^2 in 8-well cell culture slides and cultured for 24 h at 37°C and 5% CO_2 in a humidified atmosphere, followed by a 4 h incubation with RhodB-MNPs at 1 mg/mL. Lastly, cells were washed with PBS and subsequently fixed in formalin 10% (v/v) at RT during 15 min. After the incubation of the cells with Triton X100 (0.1% (v/v), in dPBS) during 5 min at RT, the cells were incubated with Flash Phalloidin Green 488 (1:100 in dPBS) at RT for 45 min and then counterstaining with DAPI (1:1000 in dPBS) for 5 min at RT. Finally, the cells were visualized by fluorescence microscopy. In **Chapter V**, the particles' uptake was also quantified. After the incubation of cells with RhodB-MNPs during 4h, cells were retrieved by enzymatic digestion with trypLE™ Express. The cell suspension of HUVECs was immunostained with APC anti-human CD31 Antibody (5 µL), whereas the cell suspension of ASCs was immunostained with APC anti-human CD90 Antibody (5 µL) for 45 min. Both samples were washed with a staining washing buffer (2% w/v BSA, 0.1% w/v sodium citrate in dPBS) and centrifuged at 500 g for 5 min, followed by a resuspension in the acquisition buffer (1% v/v formaldehyde and 0.1% w/v sodium azide in dPBS). The double positive cells for the pair CD31 and MNPs-RodB, and the pair CD90 and MNPs-RodB were sorted using a Cell Sorter.

1.4. Fabrication of the magnetized tissues

1.4.1. Shaped magnetic tissues at macroscale

Initially, the cells were seeded at the cell density of 2.4×10^6/cm^2 and cultured during 24 h at 37°C and 5% CO_2 in a humidified atmosphere, followed by a 4 h incubation with RhodB MNPs (1 mg/mL). Later, the cells were harvested using TrypLE™ Express solution at 37°C for 5 min and centrifuged at 300 g. In order to obtain magnetic tissues with flat and circular shapes, the

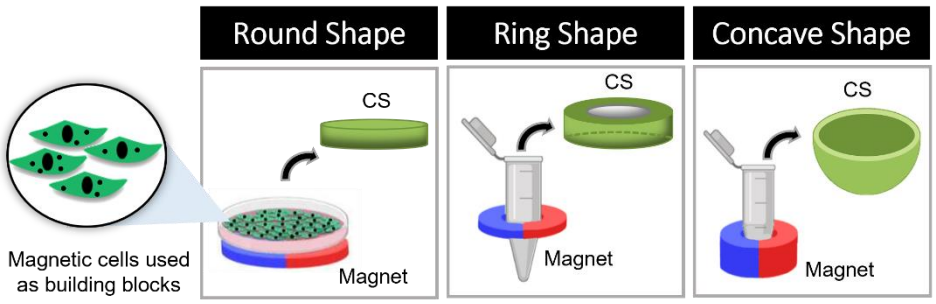

Scheme III.1: Schematic representation of the fabrication of magnetic tissues at macroscale namely round, ring and concave shape. After the successfully MNPs' internalization within cells environment, robust tissues were obtained by forcing the cell-cell interactions in the presence of a magnetic field.

magnetically labelled cells were transferred to ultralow-attachment 24, 48 or 96-well plates, previously treated with alginate (2% w/v) for 30 min. The circular tissues were explored from **Chapter IV to VII**. To provide magnetic force, commercial neodymium rod magnets (strength of 108N and standard N41 magnetization) were placed at the bottom of the reverse side of the ultralow-attachment plate. The ability to create more complex structures was investigated through the fabrication of magnetic tissues with diverse shapes based on the type of magnet, substrate and cell density. For the purpose, commercial neodymium magnets with ring and concave shapes (strength of 73.5 N and standard N42 magnetization) were used. Briefly, the magnetically labelled cells (MC3T3-E1 cell line) were transferred to an Eppendorf and then the magnets were placed around (ring shape) and at the bottom of (concave shape) the Eppendorf.

1.4.2. Hierarchical and stratified magnetic tissues

The ability to produce stratified and hierarchical tissue constructs was investigated in **Chapters IV and V**. Firstly, heterotypic magnetic tissues were produced in a double conformation (**Chapter IV**). Similar to the section *1.4.1.,* MC3T3-E1 were seeded at the cell density of $2.4 \times 10^6/cm^2$ and cultured during 24 h at 37°C and 5% CO_2 in a humidified atmosphere, followed by a 4 h incubation with MNPs (1 mg/mL). Then, the magnetized cells were transferred to ultralow-attachment 24, 48 or 96-well plates. After 24 h, the second cell phenotypic (ASCs) was added to the homotypic circular MC3T3-E1 CS, that was previously assembled. In **Chapter V**, we demonstrated the ability to produce more stratified and hierarchical structures with a final structure with a triple sheet conformation. After the seeding of magnetically labelled ASCs at the cell density of $2.4 \times 10^6/cm^2$ and their culture during 24h, the magnetically labelled HUVECs

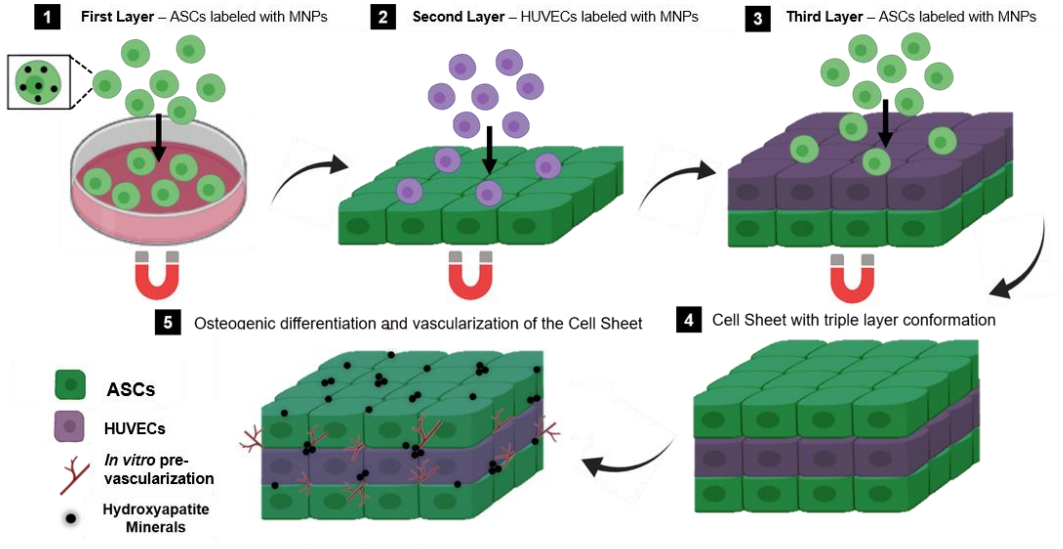

Scheme III.2: Schematic representation of the fabrication hierarchical tissue constructs in triple layer conformation composed by ASCs and HUVECs.

were added at a density of 1.2 × 10^6 cells/cm^2 on top of the previously established ASCs monolayer. Lastly, 2.4 × 10^6 cells/cm^2 of magnetic labelled ASCs were added (24 h after HUVECs magnetic deposition).

1.4.3. Shaped magnetic tissues at microscale

1.4.3.1. Production of Superhydrophobic Surfaces Patterned with Wettable Superhydrophilic Domains

After confirming the ability to produce robust magnetic CSs at the macroscale, we investigated the fabrication of magnetic microtissues. During the design of tissues *in vitro*, the engineered structures should preferentially recapitulate aspects of the architecture of the tissue microenvironment from the microscopic to macroscopic dimension levels, consistent with the hierarchical organization of biological systems.[12] By mimicking such native microstructural functional units with microarchitectural features, the emerging of modular TE aims to create more biomimetic engineered tissues, providing more guidance on the cellular level to direct tissue morphogenesis.

Based on this knowledge, we explored the fabrication of these small units by Mag-TE, using a promising high-throughput platform. The dimension and shape of the cellular construct were both controlled by the photomask design.[13]

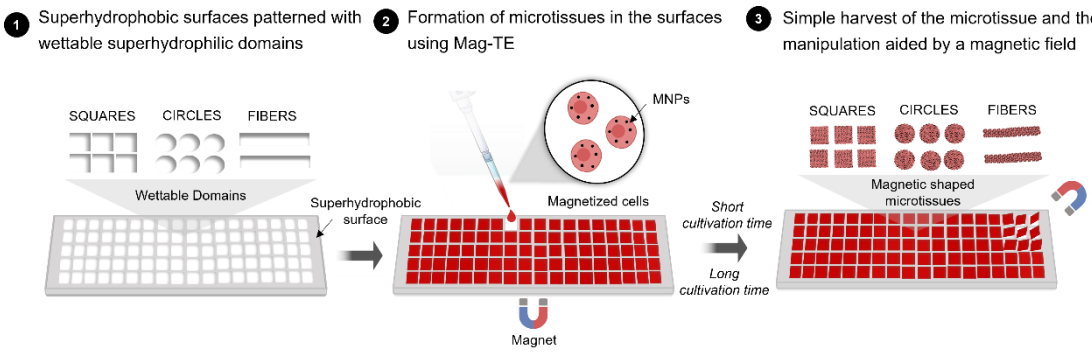

Scheme III.3: Illustration of the fabrication of micro-scale shaped magnetic tissues using a superhydrophobic platform with wettable domains. Circle, squares and fiber-like shape tissues were obtained by taking advantage of the wafer design.

Superhydrophobic surfaces (SH) patterned with wettable superhydrophilic (SL) domains were produced as reported in literature[14] Briefly, glass microscope slides were activated by immersion in 1 m sodium hydroxide (NaOH) for 1 h, followed by neutralization in 1 m hydrochloric acid (HCl) for 30 min. After activation, the glass slides were modified with 20% v/v solution of 3-(trimethoxysilyl)propyl methacrylate in ethanol for 30 min at RT. Afterward, activated glass slides were placed in a vacuumed desiccator (50 mbar, 3–5 h) under

trichloro(1H,1H,2H,2H-perfluorooctyl)silane atmosphere. Then, to create a thin polymer layer over the fluorinated glass slide, a polymerization mixture solution was prepared with 2-hydroxyethyl methacrylate (24 wt%, HEMA, Sigma-Aldrich), ethylene dimethacrylate (16 wt%, EDMA), 1-decanol (12 wt%) cyclohexanol (48 wt%), and 2,2-dimethoxy-2-phenylacetophenone (0.4 wt%, DMPA). To define the thickness of the polymer layer, two 12.5 µm thin strips of aluminum foil were applied on the corners of a fluorinated glass slide. Subsequently, the polymerization solution was applied over the fluorinated glass slide and a methacrylated glass slide was clamped on top of it. The polymerization was performed under 264 nm of UV radiation for 15 min and with 12 mW/cm^2 of intensity. After ethanol washing and nitrogen stream drying, the polymer layer was modified with 4-pentynoic acid via standard esterification. The esterification solution was prepared using dichloromethane (45 mL), 4-(dimethylamino)pyridine (56 mg), pentynoic acid (111.6 mg), and of N,N'-diisopropylcarbodiimine (180 µL), in continuous stirring for 4 h at RT. Ultimately, SH patterns with specific geometries were obtained by applying 5% v/v solution of 1H,1H,2H,2H-perfluorodecanethiol (PFDT) in acetone onto the polymer surface, followed by UV irradiation (264 nm) through a quartz photomask at 12 mW/cm^2 for 1 min. The remaining alkyne groups were subjected to a thiolyne reaction with 2-mercaptoethanol (10% v/v) under 264 nm of UV radiation for 15 min and with 12 mW/cm^2 of intensity, originating the formation of SL areas.

1.4.3.2. Development of Freestanding Microtissues through Mag-TE

The freestanding magnetic tissues at microscale were fabricated as described in the previous sections. hASCs were seeded at the cell density of 2.4 × 10^6 per cm^2 and incubated during 24 h at 37 °C and 5% CO_2 in a humidified atmosphere. Then, the cells were incubated with MNPs (1 mg/mL) for 4 h. Afterward, cells were detached by adding trypLE^{TM} Express during 5 min at 37 °C. After the centrifugation of the cells at 300 g, the magnetically labelled cells were transferred to the wettable SL domains of the SH surfaces, previously treated with 2% (w/v) alginate solution during 30 min at 37 °C to produce the magnetic microtissues. For the purpose, commercial neodymium block magnets 40 × 20 × 5 mm (strength of 137 N and standard N42 magnetization) were placed at the bottom of the micropatterned surfaces to provide magnetic force.

2. Magnetic stimulation of the produced tissue constructs

After the fabrication of the magnetized tissues, the influence of the magnetic field on cell behavior was also investigated in **Chapter VII**. MNPs attached on cellular membrane act as stress generators, which can be thus mechanically conditioned by magnetic remote actuation. Several works have shown that by incorporating MNPs in cells or scaffolds, the magnetic field can provide necessary cues to stimulate cells' differentiation. Regarding this information, we explored the use of a cyclic magnetic field (CMF) to stimulate the differentiation of magnetic tissues previously formed.[15] The produced magnetic tissues were collected from the 96-well ultralow-attachment plates after 7 days of culture, with the aid of a magnet and transferred to a mold containing the same volume of culturing medium. Then, for dynamic condition, the samples were subjected to a CMF (13mT, 14 s^{-1}) – see **Scheme III.4**. The magnetic field was measured by a hall effect magnetic field sensor. In control, the magnets were removed from the 96-well ultralow-attachment plates, and then the samples were strategically placed far from the magnetic field.

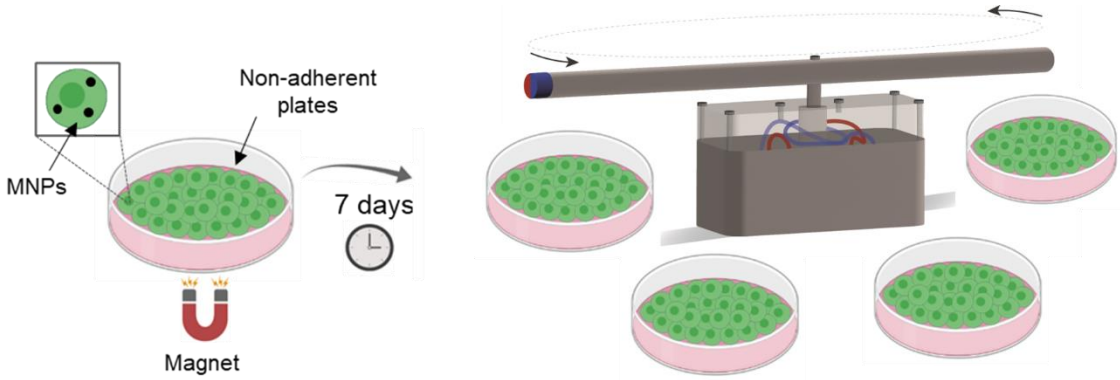

Scheme III.4: Representative image of the formation of magnetic tissues by Mag-TE during 7 days and their stimulation by a CMF magnetic field.

2.1. Magnetic characterization of the produced tissues

2.1.1. Iron content

The total iron (mass) in magnetic tissues was determined for both conditions after 7, 14 and 21 days by Inductively Coupled Plasma Optical Emission Spectrometry ICP-OES. For each measurement, the magnetic tissues (10 mg) were dried at 37°C, overnight. Then, 1 mL of nitric acid HNO_3 was added to each sample for the microwave acid digestion.

2.1.2. Magnetization of the produced tissues

The magnetic characterization of the produced magnetic tissues was performed using a Quantum Design MPMS3 SQUID magnetometer. Magnetizations versus applied magnetic field

curves were obtained at 300K. The magnetic moment measurements were performed using a 1 mm SQUID-VSM amplitude and a 30 mm DC-scan length.[16] For this purpose, magnetic tissues were dried at 37 °C during 24 h and then, the dried materials were used for each measurement, normalizing the obtained magnetization values by the mass of the magnetic tissues.

2.1.3. Magnetic mapping of the proposed apparatus

The computer simulation of the magnetic fields generated by the opposite-sided magnets setup was performed using the pcolormesh() function in pyplot module of matplotlib library. For this, the magnetostatic field was determined for each position, using an gaussmeter.

3. *In vitro* biological performance of the magnetic tissues

3.1. Cell viability

The long-term cell survival was accessed in the cell-based tissue constructs after predetermined culturing times. The viability assay is based on calcein-AM and ethidium homodimer-1dyes to distinguish between living and dead cells. Living cells are stained with green, fluorescent calcein-AM, which detects intracellular esterase activity. Dead cells are penetrated with red-fluorescent ethidium homodimer-1, indicating the loss of plasma membrane integrity. Concisely, the magnetic tissues were stained with calcein-AM (1 mg/mL, 1:500 in dPBS) and propidium iodide (PI) (1 mg/mL, 1:1000 in dPBS). After the incubation at 37°C during 15 min, protected from light, the samples were immediately washed with dPBS and visualized by fluorescence microscopy.

3.2. Metabolic activity

For **Chapters IV-VII**, mitochondrial metabolic activity was determined at predetermined time-points using a 3-(4,5-dimethylthiazol-2-yl)-5-(3-carboxymethoxyphenyl)-2-(4- sulphofenyl)-2H-tetrazolium) (MTS) colorimetric assay (CellTiter96 AQueous one solution cell proliferation assay) according to the manufacturer's recommendations. The method is based on the reduction of the tetrazolium compound by metabolically active cells into coloured brown formazan. Briefly, the samples were incubated protected from light with the reagent kit for 4 h at 37 °C in a humidified 5% CO_2 air atmosphere. The absorbance was read at a wavelength of 490 nm using a microplate reader.

3.3. Cell proliferation

The ability of magnetic cells to proliferate in CSs conformation was accessed at predetermined timepoints via double-stranded (ds) DNA quantification by Quant-iT™ Picogreen™ assay

(**Chapters IV-VII**). To promote the cell lysis, the samples were firstly incubated with 2% (v/v) of Triton-X (in ultra-pure water) 1 h at 37 °C. The DNA quantification was performed according to the manufacturer's specifications. Fluorescence was read at an excitation wavelength of 485/20 nm and 528/20 nm of emission using a microplate reader.

3.4. Morphological characterization

The morphology of the produced tissues was analysed in **Chapters IV-VII**, namely tissues' thickness, architecture and robustness. After the fixation in 4% w/v formaldehyde, the samples were dehydrated in increasing ethanol series and fixed in graphite stubs. At the end, the samples were carbon sputter-coated and visualized by SEM at accelerating voltage of 15 kV.

The cell distribution in layered-tissue constructs was accessed by the staining of the different cell phenotypes. Prior to tissue fabrication, cells were stained with 3,3'-dioctadecyloxacarbocyanine perchlorate (DiO – green, 1 mM) and 1,1'-dioctadecyl-3,3,3',3'-tetramethylindodicarbocyanine, 4-chlorobenzenesulfonate salt (DiD – purple or red, 1 mM). In **Chapter IV**, ASCs were stained with DiD and MC3T3-E1 with DiO. In **Chapter V**, ASCs were stained with DiO and HUVECs with DiD. For **Chapter VI**, the lipophilic dyes DiO and DiD were used to identify different tissue units. For both scenarios, cells were detached by trypsin-EDTA treatment for 5 min at 37 °C, and subsequently centrifuged at 300 g for 5 min. Afterwards, cells were counted and resuspended in each dye solution diluted in PBS (1 mL of PBS containing 5 µL of dye per $1x10^6$ cells) for 10 min at 37 °C protected from light. Lastly, the samples were fixed in 4% w/v formaldehyde and counterstained with DAPI (1:1000 in PBS, 1 mg/mL) for 5 min at 37°C. The tissues constructs were visualized by confocal laser scanning microscopy (CLSM).

The cell organization and tissue robustness were also accessed using the DAPI-Phalloidin fluorescence assay. DAPI (4',6-diamidino-2-phenylindole) is a blue-fluorescent DNA stain that binds to adenine-thymine regions in DNA and is extensively used to detect nuclei. Phalloidin is a bicyclic peptide with a high affinity for actin filaments. The samples were fixed in 4% w/v formaldehyde for 1 h at RT. Then, samples were permeabilized with 0.1% v/v Triton-X in dPBS for 5 min at RT, followed by incubation in Flash Phalloidin Red 594 (300 U, 1:40 in PBS) for 45 min at RT protected from light. Cells' nuclei were counterstained with DAPI (1:1000 in dPBS) for 5 min at RT protected from light. Finally, the samples were visualized by fluorescence microscopy. Such information was analysed in **Chapters IV to VI.**

3.5. Mechanical characterization

Scaffold-free strategy is normally associated to tissue constructs with low mechanical performance. Of course, tissue engineered constructs should resemble the *in vivo* mechanical

properties of the native tissues to assure their functionality.[17] Based on this, in **Chapter IV** we attested the strength and the robustness of the produced magnetic tissues by the tensile mechanical test. Magnetic tissues produced with ring shape were firstly cut to display a ribbon-like conformation and then the samples were clamped in the tensile testing machine. Tensile testes were carried out with a gauge length of 3 mm and a loading speed of 1 mm min^{-1}. For each sample, the load versus cross-head displacement data from initial until rupture load was measured using a PC data acquisition system connected to the tester. Resulting stress-strain curves allowed to determine the ultimate tensile strength (UTS), elongation at break, and Young's modulus of the produced magnetic microtissues.

3.6. Osteogenic potential

The osteogenic potential of the produced magnetic tissues was investigated by using different strategies. In **Chapters IV and V**, we explored the role of specific and targeted cell phenotypes on inducing the osteogenic differentiation of stem cells. For this, we cultured the magnetic tissues in basal medium or in the presence of osteogenic factors. In **Chapter VII**, we investigated the role of the magnetic field on stimulating the osteogenic differentiation of previously formed magnetic tissues.

3.6.1. ALP activity

The osteogenic differentiation of stem cells can be accessed by quantifying the enzymatic activity of alkaline phosphatase (ALP). Bone ALP is an ectoenzyme localized on the cell membrane of osteoblasts and is responsible for the cleavage of pyrophosphate ions, responsible for the inhibition of hydroxyapatite crystals formation. Therefore, in **Chapters IV** and **V**, the ALP activity was determined using the p-nitrophenol assay. The method is based on the hydrolysis of colourless p-nitrophenyl phosphate by ALP, producing coloured p-nitrophenol (NPh). After each time point, the samples were lysed following the same procedure described in section 3.3 - *Cell proliferation*. 25 µL of each lysate sample was added to 75 µL of a freshly prepared 4-nitrophenyl phosphate (4NPhP) solution (2 mg/mL) in 1 M diethanolamine (DEA) buffer (pH 9.8, with 0.5×10^{-3} M $MgCl_2$). Samples were incubated in the dark at 37 °C for 45 min. Enzymatic activity was then quantified by UV–Vis at 405 nm. The value was normalized against the previously determined correspondent DNA concentration (µg/mL). A standard curve of 4NPh was used as reference (0, 15×10^{-6}, 30×10^{-6}, 50×10^{-6}, 75×10^{-6}, 95×10^{-6} M in DEA buffer).

3.6.2. Cytokines detection

The release of cytokines from the magnetic tissues to the culture medium was measured without destroying the samples. At different time points, the supernatants were stored at –80 °C until further use. The amounts of osteopontin, osteocalcin, vascular endothelial growth factor (VEGF), bone morphogenetic protein-2 (BMP-2), interleukin (IL)-6 and hepatocyte growth factor (HGF) were quantified using commercially available kits according to the manufacturer's specifications from **Chapters IV** to **VII**. In **Chapter VII**, the presence of cytokines, namely extracellular signal-regulated kinases (ERK1/2), total focal adhesion kinase (FAK) and FAK phosphorylation, was also analysed in cell pellets, . Upon a mechanical stimulus, such factors are normally upregulated and prompt the osteogenic differentiation of stem cells. To this end, cells pellets were extracted using cell extraction buffer and frozen at –80 °C. Afterwards, the cytokine release was quantified following the manufacturer's recommendations.

3.6.3. Osteopontin

Since osteopontin is a major bone marker with essential roles during the formation of bone tissue,[18] its expression was also corroborated by immunofluorescence detection. The presence of osteopontin was identified in **Chapters IV**, **V** and **VII**. Firstly, the samples were washed with dPBS and fixed in 4% w/v formaldehyde for 1 h at RT. Then, the magnetic tissues were incubated with 0.1% v/v Triton-X in dPBS for 5 min and non-specific binding was blocked by immersion in 5% v/v FBS (in dPBS) during 1 h at RT. Subsequently, the primary mouse anti-human osteopontin antibody (1:100 in 5% FBS/dPBS, Biolegend, Taper) was added to the samples. After 3 h, the magnetic tissues were incubated with the secondary anti-mouse Alexa Fluor 555 antibody (1:400 in 5 % FBS/dPBS) for 1 h in dark at RT. All samples were counterstained with Flash Phalloidin Green 488 (1:40 v/v in dPBS) for 45 min and DAPI (1:1000 v/v) for 5 min at RT, protected from light, and visualized by fluorescence microscopy.

3.6.4. Histology

3.6.4.1. Sample processing and embedding

Histological assessment of samples was performed in **Chapters IV to VII**. Initially, the samples were fixed in 4% w/v formaldehyde solution (in dPBS). Samples were routinely processed manually by initial dehydration in increasing ethanol series (70%, 80%, 95% and 100% v/v), followed by xylene and paraffin infiltration, and ultimately paraffin embedding. Histological sections of 5 µm thickness were cut using a microtome.

3.6.4.2. Immunohistochemistry

In preparation for immunohistochemistry, histological sections were routinely deparaffinized in xylene/ethanol series and hydrated in distilled water. When required, samples were subjected to antigen retrieval in 10 mM tri-sodium citrate dihydrate buffer with 0.05% v/v Tween-20 at pH 6, 100 °C for 20 minutes, and blocked in FBS (5% v/v in dPBS) for 1 h at RT.

Masson's Trichrome: Masson's Trichrome stains collagen, the main protein component of bone, identifying if a bone-like ECM, mostly rich in type I collagen, was deposited by the cells (**Chapters IV and V**). Histological sections were routinely deparaffinized in xylene/ethanol series and subsequently mordant in pre-heated Bouin's solution at 56°C for 15 min. Samples were stained in Weigert's Iron Hematoxylin solution for 5 min at RT and rinsed with water. Next, samples were stained in Biebrich Scarlet-Acid Fuchsin for 5 min at RT and rinsed with acetic acid (0.2% v/v, in water).

Afterwards, the tissues were stained in Phosphotungstic/Phosphomolybic Acid for 5 min, followed by staining in Aniline Blue solution for 5 min. Samples were placed in 1% v/v acetic acid in distilled water for 30 s, rinsed, dehydrated, cleared in xylene, and mounted with DPX mountant. Samples were visualised by optical microscopy.

Von Kossa: Von Kossa staining is employed to specifically stain mineralisation deposits, used along **Chapters IV and V** to identify hydroxyapatite in samples. Still, while amorphous calcium phosphate does tend to evolve towards microcrystalline hydroxyapatite, the most thermodynamically stable calcium phosphate phase, the presence of phosphate in a sample alone cannot be an indication of hydroxyapatite.[19] Von Kossa staining is hence a useful technique to be applied in combination with alternative hydroxyapatite-identifying methodologies. Samples were incubated in 5% w/v silver nitrate solution for 60 min with exposure to UV light and rinsed, followed by incubation in 5% w/v sodium thiosulfate solution for 3 min, rinsed, and incubated with Nuclear Fast Red solution for 5 min. Samples were rinsed, dehydrated, cleared in xylene, and mounted with DPX mountant. Samples were visualised by optical microscopy.

Collagen IV and Fibronectin: The fibronectin and collagen IV are crucial to the matrix assembly and formation of sheet-like ECM of multicellular tissues, respectively.[20] The presence of these factors was visualized by incubating the histological sections with Fibronectin monoclonal antibody (FN-3) Alexa Fluor 488 (1:100 in 5 % FBS/dPBS, Thermofisher) or rabbit anti-collagen IV antibody (1:400 in 5% FBS/dPBS, Abcam) during 3 h, RT. For collagen IV, the samples were

incubated with AlexaFluor 594 Donkey anti-rabbit (1:400 in 5 % FBS/dPBS, Invitrogen) during 1 h at RT.

CD44: The expression of CD44, a transmembrane glycoprotein involved in bone formation,[21] was investigated in **Chapter IV**. For that, the sections were incubated with FITC anti-human CD44 primary antibodies (1:200 in 5 % FBS/dPBS, Biolegend) 3 h, RT, protected from the light.

Lamin A: The presence of lamin A, a protein of the nuclear envelope that is required for normal bone turnover,[22] was also accessed in **Chapter IV** after 21 days of culture. Firstly, the samples were immersed in rabbit anti-Lamin A (1:200 in 5 % FBS/dPBS, Biolegend). After 3 h, the sections were incubated with Alexa Fluor 647-labeled chicken anti-rabbit (1:400 in 5 % FBS/dPBS, Invitrogen) during 1 h, at RT.

Osteocalcin: Osteocalcin is a protein secreted specifically by osteoblasts, being essential for the alignment of apatite crystals and bone strength.[23] The expression of osteocalcin was assessed in **Chapter IV**. The sections were incubated with mouse anti-osteocalcin (1:200 in 5 % FBS/dPBS, Biolegend) for 3 h at RT. Lastly, the samples were immersed in AlexaFluor 488 Goat anti- mouse (1:400 in 5 % FBS/dPBS, Invitrogen) 1 h, RT, protected from the light.

3.6.5. In vitro biomineralization

To attest the formation of bone-like tissue, the biomineralization of the tissue constructs was also investigated. For this, we have accessed the deposition of hydroxyapatite-like minerals on the magnetic tissues (**Chapter IV to VI**), since hydroxyapatite is chemically similar to the inorganic component of bone.[24] The mineralization of the tissues was accessed through energy dispersive X-ray spectroscopy (EDS) and an OsteoImage™ assay. For both methodologies, the samples were washed with dPBS and fixed in 4% w/v formaldehyde for 15 min. Then, for OsteoImage™ assay, the samples were permeabilized with 0.1% v/v Triton X (in dPBS) for 5 min. Fluorescent staining of hydroxyapatite was performed according to the manufacturer's specifications. Samples were counterstained with DAPI (1:1000 in PBS) for 5 min at RT and visualized by fluorescence microscopy. The chemical composition of the hydroxyapatite nodules was characterized by an EDS detector coupled to the SEM apparatus. The samples were prepared as described in the section *3.4. Morphological Characterization* for SEM analysis. The calcium (Ca) and phosphorus (P) peaks were determined by EDS spectra using Esprit software.

3.6.6. Microtomography

In **Chapter VII**, microtomography was performed in the magnetic tissues, in collaboration with Professor Håvard Haugen at the Institute of Clinical Dentistry, University of Oslo, Norway.

Microtomography is a useful technique for the acquisition of 2D projections and 3D rendering of samples, as well as the identification of zones with varying mass density due to differential X-ray absorption. After the fixation of the samples in 4% w/v formaldehyde solution, the magnetic tissues were stained with lead(II) acetate trihydrate solution in 2% w/v distilled water, which has been shown to enhance early mineralization in microCT images. Samples were washed in distilled water, immersed in the staining solution for 18 h and washed again in distilled water. Subsequently, dehydration in ethanol series (40%, 50%, 60%, and 70% v/v) was performed and samples were mounted in 70% v/v ethanol. Scans were performed with acquisition parameters set to 60 kV, 260 µA, rotation step of 0.29^{o} over 360^{o}, exposure time of 0.650 ms per projection and a frame-averaging of 2. The reconstruction of the virtual slices was performed with NRecon with a final voxel size of 0.7 µm. The 3D images were rendered using Dragonfly software.

3.6.7. Flow cytometry

The successful isolation of HUVECs from umbilical cord and hASCs from adipose tissue was determined by flow cytometry, **Chapters IV** and **VI**. For hASCs, the mesenchymal stem cell markers CD105, CD90 and CD73 were analysed and for HUVECs, the surface marker CD31 was evaluated. Flow cytometry was also performed in **Chapter VII** to evaluate the stemness in the developed magnetic microtissues using the stemness marker CD105.

For both scenarios, the cells were detached from the well-plate by adding TrypLE^{TM} Express solution during 5 min at 37 °C. Then, the samples were incubated with anti-human CD105-FITC antibody (5 µL of antibody per 1x10^{6} of cells, 1:20, BioLegend), anti-human CD31-APC (5 µL of antibody per 1x10^{6} of cells, 1:20, BioLegend), Alexa Fluor 647 anti-human CD90 (5 µL of antibody per 1x10^{6} of cells, 1:20, BioLegend) and anti-human CD73-PE (5 µL of antibody per 1x10^{6} of cells, 1:20, BioLegend) for 45 min, at 4°C protected from light. Samples were acquired on a flow cytometer.

3.6.8. Gene Expression

3.5.8.1. RNA extraction and cDNA production

The gene expression of magnetic microtissues was evaluated in **Chapter VII,** by investigating the role of magnetic field in stimulating the osteogenic differentiation for both *in vitro* and *in vivo* scenarios. The isolation of total RNA was performed using a commercially available column-based kit according to the manufacturer's specifications. At predetermined times, the samples were lysed with a lysis buffer containing 1% v/v of 2- mercaptoethanol and homogenized using the potter elvehjem tissue homogenizer. Afterwards, one volume of 70% (v/v) of ethanol was

added to each volume of cell homogenate, and then the mix was entirely transferred to a spin cartridge. After washing, the membrane-bounded RNA was eluted in RNase-free water and collected in single tubes. RNA quantity and purity were determined on a nanodrop spectrophotometer. Only samples with a 260/280 purity ratio higher than 2.0 were used for cDNA synthesis. The cDNA synthesis was performed using a SuperScript™ IV VILO™ Master Mix kit and the ProFlex™ 2 x 96-well PCR System. All samples were normalized (1 ng of RNA per µL of RNase-free water).

3.5.8.2. Quantitative reverse transcription polymerase chain reaction (qRT-PCR)

The expression of the adipogenic gene peroxisome proliferator-activated receptor gamma (PPARG) and bone-related genes VEGF, Runt-related transcription factor 2 (RUNX2) and collagen type I (COLA1A) was determined in the cDNA samples using a qRT-PCR reaction. The qRT-PCR was performed on a QuantStudioTM 3 RealTime PCR system with the TaqMan® Fast Advanced Master Mix and using TaqMan® gene expression assays (Table III.1.). Glyceraldehyde 3-phosphate dehydrogenase (GAPDH) was used as the endogenous housekeeping control. Amplification profiles were analysed with QuantStudio™ Design and Analysis Software. The relative expression levels of each gene in cells were normalized to the GAPDH gene using the 2-ΔΔCt method (Perkin-Elmer). Three independent experiments were performed.

Table III.1: Gene expression assays and assays IDs.

Gene Symbol	Assay ID
GADPH	Hs99999905_m1
VEGF	Hs00900055_m1
PPARG	Hs01115513_m1
RUNX2	Hs00231692_m1
COL1A1	Hs00164004_m1

3.7. *Angiogenic potential*

The angiogenic potential of the produced magnetic tissues was evaluated in **Chapter V**. By a chick chorioallantoic membrane (CAM) assay, we investigated the ability of these tissues to migrate into the host and integrate chick vasculature by accessing the number of new capillaries formed around the implantation area and the presence of human cells in the chicken vasculature.[25]

3.7.1. Implantation in chick chorioallantoic membrane (CAM) and neo-vessel quantification

The angiogenic potential of the magnetic tissues composed by hASCs and HUVECs – referred as heterotypic CSs - was evaluated using the chick embryo CAM assay. Fertilized chick (Gallus gallus) eggs were incubated horizontally at 37.8 °C in a humidified atmosphere and referred to as embryonic day. On day 3, 1.5–2 mL of albumin was removed to allow the detachment of the developing CAM and a square window was opened in the shell. This window was sealed with a transparent adhesive tape and the eggs returned to the incubator. On day 10, a 3 mm silicon ring was placed on top of the CAM and filled with magnetic tissues under sterile conditions. Basic fibroblast growth factor (bFGF) and PBS were used as positive and negative controls, respectively. Eggs were re-sealed and returned to the incubator for 4 days, being hydrated every day. Embryos were euthanized by adding fixative (2 mL) on top of the CAM, the ring was removed, and the CAM was excised. The inoculation area (CAM host controls and CAM with the magnetic tissue) was photographed *ex ovo* under a stereoscope. The number of new/recruited vessels (less than 20 µm diameter) growing radial towards the ring area was counted in a blind fashion. All experiments were carried out according to the European Directive 2010/63/EU and the national Decreto-Lei nº113/2013.

3.7.2. *Image analysis: quantification of the total number of vessels and junctions*

For a quantitative analysis of the total number of vessels and junctions, CAM images were treated using ImageJ software, by adapting a described methodology for vessel and capillary

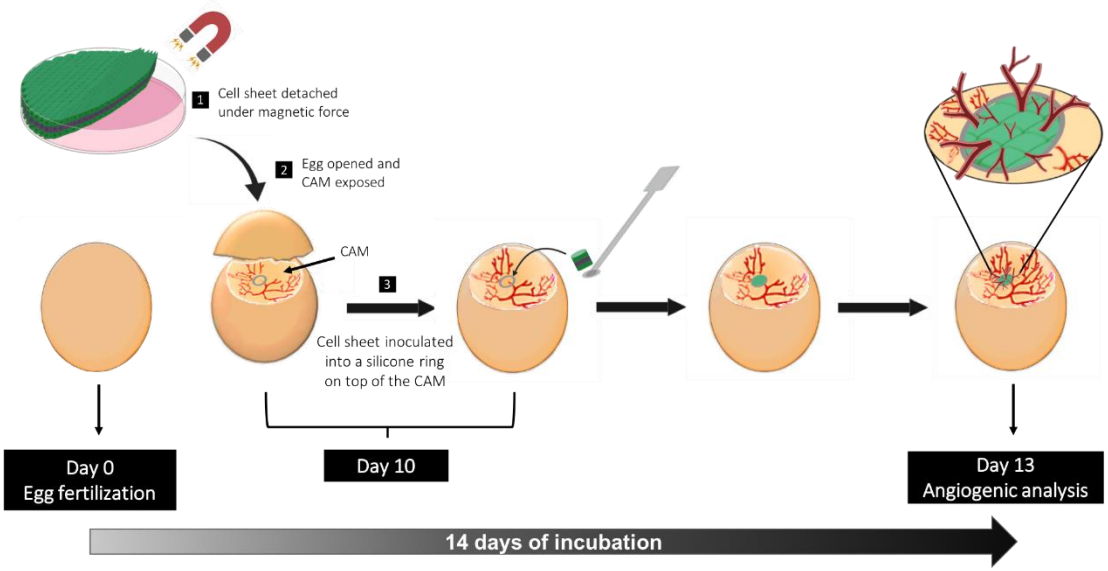

Scheme III.5: *In vivo* angiogenic potential of the produced magnetic tissues composed by hASCs and HUVECs. Schematic representation of the implementation of the tissues into the CAM.

skeletonization.[26] "FeatureJ Laplacian" plug-in was replaced by a "Mexican Hat" plug-in with a radius of 3, due to a greater adaptability to the samples, and a threshold of 1–130 was set prior to skeletonization (plug-in "Skeletonize 2D/3D"). Image skeletonization was restricted to the ROI. The number of junctions (vascular ramifications) and total number of vessels were calculated using the Image J plug-in "Analyse Skeleton 2D/3D".

3.7.3. Histological and immunohistochemical analysis of individual CSs and CAM with CS

Samples composed by the CAM and magnetic tissues were processed as described in section *3.5.4. Histology*. Sections were stained with haematoxylin and eosin (H&E) and the images were obtained using the Axio Imager M2 widefield microscope.

Expression of von Willebrand factor (VWF)/fibronectic (FN), collagen type IV/CD31, VWF/CD31 (all for CS) and VWF/human nuclei (HuNu) (for CAM with magnetic tissues) was probed after antigen recovery. Sections were incubated with rabbit anti-VWF (1:400 in 5% FBS/dPBS, Abcam) and FN monoclonal antibody (FN-3) Alexa Fluor 488 (1:100), with mouse anti-human CD31 (1:50 in 5% FBS/dPBS) and rabbit anti-collagen IV (1:400 in 5% FBS/dPBS), and mouse anti-human nuclei (1:400, Abcam) primary antibodies. This was followed by 1 h incubation with Alexa Fluor 647-labeled chicken anti-rabbit (1:400 in 5% FBS/dPBS) (VWF), AlexaFluor 488 Goat anti-mouse (1:400 in 5% FBS/dPBS) (CD31 and HuNu) and AlexaFluor 594-labeled donkey anti-rabbit (collagen IV). All sections were counterstained with DAPI. Control sections for each immunolabelling excluded primary antibody staining were performed. Images were obtained using a fluorescence inverted microscope (Zeiss).

4. *In vivo* performance of the magnetic tissues

After demonstrating the positive effect of the magnetic field in the in vitro osteogenic differentiation, we explored such phenomenon in a more complex in vivo animal model. For this purpose, magnetic tissues were produced as described in *section 2*, and placed under a RMF with similar magnetic parameters - 8-13mT, 14 s^{-1}.

All animal experiments were performed at the Universidade de Trás-os-montes e Alto Douro (UTAD) animal facility, under the reference 0421/000/000/2022. The work performed with animals was reviewed by the internal animal ethics committee and submitted to the competent authority (Direção-Geral da Alimentação e Veterinária - DGAV) for approval. Male nude mice were anesthetized using isoflurane anaesthesia with a controlled vaporizer. Heating pads were used during the whole procedure to maintain the animals' temperature. Surgical asepsis was performed using iodine and alcohol solutions alternately. The surgical procedure consisted of

one incision at the cervical dorsal area where the magnetic tissues were subcutaneously inserted by creating a small dissection tunnel. All the magnetic tissues had around 6mm of diameter and identical cell density. Each incision was closed using 5–0 polyglycolic acid suture lines. Lastly, 6 samples per condition per time point (4 and 6 weeks) were subjected to the magnetic field. As control, the same number of animals with subcutaneous implantation were kept without the

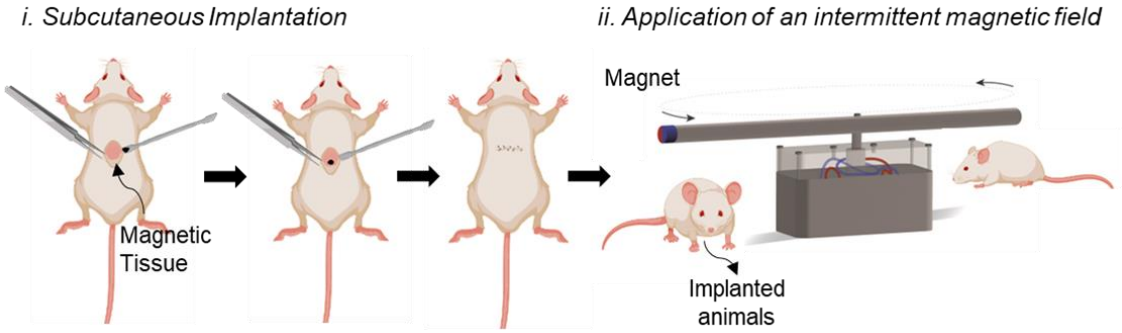

Scheme III.6: Representation of the *in vivo* procedure. The magnetic tissues were implanted subcutaneously and then, the implanted animals were subject to an RMF during 4 and 6 weeks.

presence of the magnetic stimulus. Animals were monitored daily through the rest of the experiment. After 4- and 6-weeks post-implantation, the animals were sacrificed using deep isoflurane anaesthesia followed by an injection of pentobarbital. Eventual serum toxicity from both mice populations (dynamic and control conditions) was evaluated at the end of each time-point.

Blood biochemistry of liver and kidney panels was analysed by CEDIVET Laboratories. Subsequently, the magnetic tissues were explanted by cutting the animal tissues surrounding the implant. The cell viability of the magnetized tissues *in vivo* was accessed by a live/dead assay, through the incubation of the samples with calcein/PI stains and the visualisation by CLSM. For histological evoluation, the samples were fixed in 4% v/v formaldehyde (in dPBS) during 48 h, at RT and then, embedded in paraffin blocks. Lately, the cross-sections were stained with trichrome masson, von kossa, H&E and osteopontin as described in section *3.5.4. Histology*. In order to compare both *in vitro* and *in vivo* scenarios, the gene expression was also analysed by the methodology presented in *section 3.5.8.* with some modifications. Briefly, for RNA extraction, the implant was firstly frozen in liquid nitrogen and then, mechanically destroyed. After that, the samples were incubated with cell lysis buffer as previously described. At the end, the expression of PPARG, RUNX2, COL1A1 and VEGF was determined using the TaqMan® gene expression assays described in Table III.1.

References

1. Ovsianikov, A., Khademhosseini, A. & Mironov, V. The Synergy of Scaffold-Based and Scaffold-Free Tissue Engineering Strategies. *Trends Biotechnol* **36,** 348–357 (2018).
2. Norotte, C., Marga, F. S., Niklason, L. E. & Forgacs, G. Scaffold-free vascular tissue engineering using bioprinting. *Biomaterials* **30,** 5910–5917 (2009).
3. Yang, J. *et al.* Cell sheet engineering: Recreating tissues without biodegradable scaffolds. *Biomaterials* **26,** 6415–6422 (2005).
4. Ito, A. *et al.* Tissue Engineering Using Magnetite Nanoparticles and Magnetic Force: Heterotypic Layers of Cocultured Hepatocytes and Endothelial Cells. *Tissue Eng* **10,** 833–840 (2004).
5. Castro, E. & Mano, J. F. Magnetic Force-Based Tissue Engineering and Regenerative Medicine. *J Biomed Nanotechnol* **9,** 1129–1136 (2013).
6. Gil, S., Correia, C. R. & Mano, J. F. Magnetically labeled cells with surface-modified Fe3O4 spherical and rod-shaped magnetic nanoparticles for tissue engineering applications. *Adv Healthc Mater* **4,** 883–891 (2015).
7. Birmingham, A. & McNamara, L. M. Osteogenic differentiation of mesenchymal stem cells is regulated by osteocyte and osteoblast cells in a simplified bone niche. *Eur Cell Mater* **23,** 13–27 (2012).
8. Iaquinta, M. R. *et al.* Adult Stem Cells for Bone Regeneration and Repair. *Front Cell Dev Biol* **7,** 268 (2019).
9. Kadam, S. S., Tiwari, S. & Bhonde, R. R. Simultaneous isolation of vascular endothelial cells and mesenchymal stem cells from the human umbilical cord. *In Vitro Cell Dev Biol Anim* **45,** 23–27 (2009).
10. Baudin, B., Bruneel, A., Bosselut, N. & Vaubourdolle, M. A protocol for isolation and culture of human umbilical vein endothelial cells. *Nat Protoc* **2,** 481–485 (2007).
11. Correia, C. R. *et al.* Semipermeable Capsules Wrapping a Multifunctional and Self-regulated Co-culture Microenvironment for Osteogenic Differentiation. *Sci Rep* **6,** 21883 (2016).
12. Guven, S. *et al.* Multiscale assembly for tissue engineering and regenerative medicine. *Trends Biotechnol* **33,** 269–279 (2015).
13. Nadine, S. *et al.* Geometrically Controlled Liquefied Capsules for Modular Tissue Engineering Strategies. *Adv Biosyst* **4,** 2000127 (2020).
14. Neto, A. I. *et al.* Fabrication of Hydrogel Particles of Defined Shapes Using Superhydrophobic-Hydrophilic Micropatterns. *Advanced Materials* **28,** 7613–7619 (2016).
15. Gil, S. & Mano, J. F. Magnetic composite biomaterials for tissue engineering. *Biomater Sci* **2,** 812–818 (2014).
16. Amorim, C. O., Mohseni, F., Dumas, R. K., Amaral, V. S. & Amaral, J. S. A geometry-independent moment correction method for the MPMS3 SQUID-based magnetometer. *Meas Sci Technol* **32,** 105602 (2021).
17. Courtney, T., Sacks, M. S., Stankus, J., Guan, J. & Wagner, W. R. Design and analysis of tissue engineering scaffolds that mimic soft tissue mechanical anisotropy. *Biomaterials* **27,** 3631–3638 (2006).
18. Morinobu, M. *et al.* Osteopontin Expression in Osteoblasts and Osteocytes During Bone Formation Under Mechanical Stress in the Calvarial Suture In Vivo. *Journal of Bone and Mineral Research* **18,** 1706–1715 (2003).
19. Bonewald, L. F. *et al.* Von Kossa Staining Alone Is Not Sufficient to Confirm that Mineralization In Vitro Represents Bone Formation. *Calcif Tissue Int* **72,** 537–547 (2003).
20. Werner, C., Pompe, T. & Salchert, K. Modulating extracellular matrix at interfaces of polymeric materials. *Advances in Polymer Science* **203,** 63–93 (2006).

21. Sackstein, R. *et al.* Ex vivo glycan engineering of CD44 programs human multipotent mesenchymal stromal cell trafficking to bone. *Nat Med* **14,** 181–187 (2008).
22. Li, W. *et al.* Decreased Bone Formation and Osteopenia in Lamin A/C-Deficient Mice. *PLoS One* **6,** e19313 (2011).
23. Komori, T. What is the function of osteocalcin? *J Oral Biosci* **62,** 223–227 (2020).
24. Zhou, H. & Lee, J. Nanoscale hydroxyapatite particles for bone tissue engineering. *Acta Biomater* **7,** 2769–2781 (2011).
25. Torres, A. L. *et al.* Guiding morphogenesis in cell-instructive microgels for therapeutic angiogenesis. *Biomaterials* **154,** 34–47 (2018).
26. Nowak-Sliwinska, P., Ballini, J. P., Wagnières, G. & van den Bergh, H. Processing of fluorescence angiograms for the quantification of vascular effects induced by anti-angiogenic agents in the CAM model. *Microvasc Res* **79,** 21–28 (2010).

3

Results & Discussion

Chapter IV

Complex-shaped magnetic 3d cell-based structures for tissue engineering

Chapter V

Multi-layer pre-vascularized magnetic cell sheets for bone regeneration

Chapter VI

Freestanding magnetic microtissues for tissue engineering applications

Chapter VI

A novel therapeutic strategy for in situ bone regeneration powered by magnetic stimulation

Chapter IV - Complex-shaped magnetic 3D cell-based structures for tissue engineering[2]

Abstract

The use of cells as building blocks for tissue engineering purposes has been a matter of research in the recent years. Still, the fabrication of complex-shaped 3D-like constructs using living-based materials is hampered through the difficulty in recapitulating the mechanical properties of the native tissues. In an attempt to develop robust tissue-like constructs, it is herein proposed the fabrication of complex-shaped magnetic cells sheets (CSs) with improved mechanical properties for bone TE. Hence, magnetic CSs with versatile shapes and enhanced mechanical performance are fabricated using a pre-osteoblast cell line (MC3T3-E1) through an universal approach that relies on the design of the substrate, cell density and magnetic force. Results show that such magnetic CSs exhibit a Young's modulus similar to those encountered in the soft tissues. The construction of stratified CSs is also explored using MC3T3-E1 and adipose-derived stromal cells (ASCs). The role of the pre-osteoblast cell line on ASCs osteogenesis is herein investigated for the first time, in layered scaffold-free structures. After 21 days, the level of osteogenic markers in the heterotypic CS (MC3T3-E1:ASCs) is significantly higher than in the homotypic one (ASCs:ASCs), even in the absence of osteogenic differentiation factors. These evidences open new prospects for the creation of mechanically robust, complex, higher-ordered and completely functional 3D cell-based materials that better resemble the native environment of *in vivo* tissues.

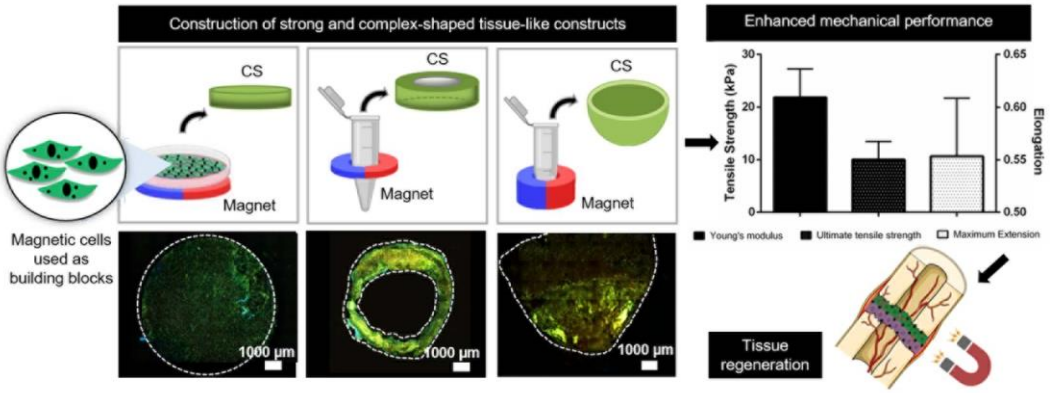

[2]Baseed on the publication: Lúcia F. Santos, A. Sofia Silva, João F. Mano. Complex-shaped magnetic 3D cell-based structures for tissue engineering. *Acta Biomaterialia* **118,** 18-31 (2020).

1. Introduction

Tissue engineering (TE) aims to generate *in vitro* biological tissues and organs to replace lost or compromised tissues.[1] In this sense, TE approaches have been focused on the creation of microenvironments that promote the regeneration of the injured site through the interaction of materials, cells and growth factors.[2] Therefore, natural and synthetic biomaterials have been serving as scaffolds for biologically active components (cells) in order to define an artificial *in vivo* milieu with complex and dynamic interactions that regulate stem cells, mimicking their natural cellular microenvironment, and consequently leading to tissue formation.[3–5] Nevertheless, the possible strong inflammatory responses that are induced upon scaffold biodegradation, the limited diffusion of nutrients that promote a necrotic core and even the use of isolated cell suspension that deprive cells of their endogenous extracellular matrix (ECM), results in the failure of tissue reconstruction and, therefore, unsatisfactory regeneration.[6] Additionally, the complex, well-organized and hierarchical architecture of tissues and organs is not fulfil by traditional TE approaches. Flat tissues, tubular structures, hallow, nanotubular, viscous organs and complex solid organs exhibit single features that became unique challenges in TE.[7,8] In such way, materials science, matrix biology and TE have been increasingly combined to generate a new class of biomimetic materials to closely mimic critical aspects of natural tissue regarding its physical and chemical properties. In this sense, scaffold-free TE has emerged as a powerful strategy using multicellular building blocks like spheroids, tissue strands and cell sheets (CSs) that are able to produce larger cohesive tissue constructs and produce ECM, that is essential to fabricate functional tissues.[6,9] In particular, CS technology has been getting momentum due to their ability to fabricate more functional, complex, and thicker heterogeneous tissues.[10] Such expertise allows the construction and harvesting of intact sheet-like cells, keeping their naturally formed cellular networks.[11–14] Thermo-responsive methodology is the most explored cell harvesting mechanism in which sheets of cells are recovered by simply changing the temperature. Nevertheless, such strategy exhibits several constraints including the high cost, alteration of cellular activity, low mechanical strength and restrains in tissue replacement.[15] Moreover, due to the complexity of organs and tissues, the fabrication of *in vivo*-like 3D constructs using CS technology may be a challenge. The development of heterotypic and stratified 3D tissue is normally achieved by individual stacking of previously formed CS monolayers. Nevertheless, such strategy could hamper the establishment of cell-cell interactions between the two different cell cultures, and hinder a

controlled spatial positioning of target cells, compromising the natural stratification of the 3D tissue.[16]

In the light of such events, magnetic-force based tissue engineering (Mag-TE) has been explored in order to produce more complex CSs through the combination of magnetic force with CS technology, enabling the easier manipulation of those cells.[10,17] In fact, Mag-TE has been implied in the production of complex tissues that are not easily achieved by conventional cell culture or co-culture methods such as 2D and 3D cell layers, tubular structures and 3D ordered assemblies consisting of several cell types.[17,18] Thus, magnetic CSs have been investigated in the regeneration of distinct tissues including skeletal and cardiac muscle,[14,16] bone[19] and angiogenesis,[20–22] emphasizing the ability of this technology over artificial synthetic scaffolding materials for a wide range of tissues. Recently, Mag-TE has shown outstanding results in the development of hierarchical 3D cohesive tissues in a simple, one-pot, cost-effective and time-saving manner, allowing the fabrication and manipulation of tissue-like constructs aided by a magnetic force.[10,23] In fact, such 3D construct revealed to be effective in stimulating *in vitro* osteogenesis and triggering the recruitment of blood vessels with empowering pre-angiogenic potential.[10] Nevertheless, the geometry, complexity and strength of the tissue-constructs still poorly-explored, which could compromise the proper function of these living materials. Tissue engineered constructs should resemble the *in vivo* structural and mechanical properties of the native tissues to assure their functionality and integration within the host.[24]

In light of such events, our group aims to investigate the ability of creating versatile and robust magnetic CSs, while guarantying the natural architecture of living tissues. Hence, the current work aims, in a first approach, at developing complex and robust magnetic membranes based exclusively on the type of magnet and substrate applied. For the purpose, mouse pre-osteoblastic cells (MC3T3-E1) were used to create different shapes of magnetic cell tissue. The robustness of such cell-dense like tissue will be validated by accessing their mechanical performance as well as by the deposition of ECM. In fact, the mechanical performance of cell-based tissue constructs was herein explored for the first time. Moreover, as a proof-of-concept, to demonstrate the ability of this technology in creating heterotypic 3D cell connected tissue, adipose derived stromal cells (ASCs), previously labelled with magnetic iron oxide nanoparticles (MNPs), were seeded on top of the magnetically labelled MC3T3-E1 CS enabling tissue stratification. We hypothesized that such approach could prompted the fabrication of cell-based constructs to create stratified cell-dense tissues for bone TE. In fact, to the best of our knowledge, the ability of pre-osteogenic linage to modulate the osteogenic differentiation of stromal cells was never tested in such layered scaffold-

free structures. We expect that the methodology herein described could be further extended for the regeneration of a wide plethora of organized tissues, enabling the creation of a living-based construct with biomimetic mechanical properties.

2. Materials and methods

2.1. Materials

All chemicals were purchased from Sigma-Aldrich and employed as received, unless otherwise specified.

2.2. Synthesis and Characterization of Magnetic Nanoparticles

Magnetite nanoparticles were synthesized as previously established by the group.[25] Briefly, Fe_3O_4 MNPs nanoparticles were synthesized by the co-precipitation reaction of ferrous ($FeCl_2 .4H_2O$) and ferric ($FeCl_3 .6H_2O$) salts at 60°C, in a nitrogen atmosphere and in the presence of ammonium hydroxide (NH_4OH). Then, MNPs surface was modified with (3-aminopropyl)triethoxysilane (APTES) by a silanization reaction and washed with water, and ethanol followed by freeze-drying. Later on, the nanoparticles were conjugated with rhodamine B isothiocyanate as previously established.[10,25] For this purpose, Fe_3O_4 –APTES MNPs were dispersed in ethanol at 5 mg mL^{-1} and then, rhodamine B (RhodB) (2.5 mg mL^{-1}) was added at RT, overnight. The modification of the MNPs with APTES was accessed by attenuated total reflectance (ATR-FTIR) by using a Bruker Tensor 27 spectrometer, as described in our previous report.[10].

2.3. Evaluation of the Fe_3O_4 – APTES RhodB-MNPs Stability

The stability of RhodB-MNPs was investigated by scanning the fluorescence of RhodB on cell culture medium and dPBS (pH=7.4). Briefly, the samples were immersed and subsequently stirred in a shaking water bath at 60 rpm and 37ºC. After 1, 3, 7, 14 and 21 days, the fluorescence spectrum was peaked at an excitation wavelength of 556 nm and 627 nm of emission using a spectrofluorometer (FP-8300, JASCO, USA).

2.4. Cell culture and *In vitro* cellular uptake of RhodB-MNPs

MC3T3-E1 cell line (ATCC® CRL-2593) and human ASCs (ATCC® PCS-500-011™) were cultured in α-MEM (minimum essential medium, ThermoFisher Scientific), supplemented with fetal bovine

serum (FBS, 10%, ThermoFisher Scientific) and penincilin-streptavidivin (1% v/v, ThermoFisher Scientific). The co-location of RhodB-MNPs was visualized in both MC3T3-E1 cell line and ASCs. Firstly, cells were seeded at density of 2.4 x 10^6 cells cm^{-2} in 8-well cell culture slides and cultured for 24 h at 37 °C and 5% CO_2 in a humidified atmosphere, followed by a 4 h incubation with RhodB-MNPs at 1 mg mL^{-1}. Lastly, cells were washed with PBS and subsequently fixed in formalin 10% (v/v) at RT during 15 min. After the incubation of the cells with Triton X100 (0.1% (v/v), in dPBS) during 5 min at RT, the cells were incubated with Flash Phalloidin Green 488 (1:100 in dPBS) at RT for 45 minutes and then counterstaining with DAPI (1:1000 in dPBS) for 5 min at RT. Finally, the cells were visualized by fluorescence microscopy (Carl Zeiss Microscopy GmbH) and using ZEN v2.3 blue edition.

2.5. Fabrication of homotypic and heterotypic magnetic CSs

Prior to cell seeding, MC3T3-E1 and ASCs were incubated during 30 minutes at 37 °C with the lipophilic dyes 3,3'-dioctadecyloxacarbocyanine perchlorate (DIO, green) and 1,1'-Dioctadecyl-3,3,3',3'-Tetramethylindodicarbocyanine (DID, purple), respectively (1mL, 2µM per 1× 10^6 cells), . Then, the labeled cells were seeded at the cell density of 2.4 × 10^6 cm^{-2} and cultured during 24 h at 37 °C and 5% CO_2 in a humidified atmosphere, followed by a 4h incubation with RhodB MNPs (1 mg mL^{-1}). Later on, the cells were harvested using TrypLE™ Express solution at 37 °C for 5 min and centrifuged at 300 g. In order to obtain CSs with flat and circular shapes, the magnetically labelled cells were transferred to ultralow-attachment 24, 48 or 96-well plates, previously treated with alginate (2% w/v) for 30 min. To provide magnetic force, commercial neodymium rod magnets (strength of 108N and standard N41 magnetization, Supermagnet) were placed at the bottom of the reverse side of the ultralow-attachment plate. The ability to create more complex structures was investigated through the fabrication of CSs with diverse shapes based on the type of magnet, substrate and cell density. For the purpose, commercial neodymium magnets with ring and concave shapes (strength of 73.5 N and standard N42 magnetization, Supermagnet) were used. Briefly, the magnetically labelled cells (MC3T3-E1 cell line) were transferred to an Eppendorf and then the magnets were placed around (ring shape) and at the bottom of (concave shape) the Eppendorf.

Heterotypic magnetic CSs were created by labelling each cell phenotype as described in the previous section. After 24 h, the second cell phenotypic (ASCs) was added to the homotypic circular MC3T3-E1 CS, that was previously assembled. The CSs with a double conformation were cultured during 7, 14 and 21 days in a-MEM medium with or without osteogenic differentiation factors - dexamethasone (10 nM), ascorbic acid (50 µg mL^{-1}) and β-glycerophosphate (10 mM). Labelled cells

in both homotypic and heterotypic magnetic CSs were visualized under fluorescence microscopy (Carl Zeiss Microscopy GmbH) and processed using ZEN v2.3 blue edition.

2.5.1. Characterization and mechanical behaviour of the developed CSs

The morphology of CSs for all conditions was visualized by SEM (S4100, Hitachi, Japan. Briefly, the samples (n=2) were washed with PBS, followed by an incubation of 15 min with formalin (10% v/v). Then, the samples were dehydrated in an increasing gradient of ethanol and gold-sputter coated using an accelerating voltage of 25 kV.

The mechanical behavior of the homotypic CS with the MC3T3-E1 cell line was investigated (n=5 independent replicas) was characterized through the tensile testing (MMT-101N, Shimazdu Scientific Instruments, Japan) with a load cell of 100 N. Briefly, CSs with ring shape were cut to form a ribbon conformation and then, the samples were clamped in tensile testing machine. Tensile testes were carried out with a gauge length of 3 mm and a loading speed of 1 mm min^{-1}. The cross-section of the CS was measured using SEM images. For each sample, the load versus cross-head displacement data from initial until rupture load was measured using a PC data acquisition system connected to the tester. Resulting stress-strain curves allowed to determine the ultimate tensile strength (UTS), elongation at break, and Young's modulus of the CSs.

2.6. Histological and immunohistochemical analysis of CSs

Prior to staining, the heterotypic CSs were fixed using formalin 10% (v/v) at RT for 15 min. After the permeabilization of the CSs with Triton X (0.1% v/v) during 5 min at RT, the CSs were incubated for 1h at RT with 5 % (v/v) FBS/dPBS. Then, the samples were immersed for 3 h at RT with the primary antibody anti-rabbit human vinculin (1:50 in 5 % FBS/dPBS, Invitrogen). Subsequently, the secondary antibody anti-rabbit AlexaFluor 594 (1:400 in 5% FBS/dPBS) was added to the samples during 1h at RT. Lastly, the CSs were incubated with Flash Phalloidin Green 488 (1:100 in dPBS) at RT for 45 min and counterstained with DAPI (1:1000 in dPBS) during 5 min at RT. At the end, the CSs were visualized by confocal microscopy LSM 880, ZEISS) and processed using ZEN v2.3 blue edition and Imaris Biteplane.

Heterotypic CSs cultured during 21 days at basal and osteogenic conditions were also visualized in histological sections. After the fixation of the samples with formalin (10% v/v), the CSs were routinely processed and embedded in paraffin. Then, sequential sections of 5 µm thickness were produced in adhesive slides to the Masson Trichrome and Van Kossa staining. Expression of

osteocalcin, lamin A and CD44 were also visualized in the histological cross-sections. Firstly, the samples were treated with TE buffer (10 mM Tris/1 mM EDTA, pH 9) for 35 min at 95–98 °C for antigen retrieval. Then, the sections were incubated during 3 h with mouse anti-osteocalcin (1:200 in 5 % FBS/dPBS, Biolegend), rabbit anti-Lamin A (1:200 in 5 % FBS/dPBS, Biolegend), FN monoclonal antibody (FN-3) Alexa Fluor 488 (1:100 in 5 % FBS/dPBS, Thermofisher), FITC anti-human CD44 primary antibodies (1:200 in 5 % FBS/dPBS, Biolegend) and rabbit anti-collagen IV antibody (1:400 in 5% FBS/dPBS, Abcam). Lastly, the samples were incubated with Alexa Fluor 647-labeled chicken anti-rabbit (1:400 in 5 % FBS/dPBS, Invitrogen) for anti-lamin A, AlexaFluor 488 Goat anti- mouse (1:400 in 5 % FBS/dPBS, Invitrogen) for anti-osteocalcin and AlexaFluor 594 Donkey anti-rabbit (1:400 in 5 % FBS/dPBS, Invitrogen) during 1h at RT. For all conditions, the histological sections were incubated with DAPI (1:500 in dPBS, Sigma) at RT for 5 min. At the end, the CSs were visualized using a fluorescence inverted microscope (AxioImager Z1, Zeiss). Statistical differences between heterotypic CSs cultured in basal or osteogenic evidenced in the histological cuts were analyzed using Image J software.

2.7. Cell viability

The survival of the cells in MC3T3-homotypic CS, ASCs-homotypic CS and heterotypic CSs was investigated through a live-dead fluorescence assay by following the manufacturer's recommendations (ThermoFisher Scientific) at 7, 14, and 21 days of culture. After washing the samples with PBS, the CSs were incubated with the kit components during 20 min at 37 °C. Finally, the samples were analyzed by fluorescence microscopy (Axio Imager 2, Zeiss).

2.8. Quantification of Mitochondrial Metabolic Activity

Mitochondrial metabolic activity was accessed through an MTS colorimetric assay (CellTiter96® AQueous one solution cell proliferation assay, Promega) according to manufacturer's recommendations. Briefly, the reagent kit (120 µl per well) was incubated with the samples (n=3) for 4h at 37 °C and then, the absorbance was determined at 490 nm using a microplate reader (Synergy HTX, BioTek Intruments, USA).

2.9. Quantification of the Cell Proliferation

Firstly, the cell lysis was performed by resuspending the CSs (n=3) in Titron 100X (2 % v/v/ in ultra-pure sterile water) at 37 °C for 1 h. The samples were stored at −80 °C until further use. Then, the

lysate DNA content was determined with Quant-iT™ PicoGreen™ dsDNA Assay Kit (Invitrogen™) according to the manufacturer's instructions. To guaranty that only DNA content would be quantified, the MNPs were firstly magnetically separated with the aid of a neodymium magnet. A standard curve for DNA analysis was generated with the provided the standard DNA solution. Lastly, the samples were incubated at RT for 10 min and the fluorescence intensity was determined at an excitation wavelength of 485/20nm and 528/20nm of emission using a microplate reader (Synergy HTX, BioTek Intruments, USA).

2.10. Analysis of osteogenic differentiation of the CSs

The role of MC3T3-E1 in the osteogenic differentiation of ASCs was evaluated in culture medium with and without osteogenic differentiating factors (dexamethasone, ascorbic acid and b-glycerol phosphate). Homotypic CSs composed of ACSs and MC3T3-E1 were used as controls. All CSs were incubated for over a period of 21 days.

2.10.1. Quantification of ALP Activity

The cell lysates were also analyzed for the quantification of the alkaline phosphatase activity (ALP) by measuring the released p-nitrophenol (4NPhP). Briefly, 75 µL of 4NPhP solution (2 mg mL^{-1} in) in 1M diethanolamine buffer were added to 25 µL of each sample. After 45 min at 37 °C in dark, the reaction was stopped with 80 µL of a NaOH (2 M) and EDTA (0.2 mM) solution. Lastly, the enzyme activity was determined at 405 nm using a multiplate reader (Synergy HTX, BioTek Intruments, USA). The value was normalized against the CS area. A standard curve with a range of 4NPh concentration was used as reference (0; 15×10^{-6}; 30×10^{-6}; 50×10^{-6}; 75×10^{-6}; 95×10^{-6} M in diethanolamine buffer).

2.10.2. Osteopontin Immunostaining

The expression of osteopontin was determined in both homotypic and heterotypic CSs, previously labelled with DIO (MC3T3-E1) and DID (ASCs). After 7, 14 or 21 days of culture, the CSs were fixed in formalin (10% v/v) at RT during 15 min. Firstly, the samples were immersed in Triton X (0.1% v/v, in dPBS) at RT for 5 min. Then, the CSs were incubated with 5 % (v/v) FBS/dPBS at RT for 1 h. Subsequently, the primary mouse anti-human osteopontin antibody (1:100 in 5% FBS/dPBS, Biolegend, Taper) was added to the samples. After 3h, the CSs were incubated with the secondary anti-mouse Alexa Fluor 555 antibody (1:400 in 5 % FBS/dPBS) for 1h in dark at RT. Lastly, all the

samples were counterstained with DAPI (1:1000 in dDPBS) during 5 min in dark at RT and visualized by fluorescence microscopy (Carl Zeiss Microscopy GmbH) and using ZEN v2.3 blue edition.

2.10.3. Quantification of Cytokines

After 21 days of culture, the culture medium from the MTS, DNA and ALP activity assays was collected and stored at -80°C until further use.
The expression of osteopontin, osteocalcin, BMP-2 and VEGF was quantified through the commercially available Human Osteopontin (Abcam), Osteocalcin (Abcam), BMP-2 (Invitrogen) and VEGF (Abcam) ELISA Kits, respectively. Lastly, the absorbance of the samples was determined at 450 nm using a microplate reader (Synergy HTX, BioTek Intruments, USA).

2.10.4. In vitro biomineralization analysis of the CS

After 7, 14 and 21 days of culture, the *in vitro* mineralization of CSs was accessed for both basal and osteogenic culture conditions using the OsteoImage™ Assay. For this purpose, the CSs were incubated with the OsteoImage™ staining reagent (1:100 v/v) during 30 min at RT. Then, the samples were counterstained with DAPI (1:1000 in dDPBS) during 5 min in dark at RT and visualized by fluorescence microscopy (Carl Zeiss Microscopy GmbH). The deposition of hydroxyapatite nodules was also visualized by SEM. Briefly, the CSs were carbon-coated and analyzed by Energy dispersive X-ray spectroscopy (EDS) (QUANTAX 400, Bruker) at an electron in intensity of 15 kV (SU-70, Hitachi).

2.11. Statistical Analysis

All the results were stated as mean ± standard error. GraphPad Prism software (GraphPad Software Inc., version 7.0) was used for the statistical analysis by two-way ANOVA following the Bonderronu pos-hoc test, with a significance level set at $P < 0.05$.

3. Results

3.1. Cell Sheet Fabrication and Characterization

RhodB-MNPs were produced and characterized according well-established protocols of the group (**Figure IV.1A**).[10,25] Prior to CSs fabrication, the stability of the magnetic nanoparticles modified with Rhodamine B (RhodB-MNPs) was confirmed in dPBS and culture medium over a course of 21

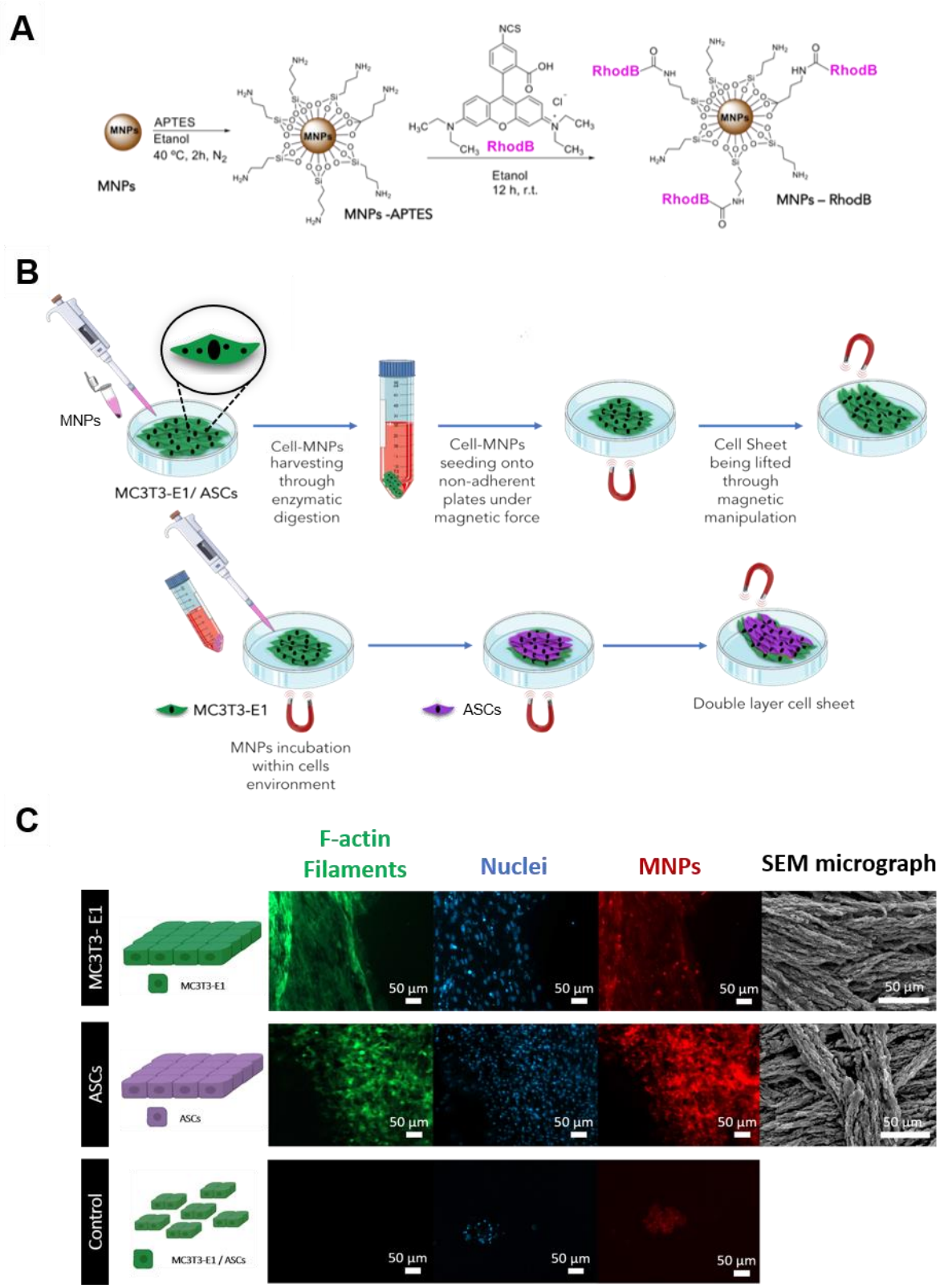

Figure IV.1: Development of CSs using Mag-TE. **A**. Schematic representation of the functionalization of MNPs used in the fabrication of CSs. **B**. Schematic illustration of the proposed approach for the development of magnetic CSs; **C**. Fluorescence and SEM images of the fabricated homotypic CSs using MC3T3-E1 and ASCs. Same cell assembly procedure without the aid of magnet was used as control and a representation of the MC3T3-E1 cell assembly is demonstrated.

days (**Figure IV.S1**). Moreover, RhodB-MNPs were successfully uptaken by MC3T3-E1 and ASCs as corroborated in **Figure IV.S2**. Afterwards, homotypic and heterotypic magnetic CSs were prepared as described elsewhere[10] and as illustrated in **Figure IV.1B**.

3.1.1. Homotypic Cell Sheet

Initially, ASCs and MC3T3-E1 cells were used for the development of homotypic CSs. As demonstrated in **Figure IV.1C**, homotypic CSs were successfully produced with the aid of the magnetic field. In the absence of the magnet only a few aggregates were formed, and no cell-cell interaction was denoted.

To further demonstrate the versatility of this approach in creating distinct and functional tissues, CSs with diverse shapes were developed based on the type of the magnet, substrate and cell density. As a proof-of concept, MC3T3-E1 cells were used to produce robust CSs with circular, ring and concave shapes. **Figure IV.2A** displays the fluorescence images of such shaped CSs, corroborating the deposition of ECM within the well-defined structures. Additionally, CSs' cell density, thickness and morphology were also investigated along time (7, 14 and 21 days) in the MC3T3-homotypic CSs through SEM (**Figure IV.S3**, **Figure IV.S4**). As hypothesized, the CS thickness and robustness increased with the cell density.[26] Nevertheless, the thickness of the CSs decreased along time (**Figure IV.S3**), thus suggesting tissue confinement and therefore, the stratification of the CS.

3.1.2. Mechanical properties

MC3T3-homotypic CSs were used to evaluate their mechanical behavior and robustness. The tests were performed using a tensile mode - see **Figure IV.2B**. Representative conventional stress– strain curve and the respective values of Young's modulus, ultimate tensile strength and maximum extension are shown in **Figure IV.2C** and **IV.2D**. Herein, CSs presented a maximum extension of 0.55 ± 0.06, a Young's modulus of 22 ± 5 kPa and an ultimate tensile strength of 10 ± 3 kPa.

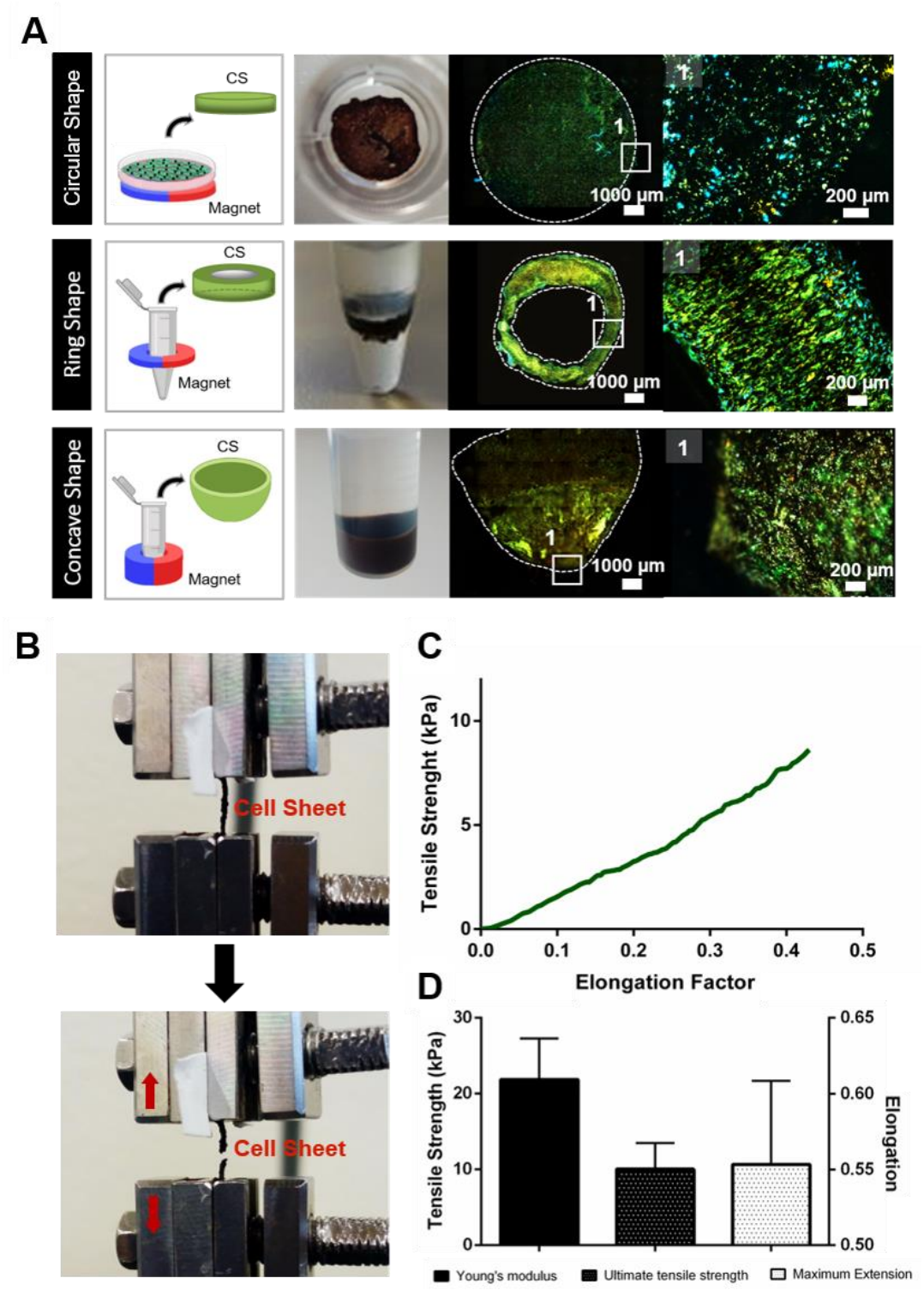

Figure IV.2: Morphological characterization of the produced CSs. **A.** Development of versatile MC3T3-homotypic CSs with different shapes, including circular, ring and concave shaped structures. **B.** Photographs of the MC3T3-homotypic CSs during the tension assay performed to evaluate their mechanical behavior; **C.** Representative conventional tensile strain–stress curve of the MC3T3-homotypic CS; **D**. Mechanical performance of the developed CSs – Young's modulus, Ultimate Tensile Strength and Maximum Extension.

3.1.3. Heterotypic Cell Sheet

The major challenge in TE prevails on the construction of highly controlled constructs able to fil distinct defects. In an attempt to investigate the ability to create heterotypic stratified cell-dense like tissue, magnetic CSs comprising MC3T3-E1 and ASCs were fabricated. The double layer CS conformation was built by seeding a suspension of magnetically labelled ASCs on the top of a previously assembled MC3T3-homotypic CS. The CS assembly was corroborated by confocal microscopy (**Figure IV.3A** and **Figure IV.S5**) with ASCs displayed in purple and MC3T3-E1 represented in green. Cell-cell interactions throughout the CS construct were confirmed by the vinculin staining (**Figure IV.3B**).

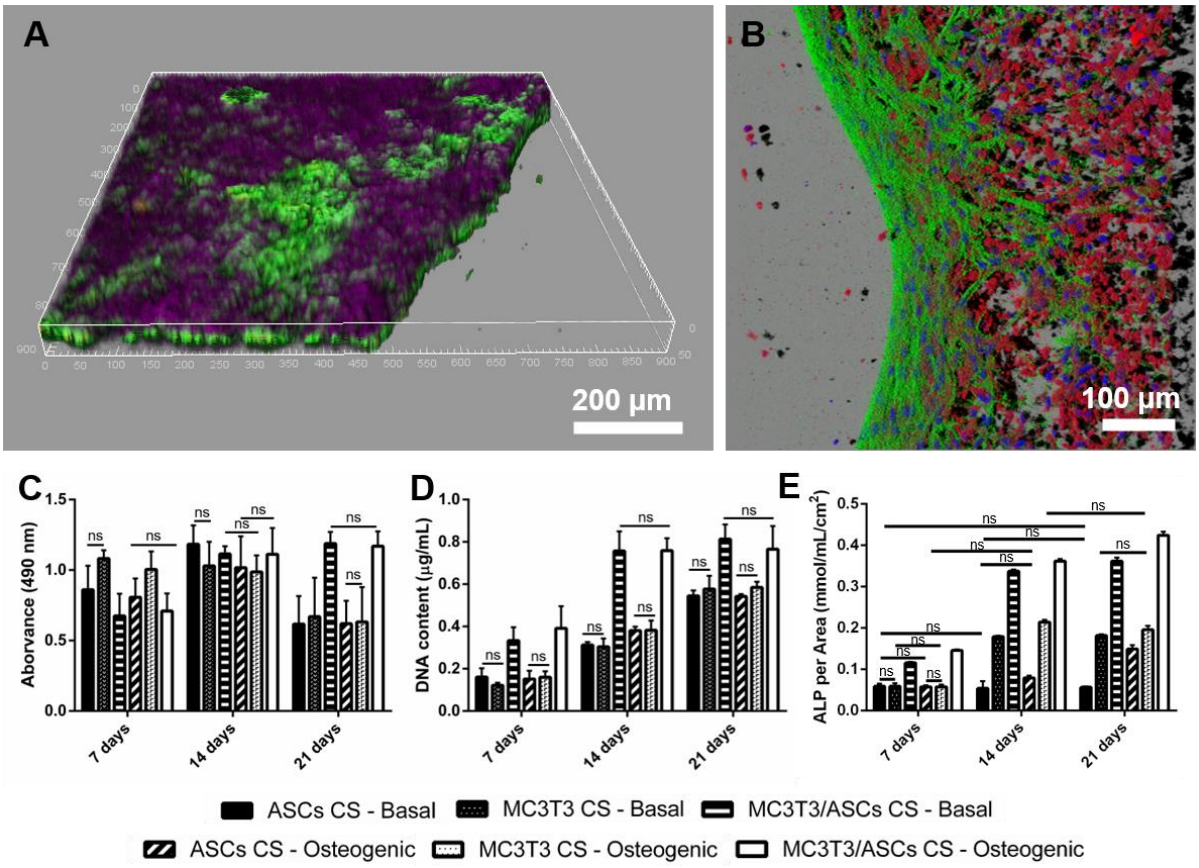

Figure IV.3: Construction of stratified heterotypic CSs. **A**. Confocal microscopy image of the 3D stratified CS with a double layer conformation: ASCs CS (purple) on the top of MC3T3-E1 CS (green); **B**. Confocal microscopy image of the heterotypic CS cultured for 7 days. The presence of vinculin (in red) in the actin cytoskeleton (in green) confirmed the cell-cell and cell-matrix junctions. Cell nuclei are depicted in blue (DAPI). **C**. Cell metabolic activity determined by MTS colorimetric assay, **D**. Cell proliferation by DNA quantification, and **E**. Alkaline phosphatase (ALP) activity normalized by the CS area. All results were significantly different unless marked with ns ($p > 0.05$).

3.2. Viability, metabolic Activity and Cell Proliferation

Heterotypic CSs in both basal and osteogenic culture media showed increased metabolic activity and DNA content up to 14 days of culture. Moreover, for all the conditions the majority of the cells remained viable after 21 days of culture (**Figure IV.S6**). On the other hand, the homotypic CSs conformations (ASCs CSs or MC3T3-E1 CSs) exhibited lower metabolic activity (**Figure IV.3C**) after 21 days of culture, suggesting a compromised viability along time for the monolayer CS conformations.

3.3. Evaluation of the *in vitro* osteogenic differentiation of the Magnetic CSs

To demonstrate the cells interactions within the CSs, we investigated the ability of MC3T3-E1 to induce the osteogenic differentiation of ASCs through the evaluation of alkaline phosphatase (ALP) activity, mineralization and cytokines detection.

3.3.1. Quantification of the ALP activity

Since enhanced levels of ALP activity are associated with the mineralization of bone,[27] we envisage that early cell differentiation had occurred on heterotypic CSs and MC3T3-homotypic CSs. The ASCs-homotypic CS presented an increment on ALP activity in the presence of the osteogenic differentiation factors after 21 days (**Figure IV.3E**). On the other hand, in basal conditions (i.e., without the supplementation of osteogenic factors such as dexamethasone, ascorbic acid and b-glycerol phosphate), ASCs-homotypic CSs do not show any increment on the ALP activity. The hypothesis that MC3T3-E1 could induce ASCs differentiation in osteogenic progenitor cells was corroborated through the increment of the ALP activity in the heterotypic CS even in basal conditions. We demonstrated that within the CSs, MC3T3-E1 and ASCs can interact in such way that leads to diffusion of signaling molecules essential for the osteogenic differentiation of stromal cells. In fact, the heterotypic CSs (MC3T3-E1/ASCs) showed higher expression of ALP (normalized by area) when compared to MC3T3-homotypic CSs, which supports our initial hypothesis that MC3T3-E1 cell line has a positive role over the ASCs osteogenic differentiation. As expected, the addition of osteogenic factors prompted to even higher cell differentiation.

3.3.2. Osteopontin Expression

Osteopontin represents one of the most-studied protein in bone matrix, playing a critical role in the maintenance of bone structure.[27] To substantiate the synergic behavior between MC3T3-E1 and

ASCs, and attest that our heterotypic CS could be further use for bone regeneration purposes, we have explored the presence of osteopontin in both homotypic and heterotypic CSs through an immunofluorescence assay. As anticipated, an earlier osteopontin detection was evidenced for the heterotypic CS in osteogenic conditions after 14 days of culture (**Figure IV.4**), corroborating the results obtained through the ALP activity. Nevertheless, after 21 days, the osteopontin staining could be depicted in both culturing conditions (even in basal media), suggesting the osteogenic induction of MC3T3-E1 over ASCs. In fact, the presence of osteopontin was more evident in heterotypic CS when compared to the MC3T3-homotypic CS (**Figure IV.S7**). As expected, the ASCs-homotypic CS cultured under basal conditions (no osteogenic supplementation), did not exhibit osteopontin expression (**Figure IV.S8**). The heterotypic-CS showed an enhanced osteopontin expression when compared to the ASCs-homotypic CS (**Figure IV.4**). Additionally, SEM micrographs were collected from all conditions to validate the cohesion of the developed tissue constructs.

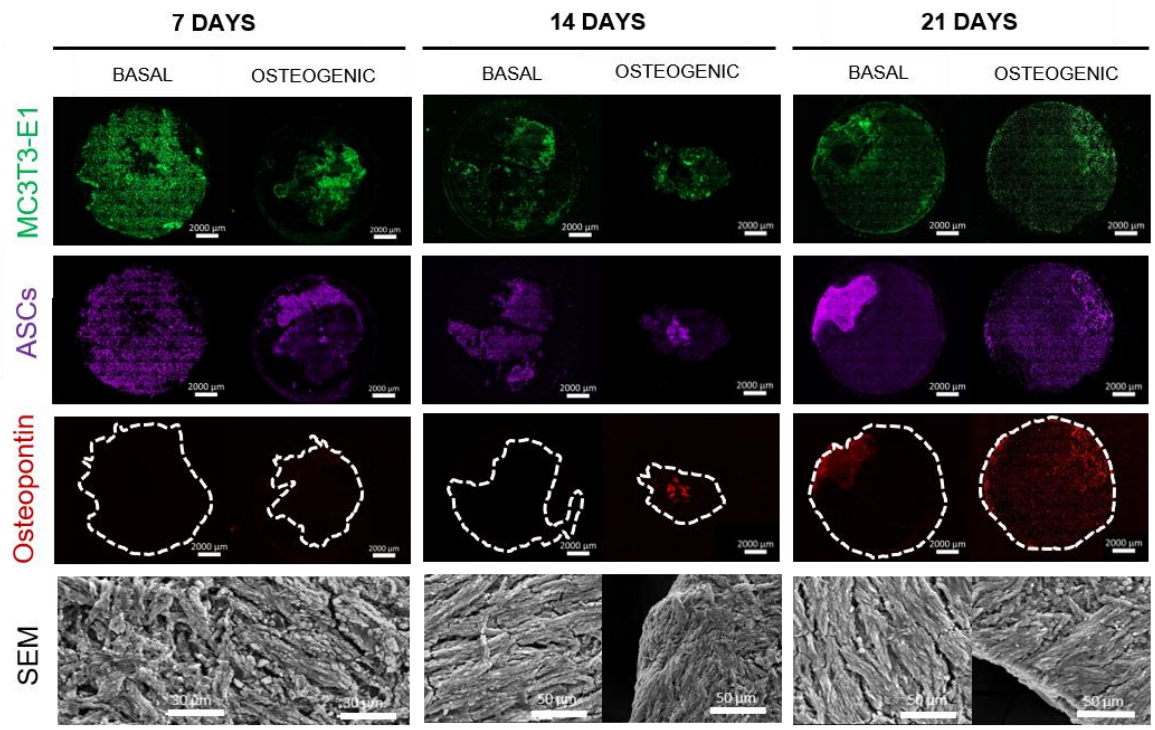

Figure IV.4: Immunofluorescence of heterotypic CSs after 7, 14 and 21 days of culture in basal and osteogenic media: MC3T3-E1 (green), ASCs (purple) and osteopontin (red). SEM micrographs corroborate the integrity of the developed CSs (bottom panel).

3.3.3. Biomineralization Assessment

The biomineralization of 3D constructs has been investigated in TE to attest the formation of bone-like tissues.[28–30] In the light this, we have also investigated the deposition of hydroxyapatite-like

minerals on both homotypic and heterotypic CSs, since hydroxyapatite is chemically similar to the inorganic component of bone. For this purpose, the mineralization of CSs was accessed through energy dispersive X-ray spectroscopy (EDS) (**Figure IV.5B**) and an OsteoImage™ assay (**Figure IV.5C**). The results supported both ALP and osteopontin findings with increased hydroxyapatite deposition overtime in both culturing conditions of the heterotypic CSs (MC3T3-E1/ASCs). The Ca/P ratio reached the maximum value at 21 days under osteogenic supplementation (1.41). As expected, a small delay was evidenced for the heterotypic CSs cultured without osteogenic supplementation (1.12).

The results suggested the formation of bone-like tissue in both culturing conditions with an enhanced deposition of hydroxyapatite-like minerals, and a Ca/P ratio similar to native apatite minerals in bone (1.67).[31,32] The deposition of hydroxyapatite minerals was also supported by SEM micrographs. Minerals with larger sizes and more defined structures were obtained after 21 days, corroborating the findings of EDS quantification. The hydroxyapatite deposition was also visualized through an OsteoImage™ Assay, attesting higher mineralization in the heterotypic CS. As expected, the deposition of hydroxyapatite-like minerals only occurred in presence of osteogenic factors for ASCs-homotypic CS. Such results were evidenced in EDS (**Figure IV.S9**) and OsteoImage™ Assay (**Figure IV.S10** and **Figure IV.S11**). Similar to osteopontin staining and ALP activity, an enhanced mineralization was obtained for the heterotypic CSs in both basal and osteogenic media, which again anticipated the synergetic effect between the two cell phenotypes and consequently the osteogenic differentiation of ASCs in the presence of MC3T3-E1.

3.3.4. Cytokines Detection

The presence of the late osteogenic markers osteopontin and osteocalcin were exhibited in the heterotypic CS after 21 days even in the absence of osteogenic factors (**Figure IV.5D** and **IV.5E**). ASCs-homotypic CSs did not secrete cytokines without osteogenic supplementation. For both culturing conditions, the heterotypic CSs presented higher expression of such osteogenic markers than the MC3T3-homotypic CS, suggesting an osteogenic role of MC3T3-E1 over ASCs, inducing their osteogenic differentiation. Furthermore, the secretion of human bone morphogenic protein-2 (BMP-2) and vascular endothelium growth factor (VEGF) was also determined after 21 days (**Figure IV.5F** and **IV.5G**). These two cytokines synergistically interact to promote the angiogenesis while guarantying the proper bone formation.

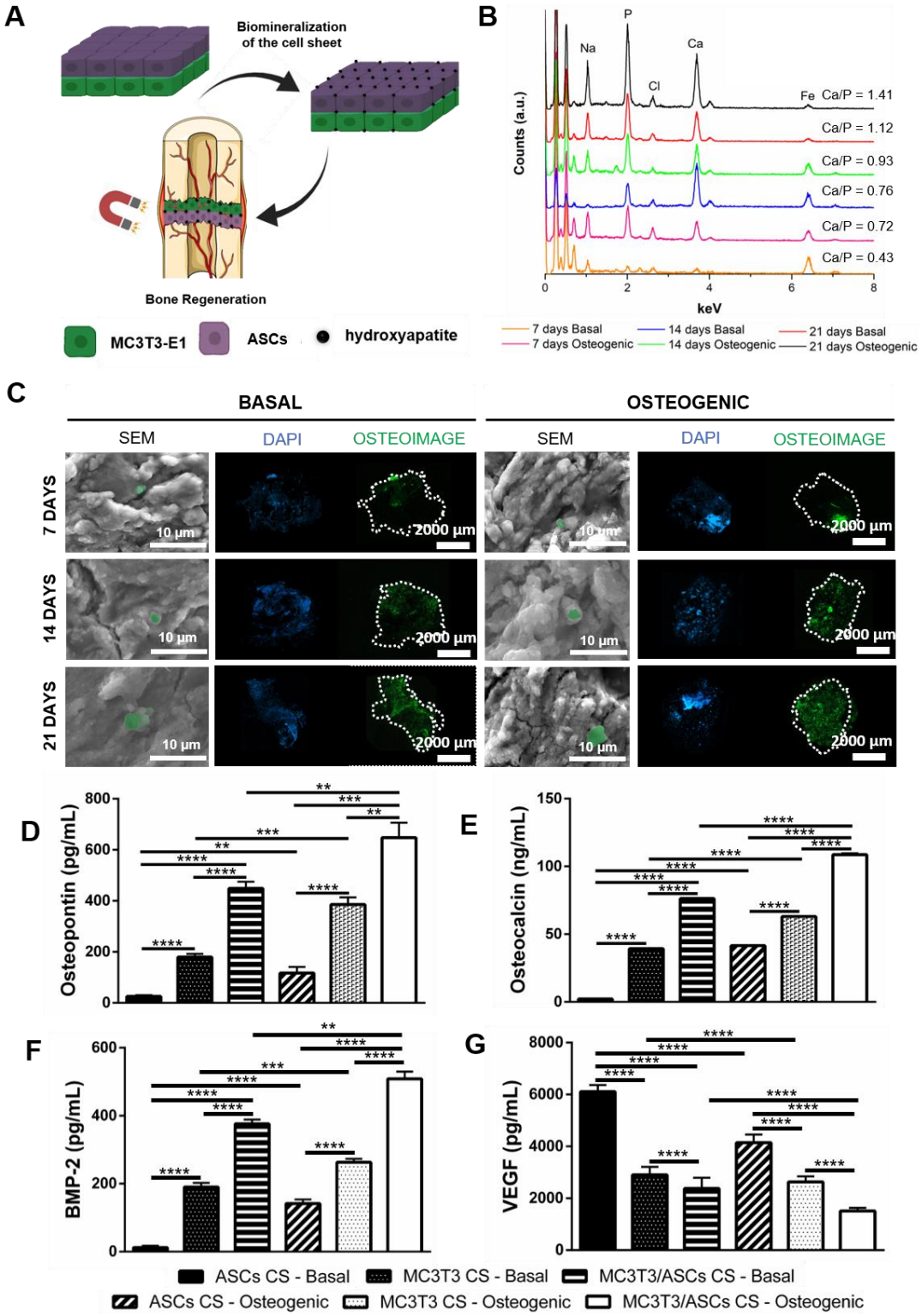

Figure IV.5: *In vitro* mineralization of the fabricated 3D heterotypic CSs in both culturing conditions. **A.** Schematic representation of the potential applications of the calcified tissues; **B.** Analysis of the mineral deposition within the CS by Energy dispersive X-ray spectroscopy (EDS); **C.** The deposition of the hydroxyapatite portion of bone-like nodules was also accessed through OsteoImage™ fluorescence assay: cell nucleus - DAPI (blue) and hydroxyapatite (green). Calcium deposits are also represented in SEM micrographs (in green) - in the right panel; Quantification of osteopontin (D) and osteocalcin (E) BMP-2 (F) and VEGF (G) expressions by ELISA. $p < 0.05$: *$p < 0.05$; **$p < 0.01$; ***$p < 0.001$; ****$p < 0.0001$.

In this work, heterotypic CSs and MC3T3-homotypic CS presented an enhanced expression of BMP-2, even in basal conditions. In contrast, the higher level of VEGF was obtained in ASCs-homotypic CS cultured in basal conditions. In fact, ASCs stimulate blood vessels growth by the secretion of growth factors like VEGF. The down-regulation of VEGF level combined with higher values of BMP-2 indicated the osteogenic differentiation of ASCs, that once differentiated lose their ability to enhance the angiogenesis by decreasing the level of VEGF.[10,33] Altogether, our results demonstrated decreased levels of VEGF with an enhanced expression of BMP-2, therefore confirming that osteogenic differentiation had occurred for both ASCs-homotypic CS in osteogenic conditions and heterotypic CSs (both culturing conditions).

3.3.5. Histological cross-sections

The mineralization of the proposed heterotypic CS was also demonstrated by the presence of the late-stage differentiation marker osteocalcin in the histological sections of the CSs. Similar to previous results, an enhanced deposition of osteocalcin was verified for both culture conditions in the heterotypic CS. Moreover, the formation of bone-like tissue was confirmed through the presence of lamin A, a protein of the nuclear envelope that is required for normal bone turnover,[34] and by the expression of CD44, an transmembrane glycoprotein involved in bone formation.[35,36] Again, the presence of such markers was verified after 21 days in both culturing conditions (**Figure IV.6**).

To corroborate the enhanced mineralization of the proposed heterotypic CS, the presence of calcium deposits was also accessed in the cross-sections of the CS through a Von Kossa staining. **Figure IV.7** reveals the deposition of calcium minerals within the *de novo* matrix formation after 21 days in both culturing conditions.

Moreover, the deposition of ECM within the heterotypic CS was accessed by Trichrome Masson, fibronectin and collagen IV stainings (**Figure IV.6, IV.7**). Results show that the proposed tissue-like

constructs are composed by a dense ECM with a collagen enriched matrix in both culturing conditions (**Figure IV.7** and **Figure IV.S12**).

Figure IV.6: Immunostaining of paraffin-embedded heterotypic CS after 21 days in both culturing conditions: osteocalcin, lamin A, CD44, collagen IV and fibronectin (red) and DAPI (in blue) stains all nuclei.

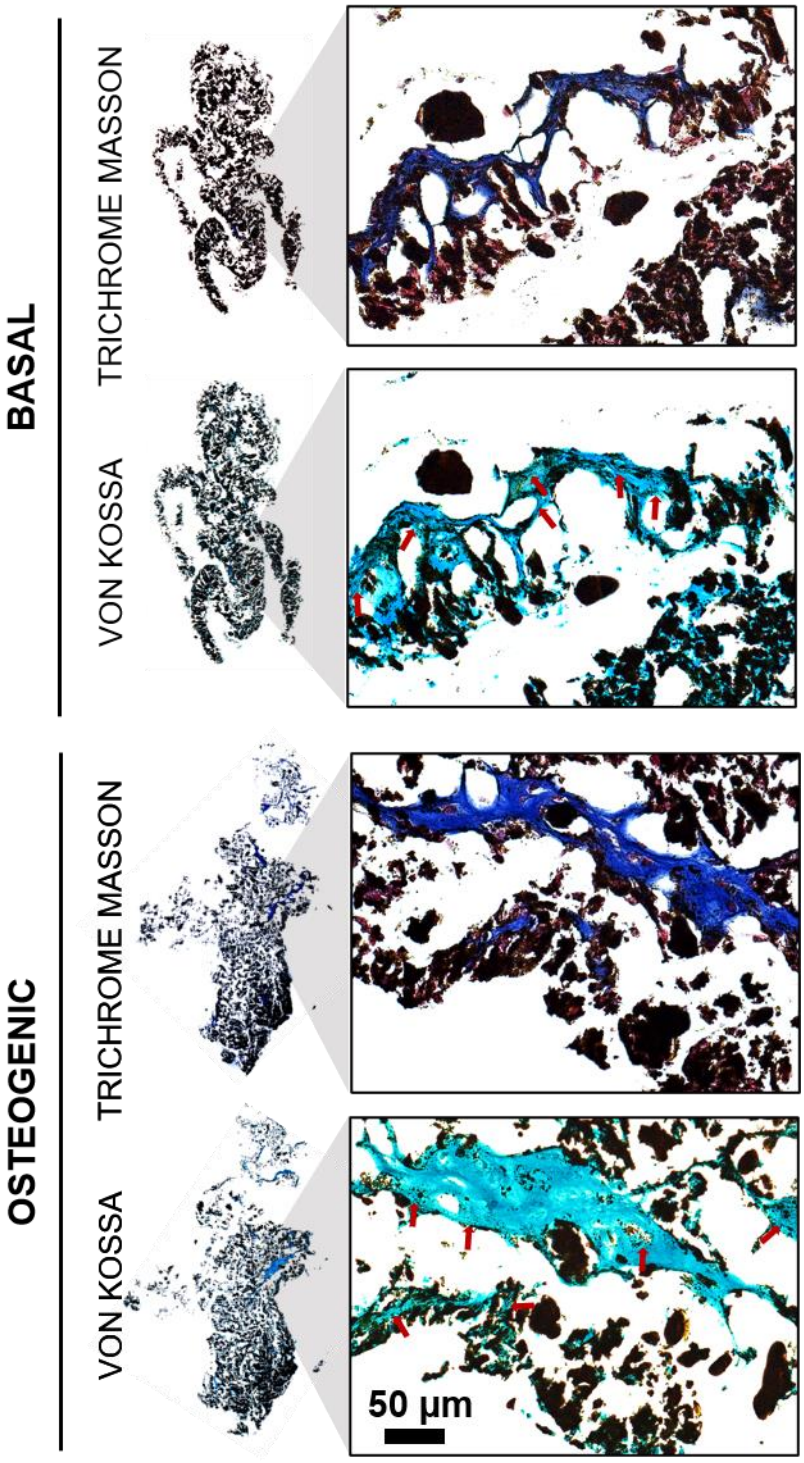

Figure IV.7: Histological sections of heterotypic CS cultured under basal (**A**) and osteogenic media (**B**) after 21 days. Trichrome Masson staining displays the collagenous connective tissue fibers and Von Kossa staining corroborates the mineralization of the heterotypic CS (calcium deposits are identified with red arrows).

4. Discussion

CS technology enables the fabrication of an entirely natural neo-tissue assembled by cells with mature ECM.[29] Nevertheless, one of the major shortcomings in the fabrication of 3D cell-like tissue from CSs is their poor mechanical properties that not only makes handling difficult, but also could compromises the proper function of tissue-like constructs.[15] Moreover, CSs tend to contract when removed from culture surfaces resulting in reduced graft sizes. Such limitations can be overcome through the construction of thicker tissues, with adequate morphologies and dimensions to fit several defects, guarantying the natural architecture of the living tissues.[37]

Within tissues and organs, cell-cell interactions are essential to maintain normal physiological conditions, playing a fundamental role in the regulation of the proliferation and differentiation of tissues.[38] In particular, homotypic and heterotypic cell-cell interactions are believed to be important in the activation of the cellular functions and in the development of more rigid and strong structures.[17] Current methodologies to produced stratified and heterotypic CSs comprise the use of the well-described thermo-responsive surfaces often associated with extra apparatus like CS layering manipulator or even automatic devices,[39,40] which requires user-knowledge, a clean room and the cost for apparatus fabrication. Moreover, such methodologies are also correlated with several constrains such as high cost, alteration of cell physiology and restriction in tissue replacement.[15,41] To overcome such limitations, Mag-TE have prompted the combination of magnetite nanoparticles and magnetic force in TE applications.[18] Cells are previously labelled with magnetic nanoparticles and then, external magnetic force promote cell-cell interactions. Magnetic cells are herein employed as building blocks for the construction of 3D tissues without requiring further artificial scaffolds. In addition, magnetic resonance imaging has been also exploring these magnetic cells as a promising candidates to assess the implanted cells and tissues, in an easier, rapid and non-invasive manner.[42,43] Despite of the physical modifications and biodegradation of MNPs along the time, it is reported that living organisms present an excellent tolerance profile for smaller spherical iron oxide nanoparticles, coordinating specific mechanisms that retard the release of free cytotoxic iron ions, until being released in a safe form.[44] Our group has been exploring the development of hierarchical 3D tissues by Mag-TE in a simple, one-pot and time-saving manner.[10] Nevertheless, the problematic associated with high complexity of living tissues and poor mechanical properties of CSs prevails and restricts their use in the creation 3D-like tissues.[37] Based on this knowledge, we herein proposed the fabrication of mechanically strong and complex-shaped magnetic CSs with an ordered and stratified conformation able to mimic the native structure of

tissues. Although we hypothesized that such organization could be used for bone TE purposes, we anticipate that the methodology herein proposed could be further used for the creation of wide range of 3D-tissues with diverse morphologies, thus demonstrating the ability of this technology in the fabrication of different CSs shapes able to fit specific tissue defects.

After confirming the successful construction of homotypic CSs composed by MC3T3-E1, we herein report the construction of robust homotypic CSs with enhanced mechanical properties using the MC3T3-E1 cell line. To the best of our knowledge, this is the first time that the mechanical behavior of cell-based constructs was accessed. In fact, an Young's Modulus of 22 ± 5 kPa was obtained for this type of CS, attaining similar values to the ones reported in the literature for soft tissues namely cornea, breast tissue, muscle and skin.[38,45] Moreover, the Young's modulus of our engineered tissue is analogous to the cartilaginous tissue model, ranging from 9 to 42 kPa.[46] Regarding the elongation rate, we herein obtained the value of 55 ± 6 % that is also similar to those find in bone-guided membranes.[47,48] Such flexible behavior represents an advantage in CS engineering by providing an easier handling of CSs that are normally damaged during the recovery process.[49] To explore the versatility of such methodology, we developed complex-shaped homotypic CSs with round, ring and concave shape exploring different types of substrates and magnet shapes. Such achievement testified the advantage of Mag-TE in the construction of tissues able to fit different shapes of defects, thus expanding their application in the TE field. Additionally, the role of cell density in CS's thickness and robustness was also investigated along time (7, 14 and 21 days). As expected, we obtained more robust CSs with increased cell density. Literature reports that the lack of sufficient vascularization induces necrosis in bioengineered tissue thicker than 100–200 μm.[20] In this work, our constructs presented the maximum thickness of 70.5 μm without presenting risks of necrosis. Nevertheless, the thickness of the CS decreased along the time, which demonstrated more CS confine and thus suggested greater cell-cell interactions and CS stratification.[50] In 3D-like constructs, the establishment of heterogeneous cell culture systems is crucial to mimic tissues and organs.[51] By taking advantage of this knowledge, we hypothesized the possibility to create stratified heterotypic CSs by magnetically forcing both homotypic and heterotypic cell-cell interactions. For the purpose, magnetically labelled ASCs were seeded on top of a previously assembled (24 h before) monolayer of magnetically labelled MC3T3-E1, creating a CS with a double layer conformation. To attest the interaction between the two cell phenotypes within the CS, we evaluated the ability of MC3T3-E1 inducing osteogenic differentiation over ASCs, even in the absence of osteogenic supplements. Firstly, MC3T3-E1 and ASCs-homotypic CSs were successfully engineered (**Figure IV.1**) and used as controls. Then, the heterotypic CS with a double layer

conformation was developed, as demonstrated by confocal microscopy (**Figure IV.3A**). After confirming their structural conformation by SEM, the cell-cell interactions within the heterotypic CS were also confirmed through a vinculin red-staining (**Figure IV.3C**). Later, the synergetic interaction between MC3T3-E1 and ASCs was confirmed through the osteogenic differentiation of the CSs. MC3T3-E1, as pre-osteoblastic cell linage, has been widely explored as model for *in vitro* osteoblast differentiation. In fact, MC3T3-E1 present similar behavior to primary osteoblasts and are already anticipated to exhibit osteogenic markers.[52] Previous works showed that osteoblasts have a great ability to modulate the osteogenic differentiation of stromal cells without requiring any osteogenic supplementation.[52–54] However, to the best of our knowledge such behavior was never tested in layered scaffold-free structures.

The stemness of ASCs-homotypic CS, corroborated by the absence of osteogenic markers over time, and the increased concentration of osteogenic markers in the heterotypic CS suggested a positive effect of MC3T3-E1 over ASCs osteogenic differentiation. The stagnation on the metabolic activity together with increased ALP activity (normalized by area) suggested osteogenic differentiation of the heterotypic CS and MC3T3-homotypic CS in both culturing conditions. In contrast, the osteogenic differentiation of the ASCs-homotypic CS only occurred in the presence of osteogenic differentiation factors. Such results corroborated the hypothesis that MC3T3-E1 induced ASCs differentiation in such layered structures. The combination of ASCs CS with MC3T3-E1 CS showed an increment on ALP activity, even with basal culture medium. When compared to heterotypic CS, the homotypic CSs presented a decreased metabolic activity after 21 days, which suggested that the stratification of tissues could promote greater CS's nutrition and consequently cell survival and viability.[55]

Native bone tissue presents an hierarchical organization that comprises both non-mineralized organic component (predominantly Collagen type I) and a mineralized inorganic component composed by apatite minerals.[55] By taking advantage of this expertise, we explored the presence of such indicators in the proposed CSs to demonstrate the potential of this methodology in the creation of mineralized 3D-like *in vitro* tissues.[56] Thick and collagen-enriched matrices were verified in the heterotypic CSs cultured with or without osteogenic differentiation factors. These non-collagenous proteins, including collagen I, ostepontin and osteocalcin, are involved in bone matrix organization and in the intracellular signaling during the osteogenic differentiation, including in the recruitment of osteoblasts to the injured bone and regulation of bone structure and morphology.[57,58] According to **Figure IV.4** and **Figure IV.5D**, osteopontin started to be expressed at day 7, especially when CSs were cultured with osteogenic differentiating factors. Nevertheless,

similar results were obtained for the heterotypic CSs in both culturing conditions after 21 days. A similar tendency was also observed for the secretion of osteocalcin. Moreover, the heterotypic CSs presented higher expression of such osteogenic markers than the MC3T3-E1 homotypic CS, thus suggesting the osteogenic role of the MC3T3-E1 over ASCs. As anticipated, ASCs-homotypic CS only expressed such cytokines under osteogenic supplementation. Such results corroborated the ALP trends above mentioned. Additionally, we also evaluated the mineral component of bone-like tissue that normally comprises a crystalline complex of calcium and phosphate commonly denominated hydroxyapatite.[59] The results of OsteoImage™ demonstrated similar deposition of hydroxyapatite in basal and osteogenic culturing conditions after 21 days, thus suggesting the synergetic interaction between MC3T3-E1 and ASCs within the heterotypic CS. To corroborate these results, the chemical composition of such minerals was also assessed. Once again, analogous Ca/P ratios were obtained after 21 days with both culturing conditions. In fact, the Ca/P ratio was similar to the one found in the apatite minerals in bone matrix, thus suggesting the tendency of the heterotypic CS in simulating the natural structure of bone.[60] After 21 days, the formation of bone-like tissue was also validated through the expression of fibronectin, lamin A, CD44 in both culturing conditions, essential for proper bone formation.[34–36] Moreover, the fibronectin and collagen IV are crucial to the matrix assembly and formation of sheet-like ECM of multicellular tissues, respectively.[61] Such essential ECM proteins were found in the heterotypic CSs developed for both culturing conditions. Additionally, ASCs and osteoblasts are known to be involved in blood vessels formation by secreting pro-angiogenic factors, such as VEGF, combining osteogenesis and vascularization during bone development and growth.[62,63] In this sense, VEGF and BMP-2 have been widely explored in TE to synergically incite angiogenesis and bone formation.[10,64] As anticipated, the heterotypic CSs secreted the highest amount of BMP-2 and more pronounced effect was noticed upon the supplementation with osteogenic differentiating factors. Such results corroborated our hypothesis that the co-culture of ASCs and MC3T3-E1 induced an enhanced release of BMP-2. Moreover, the synergic behavior between VEGF and BMP-2 was also visualized in the developed CSs. Heterotypic CSs and MC3T3-homotypic CS demonstrated an increased osteogenic differentiation after 21 days, presenting low expression of VEGF and consequently, a diminished capacity to induce angiogenesis. Nevertheless, thick and high-dense CSs without adequate vascularization are reported to induce necrosis in tissues.[65,66] To overcome this limitation, the group proved that co-culture with endothelial cells could improve the angiogenic potential of the 3D construct, showing outstanding results in the migration and integration of the CS within the host.[10]

By providing magnetic cells as building blocks, we herein proposed the fabrication of mechanically strong and complex-shaped 3D-like tissues using Mag-TE in a simple, versatile, cost-effective and time-saving fashion. By simply adjusting the shapes of magnet and substrates we could obtain tissue-like constructs to be employed in diverse tissue defects, adapting the cell phenotypes of the CS to be fabricated. Regarding the current biofabrication strategies including the highly-explored 3D bioprinting, the strategy herein proposed does not require sophisticated apparatus or user-knowledge, which can prompt the fabrication of such tissue-like constructs in a large scale, overcoming the challenges of the remote control strategies in TE. 3D bioprinting is still not only facing technical challenges in terms of high-resolution cell deposition, controlled cell distributions and vascularization within complex 3D tissues but also require sophisticated apparatus, increasing the cost of the process and the need of user-knowledge.[67] As demonstrated by the group, the vascularization of the constructs is crucial to fabricate cell-dense tissues for supplying oxygen and nutrients while removing metabolic wastes.[10] According to previous works, this magnetic-based strategy showed the ability to engineer pre-vascularized constructs that were also able to migrate and integrate the host vasculature, overcoming the main issues of 3D bioprinting technique. Additionally, the capability to sequentially accommodate layers of different cells can be useful for the development of complex tissues using bottom-up TE strategies.[68]

By taking advantage of this expertise, the next steps of tissue manufacturing aim to recapitulate the geometry, complexity and architecture of human tissues while guarantying the survival of the 3D tissues and easier interaction with host tissue. An idyllic prospective of Mag-TE would encompass the fabrication of a total scaffold- and biomaterial-free tissue constructs, without internalization of MNPs within cells environment.

5. Conclusion

Current strategies for tissue manufacturing fail to recapitulate the geometry, complexity, strength and longevity of human tissues. Mag-TE has been implied in the production of more complex tissues that are not easily achieved by conventional TE methodologies. Herein, we anticipated that Mag-TE could enable the fabrication of versatile and robust 3D tissues with a biomimetic architecture based on cell phenotype and shapes of the magnet and substrate. Therefore, we proposed the construction of complex-shaped 3D-like tissues (CSs) in a simple, one-pot, versatile, cost-effective and time-saving strategy that could scale-up fabrication of 3D tissues. For the purpose, magnetic cells were used as building blocks and mechanical behavior of CSs was for the first time accessed. Moreover, we also evaluated the influence of cell density and time in the thickness of CSs, a crucial

feature in the development of strong cellular constructs. As a proof-of-concept, we developed more complex and hierarchical 3D tissues using pre-osteoblast MC3T3-E1 cell line and ASCs in a double CS conformation. The ability of this construct for bone regeneration purposes was revealed even in the absence of osteogenic differentiation factors, attesting for the first time the role of the pre-osteoblast cell linage in stromal cells in such kind of living materials. Although this work is intended for bone TE, we anticipate that this methodology could be further extended for a plethora of organized tissues, opening new avenues for the fabrication of 3D constructs that better mimics the complex environmental of native tissues with potential applications in the production of *in vitro* disease models or implantable structures for tissue/organ repair and regeneration.

Acknowledgements

This work was developed within the scope of the project CICECO-Aveiro Institute of Materials, UIDB/50011/2020 & UIDP/50011/2020, financed by national funds through the FCT/MEC and when appropriate co-financed by FEDER under the PT2020 Partnership Agreement and PROMENADE (Ref. PTDC/BTM-MAT/29830/2017). This work was also sponsored by the project ATLAS (ref.ERC-2014-ADG-669858) and through the doctoral grant SFRH/BD/141523/2018 (Lúcia F. Santos).

References

1. E.S. Place, J.H. George, C.K. Williams & M.M. Stevens. Synthetic polymer scaffolds for tissue engineering. *Chem. Soc. Rev.* **38,** 1139–1151 (2009).
2. G. Chan & D.J. Mooney. New materials for tissue engineering: towards greater control over the biological response. *Trends Biotechnol.* **26,** 382–392 (2008).
3. X. Liu & P.X. Ma. Polymeric scaffolds for bone tissue engineering. *Ann. Biomed. Eng*. **32,** 477–486 (2004). .
4. F.J. O'Brien. Biomaterials & scaffolds for tissue engineering. *Mater. Today.* **14,** 88–95 (2011).
5. F.M. Chen & X. Liu. Advancing biomaterials of human origin for tissue engineering. *Prog. Polym. Sci.* **53,** 86–168 (2016).
6. A. Ovsianikov, A. Khademhosseini & V. Mironov. The Synergy of Scaffold-Based and Scaffold-Free Tissue Engineering Strategies. *Trends Biotechnol.* **36,** 348–357 (2018).
7. A. Atala, F. Kurtis Kasper& A.G. Mikos, Engineering complex tissues, *Sci. Transl. Med*. **4,** 1–12 (2012).
8. A. Shahin-Shamsabadi & P.R. Selvaganapathy. Tissue-in-a-Tube: three-dimensional in vitro tissue constructs with integrated multimodal environmental stimulation. *Mater. Today Bio.* **7,** 100070 (2020).
9. C. Norotte, F.S. Marga, L.E. Niklason & G. Forgacs. Scaffold-free vascular tissue engineering using bioprinting. *Biomaterials* **30,** 5910–5917 (2009).
10. A.S. Silva, L.F. Santos, M.C. Mendes & J.F. Mano. Multi-layer pre-vascularized magnetic cell sheets for bone regeneration. *Biomaterials* **231,** 119664 (2020).
11. J. Yang, M. Yamato, C. Kohno, A. Nishimoto, H. Sekine, F. Fukai & T. Okano. Cell sheet

engineering: Recreating tissues without biodegradable scaffolds. *Biomaterials* **26,** 6415–6422 (2005).

12. M. Yamato & T. Okano. Cell sheet engineering. *Mater. Today* **7,** 42–47 (2004).
13. J. Yang, M. Yamato, T. Shimizu, H. Sekine, K. Ohashi, M. Kanzaki, T. Ohki, K. Nishida & T. Okano. Reconstruction of functional tissues with cell sheet engineering. *Biomaterials* **28,** 5033–5043 (2007).
14. T. Owaki, T. Shimizu, M. Yamato & T. Okano. Cell sheet engineering for regenerative medicine: Current challenges and strategies. *Biotechnol. J.* **9,** 904–914 (2014).
15. I.Y. Kim, R. Iwatsuki, K. Kikuta, Y. Morita, T. Miyazaki & C. Ohtsuki. Thermoreversible behavior of κ-carrageenan and its apatite-forming ability in simulated body fluid. *Mater. Sci. Eng.* 1472–1476
16. A. Ito, Y. Takizawa, H. Honda, K. Hata, H. Kagami, M. Ueda & T. Kobayashi. Construction and Harvest of Multilayered Keratinocyte Sheets Using Magnetite Nanoparticles and Magnetic Force. *Tissue Eng.* **10,** 873–880 (2004).
17. E. Castro & J.F. Mano Magnetic Force-Based Tissue Engineering and Regenerative Medicine. *J. Biomed. Nanotechnol.* **9,** 1129–1136 (2013).
18. A. Ito, Y. Takizawa, H. Honda, K. Hata, H. Kagami, M. Ueda & T. Kobayashi. Tissue Engineering Using Magnetite Nanoparticles and Magnetic Force: Heterotypic Layers of Cocultured Hepatocytes and Endothelial Cells. *Tissue Eng*. **10,** 833–840 (2004).
19. J. Dobson. Remote control of cellular behaviour with magnetic nanoparticles. *Nat. Nanotechnol.* **3,** 139–143 (2008).
20. N. Asakawa, T. Shimizu, Y. Tsuda, S. Sekiya, T. Sasagawa, M. Yamato, F. Fukai & T. Okano. Pre-vascularization of in vitro three-dimensional tissues created by cell sheet engineering. *Biomaterials* **31,** 3903–3909 (2010).
21. H. Akiyama, A. Ito, Y. Kawabe & M. Kamihira. Biomaterials Genetically engineered angiogenic cell sheets using magnetic force-based gene delivery and tissue fabrication techniques. *Biomaterials* **31,** 1251–1259 (2010).
22. T. Kito, R. Shibata, M. Ishii, H. Suzuki, T. Himeno, Y. Kataoka, Y. Yamamura, T. Yamamoto, N. Nishio, S. Ito, Y. Numaguchi, T. Tanigawa, J.K. Yamashita, N. Ouchi, H. Honda, K. Isobe & T. Murohara. iPS cell sheets created by a novel magnetite tissue engineering method for reparative angiogenesis. *Sci. Rep.* **3,** 1418 (2013).
23. A. Ito, H. Jitsunobu, Y. Kawabe & M. Kamihira. Construction of Heterotypic Cell Sheets by Magnetic Force-Based 3-D Coculture of HepG2 and NIH3T3 Cells. *J. Biosci. Bioeng*. **104,** 371–378 (2007).
24. T. Courtney, M.S. Sacks, J. Stankus, J. Guan & W.R. Wagner. Design and analysis of tissue engineering scaffolds that mimic soft tissue mechanical anisotropy. *Biomaterials* **27,** 3631–3638 (2006).
25. S. Gil, C.R. Correia & J.F. Mano. Magnetically Labeled Cells with Surface-Modified Fe_3O_4 Spherical and Rod-Shaped Magnetic Nanoparticles for Tissue Engineering Applications. *Adv. Healthc. Mater.* **4,** 883–891 (2015).
26. T. Kikuchi, T. Shimizu, M. Wada, M. Yamato & T. Okano. Automatic fabrication of 3-dimensional tissues using cell sheet manipulator technique. *Biomaterials* **35,** 2428–2435 (2014).
27. G.J. Atkins, D.M. Findlay, P.H. Anderson, H.A. Morris. Target Genes: Bone Proteins. *Vitam. D* **23,** 411–424 (2011).
28. T. Kaito, A. Myoui, K. Takaoka, N. Saito, M. Nishikawa, N. Tamai, H. Ohgushi & H. Yoshikawa. Potentiation of the activity of bone morphogenetic protein-2 in bone regeneration by a PLA-PEG/hydroxyapatite composite. *Biomaterials* **26,** 73–79 (2005).
29. N. Matsuda, T. Shimizu, M. Yamato & T. Okano. Tissue Engineering Based on Cell Sheet Technology. *Adv. Mater.* **19,** 3089–3099 (2007).

30. H. Zhou & J. Lee. Nanoscale hydroxyapatite particles for bone tissue engineering. *Acta Biomater.* **7,** 2769–2781 (2011).
31. B.W. T, J.D. Pasteris. A mineralogical perspective on the apatite in bone. *Materials Science and Engineering: C* **25,** 131–143 (2005).
32. S. Raynaud & E. Champion. Calcium phosphate apatites with variable Ca / P atomic ratio II . Calcination and sintering. *Biomaterials* **23,** 1073–1080 (2002).
33. C.R. Correia, R.P. Pirraco, M.T. Cerqueira, A.P. Marques, R.L. Reis & J.F. Mano. Semipermeable Capsules Wrapping a Multifunctional and Self-regulated Co-culture Microenvironment for Osteogenic Differentiation. *Sci. Rep.* **6,** 21883 (2016).
34. W. Li, L.S. Yeo, C. Vidal, T. McCorquodale, M. Herrmann, D. Fatkin & G. Duque. Decreased Bone Formation and Osteopenia in Lamin A/C-Deficient Mice. *PLoS One*. **6,** e19313 (2011).
35. R. Sackstein, J.S. Merzaban, D.W. Cain, N.M. Dagia, J.A. Spencer, C.P. Lin, R. Wohlgemuth. Ex vivo glycan engineering of CD44 programs human multipotent mesenchymal stromal cell trafficking to bone. *Nat. Med.* **14,** 181–187 (2008).
36. T.J. de Vries, T. Schoenmaker & W. Beertsen, R. van der Neut, V. Everts. Effect of CD44 deficiency on in vitro and in vivo osteoclast formation. *J. Cell. Biochem.* **94,** 954–966 (2005).
37. C.K. Griffith, C. Miller, R.C.A. Sainson, J.W. Calvert, N.L. Jeon, C.C.W. Hughes & S.C. George. Diffusion limits of an in vitro thick prevascularized tissue. *Tissue Eng.* **11,** 257–266 (2005).
38. J.F. Mano, R.A. Sousa, L.F. Boesel, N.M. Neves & R.L. Reis. Bioinert, biodegradable and injectable polymeric matrix composites for hard tissue replacement: State of the art and recent developments. *Compos. Sci. Technol.* **64,** 789–817 (2004).
39. N. Asakawa, T. Shimizu, Y. Tsuda, S. Sekiya, T. Sasagawa, M. Yamato, F. Fukai & T. Okano. Pre-vascularization of in vitro three-dimensional tissues created by cell sheet engineering. *Biomaterials* **31,** 3903–3909 (2010).
40. N. Yamada, T. Okano, H. Sakai, F. Karikusa, Y. Sawasaki & Y. Sakurai. Thermo-responsive polymeric surfaces; control of attachment and detachment of cultured cells. *Die Makromol. Chemie, Rapid Commun.* **11,** 571–576 (1990).
41. M. Nakayama, T. Okano & F.M. Winnik. Poly(N-isopropylacrylamide)-based Smart Surfaces for Cell Sheet Tissue Engineering. *Mater. Matters* **5,** 56 (2010).
42. H. Xu, S.F. Othman & R.L. Magin. Monitoring Tissue Engineering Using Magnetic Resonance Imaging. J*. Biosci. Bioeng.* **106,** 515–527 (2008).
43. K.. J. Saldanha, S.L. Piper, K.M. Ainslie, H.T. Kim & S. Majumdar. Magnetic resonance imaging of iron oxide labelled stem cells: applications to tissue engineering based regeneration of the intervertebral disc. *Eur. Cells Mater.* **16,** 17–25 (2008).
44. L. Lartigue, D. Alloyeau, J. Kolosnjaj-Tabi, Y. Javed, P. Guardia, A. Riedinger, C. Péchoux, T. Pellegrino, C. Wilhelm, F. Gazeau. Biodegradation of iron oxide nanocubes: High-resolution in situ monitoring. *ACS Nano* **7**, 3939–3952 (2013).
45. C.T. McKee, J.A. Last, P. Russell & C.J. Murphy. Indentation versus tensile measurements of young's modulus for soft biological tissues. *Tissue Eng. - Part B Rev.* **17,** 155–164 (2011).
46. S. Miyata, T. Numano, K. Homma, T. Tateishi & T. Ushida. Feasibility of noninvasive evaluation of biophysical properties of tissue-engineered cartilage by using quantitative MRI. *J. Biomech.* **40,** 2990–2998 (2007).
47. C. Xianmiao, L. Yubao, Z. Yi, Z. Li, L. Jidong & W. Huanan. Properties and in vitro biological evaluation of nano-hydroxyapatite/chitosan membranes for bone guided regeneration. *Mater. Sci. Eng. C* **29,** 29–35 (2009).
48. M.A. Basile, G.G. D'Ayala, M. Malinconico, P. Laurienzo, J. Coudane, B. Nottelet, F. Della Ragione & A. Oliva, Functionalized PCL/HA nanocomposites as microporous membranes for bone regeneration. *Mater. Sci. Eng. C* **48,** 457–468 (2015).
49. A. Ito, K. Ino, T. Kobayashi & H. Honda. The effect of RGD peptide-conjugated magnetite cationic liposomes on cell growth and cell sheet harvesting. *Biomaterials* **26,** (2005) 6185–

6193.
50. T.J. Klein, B.L. Schumacher, T.A. Schmidt, K.W. Li, M.S. Voegtline, K. Masuda, E.J.M.A. Thonar & R.L. Sah. Tissue engineering of stratified articular cartilage from chondrocyte subpopulations. *Osteoarthr. Cartil.* **11,** 595–602 (2003).
51. Y. Haraguchi, T. Shimizu, M. Yamato & T. Okano. Scaffold-free tissue engineering using cell sheet technology. *RSC Adv*. **2,** 2184–2190 (2012).
52. A. Birmingham & L.M. McNamara. Osteogenic differentiation of mesenchymal stem cells is regulated by osteocyte and osteoblast cells in a simplified bone niche. *Eur. Cells Mater.* **23,** 13–27 (2012).
53. A. Tevlek, S. Odabas, E. Çelik & H.M. Aydin. Preparation of MC3T3-E1 cell sheets through short-term osteogenic medium application. *Artif. Cells, Nanomedicine, Biotechnol.* **46,** 1145–1153 (2018).
54. S. Nadine, S.G. Patrício, C.R. Correia & J.F. Mano. Dynamic microfactories co-encapsulating osteoblastic and adipose-derived stromal cells for the biofabrication of bone units. *Biofabrication* **12,** 015005 (2019).
55. M.M. Stevens. Biomaterials for bone tissue engineering. *Mater. Today* **11,** 18–25 (2008).
56. M.B. Keogh, F.J. O'Brien & J.S. Daly. A novel collagen scaffold supports human osteogenesis - Applications for bone tissue engineering. *Cell Tissue Res.* **340,** 169–177 (2010).
57. Z. Lin, K.L. Solomon, X. Zhang, N.J. Pavlos, T. Abel, C. Willers, K. Dai, J. Xu, Q. Zheng & M. Zheng. In vitro evaluation of natural marine sponge collagen as a scaffold for bone tissue engineering. *Int. J. Biol. Sci*. **7,** 968–977 (2011).
58. R. Marom, I. Shur, R. Solomon & D. Benayahu. Characterization of adhesion and differentiation markers of osteogenic marrow stromal cells. *J. Cell. Physiol.* **202,** 41–48 (2005).
59. T.A. Grünewald, H. Rennhofer, B. Hesse, M. Burghammer, S.E. Stanzl-Tschegg, M. Cotte, J.F. Löffler, A.M. Weinberg & H.C. Lichtenegger. Magnesium from bioresorbable implants: Distribution and impact on the nano- and mineral structure of bone. *Biomaterials* **76,** 250–260 (2016).
60. B. Wopenka & J.D. Pasteris. A mineralogical perspective on the apatite in bone. *Mater. Sci. Eng. C* **25,** 131–143 (2005).
61. C. Werner, T. Pompe & K. Salchert. Modulating extracellular matrix at interfaces of polymeric materials. *Adv. Polym. Sci.* **203,** (2006) 63–93.
62. M.M.L. Deckers, R.L. van Bezooijen, G. van der Horst, J. Hoogendam, C. van der Bent, S.E. Papapoulos & C.W.G.M. Löwik, Bone Morphogenetic Proteins Stimulate Angiogenesis through Osteoblast-Derived Vascular Endothelial Growth Factor A. *Endocrinology* **143,** 1545–1553 (2002).
63. F. Verseijden, H. Jahr, S.J. Posthumus-van Sluijs, T.L. Ten Hagen, S.E.R. Hovius, A.L.B. Seynhaeve, J.W. van Neck, G.J.V.M. van Osch & S.O.P. Hofe. Angiogenic Capacity of Human Adipose-Derived Stromal Cells During Adipogenic Differentiation: An *In Vitro* Study. *Tissue* Eng. Part A. **15,** 445–452 (2009).
64. X. Jiang & D.L. Kaplan. VEGF and BMP-2 promote stem cell homing. *Eur. Cells Mater*. **27,** 1–12 (2014).
65. K. Moschouris, N. Firoozi & Y. Kang. The application of cell sheet engineering in the vascularization of tissue regeneration, *Regen. Med.* **11,** 559–570 (2016).
66. Y. Naka, S. Kitano, S. Irie & M. Matsusaki. Wholly vascularized millimeter-sized engineered tissues by cell-sized microscaffolds. *Mater. Today Bio*. **6,** 100054 (2020).
67. E.S. Bishop, S. Mostafa, M. Pakvasa, H.H. Luu, M.J. Lee, J.M. Wolf, G.A. Ameer, T.C. He & R.R. Reid. 3-D bioprinting technologies in tissue engineering and regenerative medicine: Current and future trends. *Genes Dis.* **4,** 185–195 (2017).
68. V.M. Gaspar, P. Lavrador, J. Borges, M.B. Oliveira & J.F. Mano. Advanced Bottom-Up

Engineering of Living Architectures, *Adv. Mater.* **6,** 1903975 (2019).

.

Supporting Information

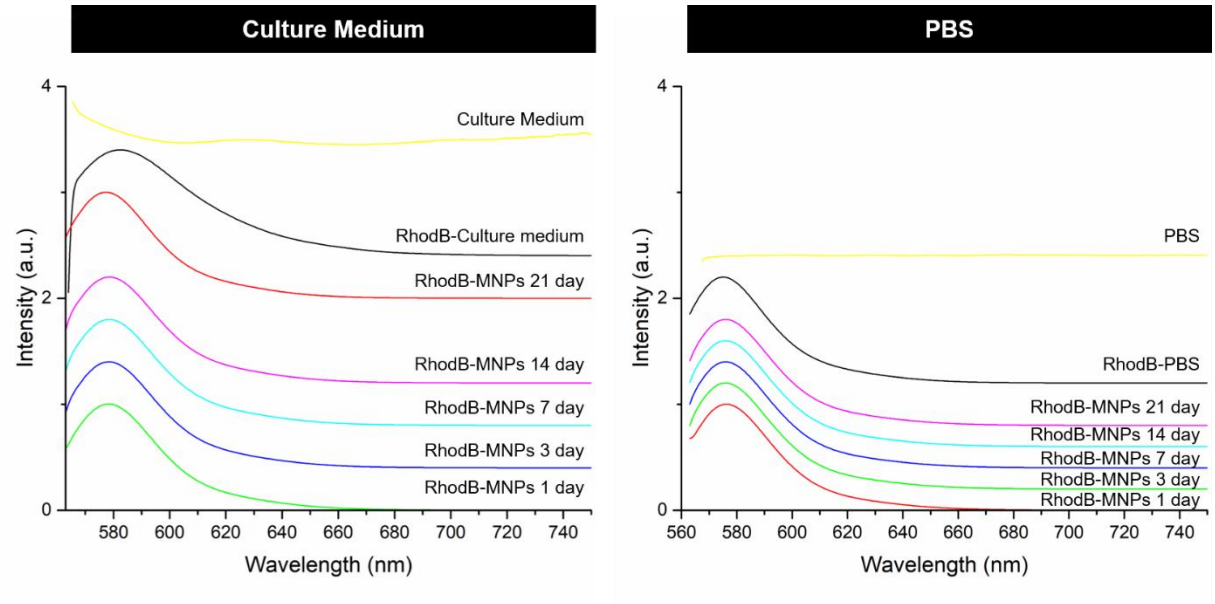

Figure IV.S1: Stability of RhodB-MNPs incubated in dPBS and α-MEM culture medium during 21 days at 37°C.

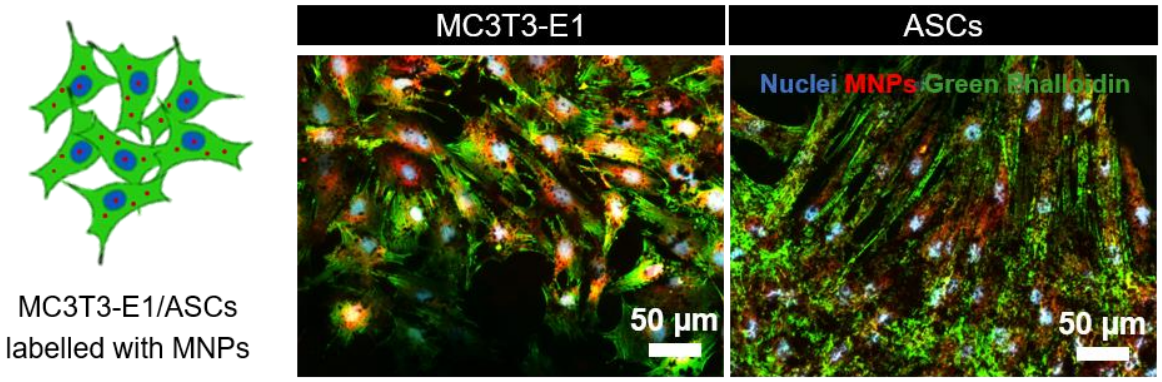

Figure IV.S2: Cellular uptake of RhodB-MNPs in ASCs and MC3T3-E1: actin filaments of MC3T3-E1 and ASCs (green phalloidin), RhodB-MNPs (red) and cell nucleus - DAPI (blue).

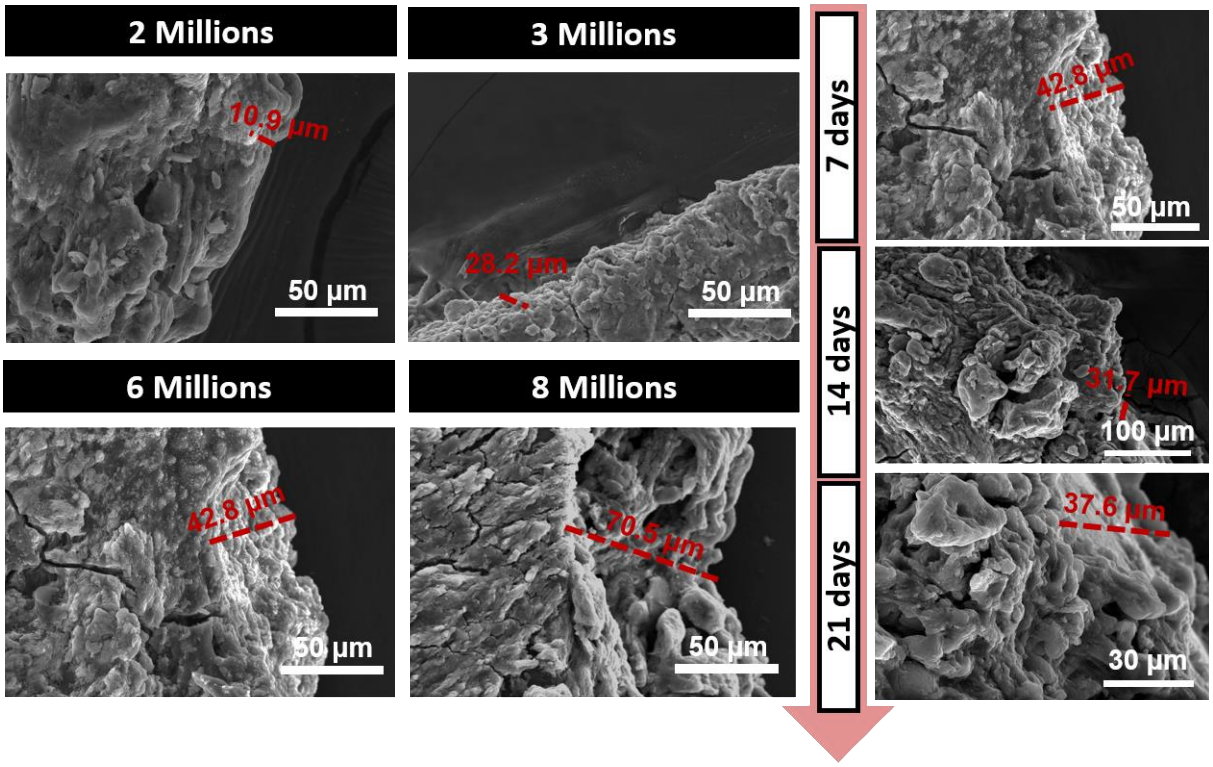

Figure IV.S3: SEM micrographs of the developed MC3T3-homotypic CS with different cell density (namely 2, 3, 6 and 8 million cells) and along the time (at 7, 14 and 21 days).

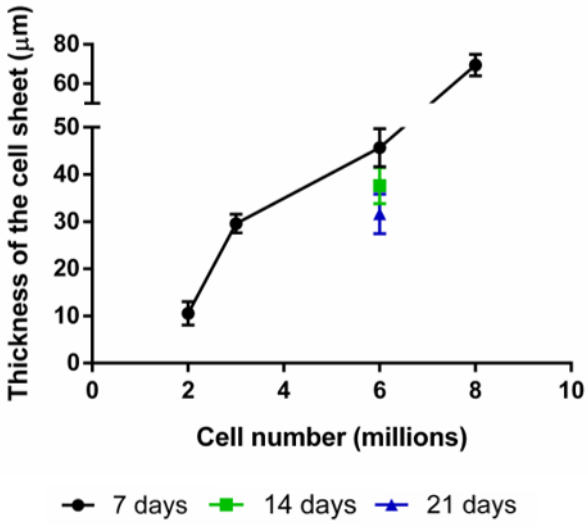

Figure IV.S4: Graphical representation of the thickness of the CS along the time and varying the cell density.

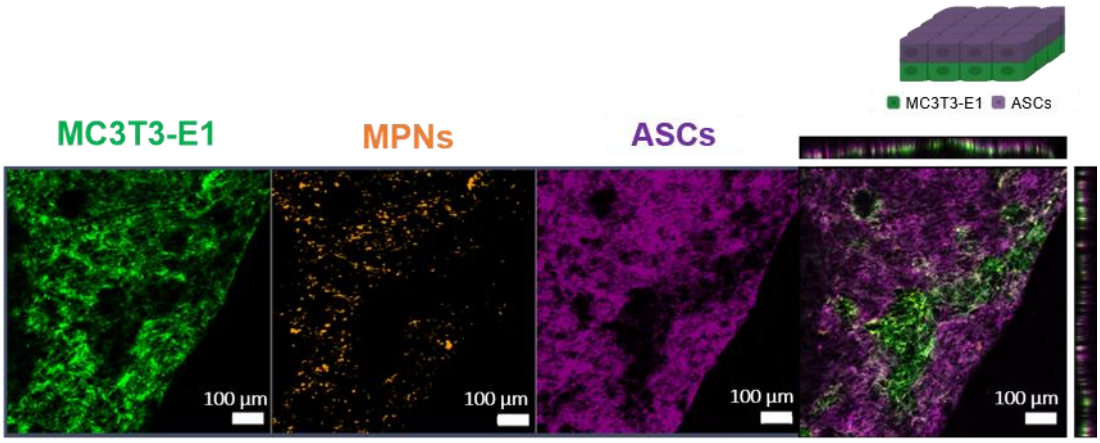

Figure IV.S5: Confocal microscopy of the magnetically labelled CS composed by MC3T3-E1 (green) and ASCs (purple) in double sheet conformation.

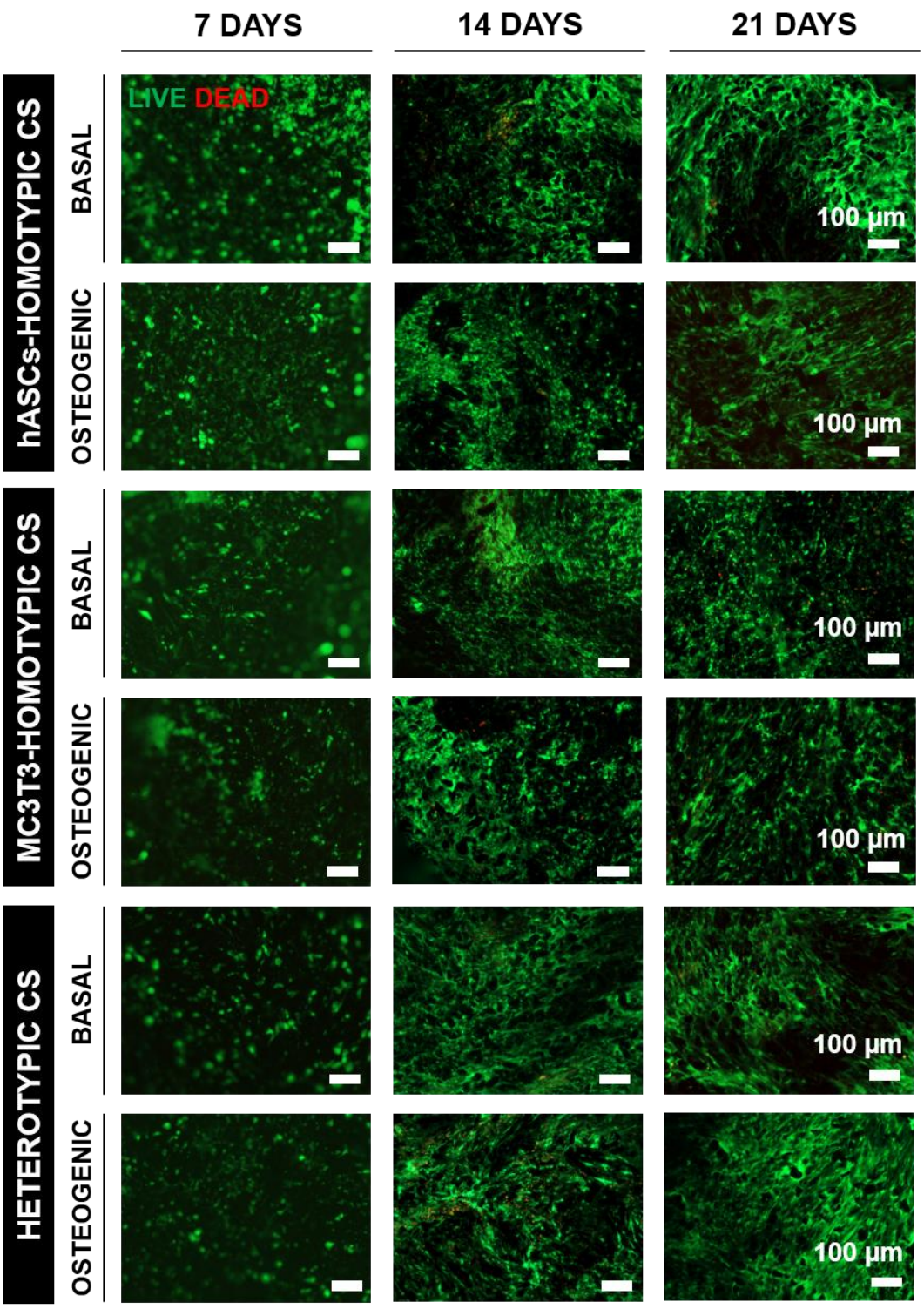

Figure IV.S6*:* Live-dead fluorescence assay *of homotypic and heterotypic CSs after* 7, 14 and 21 of culture in basal and osteogenic *conditions.* Living cells were stained by calcein (green) and dead cells by propidium iodide (red).

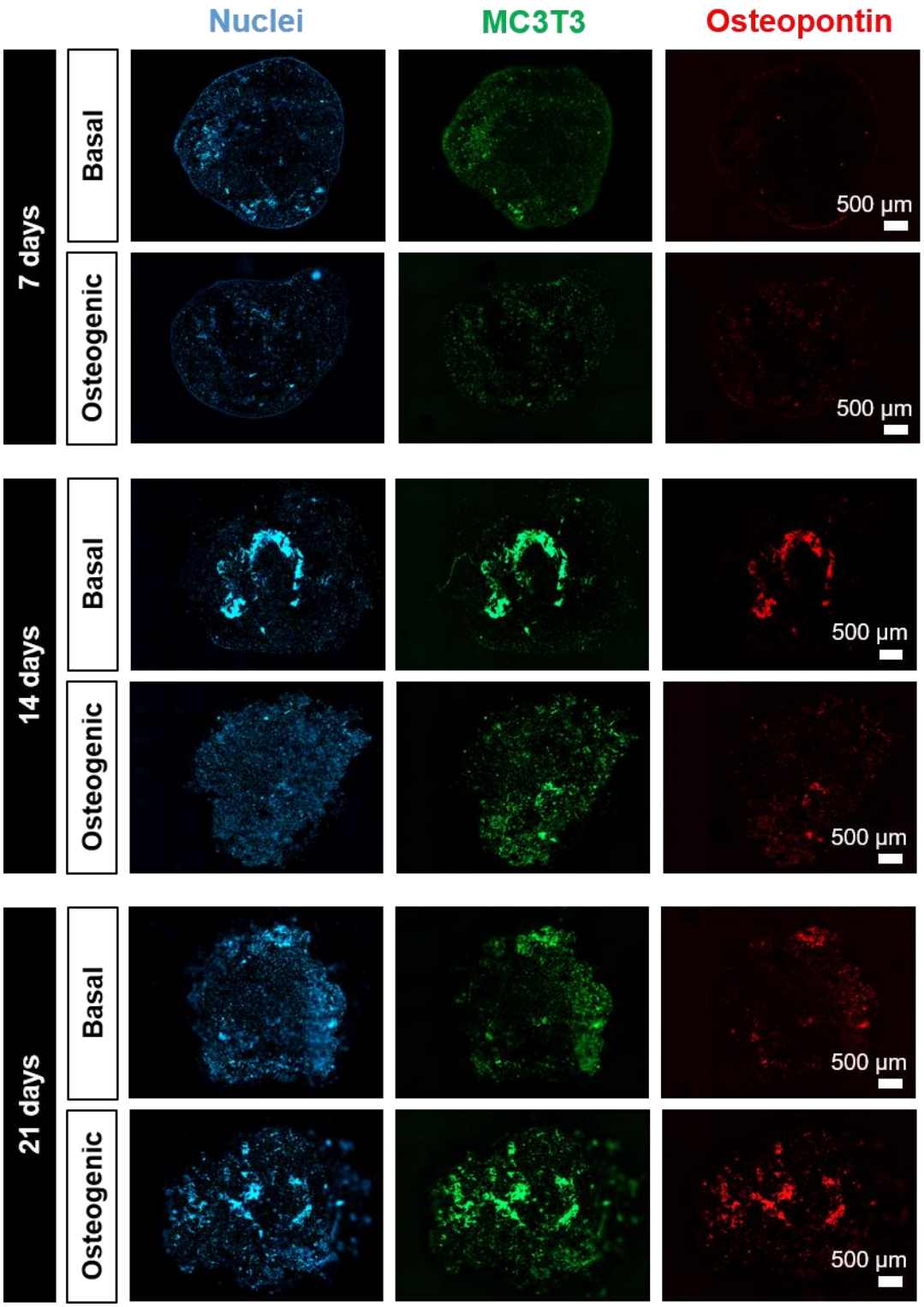

Figure IV.S7: Immunofluorescence of MC3T3-homotypic CS after 7, 14 and 21 days in both culture conditions: MC3T3-E1 (green), osteopontin (red) and cell nucleus-DAPI (blue).

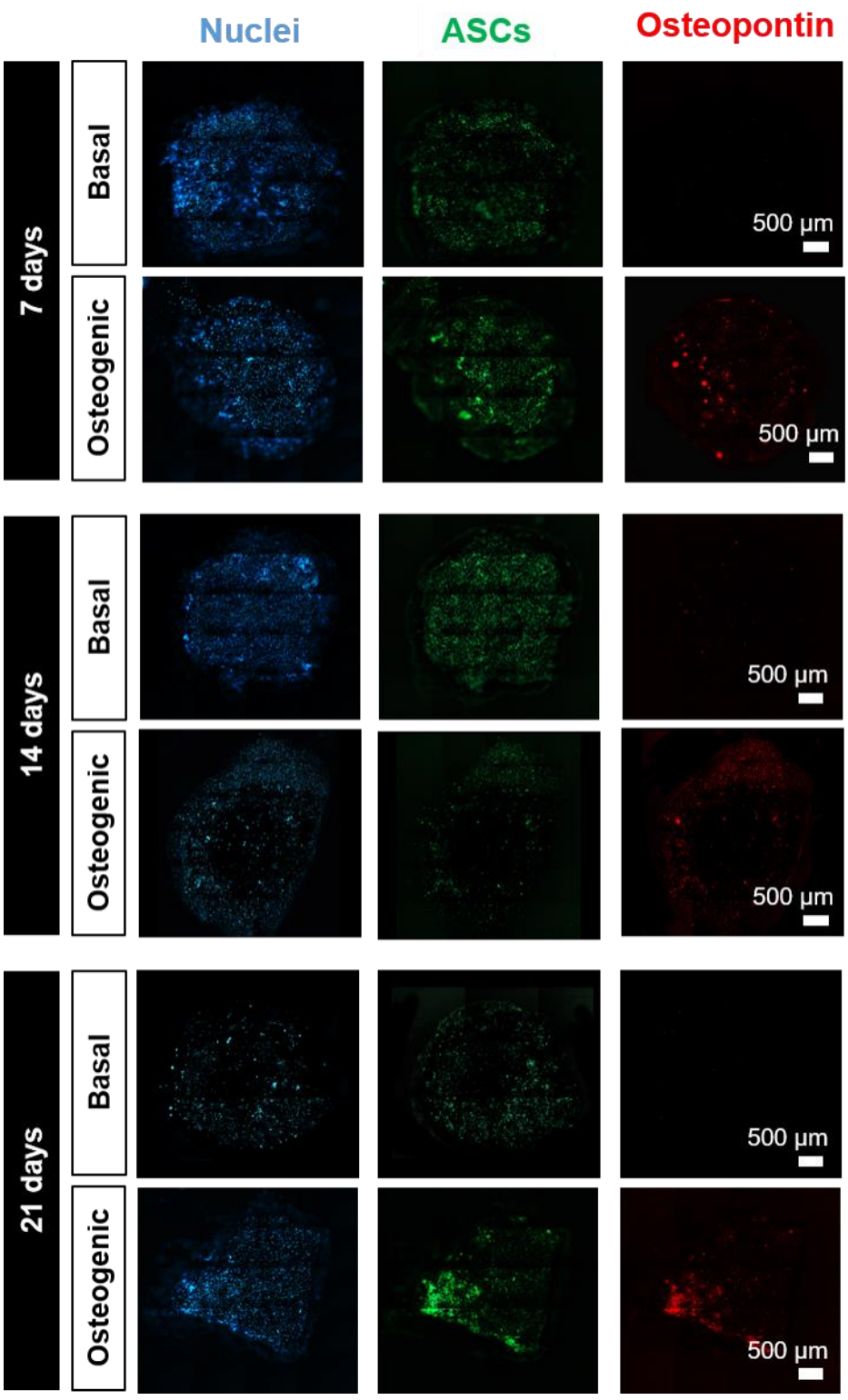

Figure IV.S8: Immunofluorescence of ASCs-homotypic CS after 7, 14 and 21 days in both culture conditions: ASCs (green), osteopontin (red) and cell nucleus-DAPI (blue).

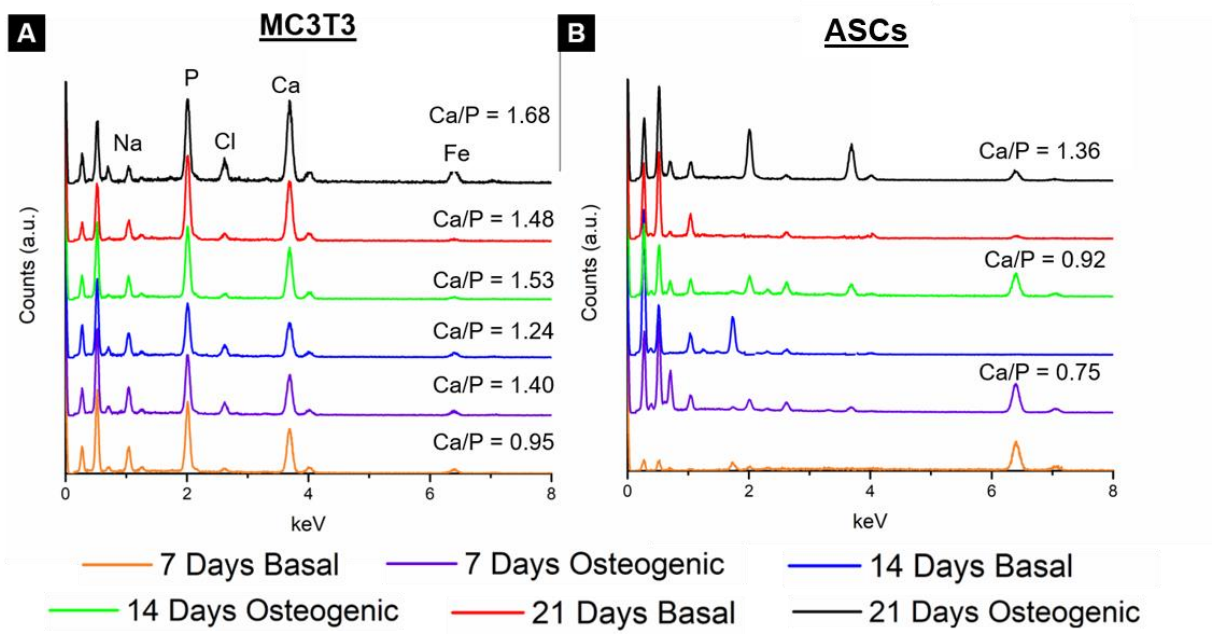

Figure IV.S9: Energy dispersive X-ray spectroscopy (EDS) spectra of deposited minerals in CSs composed by MC3T3-E1 or ASCs after 7, 14 and 21 days in both basal and osteogenic conditions.

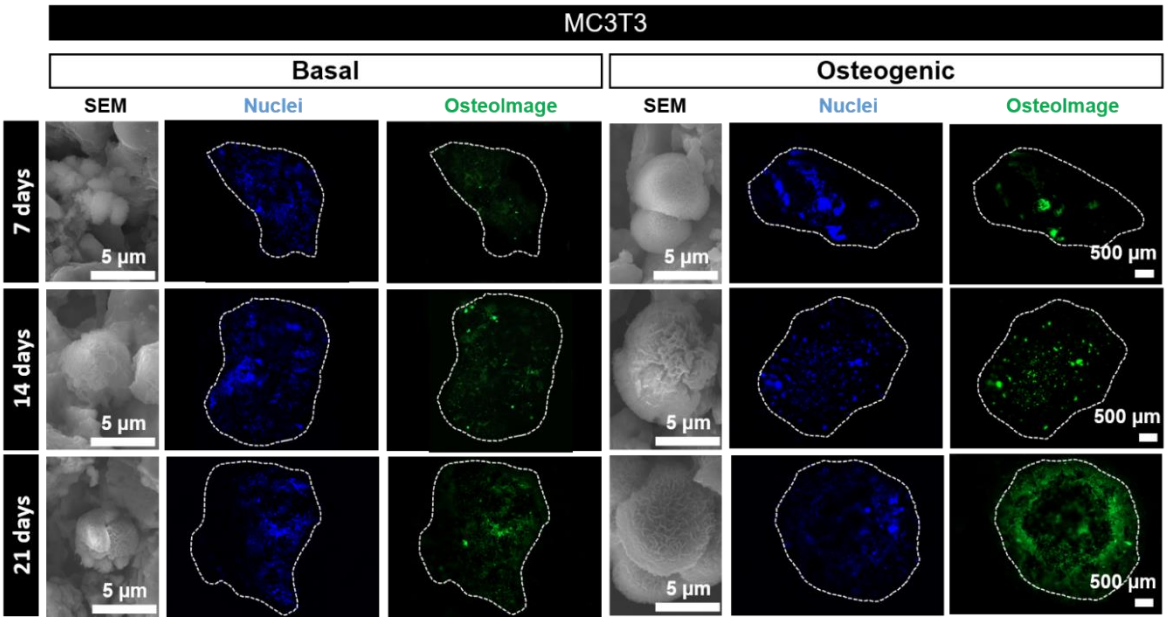

Figure IV.S10: Assessment of the of hydroxyapatite portion of bone-like nodules deposition in MC3T3-homotypic CS through fluorescent OsteoImage™ Mineralization Assay: cell nucleus - DAPI (blue) and hydroxyapatite (green). Calcium deposits were also identified in SEM micrographs (right panel).

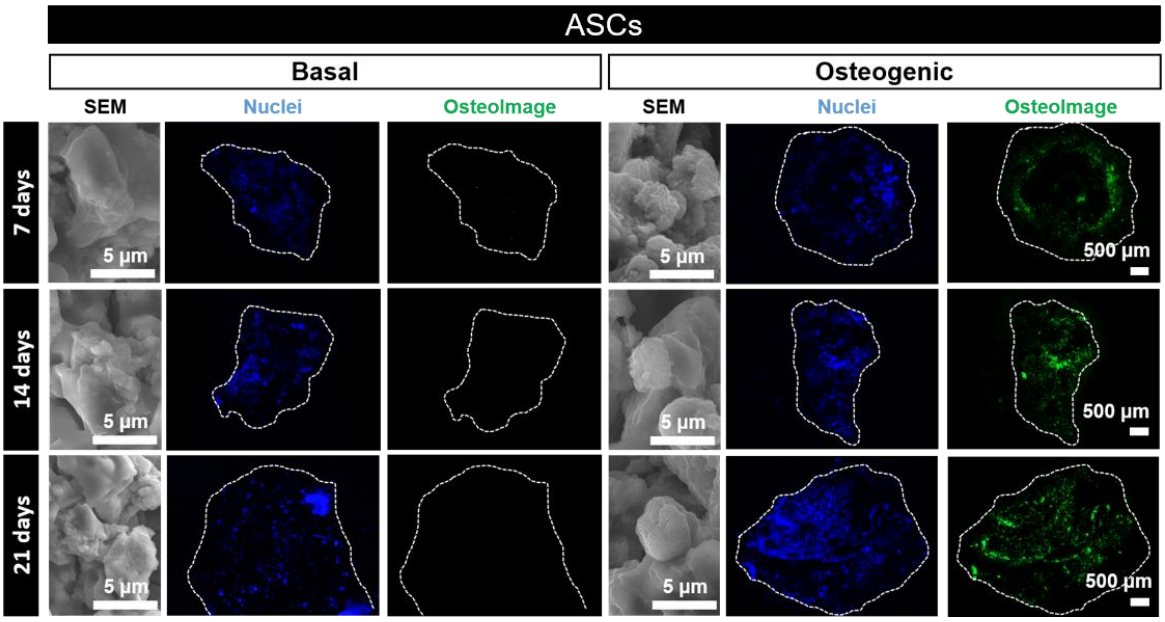

Figure IV.S11: Assessment of the of hydroxyapatite portion of bone-like nodules deposition in ASCs-homotypic CS through fluorescent OsteoImage™ Mineralization Assay: cell nucleus - DAPI (blue) and hydroxyapatite (green). Calcium deposits were also identified in SEM micrographs (right panel).

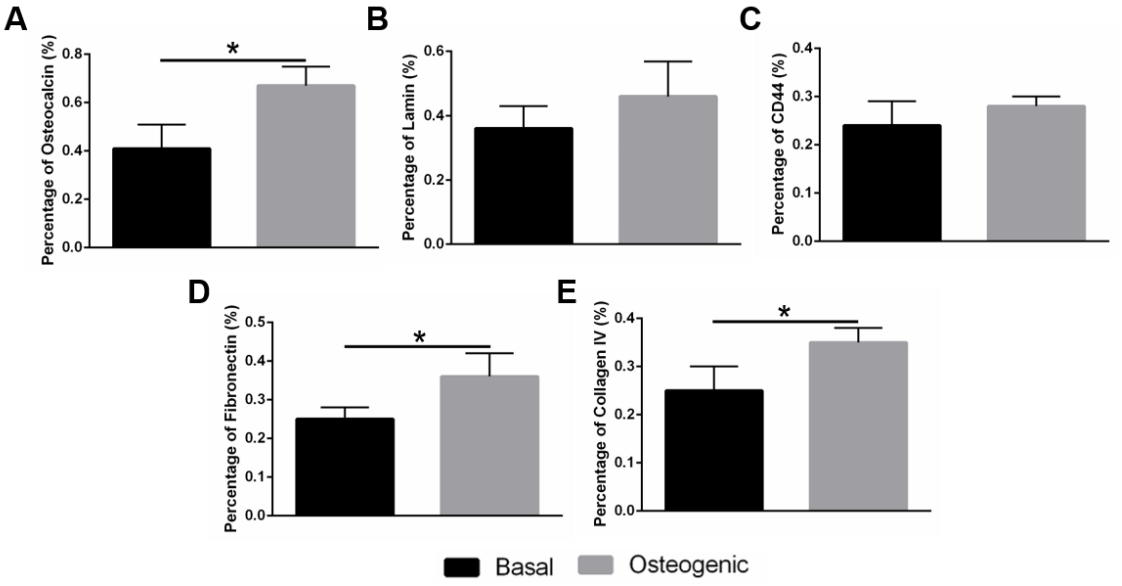

Figure IV.S12: Percentage of osteocalcin (**A**), lamin (**B**), CD44 (**C**), fibronectin (**D**) and collagen IV (**E**) in the representative histological cuts (displayed in Figure 6) of CSs cultured in basal and osteogenic conditions.

Chapter V - Multi-layer pre-vascularized magnetic cell sheets for bone regeneration[3]

Abstract

The lack of effective strategies to produce vascularized 3D bone transplants *in vitro,* hampers the development of thick-constructed bone, limiting the translational of lab-based engineered system to clinical practices. Cell sheet (CS) engineering techniques provide an excellent microenvironment for vascularization since the technique can maintain the intact cell matrix, crucial for angiogenesis. In an attempt to develop hierarchical vascularized 3D cellular constructs, we herein propose the construction of stratified magnetic responsive heterotypic CS by making use of iron oxide nanoparticles previously internalized within cells. Magnetic force-based CS engineering allows for the construction of thick cellular multilayers. Results show that osteogenesis is achieved due to a synergic effect of human umbilical vein endothelial cells (HUVECs) and adipose-derived stromal cells (ASCs), even in the absence of osteogenic differentiating factors. Increased ALP activity, matrix mineralization, osteopontin and osteocalcin detection were achieved over a period of 21 days for the heterotypic CS conformation (ASCs/HUVECs/ASCs), over the homotypic one (ASCs/ASCs), corroborating our findings. Moreover, the validated crosstalk between BMP-2 and VEGF releases triggers not only the recruitment of blood vessels, as demonstrated in an *in vivo* CAM assay, as well as the osteogenesis of the 3D cell construct. The *in vivo* angiogenic profile also demonstrated preserved human vascular structures and human cells showed the ability to migrate and integrate within the chick vasculature.

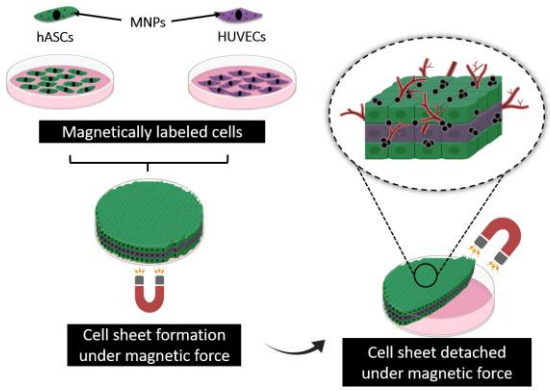

[3]Baseed on the publication: A. Sofia Silva, Lúcia F. Santos, Maria C. Mendes, João F. Mano. Multi-layer pre-vascularized magnetic cell sheets for bone regeneration. *Biomaterials* **231,** 119664 (2020).

1. Introduction

Tissue engineering (TE) aims to develop biological substitutes to replace, repair or regenerate lost tissue function or damaged tissues/organs.[1–5] Despite the notable advances in the field, the struggle in mimicking the complex environment of biological tissues, including vascularization, hampers the fabrication of complex organs limiting translational and clinical success.[2,3,6–8] In fact, traditional TE methods, which either focus on the injection of isolated cell suspensions or on the use of biodegradable scaffolds to support tissue formation, deprive cells of their endogenous extracellular matrix (ECM), which may dampen cell differentiation.[2] Cell-sheet (CS) technology, which has arisen as a reliable alternative to such conventional and limiting strategies,[2–5] allows for the creation of cell-dense tissues that can be harvested as a whole, preserving their ECM.[9] Upon *in vivo* transplantation, tissues fabricated by CS engineering are able to adhere to the surface of the host tissue without suture and form cell-like dense structure,[10] enabling the maintenance of cell-cell interactions that lead to a proper tissue regeneration.[1] CS technology has been applied to several types of tissues such as heart, liver, bladder, bone, cornea and esophagus,[9] with the two latter having achieved successful clinical outcomes.[11] Yet, engineering CS for bone regeneration is still in its infancy. The difficulty in reproducing the high levels of hierarchical organization of bone, including vascularization, may hamper the development of totally functional tissues.[12–15] In fact, engineering thick tissue replacements to fit bone defects depends on rapid and sufficient vascularization in the tissue-engineered constructs, which is a pre-requisite for optimal cell survival and perfect tissue integration *in vivo*.[9] Apart from bone growth, vascularization is also involved in bone healing, both in natural and artificial bone implants.[16] Therefore, tissue ischemia and low mechanical strength of thin CS limits their application towards bone repair. Recent studies have focused on the pre-vascularization of CS for bone regeneration priori *in vivo* implantation in order to promote a vascular network using the thermo-responsive dishes of poly(N-isopropylacrylamide) (PIPAAm) proposed by Okano and co-workers.[5,7,8,17–19] In fact, pre-vascularization strategies have already demonstrated to significantly reduce the time needed to vascularize the implant when compared with approaches that depend on scaffold design and delivery of angiogenic factors. However, both works describing CS pre-vascularization consisted on the individual stacking of previously formed CS monolayers, which may hinder the assembly and stratification of heterotypic cells into complex tissues such as ductlike constructs, and the development of more rigid cell structures.[20] Additionally, such methodology can be time consuming, resulting in thin cell layers difficult to manipulate and encumber to spatially control the positioning of target cells.[21,22] To

circumvent those issues, Ito and co-workers have proposed a successful methodology consisting of magnetically forcing human aortic endothelial cells (HAECs), previously labeled with magnetite cationic liposomes, to deposit and adhere to a surface containing human hepatocytes, promoting cell-cell adhesion to form a 3D construct.[1,23]

More recently, Gil and co-workers have also demonstrated in a proof-of-concept study the ability to create magnetic CSs by making use of rod and sphere shapes of amino-functionalized iron oxide nanoparticles.[24]

In an attempt to develop thick, stratified and hierarchical cellular 3D vascularized constructs to fit bone TE purposes, we herein propose the construction of magnetic responsive heterotypic CS by making use of iron oxide nanoparticles in a concept named magnetic force-based TE (Mag-TE). For this purpose, magnetically labeled adipose-derived stromal cells (ASCs) and human umbilical vein endothelial cells (HUVECs) were organized in a triple sheet conformation with HUVECs in between two sheets of ASCs. By forcing both heterotypic and homotypic cell-cell interactions we attempt to construct thicker and fully functional tissues. These tissues will be able to interact in a synergic trend, easing viability and proliferation as well as the secretion of growth factors and proteins that trigger both osteo- and angiogenesis in the developed tissue construct. Moreover, the sequential deposition of cells enables the accelerated development of a stratified tissue in a one-pot methodology. We therefore hypothesized that our pre-vascularized magnetically labeled CS could orchestrate the right signals towards new bone formation without requiring the supplementation of main osteogenic differentiation factors, such as dexamethasone, ascorbic acid and β-glycerophosphate; and exhibit angiogenic potential both *in vitro* and *in vivo*. The methodology herein used to create pre-vascularized and stratified cell-dense tissue opens new insights for the fabrication and repositioning of complex and higher ordered 3D connected tissue that better resembles the native *in vivo* environment.

2. Materials and Methods

All chemicals were purchased from Sigma-Aldrich and used as received, unless otherwise specified.

2.1. Synthesis and characterization of magnetic nanoparticles

Magnetite nanoparticles (MNPs) were synthesized based on the procedure previously published procedure.[24] Briefly, Fe_3O_4 MNPs were synthesized by the co-precipitation reaction of ferrous ($FeCl_2 .4H_2O$) and ferric ($FeCl_3 .6H_2O$) salts in the presence of ammonium hydroxide (NH_4OH), at

60°C and under a nitrogen atmosphere. Afterwards, MNPs' surface was modified with (3-aminopropyl)triethoxysilane (APTES) through a silanization reaction and then washed with deionized water and ethanol. Consequently, MNPs-APTES were conjugated with rhodamine B isothiocyanate (RodB) (MNPs-RodB). MNPs-APTES (previously freeze dried) were dispersed in ethanol (5 mg/mL) and then RodB (2.5 mg/mL) was added and stirred overnight at RT. Lastly, MNPs-RodB were washed until no traces of RodB were detected and freeze dried. MNPs, MNPs-APTES and MNPs-RodB were visualized by TEM (20kV, HR-TEM20-SE, JEOL), which were previously added dropwise to a carbon film copper grid and. Then, the images were analyzed by Image J software. The successful modification of the particles with APTES was confirmed by attenuated total reflectance (ATR-FTIR) by using a Bruker Tensor 27 spectrometer. The spectra were recorded at a 4 cm^{-1} resolution with a total of 256 scans in the spectral width of 4000-350 cm^{-1}.

2.2. Cell culture and cellular uptake

The collected umbilical cord was obtained under a cooperation agreement between the Aveiro Institute of Materials, University of Aveiro and Hospital do Baixo Vouga (Aveiro, Portugal), after approval of the Competent Ethics Committee (CEC). The human tissues received were handled in accordance with the guidelines approved by the CEC. Informed consent was obtained from all subjects. HUVECs were isolated following well-established protocols in the group. The enzymatic mixture containing dispase II (Sigma-Aldrich) and collagenase type IV (Sigma-Aldrich) was used for the isolation of HUVECs from cord vein. Cord vein was filled with the enzyme cocktail along the multiple site injection of enzyme cocktail in cord matrix. Afterward, the cord was incubated at 37ºC for 20 min and then, HUVECs were seeded in M199 growth medium and incubated in humidified atmosphere of 5% CO_2 at 37ºC. At the end of 4-6h, the medium was changed to M199 containing 20% umbilical cord blood serum (UCBS), 2mM L-glutamine, 5 ng/mL vascular endothelial growth factor, 10 µg/mL heparin, 100 U/mL penicillin and 100 µg/mL streptomycin.[25,26]

Human ASCs (ATCC® PCS-500-011™) were cultured in α-MEM (minimum essential medium, ThermoFisher Scientific), supplemented with 10 % of heat-inactivated FBS (Fetal bovine serum, ThermoFisher Scientific), 100 U/mL of penicillin and 0.1 mg/mL of streptomycin (ThermoFisher Scientific).

The co-location of MNPs-RodB in both HUVECs and ASCs was assessed by seeding both types of cells in well plates at cell densities of 2.4 x 10^6 cells/cm^2 for ASCs and 1.2 x 10^6 cells/cm^2 for HUVECs. Cells were cultured for 24 h at 37 °C and 5% CO_2, followed by a 4-hour incubation with MNPs-RodB at 1mg/mL. Afterwards, cells were retrieved by enzymatic digestion with trypLE Express. The cell

suspension of HUVECs was immunostained with APC anti-human CD31 Antibody (5μL) (Biolegend), whereas the cell suspension of ASCs was immunostained with APC anti-human CD90 Antibody (5μL) (Biolegend) for 45 min. Both samples were washed with a staining washing buffer (2% w/v BSA, 0.1% w/v sodium citrate in PBS) and centrifuged at 500g for 5 min, followed by a resuspension in the acquisition buffer (1% v/v formaldehyde and 0.1% w/v sodium azide in PBS). The double positive cells for the pair CD31 and MNPs-RodB, and the pair CD90 and MNPs-RodB were sorted using a Cell Sorter (BD Accuri C6 Plus).

Cellular uptake was also verified using fluorescent microscopy *a priori* the formation of CSs. For this purpose, ASCs and HUVECs were seeded at the same cellular density previously mentioned and upon 24 hours of incubation at 37 °C and 5% CO_2, MNPs-RodB (1 mg/mL), were added. After 4h cells were washed with PBS and fixed at RT in formalin (10% v/v) for 15 min. Subsequently, cells were incubated with 0.1% (v/v) Triton X100 in dPBS at RT for 5 min and incubated with Flash Phalloidin Green 488 (1:100 in dPBS) during 45 min at RT and then counterstaining with DAPI (1:1000 in dPBS) for 5 min at RT. Fluorescence microscopy analysis was performed using Axio Imager M2 widefield microscope (Carl Zeiss Microscopy GmbH) and using ZEN v2.3 blue edition.

2.3. Development of homotypic and heterotypic magnetic CS

To achieve a heterotypic CS, ASCs and HUVECs were organized in a stratified triple sheet conformation with the endothelial cells layered in between the two sheets of ASCs. For the purpose, ASCs were seeded at density of 2.4 x 10^6 cells/cm^2. After 24 h of incubation at 37 °C and 5% CO_2, MNPs-RodB (1 mg/mL), were added. After 4h, cells were detached by adding trypLE Express followed by a 5 min incubation at 37 °C. Cells were then centrifuged at 300 g and then, the magnetically labeled cells were transferred to ultralow-attachment 24, 48 or 96-well plates (previously treated with 2%, w/v alginate solution during 30 min). Commercial neodymium rod magnets Ø 10 mm, height 40 mm (strength of 108N and standard N41 magnetization) (Supermagnet) were placed at the bottom of the reverse side of the ultralow-attachment plate to provide magnetic force to the plate, during the timeframe of the culture. After 24h, the magnetically labeled HUVECs were added at a density of 1.2 x 10^6 cells/cm^2 on top of the previously established ASCs monolayer. Lastly, 2.4 x 10^6 cells/cm^2 of magnetic labeled ASCs were added (24h after HUVECs magnetic deposition) and the final structure with a triple sheet conformation was cultured for 7, 14 and 21 days. Homotypic CS were used as control and were produced following the same above-mentioned methodology but omitting the addition of HUVECs. A second ASCs layer

was added to the ASCs monolayer after 24h. Homotypic CS were also cultured during 7, 14 and 21 days. Both homotypic and heterotypic CSs were cultured in M199 medium supplement with heparin and ECGS with or without osteogenic differentiation factors, namely dexamethasone (10nM), ascorbic acid (50µg/mL) and β-glycerophosphate (10mM).

2.4. CS characterization

Heterotypic and homotypic CSs cultured for 7 days in basal conditions (no osteogenic factors), were fixed in formalin 10% (v/v) during 15 min at RT. Then, the CSs were permeabilized with 0.1 (v/v) Triton X for 5 min at RT. Afterwards, CSs were immersed in 5 % (v/v) FBS/dPBS for 1h at RT and then incubated with the anti-rabbit human vinculin antibody (1:50 in 5% FBS/dPBS, Invitrogen) for 3h at RT. After washing the samples with PBS, the CSs were incubated with the secondary antibody donkey anti-rabbit AlexaFluor 594 (1:400 in 5% FBS/dPBS). To confirm the presence of HUVECs in the developed heterotypic CSs, a similar immunofluorescence procedure was performed with the addition of the mouse anti-human CD31 (1:50 in 5% FBS/dPBS, BioLegend) conjugated with the secondary antibody goat anti-mouse AlexaFluor 647 (1:400 in 5% FBS/dPBS). The CSs were incubated with Flash Phalloidin Green 488 (1:100 in dPBS) during 45 min at RT and then counterstaining with DAPI (1:1000 in dPBS) for 5 min at RT. Finally, the samples were analyzed by confocal microscopy (LSM 880, ZEISS). The morphology of both homotypic and heterotypic CSs cultured for 7, 14 and 21 days under basal and osteogenic media was also accessed by Scanning Electron Microscopy (SEM). For the purpose, samples were washed with PBS and fixed at RT in formalin (10% v/v) for 15 min. After 1 h, samples were dehydrated in an increasing gradient series of ethanol for 10 min each. The samples were gold sputter-coated using an accelerating voltage of 25 kV and visualized by SEM (S4100, Hitachi, Japan).

2.5. Mitochondrial metabolic activity quantification

Mitochondrial metabolic activity was determined using a MTS colorimetric assay (CellTiter96® AQueous one solution cell proliferation assay, Promega) in agreement to manufacture's specifications. CSs (n=3) were incubated with the reagent kit (120 µl per well) and incubated at 37 °C during 4 h, protected from light. Lastly, the absorbance was read at 490 nm using a microplate reader (Synergy HTX, BioTek Intruments, USA).

2.6. Cell proliferation quantification

Total DNA quantification of the CSs (previously cultured during 7, 14 and 21 days) was performed after cell lysis (Quant-iT™ PicoGreen™ dsDNA Assay Kit, Invitrogen™). CSs (n=3) were suspended in ultra-pure sterile water with 2 % (v/v) Triton 100X during 1 h at 37 °C and then the samples were frozen at −80 °C and stored until further use. Samples were defrosted and used according to the specifications of the kit. MNPs-RodB were magnetically segregated using a neodymium magnet to assure that only DNA content would be selected for the quantification assay. A standard curve for DNA analysis was generated with the provided DNA standard from the DNA assay kit. After 10 min of incubation at RT, fluorescence was read at an excitation wavelength of 485/20 nm and 528/20 nm of emission using a microplate reader (Synergy HTX, BioTek Intruments, USA).

2.7. Cell viability

The survival of the developed CSs was evaluated by a live-dead fluorescence assay according to the manufacturer's recommendation (ThermoFisher Scientific). On days 7, 14, or 21, samples were washed with PBS and then stained with the kit components at 37ºC for 20 min and protected from light. Afterwards, samples were visualized by fluorescence microscopy (Axio Imager 2, Zeiss).

2.8. Analysis of osteogenic differentiation of CS

The ability of HUVECs to induce osteogenic differentiation over ASCs was evaluated in growth medium with and without osteogenic differentiation factor. Homotypic CSs with ACSs were used as control. All CSs were incubated for 7, 14 and 21 days.

2.9. ALP activity measurement assays

After each time point, the CSs were lysed by the same procedure in the section of cell proliferation quantification. ALP activity was determined in the lysates by using 4NPhP ALP-mediated hydrolysis to quantify 4NPh release. 25 µL of each lysate sample was added to 75 µL of a freshly prepared 4NPhP solution (2 mg/mL) in 1M diethanolamine (DEA) buffer (pH 9.8, with 0.5 × 10^{-3}M $MgCl_2$). Samples were incubated in the dark at 37 °C for 45 minutes. Enzymatic activity was then quantified by UV–vis 405 nm (Synergy HTX, BioTek Intruments, USA). The value was normalized against the previously determined correspondent DNA concentration (µg/mL). A standard curve of 4NPh was used as reference (0, 15 × 10^{-6}, 30 × 10^{-6}, 50 × 10^{-6}, 75 × 10^{-6}, 95 × 10^{-6} M in DEA buffer).

2.10. Osteopontin immunostaining

Prior to cell seeding, ASCs and HUVECs were incubated with the lipophilic dyes 3,3'-dioctadecyloxacarbocyanine perchlorate (DIO, green) and 1,1'-Dioctadecyl-3,3,3',3'-Tetramethylindodicarbocyanine (DID, purple), respectively. Cells were incubated with each dye (1mL, 2µM per 1× 10^6 cells) at 37 °C for 30 min, as described by the manufacturer. The expression of osteopontin on the CSs was visualized by fluorescence microscopy. At each time point, the samples were washed with PBS and fixed at RT in formalin (10% v/v) for 15 min. Initially, CSs were incubated with 0.1% (v/v) Triton X100 in dPBS at RT for 5 min. Subsequently, the samples were rinsed and incubated in 5% (v/v) FBS/dPBS solution during 1h at RT. Afterwards, CSs were washed and incubated with 400 µl of mouse anti-human osteopontin antibody (1:100 in 5% FBS/dPBS, Biolegend, Taper) during 3h at RT. Then, the samples were incubated with the anti-mouse Alexa Fluor 555 conjugated dye solution (1:400 in 5% FBS/dPBS) for 1h in dark at RT. Lastly, the CSs were incubated with 400 µl of DAPI solution to nuclei staining (1:1000 in dPBS) during 5 min in the dark at RT. Homotypic CSs were used as control. Fluorescence microscopy analysis were performed in Axio Imager M2 widefield microscope (Carl Zeiss Microscopy GmbH) and using ZEN v2.3 blue edition.

2.11. ELISA immunoassay quantification of cytokines

The expression of osteopontin and osteocalcin was determined through Human Osteopontin and Osteocalcin ELISA Kits (Abcam), respectively according to the manufacturer's instructions. Human bone morphogenic protein-2 (BMP-2) and vascular endothelium growth factor (VEGF) were also quantified using BMP-2 (Invitrogen) and VEGF (Abcam) ELISA Kits, and used according manufacture's specifications. Culture media from the MTS, DNA and ALP activity assays over 21 days were collected and stored at -80^{o}C until further use. The absorbance was then read at 450 nm using a microplate reader (Synergy HTX, BioTek Intruments, USA) (21 days for osteopontin and osteocalcin and 7,14, 21 for BMP-2 and VEGF).

2.12. Analysis of biomineralization of the CS

In vitro mineralization of CSs was accessed at 7, 14 and 21 days of culture in medium with or without osteogenic differentiation factors. Firstly, the CSs were fixed at RT in formalin (10% v/v) for 15 min. Posteriorly the OsteoImage™ Assay was used to visualize the hydroxyapatite portion of bone-like nodules deposited by cells. The OsteoImage™ Staining reagent (1:100 v/v) was added to the

previously fixed CSs and incubated for 30 min. After this, the CSs were washed 3 times and visualized under fluorescence microscope. The mineral formation was also accessed using SEM. Energy dispersive X-ray spectroscopy (EDS) (QUANTAX 400, Bruker) was used to examine the chemical composition of the mineral's deposits within the CS. The samples were carbon-coated and imaged at an electron in intensity of 15 kV (SU-70, Hitachi). The immunofluorescence staining in the histological sections was also performed for the heterotypic CSs at 21 days cultured with or without osteogenic differentiation factors. The samples were previously fixed with 10% (v/v) and then, CSs were routinely processed in an automated system and embedded in paraffin. Afterwards, sequential sections of 5 µm thickness were made in adhesive slides for Von Kossa and Masson's Trichrome staining. The percentage of collagen matrix and number of Ca deposits in the histological cuts were analyzed using Image J software.

2.13. Assessment of *in vivo* angiogenic potential using a chick embryo model

2.13.1. Implantation in chick chorioallantoic membrane (CAM) and neo-vessel quantification

The angiogenic potential of the heterotypic CS (previously cultured in basal media for 7 days) was evaluated using the chick embryo CAM assay. Fertilized chick (Gallus gallus) eggs were incubated horizontally at 37.8 °C in a humidified atmosphere and referred to as embryonic day (E). On E3, 1.5–2 mL of albumin was removed to allow the detachment of the developing CAM and a square window was opened in the shell. This window was sealed with a transparent adhesive tape and the eggs returned to the incubator. On E10, a 3-mm silicon ring was placed on top of the CAM and filled with CSs under sterile conditions. Basic fibroblast growth factor (bFGF) and PBS were used as positive and negative controls, respectively. Eggs were re-sealed and returned to the incubator for 4 days, being hydrated every day. Embryos were euthanized by adding fixative (2 mL) on top of the CAM, the ring was removed, and the CAM was excised. The inoculation area (CAM host controls and CAM with the CS) was photographed *ex ovo* under a stereoscope, at 20x magnification (Olympus, SZX16 coupled with a DP71 camera). The number of new/recruited vessels (less than 20 µm diameter) growing radial towards the ring area was counted in a blind fashion. All experiments were carried out according to the European Directive 2010/63/EU and the national Decreto-Lei nº113/2013.

2.13.2. Image analysis: quantification of the total number of vessels and junctions

For a quantitative analysis of the total number of vessels and junctions, CAM images were treated using ImageJ, by adapting a described methodology[27] for vessel and capillary skeletonization. "FeatureJ Laplacian" plug-in was replaced by a "Mexican Hat" plug-in with a radius of 3, due to a greater adaptability to the samples, and a threshold of 1-130 was set prior to skeletonization (plug-in "Skeletonize 2D/3D"). Image skeletonization was restricted to the ROI. The number of junctions (vascular ramifications) and total number of vessels was calculated using the ImageJ plug-in "Analyse Skeleton 2D/3D" (n=3).

2.14. Histological and immunohistochemical analysis of individual CSs and CAM with CS

Samples of CS and CAM with CS were paraffin-embedded and 5-µm cross-sections were obtained from 2 to 3 standardized transversal planes using a Thermo Scientific HM550 microtome. Sections were stained with H&E and images were obtained using the Axio Imager M2 widefield microscope (Carl Zeiss Microscopy GmbH).

Expression of von Willebrand factor (VWF)/fibronectic (FN), CD31/collagen type IV, VWF/CD31 (all for CS) and VWF/human nuclei (HuNu) (for CAM with CS) was probed after antigen recovery. For this, masked epitopes were exposed by treatment with TE buffer (10 mM Tris/1 mM EDTA, pH 9) for 35 min at 95–98 °C. Sections were incubated with rabbit anti-VWF (1:400 in 5% FBS/dPBS, Abcam) and FN monoclonal antibody (FN-3) Alexa Fluor 488 (1:100, Thermofisher), with mouse anti-human CD31 (1:50 in 5% FBS/dPBS,BioLegend) and rabbit anti-collagen IV (1:400 in 5% FBS/dPBS, Abcam), and mouse anti-human nuclei (1:400, Abcam) primary antibodies. This was followed by 1 h–incubation with Alexa Fluor 647-labeled chicken anti-rabbit (1:400 in 5% FBS/dPBS, Invitrogen) (VWF), AlexaFluor 488 Goat anti- mouse (1:400 in 5% FBS/dPBS, Invitrogen) (CD31 and HuNu) and AlexaFluor 594-labeled donkey anti-rabbit (collagen IV). All sections were counterstained with DAPI (Sigma). Control sections for each immunolabelling excluded primary antibody staining were performed. Images were obtained using a fluorescence inverted microscope (AxioImager Z1, Zeiss).

2.15. Statistical analysis

Statistical analysis was performed using GraphPad Prism software (GraphPad Software Inc., version 7.0) with two-way ANOVA following the Bonferroni post hoc test, with a significance level at $p < 0.05$: *$p < 0.05$; **$p < 0.01$; *** $p< 0.001$; ****$p < 0.0001$.

3. Results

3.1. MNPs characterization

Continuous homotypic and heterotypic magnetic CSs were prepared via Mag-TE. For this purpose, MNPs were synthetized as described in **Figure V.S1A**. Upon characterization via TEM, it was determined that MNPs presented sizes ranging from 5-15nm (**Figure V.S1B**). Subsequently, MNPs were amino-functionalized as previously described,[24] and such modification was confirmed through FTIR-ATR. The characteristic bands of MNPs associated with the Fe-O vibration were evidenced below 700 cm^{-1} (**Figure V.S1C-i**).[28] The characteristic band at 1634 cm^{-1} was associated with the N-H bend in primary amines, which may be correlated with the fabrication method employed (using ammonium hydroxide). The functionalization of MNPs with APTES (**Figure V.S1C-ii**) caused slight deviations from the characteristic bands below 700 cm^{-1}. Further characteristic bands appeared on the APTES modified MNPs. Specifically, the absorption band at 993 cm^{-1} was associated with Fe-O-Si vibration, the low-intensity bands in the 1300–1600 cm^{-1} range are attributed to the amino-propyl segment and free amino groups and the bands in the range 2853-2954 cm^{-1} match the vibration of the CH_2 group.[28] The modification of MNPs-APTES with RodB was also confirmed by FTIR-ATR (**Figure V.S1C-iii**). Upon the incorporation of RodB (Fig.S1C-iv), the carboxylic groups of the compound, represented by the C=O characteristic band at 1709 cm^{-1}, undergo esterification causing a shift in the C=O vibration. Moreover, the incorporation of RodB caused a shift in the Fe-O-Si characteristic band evidenced in APTES-MNPs (993- 1007 cm^{-1}). A new low intensity peak appeared at 1222 cm^{-1} and was associated with C-H in plane bend. The characteristic peak evidenced in the whole spectra at approximately 3400 cm^{-1} was attributed to the O-H vibration.[29]

3.2. CS fabrication, 3D stratification and their characterization

The successful isolation of HUVECs from umbilical cord was determined by flow cytometry (**Figure V.S2**). More than 98% of HUVECs revealed positive markers for CD31.

Prior to CS formation, MNPs-RodB were successfully uptaken by HUVECs (81.4 $\pm$ 1.5%) and ASCs (93.1$\pm$ 4.6%), as corroborated in Fig.1A and B.

Homotypic CSs comprising of two ASCs and heterotypic CSs composed of two ASCs layers with one CS of HUVECs in between, were produced following the methodology represented in **Figure V.1C**. As previously described by Ito and co-workers, the thickness of individual CS was controlled by manipulating the amount of cells in suspension and the area of the well plate.[1,20,30]

CD31 immunodetection highlighted the presence of HUVECs in the middle of the fabricated CS (**Figure V.2A**) where, via vinculin staining, it was possible to attest the existence of cell-cell adhesions throughout the developed construct (**Figure V.S3**). 3D reconstruction and different side views (top and middle) are displayed in Fig.2B. The integrity of the vascularized CS membrane was corroborated by SEM (**Figure V.2C**). Moreover, tubular-like structures (represented in red), were evidenced in between two ASCs layers, displayed in green.

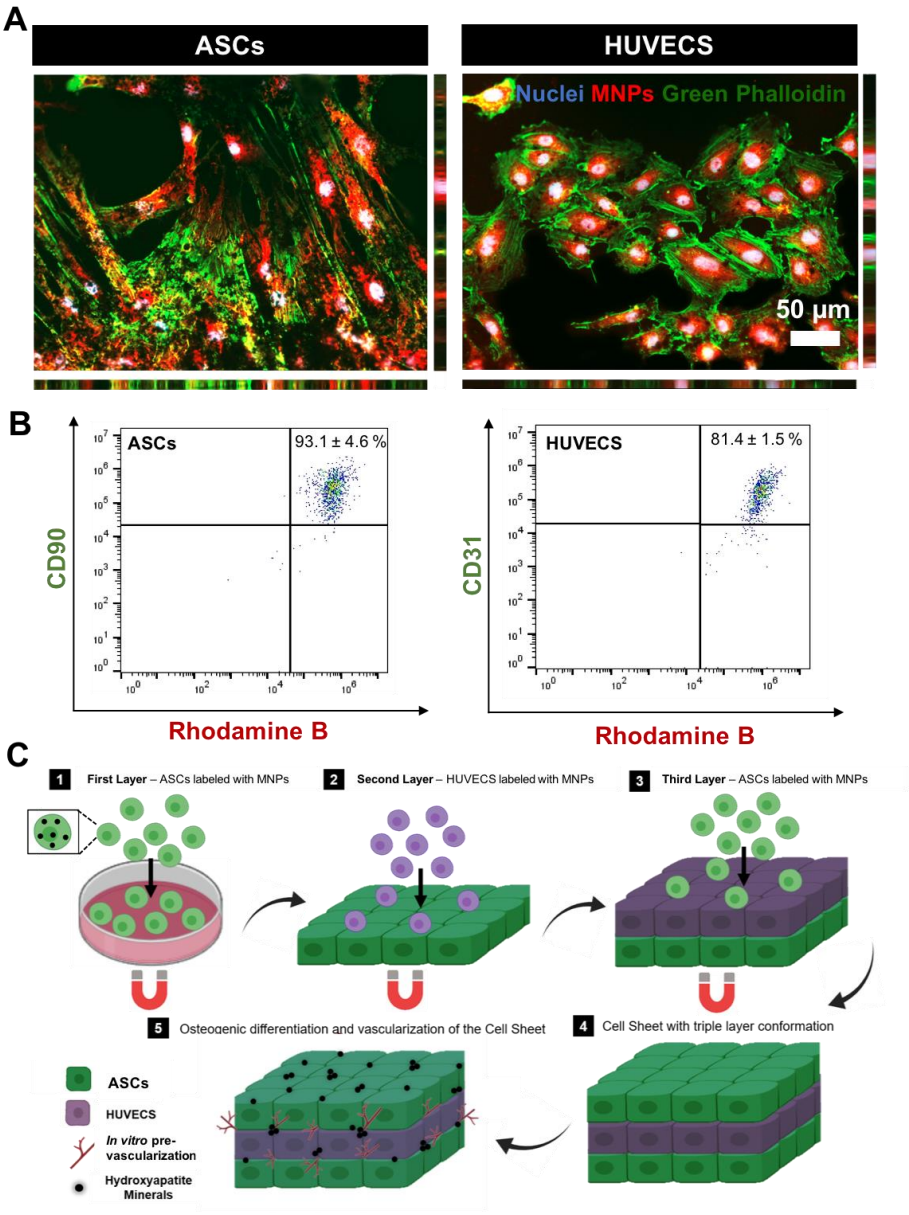

Figure V.1: Cellular uptake and graphical illustration of the CS fabrication. **A.** Internalization of MNPs-RodB in ASCs and HUVECs: actin filaments of HUVECs and ASCs (green phalloidin), MNPs-RodB (red) and cell nucleus - DAPI (blue). **B**. Flow cytometry analysis of MNPs-RodB uptake after 4 hours. (**C**) Schematic representation of the fabricated 3D vascularized heterotypic CS.

3.3. Metabolic activity and cell proliferation and survival

Homotypic and heterotypic CS in both basal and osteogenic medium showed an increased metabolic activity (**Figure V.2D**) and DNA (**Figure V.2E**) content up to 14 days of culture. Live-dead

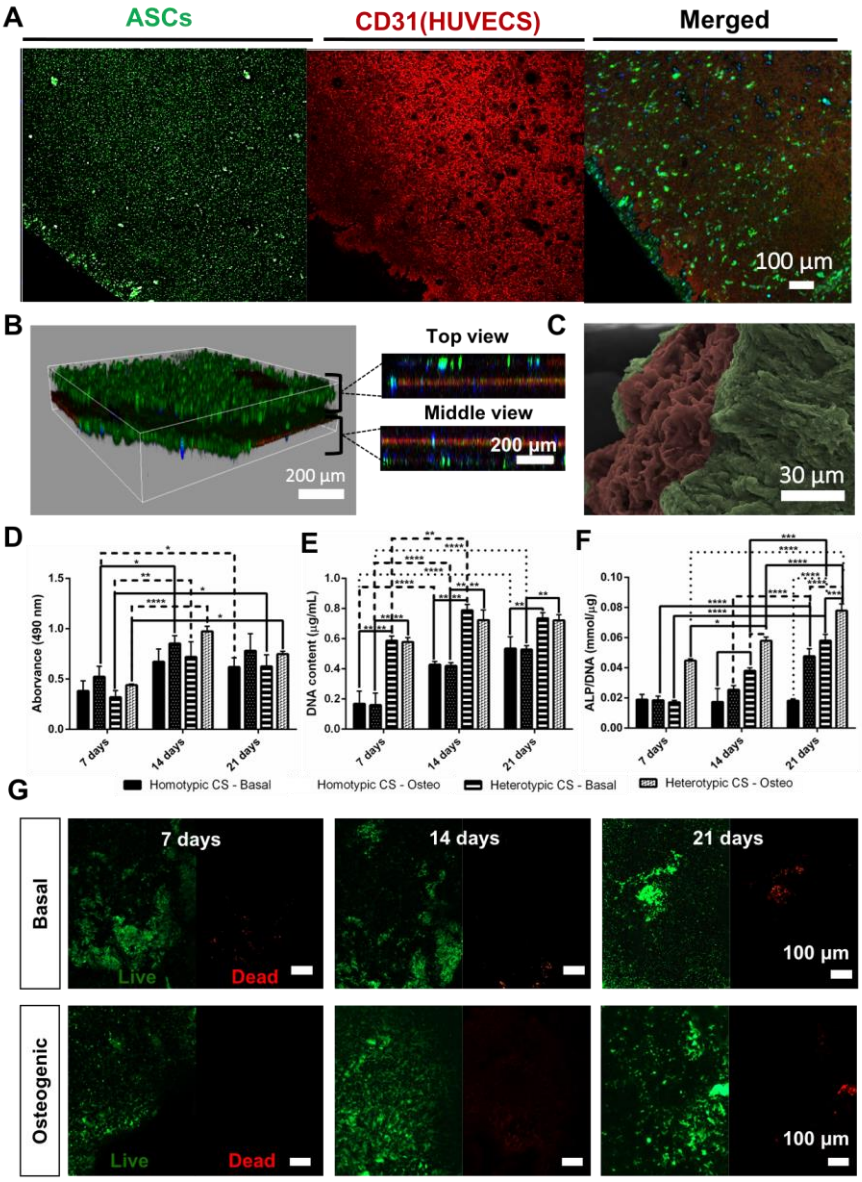

Figure V.2: Cell sheet integrity, metabolic activity, cell survival and proliferation, and *in vitro* osteogenic potential. **A**. Confocal microscopy of the magnetically labeled CS demonstrating CD31 staining HUVECs in between two ASCs sheets – CD31: HUVECs (red) and ASCs (green); **B**. 3D reconstruction of B and side sections exhibiting CD31 (HUVECs) in the middle of two ASCs sheets (Phalloidin – green, DAPI – blue). **C**. SEM micrographs of the triple layer conformation of the developed CS: HUVECs (represented in red) and ASCs (represented in green). **D.** Cell metabolic activity determined by MTS colorimetric assay, **E.** Cell proliferation by DNA quantification and **F.** Alkaline phosphatase (ALP) activity normalized by DNA content for both homotypic and heterotypic CS. All results were significantly different unless marked with ns ($p > 0.05$). (**G**) Live-dead fluorescence assay at day 7, 14 and 21 of culture in basal and osteogenic medium. Living cells were stained by calcein (green) and dead cells by propidium iodide (red).

assay showed that up to 21 days post-CSs' formation, the majority of the cells remained viable for all formulations (**Figure V.2F** and **Figure V.S4**). Notably, these results also evidenced the ability of CSs for long-term cell survival, which is a major challenge in tissue engineering strategies aiming CSs fabrication.

3.4. *In vitro* assessment of the osteogenic potential of the Mag-TE Cell sheets

3.4.1. Quantification of the ALP activity and mineralization assessment

Based on the knowledge that increased levels of ALP activity are correlated with enhanced osteogenic differentiation, it is possible to assure that cell differentiation had occurred earlier (7 days) for the heterotypic CS cultured with osteogenic media (**Figure V.2G**). However, at the end of 21 days both heterotypic CS cultured in either basal or osteogenic media, showed enhanced ALP activity, corroborating the fact that ASCs co-cultured with HUVECs lead to an enhanced cell differentiation, although delayed (7 days) when compared with the heterotypic CS cultured in osteogenic media. As expected, the ACSs monolayer cultured under osteogenic conditions revealed some ALP increment after the 21 days, as the ACSs monolayer in basal conditions did not show any ALP increment over time.

The mineralization of the heterotypic CSs was also evidenced by EDS and Osteoimage™ assay and the results support the ALP findings. Hydroxyapatite crystals were also evidenced in both culturing conditions after 14 days (**Figure V.3A**). The chemical analysis of the minerals by EDS displayed calcium (Ca) and phosphate (P) peaks increasing over time in both basal and osteogenic conditions, with a higher Ca/P ratio attained for the heterotypic CS cultured for 21 days under osteogenic media (**Figure V.3B**). The ratio between Ca/P achieved for the heterotypic CSs cultured in basal conditions re-suggests a delayed (7 days) osteogenic differentiation. The enhanced deposition of hydroxyapatite-like minerals evidenced in both conditions with the ratio of Ca/P approaching the one of the apatite minerals in bone (*1.66),[31,32] indicates the formation of bone-like tissue for the heterotypic CS, even in the absence of osteogenic factors. Nevertheless, no significant differences were evidenced. In addition, the decline in iron (Fe) detection overtime was in agreement with cell proliferation and *de novo* matrix formation that leads to a decrease signal.

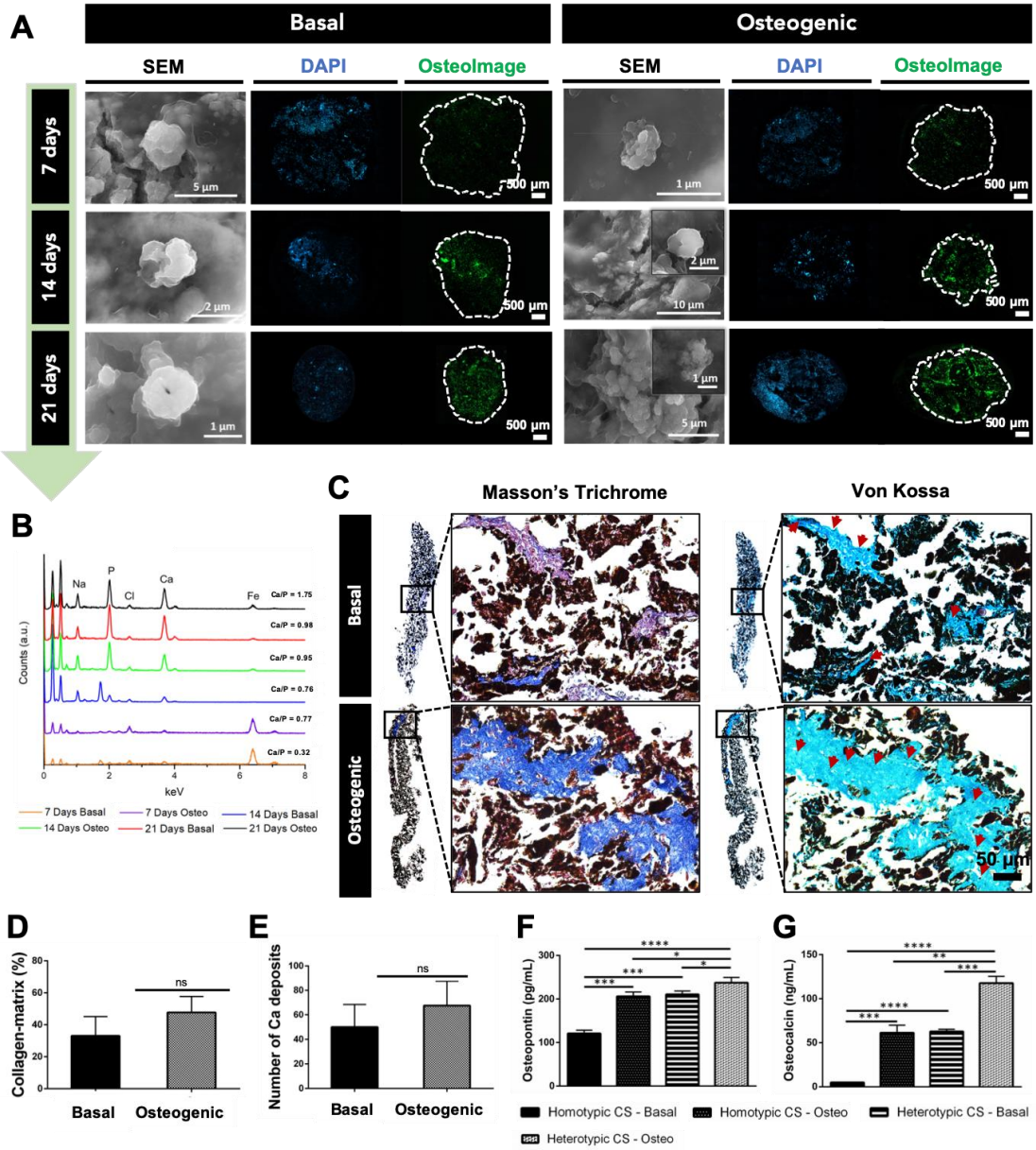

Figure V.3: Mineralization of the developed 3D heterotypic CS in basal and osteogenic media. **A**. The hydroxyapatite portion of bone-like nodules deposited by cells was visualized through fluorescent OsteoImage™ Mineralization Assay: cell nucleus - DAPI (blue) and hydroxyapatite (green). SEM micrographs displaying calcium deposits are depicted in the right panel; **B**. Energy dispersive X-ray spectroscopy (EDS) spectra of minerals formed within the CS; **C**. mineralization of the heterotypic CS accessed by Von Kossa staining and collagenous connective tissue fibers identified by Trichrome Masson staining on histological sections CS cultured in basal or osteogenic media after 21 days. **D**. Percentage of collagen-matrix in the representative histological cut; **E**. Number of Ca deposits in the *de novo* cell matrix; **F.** Quantification of osteopontin and osteocalcin (**G**) expression by ELISA. $p < 0.05$: *$p < 0.05$; **$p < 0.01$; ***$p < 0.001$; ****$p < 0.0001$.

Furthermore, Von Kossa staining revealed the presence of Ca deposits within the *de novo* matrix formed, and Masson's Trichrome technique also demonstrated a collagen enriched matrix in the developed construct (**Figure V.3C**, **V.3D** and **V.3E**).

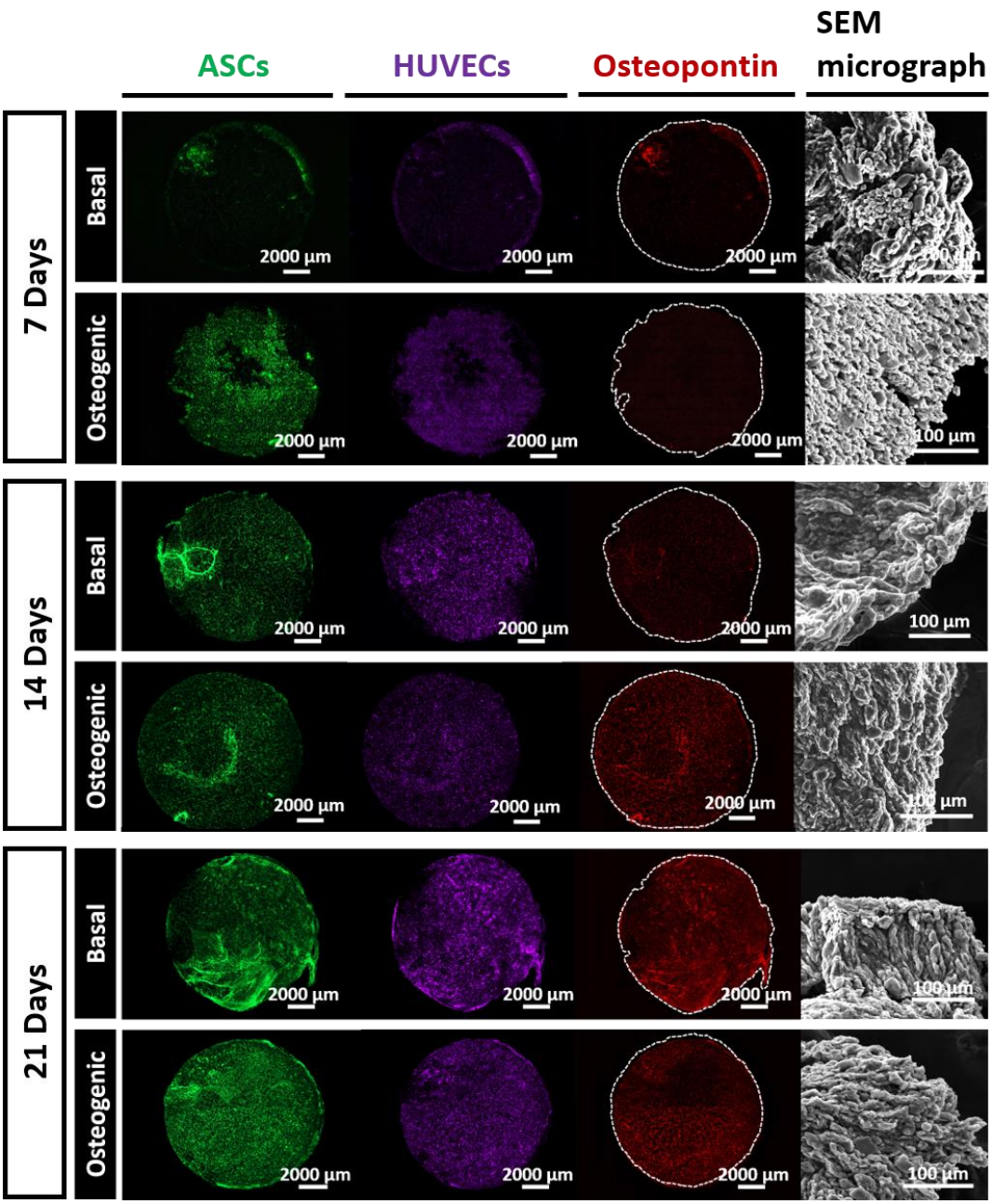

Figure V.4: Osteopontin staining and SEM micrographs of heterotypic CS. Immunofluorescence of ASCs (green), HUVECs (purple) and osteopontin (red) in 3D heterotypic CS cultured for 7, 14 and 21 days in basal and osteogenic media**.** SEM micrographs of the developed CSs are represented in the right panel demonstrating CS integrity.

3.4.2. Cytokines detection

The secretion of the late osteogenic markers osteopontin and osteocalcin was evidenced after 21 days in both culturing conditions in the homotypic and heterotypic CSs (**Figure V.3F** and **V.3G**, respectively). As anticipated, magnetically labeled homotypic CS in the absence of osteogenic

factors secreted none (for osteocalcin) or few (for osteopontin) of the osteogenic markers. The obtained results for the release of both osteopontin and osteocalcin cytokines suggested a similar tendency between the magnetically labeled homotypic CS cultured with osteogenic factors and the heterotypic CS cultured in the absence of the osteogenic factors. Again, the results suggested an osteogenic role of HUVECs over ASCs. To further explore other forms of osteopontin presence in the magnetically labeled heterotypic CS, an immunofluorescence assay was also performed. The results, displayed in **Figure V.4**, demonstrated a complete osteopontin staining after 21 days in both culturing conditions. SEM micrographs were taken from every representative condition. **Figure V.S5**, which demonstrated the immunofluorescence assay of osteopontin for homotypic CSs, also exhibited a complete osteopontin staining after 21 days in osteogenic conditions. As expected, no osteopontin staining was evidenced in the homotypic CSs under basal conditions.

The secretion of BMP-2 and VEGF was also investigated over a period of 21 days (**Figure V.5A,B**). The results insinuate a synergic behavior between BMP-2 and VEGF. BMP-2 was found to be enhanced for the heterotypic conditions, with a more pronounced effect ($P<0.01$) on the CSs cultured with osteogenic supplements, for every single timepoint, with increased expression at 21 days. On the other hand, the highest levels of VEGF were achieved for the homotypic CS cultured in basal conditions, followed by the ones cultured in osteogenic condition, again regardless of the timepoint. The decreased VEGF values obtained for the heterotypic CS supported osteogenic differentiation. In fact ASCs stimulate blood vessel growth via the secretion of angiogenic and anti-apoptotic growth factors, such as VEGF, enhancing the biological activity of endothelial cells.[7,13,33,34] Nevertheless, decreased levels of VEGF with enhanced values of BMP-2 suggested the osteogenic differentiation of ASCs that, once differentiation has occurred, lose their ability to enhance angiogenesis by down-regulating VEGF levels. Moreover, the effect of VEGF over endothelial cells is known to induce the release of BMP-2,[13,35,36] which is in agreement with the data herein acquired: even in the absence of osteogenic factors, BMP-2 is increased in the endothelized CS. The results insinuate the synergic interaction between the layers of ASCs and HUVECs, even in the absence of osteogenic differentiation factors, corroborating CS stratification, achieved through Mag-TE.

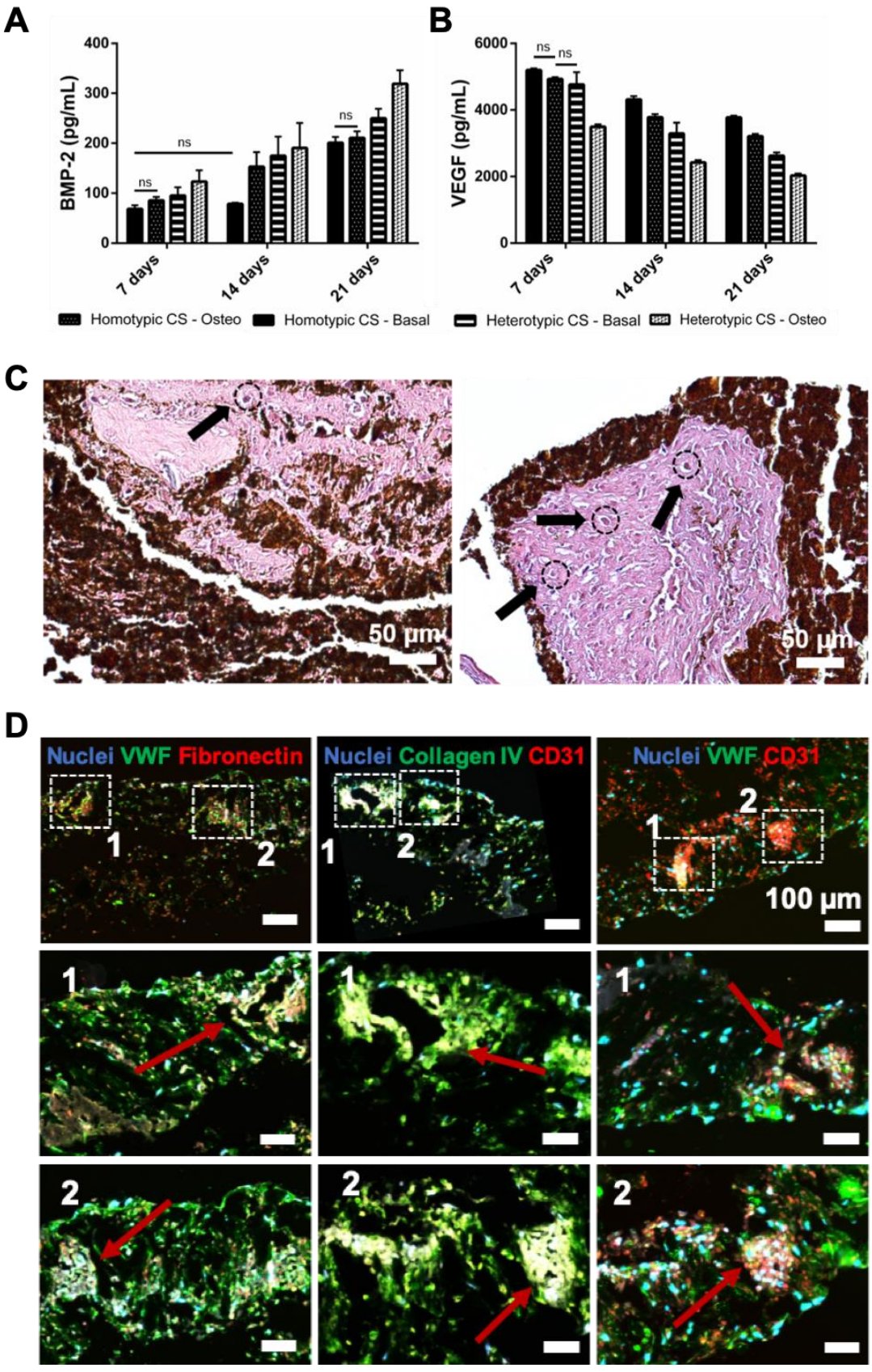

Figure V.5: Pre-vascularization of the heterotypic CS cultured during 7 days with basal media. **A.** Quantification of BMP-2 and **B**. VEGF release by Elisa on the homotypic and heterotypic CS cultured over 21

days in basal and osteogenic media; **C**. H&E staining of paraffin-embedded heterotypic CSs cultured under basal conditions for 21 days; **D.** Immunostaining of CS: VWF (green) and FN (red); collagen IV (green) and CD31 (red); and VWF (green) and CD31 (red) demonstrating the presence of capillary-like structures (white arrows). DAPI (in blue) stains all nuclei.

3.5. Angiogenic potential

De novo matrix formation and pre-vascularization of heterotypic CSs cultured under basal conditions were evidenced after 21 days of culture (**Figure V.5C**). H&E staining of the CSs revealed the presence of tubular-like structures in the *de novo* matrix formed. To corroborate the presence of vascular structures within the CS, the sections were stained with the endothelial marker CD31 and collagen IV, a main protein component of all basement membrane that has a crucial role in endothelial cell proliferation and cell behavior.[37] VWF and FN immunostaining also exposed the presence of capillary-like structures within the CS, corroborating our findings. All sections were counterstained with DAPI to stain the cells' nuclei. For a better visual interpretation of the capillary-like structures, a VWF and CD31 immunostaining was also performed (**Figure V.5D** and **Figure V.S6**) A CAM assay was performed to evaluate the *in vivo* angiogenic potential of our magnetic heterotypic CSs cultured in basal medium. The developed CSs were harvested with the aid of a neodymium magnet and implanted inside a silicon ring placed on top of the CAM and cultured for 4 days, as represented in **Figure V.6A**. Photomicrographs were taken to count the number of newly formed blood vessels (**Figure V.6B**). The results demonstrate that our endothelized CS was able to recruit new microvessels at a same extent of bFGF, used as a positive control, and significantly higher than the negative control (PBS) **Figure V.6C**. The total number of vessels and junctions were also quantified using ImageJ. Although higher values were verified for the heterotypic CSs in comparison with the negative and positive controls (**Figure V.S7**), no significant differences were observed.

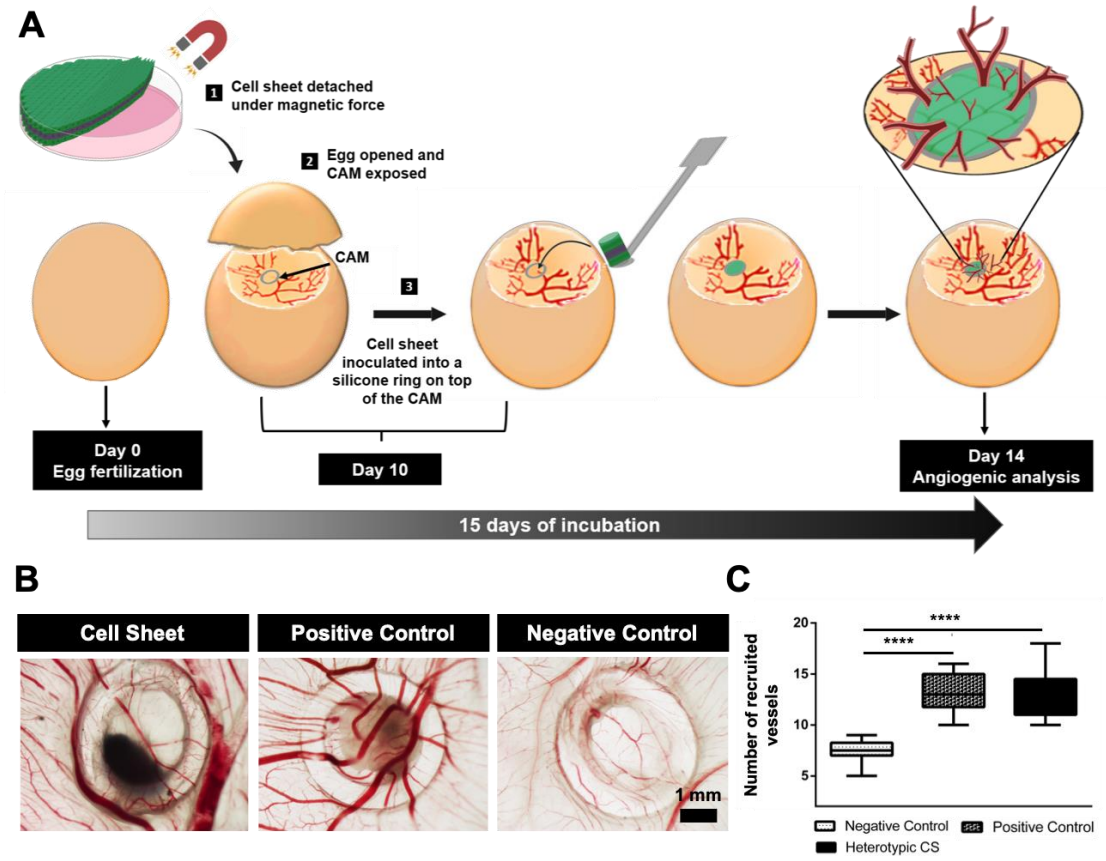

Figure V.6: *In vivo* angiogenic potential of the heterotypic CS cultured during 7 days with basal media. PBS was used as negative control and bFGF as a positive control. **A.** Schematic representation of the implementation of the CS into the CAM; **B.** Photomicrographs of the newly formed vessels; **C.** Quantification of the newly formed vessels after 14 days of maturation (****$p < 0.0001$).

H&E staining of paraffin-embedded CAMs showed that our magnetically labeled CSs were able to incorporate into the host tissue. The appearance of MNPs within the CAM of the host supported this finding (**Figure V.7A**). To further track the implanted human cells, the specific human nuclei marker was also used (HuNu, stained in pink). Human nuclei were found all over the host membrane corroborating the cellular invasion from the cells of our heterotypic CS (**Figure V.7B**). Moreover, the combination of HuNu with VWF immunostaining exposed HUVECs organized in capillary-like structures within the CS tissue, as well as human cells integrating chick vasculature (zoom sections of **Figure V.7C**). In fact, the combination of HuNu with VWF inside chick vessels lead us to conclude that human endothelial cells were in fact integrating such vascular regions (**Figure V.S8**). The positive control (bFGF) was used to corroborate our findings.

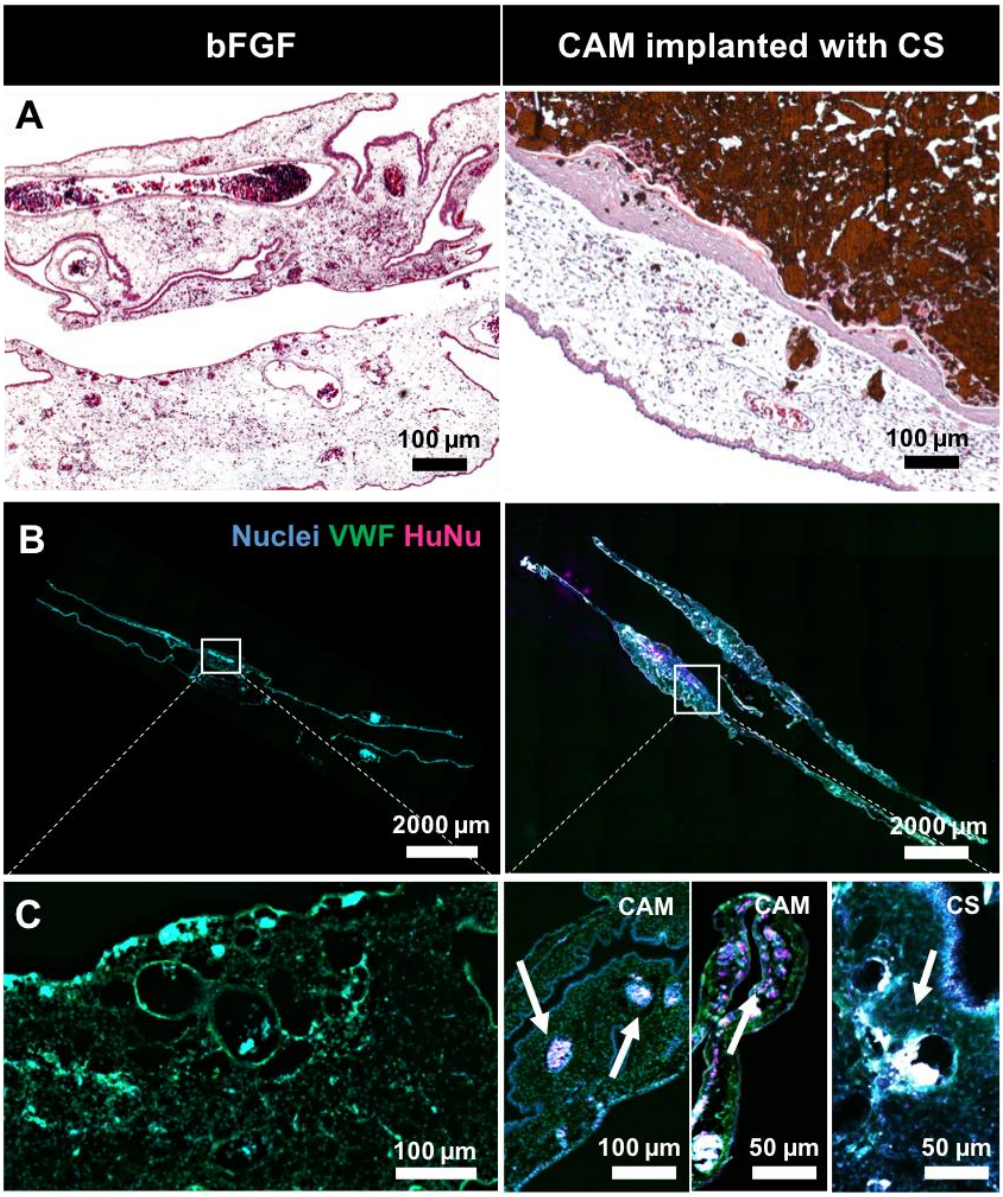

Figure V.7: CS integration within the CAM. **A.** H&E staining of paraffin-embedded CAMs; **B.** Immunostaining of CAM with implanted CS and CAM implanted with bFGF (positive control). VWF (in green) labels both human and chick endothelial cells, DAPI (in blue) stains all nuclei, and HuNu (in pink) stains the human nuclei. **C.** Zoom of CAMs sections. As displayed in CAM with implanted CS, human nuclei are integrated within the CAM and have integrated chick vasculature (white arrows). The presence of human vessels within the CS is also corroborated by the overlapping of HuNu and VWF (white arrow).

4. Discussion

One of the major hurdles in fabricating 3D tissues from CSs involved the engineering of mechanically resistant cell-constructs for vascularized tissues. The poor mechanical properties of CSs monolayers can be overcome through the construction of thicker ones. However, the thickness

limitation of multilayered CSs is correlated with the need for blood vessels supplying oxygen and essential nutrients throughout the 3D construct,[5,10] while removing metabolic waste.[38] In fact, thick and highly-dense CSs without blood vessels have already been reported to be unable to survive *in vivo*.[10] It has also been reported that the lack of adequate vascularization induces necrosis in tissues thicker than 100-200μm.[9,38] To overcome such limitations pre-vascularization strategies have been used to accelerate its perfusion after CS implantation, guarantying the survival of the 3D construct and the correct interaction with the host tissue.[5,7,10,11,38–41]

The works reported in the literature regarding the establishment of pre-vascularized CS consist on the individual stacking of previously formed CS monolayers by making use of thermo-responsive surfaces. To aid in such CS fabrication, Okano and co-workers have proposed a methodology that encompasses the use of a CS layering manipulator that avoids the shrinkage of the developed CS after detachment from the thermo-responsive surfaces. Such devices have been used to lift up to three CS monolayers from individual PIPAAm surfaces,[19,38] yet the ability to lift up to ten monolayers is reported.[5] However, this manipulation requires skills and user-knowledge to successful deposit the CS into layers. To overcome this limitation the same researchers have developed an automatic apparatus able to stack several CSs in a reproducible manner without requiring the expertise of the operator. Nevertheless, the cost for the fabrication of the apparatus and the need for a clean room facility make the process unsuitable for most research facilities. In addition, PIPAAm thermo-responsive surfaces are also known to exhibit some limitations such as high cost, abnormal cellular activity due to physiological alteration within cell microenvironment and restrains in tissue replacement.[42] Also, the spatial control of the positioning of target cells is challenging in such approach.[21] In Mag-TE, cells are labeled with magnetic biocompatible nanoparticles and forced to interact with each other, prompting cell-cell adhesion.[43] In fact, the use of biocompatible magnetite nanoparticles in the TE and regenerative field has long been proven to provide outstanding biological and medical applications.[43–46] Mag-TE technology has been used to produce heterotypic CS of HAECs and human hepatocytes with satisfactory outcomes.[1,20,23]

By taking advantage of this expertise, we herein report the development of a stratified and hierarchical 3D vascularized construct to fit bone TE purposes. CS applications towards bone regeneration using thermo-responsive surfaces have already been proposed.[7–9,47] In published studies, a co-culture of endothelial cells and bone marrow derived stromal cells (hBMSCs) was performed in culture media supplemented with osteogenic factors such as dexamethasone and ascorbic acid. Pirraco *et al.* and Mendes *et al.* stacked such co-cultured layers with a layer of hBMSCs. In turn, Ren *et al.* and Li *et al.* folded the co-cultured CS construct to create a 3D

vascularized tissue.[8,17,33,48] Recently, Zhang *et al.* created a double CS complex through the stacking of previously differentiated ASCs into either osteogenic CSs or endothelial CSs. The authors investigated the influence of stacking both layers in different orders and, in further conjugation with a coral hydroxyapatite scaffold, assessed the newly formed vessels after subcutaneous heterotypic transplantation in nude mice. Again, the contractile nature of such CS hinders the manipulation of the construct.[30]

Here, we proposed the developed of a pre-vascularized heterotypic CS by making use of Mag-TE technology, in simple, one-pot, cost effective and time-saving fashion. By magnetically pushing both heterotypic and homotypic cell-cell interactions we attempted to easily create a fully functional pre-vascularized tissue, and to demonstrate the synergic interaction between HUVECs and ASCs, as well as the self-generation of growth factors and proteins that boost both osteo- and angiogenesis in the developed tissue construct. Thus, we hypothesized that our endothelized magnetically labeled CS could coordinate the precise signals towards new bone formation without requiring the supplementation of the three main osteogenic differentiation factors, such as dexamethasone, ascorbic acid and β-glycerophosphate, while exhibiting angiogenic potential both *in vitro* and *in vivo*. Such hypothesis is in line with other studies and emphasizes the potential use of endothelial cells in the osteogenic differentiation of ASCs, when compared to the monoculture counterparts.[6,13,49,50]

In this sense, ASCs and HUVECs were successfully labeled with magnetic nanoparticles. Homotypic ASCs CS and heterotypic CSs comprising of an HUVECs CS in between two ACSs CSs, were engineered as described above. An identical number of ASCs was used for both assemblies. With the aid of magnetic force, cell-cell homotypic and heterotypic interactions were enforced, enabling the development of a cohesive and stratified tissue. In addition, visual perception of both CS constructs revealed that a more cohesive CS was obtained for the heterotypic condition. CS integrity in both homotypic and heterotypic tissues was corroborated via SEM imaging and by H&E staining, where *de novo* matrix was also identified. Cell-cell interactions in the heterotypic CS were corroborated through vinculin orange-staining. An immunodetection of CD31 confirmed the presence of a CS of HUVECs in between the two CSs of ASCs, as demonstrated by the side sections of the confocal image. The cross talk between ASCs and HUVECs was confirmed through CS osteogenic differentiation. Thick and collagen-enriched matrices were achieved in heterotypic CS for both culture media conditions. The metabolic activity stagnation together with ALP/DNA increase in the heterotypic stratified CS and monotypic CS cultured in osteogenic media also suggested osteogenic differentiation. Moreover, ALP, which is secreted by active osteoblasts, is

known to cleave the pyrophosphate ions that hamper the formation of hydroxyapatite crystals. Such ALP-induced hydrolysis results in the saturation of the extracellular fluid with orthophosphates that stimulate matrix mineralization.[13,51,52] This has been well-documented by the calcium deposition, hydroxyapatite crystals and Ca/P ratio approaching the one found in cortical bone.[31,32] The obtained results for ALP and hydroxyapatite deposition also suggest a delay in osteogenesis for the homotypic CS when compared to the heterotypic CS cultured in osteogenic conditions. Such effect was already expected as the combination of both strategies triggers a faster osteogenic differentiation.[13]

The pro-osteogenic potential of CS was also evaluated through the secretion of the two major non-collagenous proteins osteopontin and osteocalcin, involved in bone matrix organization and deposition. Both proteins are secreted by bone differentiated cells and are produced during bone formation, late in the mineralization process controlling mass, mineral size and orientation, regulating whole-bone structure and morphology.[53] The results suggested osteogenic differentiation in both heterotypic and homotypic CSs cultured under the influence of osteogenic factors, suggesting a similar effect for these factors and endothelial cells in the expression of this non-collagenous proteins. Residual osteopontin expression was also achieved for ASCs monoculture CS. Osteocalcin secretion follows a similar tendency. Nevertheless, as osteocalcin is only expressed by active osteoblasts, the differences between conditions appear to be more pronounced, as the osteocalcin expression in ASCs is negligent. Such effect re-suggests a seven-day late osteogenic differentiation in the homotypic CS cultured under osteogenic factors and in the heterotypic CS cultured in the absence of those components (basal media). Immunodetection of all forms of osteopontin in both heterotypic CS revealed a similar fluorescence intensity after 21 days of culture.

As has been widely reported, osteogenesis and vascularization are coupled during bone development and growth. In fact, angiogenesis is known to play a fundamental role in bone growth and remodeling.[7,8,13,17,33,35] VEGF and BMP-2 have been widely used in TE and regenerative medicine to synergically incite angiogenesis and bone formation.[54] VEGF, which is known to be expressed in ASCs,[13,55] is a strong angiogenic factor, and plays a fundamental role in blood vessel invasion and in the secretion of growth factors that stimulate osteogenesis.[35] On the other hand, BMP-2 is an osteogenic growth factor that is involved in improved bone tissue regeneration,[13,56–59] is expressed in several cell types including endothelial ones. The ability of endothelial cells to release BMP-2 by the action of VEGF is well document in the literature and supports our findings. As expected, pre-vascularized heterotypic CS secrete more BMP-2. Moreover, the synergic effect

of the co-culture together with the differentiating osteogenic factors resulted in a higher BMP-2 release, measure at the end of the experiment (21 days). Nevertheless, the results confirm that the co-culture of endothelial cells and ASCs was sufficient to induce the release of BMP-2, since the amount released is higher than the one evidenced in homotypic CS. Also, the crosstalk between BMP-2 and VEGF was likewise corroborated by the VEGF release. As time increased and upon osteogenic differentiation (evidenced by BMP-2, osteopontin, osteocalcin, ALP and Ca/P ratio increase overtime), ASCs capability to induce angiogenesis is diminished, which in turn down-regulated VEGF expression. Equivalent results were evidenced in a co-culture of microvascular endothelial cells and ASCs within a 3D system of liquified capsules.[13] Similarly, the delayed osteogenesis observed for the heterotypic CS cultured in the absence of osteogenic factors, could in fact represent an added value. In fact, the amount of VEGF being released may further trigger the recruitment of new vessels, enhancing angiogenesis and enabling the formation of a more vascularized osteogenic tissue. In light of such events, the angiogenic potential of the heterotypic CS cultured under basal conditions was investigated. After 21 days of *in vitro* culture, the developed CSs revealed the presence of vascular structures, which was corroborated through i) the combination of CD31 (endothelial cells' marker) and the deposition of the basement membrane protein collagen IV; and ii) the association of FN, that is particularly relevant during blood vessel formation and VWF (another endothelial cells' marker).

The *in vivo* angiogenic potential of heterotypic CS cultured in basal medium for 7 days was also investigated through a CAM assay,[37] and compared to the effect of the angiogenic stimulant bFGF.[60] The number of new capillaries formed around the implantation area suggests a similar performance between the heterotypic CS and the positive control, only 4 days after the CS implantation, likely due to the increased VEGF levels during that period. Human cells showed to be able to migrate into the host and integrate chick vasculature as corroborated by H&E staining, where MNPs have integrated the CAM and its vasculature, as well as by the presence of a specific human nuclei marker. Moreover, the presence of human vessels in the CAM chick and in our CS was identified by the overlapping of HuNu with VWF. Although this preliminary *in vivo* angiogenic assay demonstrated that our magnetically labeled heterotypic CSs stimulates blood vessels recruitment and integration within the host environment, forthcoming studies including the implementation of this CS in more realistic models for clinical applications, where angiogenesis and *de novo* bone formation could be fully evaluated. With this technology, we intend to create personalized CSs with patient own cells. Although we suggest using endothelial cells from umbilical cord source, in case of impossibility, human adipose microvascular endothelial cells (ECs) can be

retrieved from adipose tissue. As already demonstrated in the group, the combination ASCs and ECs is also expected to produce bone-like tissues under similar conditions.[13] IPSC technology may also be used to create patient-specific CSs. In fact, the tremendous potential of IPSC in regenerative medicine, particularly in the development CSs for heart, liver and retinal therapies, has already been disclosed.[61–63] The developed CSs can be used as membranes for guided bone regeneration either by placing the CSs on top of cranial or maxillofacial defects, or by wrapping around femoral bone injury.[64] In fact, CSs for bone regeneration are commonly used as membranes for periosteum repair, a highly vascularized tissue that resides in a dynamic mechanically loaded environment and envelopes the bone surface of long bones.[65] Even though this study focused on bone regeneration, we believe that the easiness of the methodology herein describe could be extended to further applications for a plethora of hierarchical tissues by adapting the cell phenotypes within the fabricated CS.

5. Conclusion

Mag-TE has shown remarkable outcomes in the fabrication of both homotypic and heterotypic CS in a simple, one-pot, cost-effective and time-saving manner, enabling the construction and manipulation with the aid of mild magnetic force. Stimulated by the high vascularization nature of bone tissue, we herein developed a hierarchical 3D cohesive tissue of HUVECs and ASCs based on CS technology and Mag-TE, to be used in bone regeneration purposes. The hierarchical construct (ASCs/HUVECs/ASCs) revealed to be effective in stimulating *in vitro* osteogenesis through the crosstalk of both cells' phenotypes, even in the absence of osteogenic differentiating factors such as dexamethasone, ascorbic acid and β-glycerophosphate. Furthermore, VEGF and BMP-2 release triggered the recruitment of more blood vessels, empowering the outstanding potential of the developed system for TE practices. The development of pre-vascularized/angiogenic magnetically actuated CS is expected to improve to a great extent the use of such technology in the creation of robust and easily manipulated cell constructs to fit TE purposes.

Acknowledgments

We acknowledge the project CICECO – Aveiro Institute of Materials, POCI-01-0145-FEDER-007679 [Fundação para a Ciência e Tecnologia (FCT) Ref. UID/CTM/50011/2013], financed by national funds through the FCT/Ministério da Educação e Ciência, and PROMENADE (Ref. PTDC/BTM-MAT/29830/2017). This work was also supported by the project ATLAS (ref.ERC-2014-ADG-669858)

and through the doctoral grants SFRH/BD/141523/2018 (Lúcia F. Santos) and SFRH/BD/146740/2019 (Maria C. Mendes).
Confocal image acquisition was performed in the LiM facility of iBiMED, a node of PPBI (Portuguese Platform of BioImaging): POCI-01-0145-FEDER-022122. We also acknowledge to Marta Teixeira Pinto for the CAM assay technique performed at the "*in vivo* CAM assays" i3S Scientific Platform and for the helpful discussions.

References

1. Ito, A.; Jitsunobu, H.; Kawabe, Y. & Kamihira, M. Construction of Heterotypic Cell Sheets by Magnetic Force-Based 3-D Coculture of HepG2 and NIH3T3 Cells. *J. Biosci. Bioeng.* **104,** 371–378 (2007).
2. Yang, J.; Yamato, M.; Kohno, C.; Nishimoto, A.; Sekine, H.; Fukai, F. & Okano, T. Cell Sheet Engineering: Recreating Tissues without Biodegradable Scaffolds. *Biomaterials* **26,** 6415–6422 (2005).
3. Yamato, M. & Okano, T. Cell Sheet Engineering. *Mater. Today* **7,** 42–47 (2004).
4. Yang, J.; Yamato, M.; Shimizu, T.; Sekine, H.; Ohashi, K.; Kanzaki, M.; Ohki, T.; Nishida, K.; Okano, T. Reconstruction of Functional Tissues with Cell Sheet Engineering. *Biomaterials* **28,** 5033–5043 (2007).
5. Owaki, T.; Shimizu, T.; Yamato & M.; Okano, T. Cell Sheet Engineering for Regenerative Medicine : Current Challenges and Strategies. *Biotechnol. J.* **9,** 904–914 (2014).
6. Costa, M.; Cerqueira, M. T.; Santos, T. C.; Sampaio-Marques, B.; Ludovico, P.; Marques, A. P.; Pirraco, R. P. & Reis, R. L. Cell Sheet Engineering Using Stromal Vascular Fraction of Adipose Tissue as a Vascularization Strategy. *Acta Biomater.* ***55*****,** 131–143 (2017).
7. Pirraco, P.; Iwata, T.; Yoshida, T.; Marques, A. P.; Yamato, M. & Reis, R. L. Endothelial Cells Enhance the in Vivo Bone-Forming Ability of Osteogenic Cell Sheets. *Lab. Investig.* ***94*****,** 663–673 (2014).
8. Mendes, L. F.; Pirraco, P.; Szymczyk, W.; Frias, A. M.; Santos, T. C.; Reis, R. L. & Marques, A. P. Perivascular-Like Cells Contribute to the Stability of the Vascular Network of Osteogenic Tissue Formed from Cell Sheet-Based Constructs. *PLoS One* ***7*****,** 1–12 (2012).
9. Moschouris, K.; Firoozi, N.& Kang, Y. The Application of Cell Sheet Engineering in the Vascularization of Tissue Regeneration. *Regen. Med.* **11,** 559–570 (2016).
10. Sekine, W.; Haraguchi, Y.; Shimizu, T.; Umezawa, A. & Okano, T. Thickness Limitation and Cell Viability of Multi-Layered Cell Sheets and Overcoming the Diffusion Limit by a Porous-Membrane Culture Insert. *J. Biochips Tissue chips* ***S1:007*****,** (2011)
11. Hong, S.; Young, B. & Changmo, J. Multilayered Engineered Tissue Sheets for Vascularized Tissue Regeneration. *Tissue Eng. Regen. Med.* **14,** 371–381 (2017).
12. Lopes, D.; Martins-Cruz, C.; Oliveira, M. B.; Mano, J. F. Bone Physiology as Inspiration for Tissue Regenerative Therapies. *Biomaterials* **185,** 240–275 (2018).
13. Correia, C. R.; Pirraco, R. P.; Cerqueira, M. T.; Marques, A. P.; Reis, R. L. & Mano, J. F. Semipermeable Capsules Wrapping a Multifunctional and Self-Regulated Co-Culture Microenvironment for Osteogenic Differentiation. *Sci. Rep.* **6,** 21883 (2016).
14. Amini, A. R.; Laurencin, C. T. & Nukavarapu, S. P. Bone Tissue Engineering: Recent Advances and Challenges. *Crit. Rev. Biomed. Eng.* **40,** 363–408 (2012).
15. Rouwkema, J.; Khademhosseini, A. Trends in Biotechnology. *Trends Biotechnol.* **34,** 734–745 (2016).
16. Rouwkema, J.; Boer, J. De; Blitterswijk & C. A. Van. Endothelial Cells Assemble into a 3-Dimensional Prevascular Network in a Bone Tissue Engineering Construct. *Tissue Eng.* **12,**

2685–2693 (2006).
17. Ren, L.; Kang, Y.; Browne, C.; Bishop, J. & Yang, Y. Fabrication, Vascularization and Osteogenic Properties of a Novel Synthetic Biomimetic Induced Membrane for the Treatment of Large Bone Defects Liling. *Bone* **64,** 173–182 (2015).
18. Mano, F.; Reis, R. L. & Silva, R. M. P. Smart Thermoresponsive Coatings and Surfaces for Tissue Engineering : Switching Cell-Material Boundaries. *Trends Biotechnol.* **25,** 12–15 (2007).
19. Yamada, N.; Okano, T.; Sakai, H.; Karikusaa, F.; Sawasaki, Y.; Sakurai, Y. Thermo-Responsive Polymeric Surfaces ; Control of Attachment and Detachment of Cultured Cells. *Macromol. Rapid Commun.* **576,** 571–576 (1990).
20. Ito, A.; Takizawa, Y.; Honda, H.; Hata, K.; Kagami, H.; Ueda & M.; Kobayashi, T. Construction and Harvest of Multilayered Keratinocyte Sheets Using Magnetite Nanoparticles and Magnetic Force. *Tissue Eng.* **10,** 873–880 (2004).
21. Dobson, J. Remote Control of Cellular Behaviour with Magnetic Nanoparticles. *Nature Nanotechnology* **3,** 139–143 (2008).
22. Goncalves, A. I.; Miranda, M. S.; Rodrigues, M. T.; Reis, R. L.& Gomes, M. E. Magnetic Responsive Cell-Based Strategies for Diagnostics and Therapeutics. *Biomedical Materials* **13,** 54001 (2018).
23. Ito, A.; Takizawa, Y.; Honda, H.; Hata, K.; Kagami, H.; Ueda & M.; Kobayashi, T. Tissue Engineering Using Magnetite Nanoparticles and Magnetic Force: Heterotypic Layers of Cocultured Hepatocytes and Endothelial Cells. *Tissue Eng.* **10,** 833–840 (2004).
24. Gil, S.; Correia, C. R. & Mano, J. F. Magnetically Labeled Cells with Surface-Modified Fe3O4 Spherical and Rod-Shaped Magnetic Nanoparticles for Tissue Engineering Applications. *Adv. Healthc. Mater.* **4,** 883–891 (2015).
25. Baudin, B.; Bruneel, A.; Bosselut, N. & Vaubourdolle, M. A Protocol for Isolation and Culture of Human Umbilical Vein Endothelial Cells. *Nat. Protoc.* **2,** 481–485 (2007).
26. Kadam, S. S.; Tiwari, S. & Bhonde, R. R. Simultaneous Isolation of Vascular Endothelial Cells and Mesenchymal Stem Cells from the Human Umbilical Cord. *Vitr. Cell. Dev. Biol.- Anim.* ***45,*** 23–27 (2009).
27. Nowak-sliwinska, P.; Ballini, J.; Wagnières, G.; Bergh & H. Van Den. Processing of Fl Uorescence Angiograms for the Quanti Fi Cation of Vascular Effects Induced by Anti-Angiogenic Agents in the CAM Model. *Microvasc. Res.* **79,** 21–28 (2010).
28. Bayrakcı, M.; Maltaş, E.; Yiğiter, Ş.& Özmen, M. Synthesis and Application of Novel Magnetite Nanoparticle Based Azacrown Ether for Protein Recognition. *Macromol. Res.* **21,** 1029–1035 (2013).
29. Coates, J. Interpretation of Infrared Spectra, A Practical Approach. In *Encyclopedia of Analytical Chemistry*; Meyers, R.; McKelvy, M., Eds.; John Wiley & Sons, Inc., Chichester, (2006).
30. Zhang, H.; Zhou, Y.; Zhang, W.; Wang, K.; Xu, L.; Ma, H.& Deng, Y. Construction of Vascularized Tissue-Engineered Bone with a Double-Cell Sheet Complex. *Acta Biomater.* **77,** 212–227 (2018).
31. T, B. W. & Pasteris, J. D. A Mineralogical Perspective on the Apatite in Bone. *Materials Science and Engineering: C* **25,** 131–143 (2005).
32. Raynaud, S. & Champion, E. Calcium Phosphate Apatites with Variable Ca / P Atomic Ratio II . Calcination and Sintering. *Biomaterials* **23,** 1073–1080 (2002).
33. Pirraco, R. .; Melo-Ferreira, B.; Santos, T. C.; Frias, A. M.; Marques, A. P. & Reis, R. L. Adipose Stem Cell-Derived Osteoblasts Sustain the Functionality of Endothelial Progenitors from the Mononuclear Fraction of Umbilical Cord Blood. *Acta Biomater.* **9,** 5234–5242 (2013).
34. Tumarkin, E.; Lsan, T.; Csaszar, E.; Seo, M.; Zhang, H.; Lee, A.; Peerani, R.; Purpura, K.; Zandstra, P. W. & Kumacheva, E. High-Throughput Combinatorial Cell Co-Culture Using

Microfluidics. *Integr. Biol.* **3,** 653–662 (2011).
35. Hu, K. & Olsen, B. R. The Roles of Vascular Endothelial Growth Factor in Bone Repair and Regeneration. *System* **91,** 30–38 (1997).
36. Barati, D.; Ramin, S.; Shariati, P.; Moeinzadeh, S.; Melero-, J. M.; Khademhosseini, A. & Jabbari, E. Spatiotemporal Release of BMP-2 and VEGF Enhances Osteogenic and Vasculogenic Differentiation of Human Mesenchymal Stem Cells and Endothelial Colony-Forming Cells Co-Encapsulated in a Patterned Hydroge. *J. Control. Release* **223,** 126–136 (2017).
37. Torres, A. L.; Bidarra, S. J.; Pinto, M. T.; Aguiar, P. C.; Silva, E. A. & Barrias, C. C. Guiding Morphogenesis in Cell-Instructive Microgels for Therapeutic Angiogenesis. *Biomaterials* **154,** 34–47 (2018).
38. Asakawa, N.; Shimizu, T.; Tsuda, Y.; Sekiya, S.; Sasagawa, T.; Yamato, M.; Fukai, F. & Okano, T. Pre-Vascularization of in Vitro Three-Dimensional Tissues Created by Cell Sheet Engineering. *Biomaterials* **31,** 3903–3909 (2010).
39. Costa, M.; Cerqueira, M. T.; Santos, T. C.; Sampaio-Marques, B.; Ludovico, P.; Marques, A. P.; Pirraco, R. P. & Reis, R. L. Cell Sheet Engineering Using the Stromal Vascular Fraction of Adipose Tissue as a Vascularization Strategy. *Acta Biomater.* **55,** 131–143 (2017).
40. Sekiya, S.; Muraoka, M.; Sasagawa, T.; Shimizu, T.; Yamato, M. & Okano, T. Three-Dimensional Cell-Dense Constructs Containing Endothelial Cell-Networks Are an Effective Tool for in Vivo and in Vitro Vascular Biology Research. *Microvasc. Res.* **80,** 549–551 (2010).
41. Takeuchi, R.; Kuruma, Y.; Sekine, H.; Dobashi, I.; Yamato, M.; Umezu, M.; Shimizu, T. & Okano, T. In Vivo Vascularization of Cell Sheets Provided Better Long-Term Tissue Survival than Injection of Cell Suspension. *J. Tissue Eng. Regen. Med.* **10,** 700–710 (2016).
42. Kim, I. Y.; Iwatsuki, R.; Kikuta, K.; Morita, Y.; Miyazaki, T. & Ohtsuki, C. Thermoreversible Behavior of κ-Carrageenan and Its Apatite-Forming Ability in Simulated Body Fluid. *Mater. Sci. Eng. C* **31,** 1472–1476 (2011).
43. Castro, E. & Mano, J. F. Magnetic Force-Based Tissue Engineering and Regenerative Medicine. *J. Biomed. Nanotechnol.* **9,** 1129–1136 (2013).
44. Gupta, A. K.; Naregalkar, R. R.; Vaidya, V. D. & Gupta, M. Recent Advances on Surface Engineering of Magnetic Iron Oxide Nanoparticles and Their Biomedical Applications. *Nanomedicine* **2,** 23–39 (2007).
45. Ito, A.; Shinkai, M.; Honda, H. & Kobayashi, T. Medical Application of Functionalized Magnetic Nanoparticles. *J. Biosci. Bioeng.* **100,** 1–11 (2005).
46. Shubayev, V. I.; Pisanic, T. R. & Jin, S. Magnetic Nanoparticles for Theragnostics. *Adv. Drug Deliv. Rev.* **61,** 467–477 (2009).
47. Nakamura, A.; Akahane, M.; Shigematsu, H.; Tadokoro, M. & Morita, Y. Cell Sheet Transplantation of Cultured Mesenchymal Stem Cells Enhances Bone Formation in a Rat Nonunion Model. *Bone* **46,** 418–424 (2010).
48. Liu, H.; Zhou, W.; Ren, N.; Feng, Z.; Dong, Y.; Bai, S. & Jiao, Y. Cell Sheets of Co-Cultured Endothelial Progenitor Cells and Mesenchymal Stromal Cells Promote Osseointegration in Irradiated Rat Bone. **1,** 1–12 (2017).
49. Lee, K.; Silva, E. A. & Mooney, D. J. Growth Factor Delivery-Based Tissue Engineering : General Approaches and a Review of Recent Developments. **4,** 153–170 (2011).
50. Baldwin, J.; Antille, M.; Bonda, U.; De-Juan-Pardo, E. M.; Khosrotehrani, K.; Ivanovski, S.; Petcu, E. & Hutmacher, D. In Vitro Pre-Vascularisation of Tissue-Engineered Construct: A Co-Culture Perspective. *Vasc. Cell* **6,** 13 (2014).
51. Grover, L. M.; Wright, A. J.; Gbureck, U.; Bolarinwa, A.; Song, J.; Liu, Y.; Farrar, D. F.; Howling, G.; Rose, J. & Barralet, J. E. Biomaterials The Effect of Amorphous Pyrophosphate on Calcium Phosphate Cement Resorption and Bone Generation. *Biomaterials* **34,** 6631–6637 (2013).
52. Liu, J.; Nam, H. K.; Campbell, C.; Gasque, K. C. da S.; Millán, J. L. & Hatch, N. E. Tissue-

Nonspecific Alkaline Phosphatase Deficiency Causes Abnormal Craniofacial Bone Development in the Alpl-/- Mouse Model of Infantile Hypophosphatasia. *Bone* **67,** 81–94 (2014).

53. Bailey, S.; Karsenty, G.; Gundberg, C.; Vashishth, D. & Haven, N. Osteocalcin and Osteopontin Influence Bone Morphology and Mechanical Properties. *Annals of the New York Academy of Sciences* **1409,** 79–84 (2018).
54. Zhang, W.; Zhu, C.; Wu, Y.; Ye, D.; Wang, S.; Zou, D.; Zhang, X.; Kaplan, D. & Jiang, X. VEGF and BMP-2 Promote Bone Regeneration by Facilitating Bone Marrow Stem Cell Homing and Differentiation. *Eur. Cells Mater.* **27,** 1–12 (2016).
55. Verseijden, F.; Jahr, H.; Posthumus-van Sluijs, S. J.; Hagen, T. L. T. Ten; Hovius, S. E. R.; Seynhaeve, A. L. B.; van Neck, J. W.; van Osch, G. J. V. M.; Hofer, S. O. P.; Hovious, S. E. R.; *et al.* Angiogenic Capacity of Human Adipose-Derived Stromal Cells During Adipogenic Differentiation: An In Vitro Study. *Tissue Eng. - Part A* **15,** 445–452 (2008).
56. Marupanthorn, A.; Tantrawatpan, C.; Kheolamai, P.; Tantikanlayaporn, D. & Manochantr, S. Bone Morphogenetic Protein-2 Enhances the Osteogenic Differentiation Capacity of Mesenchymal Stromal Cells Derived from Human Bone Marrow and Umbilical Cord. *Int. J. Mol. Med.* **39,** 654–662 (2017).
57. Thébaud, N. B.; Siadous, R.; Bareille, R.; Remy, M.; Daculsi, R.; Amédée, J. & Bordenave, L. Whatever Their Differentiation Status, Human Progenitor Derived – or Mature – Endothelial Cells Induce Osteoblastic Differentiation of Bone Marrow Stromal Cells. *Tissue Eng. Regen. Med.* ***6*****,** e51–e60 (2012).
58. Saleh, F. A.; Whyte, M. & Genever, P. G. Effects of Endothelial Cells on Human Mesenchymal Stem Cell Activity in a Three-Dimensional in Vitro Model. *Eur. Cells Mater.* **22,** 242–257 (2011).
59. Leszczynska, J.; Zyzynska-Granica, B.; Koziak, K. & Ruminski, S.; Lewandowska-Szumiel, M. Contribution of Endothelial Cells to Human Bone-Derived Cells Expansio in Coculture. *Tissue Eng. - Part A*, **19,** 393–402 (2012).
60. Miller, W. J.; Kayton, M. L.; Patton, A.; O'Connor, S.; He, M.; Vu, H.; Baibakov, G.; Lorang, D.; Knezevic, V.; Kohn, E.; *et al.* A Novel Technique for Quantifying Changes in Vascular Density, Endothelial Cell Proliferation and Protein Expression in Response to Modulators of Angiogenesis Using the Chick Chorioallantoic Membrane (CAM) Assay. *J. Transl. Med.* **2,** 1–12 (2004).
61. Nagamoto, Y.; Takayama, K.; Ohashi, K.; Okamoto, R.; Sakurai, F.; Tachibana, M.; Kawabata, K.& Mizuguchi, H. Transplantation of a Human IPSC-Derived Hepatocyte Sheet Increases Survival in Mice with Acute Liver Failure. **64,** 1–6 (2016).
62. Takagi, S.; Mandai, M.; Hirami, Y.; Kurimoto, Y.; Takahashi, M. Induced Pluripotent Stem Cell-Based Cell Therapy of the Retina. In *Medical Applications of iPS Cells : Innovation in Medical Sciences*; Inoue, H.; Nakamura, Y., Eds.; Springer Singapore: Singapore, 133–147 (2019).
63. Kawamura, M.; Miyaga, S.; Fukushima, S.; Saito, A.; Miki, K.; Miyagawa, S.; Fukushima, S.; Saito, A.; Miki, K.; Funakoshi, S.; *et al.* Enhanced Therapeutic Effects of Human IPS Cell Derived-Cardiomyocyte by Combined Cell-Sheets with Omental Flap Technique in Porcine Ischemic Cardiomyopathy Model. *Sci. Rep.* **7,** 8824–8824 (2017).
64. Lu, Y.; Zhang, W.; Wang, J.; Yang, G.; Yin, S.; Tang, T.; Yu, C. & Jiang, X. Recent Advances in Cell Sheet Technology for Bone and Cartilage Regeneration : From Preparation to Application. *Int. J. Oral Sci.* **11,** 17 (2019).
65. Wang, T.; Zhai, Y.; Nuzzo, M.; Yang, X.; Yang, Y. & Zhang, X. Layer-by-Layer Nanofiber-Enabled Engineering of Biomimetic Periosteum for Bone Repair and Reconstruction. *Biomaterials* **182,** 279–288 (2018).

Supporting Information

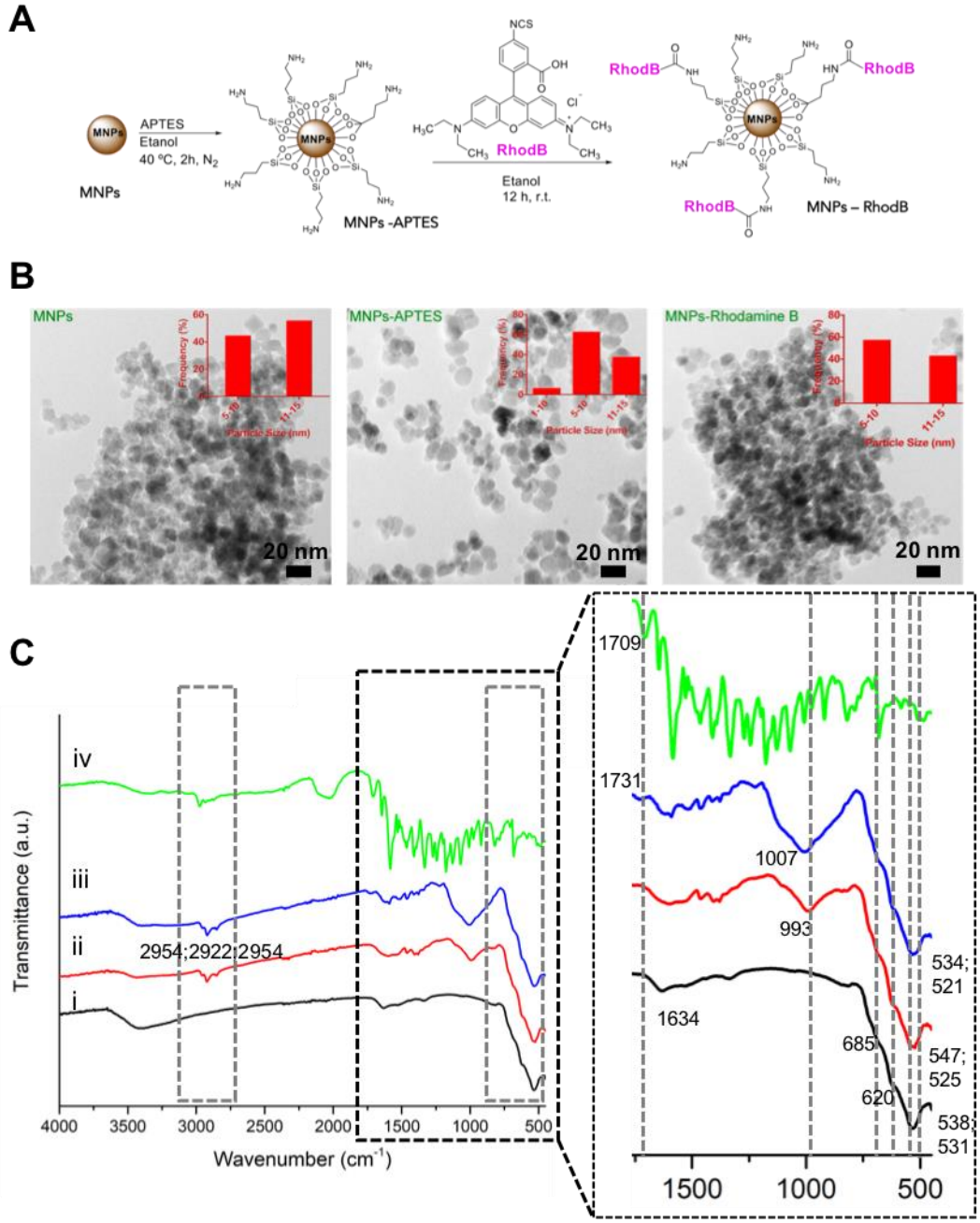

Figure V.S1: Characterization of MNPs. **A.** Schematic representation of the functionalization of the particles; **B.** TEM micrographs and size distribution of MNPs and its modifications. **C.** FTIR-spectra of i) MNPs unmodified; ii) MNPs-APTES; iii) MNPs-RodB; and RodB.

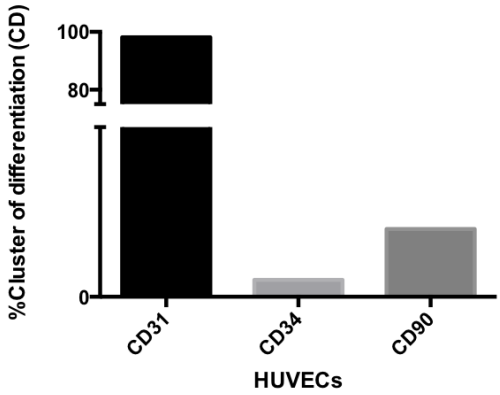

Figure V.S2: Flow cytometry analysis of surface markers expression of HUVECs.

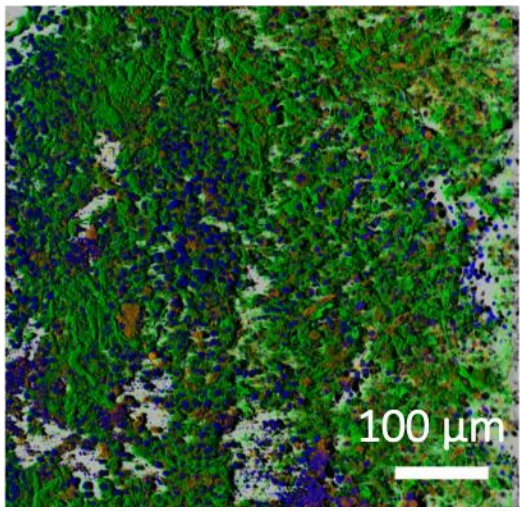

Figure V.S3: Confocal microscopy of vinculin staining in heterotypic CS. After 7 days of culture, the cell-cell and cell-matrix junctions were demonstrated by the presence of vinculin (in orange) in actin cytoskeleton (in green). Cell nuclei are depicted in DAPI (blue).

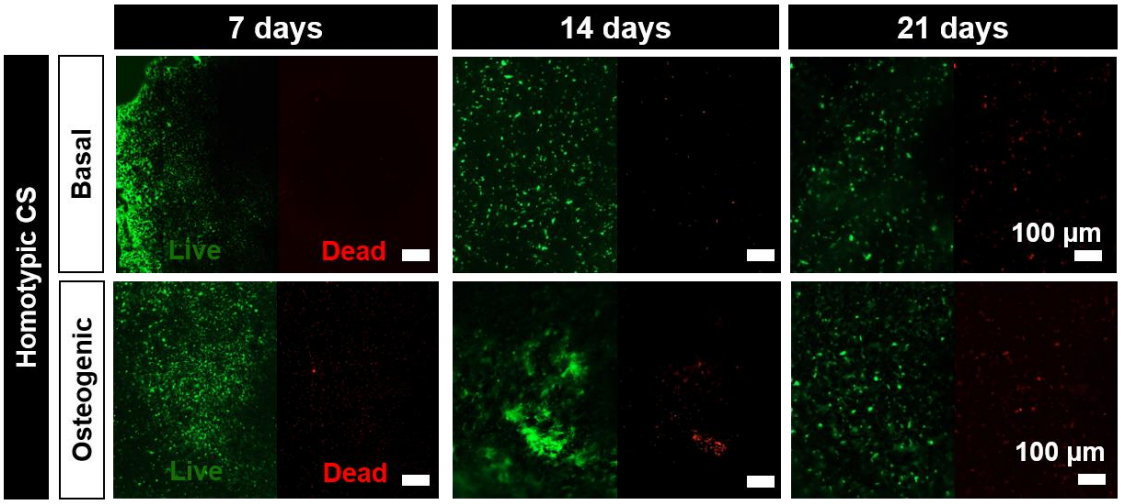

Figure V.S4: Live-dead assay of homotypic CSs. Live-dead fluorescence assay at day 7, 14 and 21 of culture in basal and osteogenic medium. Living cells were stained by calcein (green) and dead cells by propidium iodide (red).

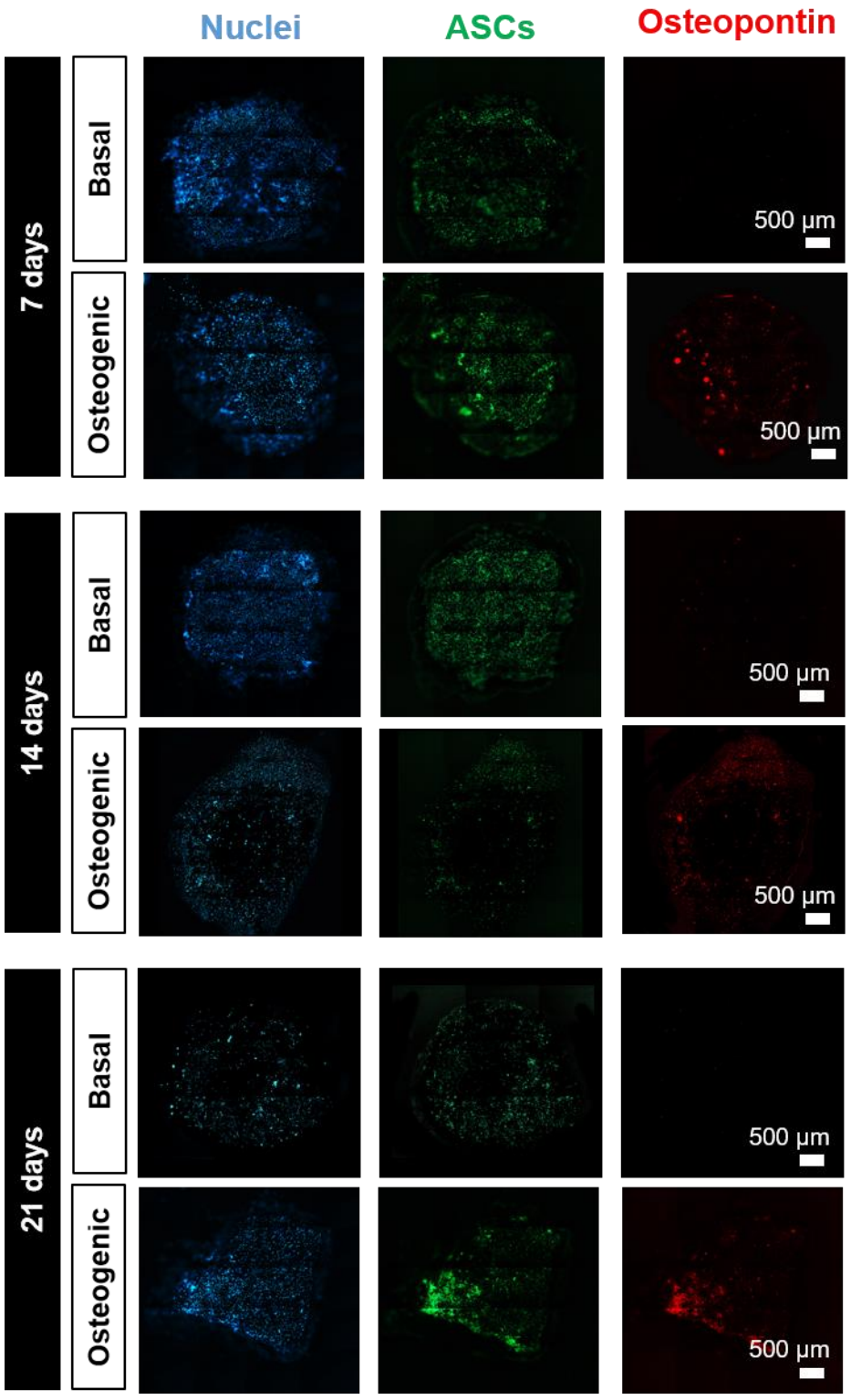

Figure V.S5: Osteopontin staining of homotypic CS. Immunofluorescence of ASCs (green), osteopontin (red) and cell nucleus- DAPI (blue) in 3D homotypic CS cultured for 7, 14 and 21 days in basal and osteogenic media.

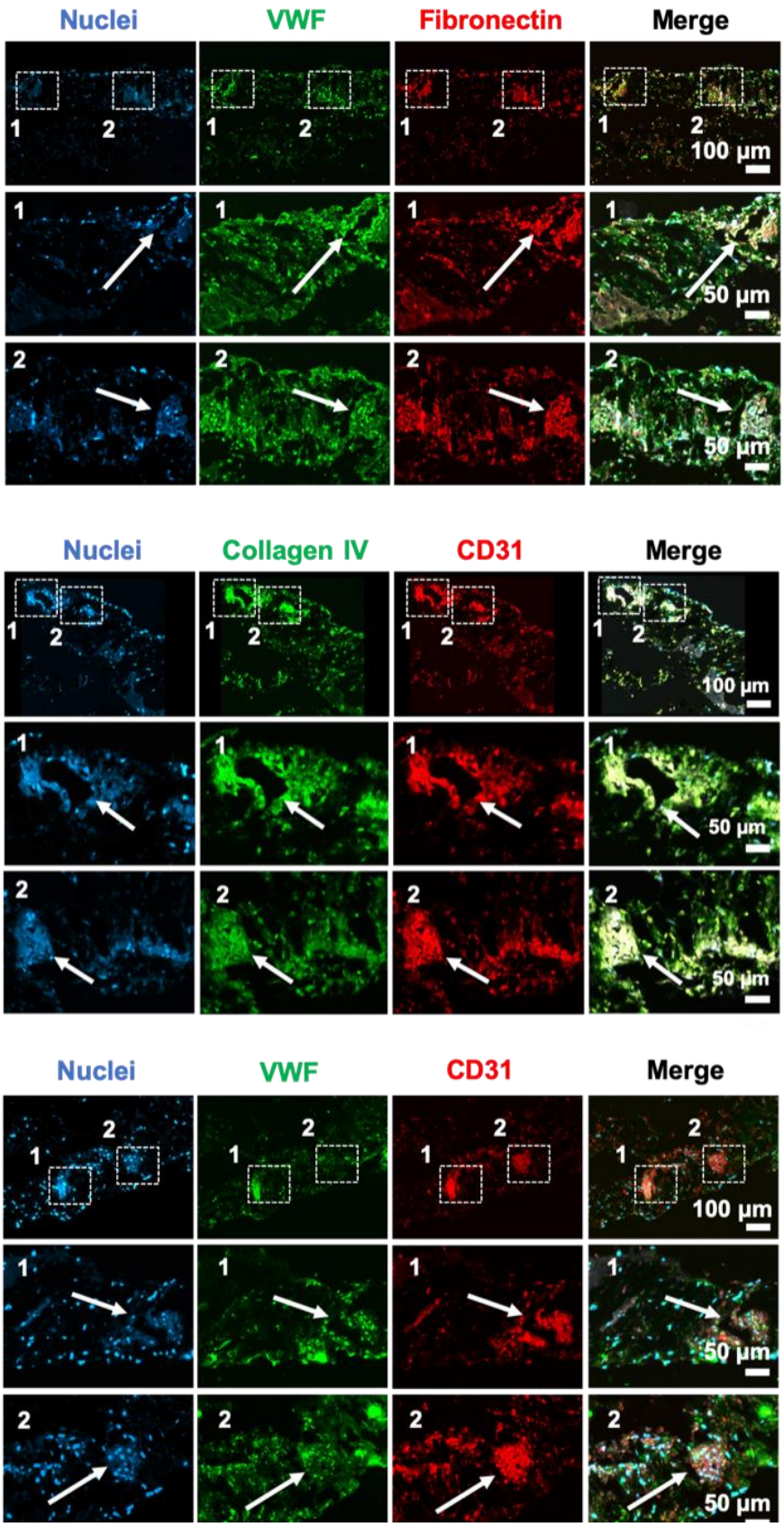

Figure V.S6: Immunostaining of CS with VWF(green)/FN(red); collagen IV(green)/CD31(red) and VWF(green)/CD31(red) demonstrating the presence of capillary-like structures (white arrows). DAPI stains the cells' nuclei.

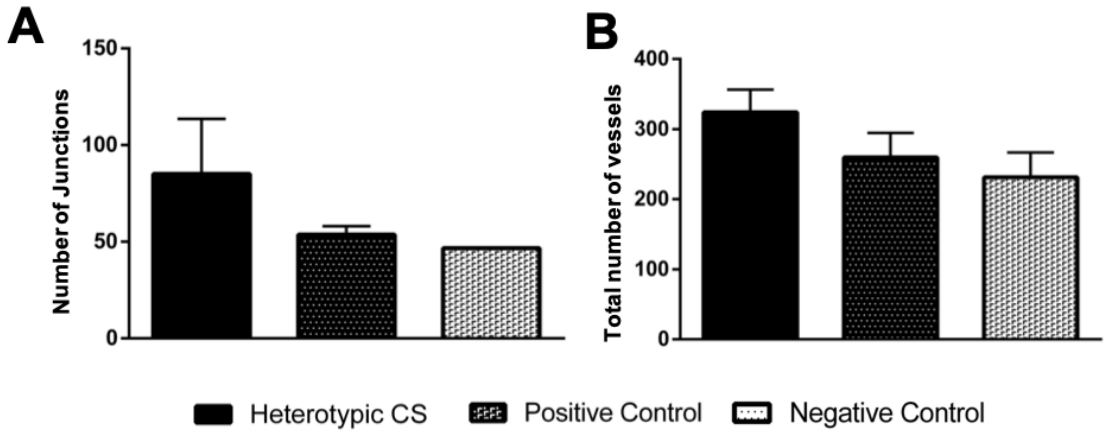

Figure V.S7: Number of junctions (**A**) and total number of vessels (**B**). Although higher values were evidenced for the heterotypic CS implanted within the CAM, no significant differences were evidenced.

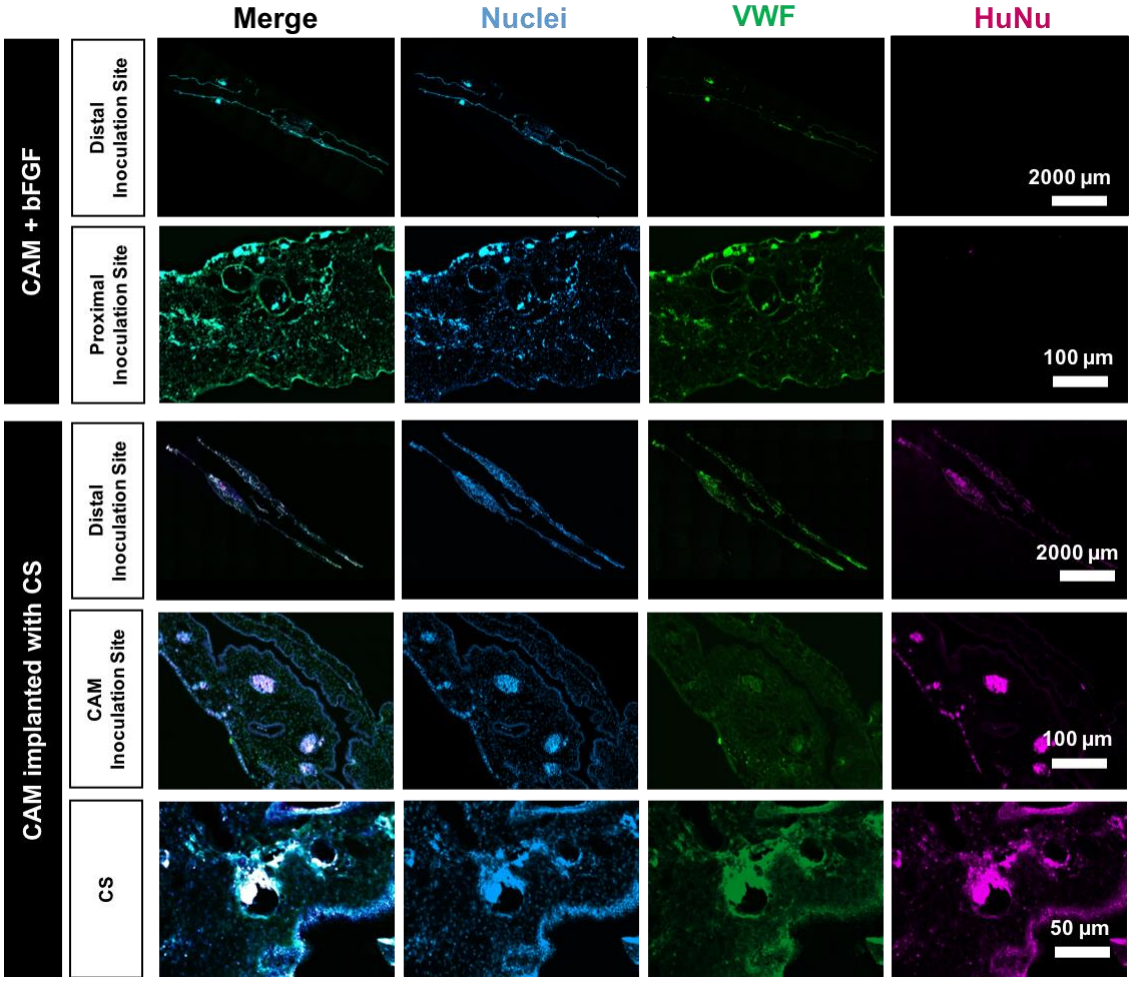

Figure V.S8: Immunostaining of CAM + bFGF (positive control) and CAM with implanted CS. VWF (in green) labels both human and chick endothelial cells, DAPI (in blue) stains all nuclei, and HuNu (in pink) stains the human nuclei. As displayed, human nuclei are integrated within the CAM and have integrated chick vasculature corroborated by the overlapping of VWF and HuNu stainings.

Chapter VI - Freestanding magnetic microtissues for tissue engineering applications[4]

Abstract

A long-sought goal in tissue engineering is the development of tissues able to recapitulate the complex architecture of the native counterpart. Microtissues, by resembling the functional units of living structures, can be used to recreate tissues' architecture. Howbeit, microfabrication methodologies fail to reproduce cell-based tissues with uniform shape. At the macroscale, complex tissues were already produced by magnetic-tissue engineering using solely magnetized cells as building materials. The enhanced extracellular matrix deposition guaranties the conservation of tissues' architecture, leading to a successful cellular engraftment. Following the same rational, we now propose the combination of a versatile microfabrication-platform with magnetic-tissue engineering to generate robust micro-tissues with complex architecture for tissue engineering purposes. Small tissue units with circle, square and fiber-like shapes were designed with high fidelity acting as building blocks for engineering complex tissues. Notably, freestanding microtissues maintained their geometry after 7 days post-culturing, overcoming the challenges of microtissues fabrication. Lastly, the ability of microtissues in invading distinct tissue models while releasing trophic factors was substantiated in methacryloyl laminarin and platelet lysates hydrogels. By simply using cells as building units and such microfabrication-platform, we envisage the fabrication of complex multiscale and multifunctional tissues with clinical relevance, including for therapies or disease models.

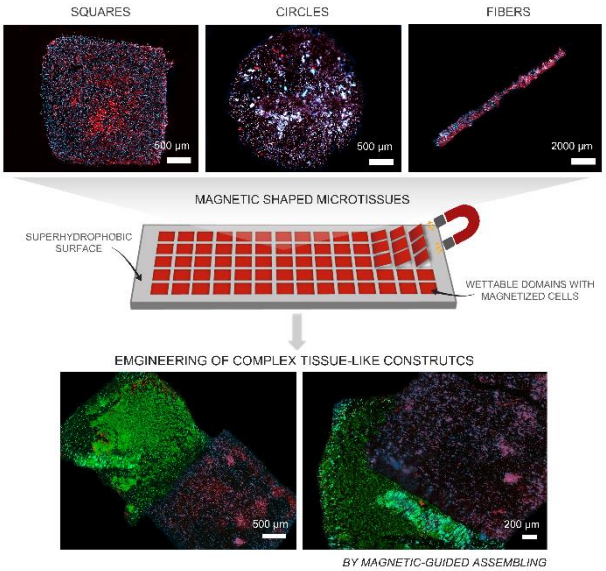

[4]Baseed on the publication: Lúcia F. Santos, Sónia G. Patrício, A. Sofia Silva, João F. Mano. Freestanding Magnetic Microtissues for Tissue Engineering Applications. *Advanced Healthcare Materials* **11,** 2101532 (2022).

1. Introduction

Despite of the incredible efforts of tissue engineering (TE) in integrating cell biology principles with materials science, the translation to clinical practice remains a challenge.[1] A feasible justification for such event relies in the lack of satisfactory morphological and functional features of the tissue engineered constructs. During the design of tissues *in vitro*, the engineered structures should preferentially recapitulate aspects of the architecture of the tissue microenvironment from the microscopic to macroscopic dimension levels, consistent with the hierarchical organization of biological systems.[2] In tissues, such complex hierarchy is formed by heterogeneous building blocks that are responsible for regulating their functionality.[2] By mimicking such native microstructural functional units with microarchitectural features, the emerging of modular TE aims to create more biomimetic engineered tissues, providing more guidance on the cellular level to direct tissue morphogenesis.[3] Several methodologies have been explored for the production of tissue building blocks, including fabrication of cell-encapsulating microscale hydrogels (microgels) or liquified compartments, self-assembled cell aggregation, generation of cell sheets (CSs) and direct printing of cells.[4,5] These small tissue units can be used as building blocks to engineer larger and heterogenous tissues, where each component can be easily adapted to fulfil the requirement of complex and hierarchical tissues. Although biomaterials have played a central role in the production of tissues *in vitro,* many works have evidenced the primordial role of cells as the local basic unit tissue builders and strategies have been focusing on minimizing the amount of biomaterials to increment the regenerative process.[6]

At the extreme of such minimalistic-engineering approaches, scaffold-free TE has emerged as a powerful strategy using multicellular building blocks, including spheroids, tissue strands and CSs to fabricate larger cohesive tissue constructs and produce extracellular matrix (ECM), essential for naturally developing their tissue architecture.[7,8] Particularly, CS engineering has been widely explored due to its ability to fabricate functional, complex and robust tissues.[9] Such approach allows to keep the natural networks of tissues without breaking them, through the harvesting of entire sheet-like cells, guarantying the maintenance of cell-cell and cell-ECM interactions.[10] Classically, CSs are recovery by thermo-responsive methodologies in a non-invasive manner, typically by using poly(N-isopropylacrylamide) thermo-responsive substrates. Such substrates are mainly limited by their high cost and low mechanical strength, as well as, by the cellular abnormalities linked to physiological changes within cell microenvironment.[11] Additionally, traditional CS engineering may be a challenge for the development of larger 3D tissue-like constructs due to their high complexity. In fact, stratified and heterotypic CSs have been previously produced through the individual stacking of formerly built CS monolayers in a time-consuming methodology, that may limits the establishment of cell-cell

interactions and hinder the spatial positioning control of the target cells.[12] As an alternative approach, magnetic-force based tissue engineering (Mag-TE) has been explored to produce CSs by combining magnetic force with CS technology, enabling an easier manipulation of those cells by a magnetic field.[13,14] A simple, one-pot and cost-effective strategy was recently proposed by our group, permitting the fabrication of robust 3D-like tissues by Mag-TE.[15] This strategy allowed the development of complex-shaped magnetic tissues at the macroscale, while exhibiting mechanical properties similar to soft tissues.[16] Hereto, complex magnetic tissues may be attained through the stacking of CSs or simple suspensions of magnetized cells (z-direction), in a stratified conformation.[12,17] To design 3D tissues akin to biological organisms it is crucial not only the fabrication of stratified constructs, but also the assembling of the tissues modules in a puzzle-like manner (x,y-directions).[3] To address this challenge, small basic units could be design at the microscale by Mag-TE and then, these micro-constructs could be assembled in heterogeneous, multi-layered tissue-like structures, with extreme control over x,y,z directions by using magnetic forces, avoiding contractibility issues.

In this work, we propose the fabrication of radically new freestanding microtissues with geometrically controlled shape and dimensions by Mag-TE using an accessible, scalable and high-throughput microfabrication platform. By miniaturizing the magnetic tissues, we hypothesize that these microstructures could be used as individual miniaturized tissues to be implanted using minimally invasive procedures or to be used as biological/ disease models. Additionally, they could act as building blocks to engineer complex and hierarchical tissue-like constructs. Overall, by combining a microfabrication platform with an optimized methodology of Mag-TE, we herein demonstrate the ability to fabricate living microtissues with well-defined sizes and architectures, circumventing one of the major problematics around CS fabrication that is tissue contractability. We envision that this newly explored methodology could open new insights for the use of such living microunits for tissue regenerative purposes.

2. Materials and Methods

All chemicals were purchased from Sigma-Aldrich and used as received, unless otherwise specified.

2.1. Production of superhydrophobic surfaces patterned with wettable superhydrophilic domains

The methodology followed to produce superhydrophobic surfaces (SH) patterned with wettable superhydrophilic (SL) domains has already been reported in the literature.[19] Briefly, glass microscope slides were activated by immersion in 1 M sodium hydroxide (NaOH, Eka) for 1 h, followed by neutralization in 1 M hydrochloric acid (HCl, Sigma-Aldrich) for 30 min. After activation, the glass slides

were modified with 20% v/v solution of 3-(trimethoxysilyl)propyl methacrylate (Sigma-Aldrich) in ethanol for 30 min at room temperature (RT). Afterwards, activated glass slides were placed in a vacuumed desiccator (50 mbar, 3-5 h) under trichloro(1H,1H,2H,2H-perfluorooctyl)silane (Sigma-Aldrich) atmosphere. Then, to create a thin polymer layer over the fluorinated glass slide, a polymerization mixture solution was prepared with 2- hydroxyethyl methacrylate (24 wt%, HEMA, Sigma-Aldrich), ethylene dimethacrylate (16 wt%, EDMA, Sigma-Aldrich), 1-decanol (12 wt%, Sigma-Aldrich), cyclohexanol (48 wt%, Sigma-Aldrich), and 2,2-dimethoxy-2-phenylacetophenone (0.4 wt%, DMPA, Sigma-Aldrich). To define the thickness of the polymer layer, two 12.5 µm thin strips of aluminium foil were applied on the corners of a fluorinated glass slide. Subsequently, the polymerization solution was applied over the fluorinated glass slide and a methacrylated glass slide was clamped on top of it. The polymerization was performed under 264 nm of UV radiation for 15 min and with 12 mW/cm^2 of intensity. After ethanol washing and nitrogen stream drying, the polymer layer was modified with 4-pentynoic acid via standard esterification. The esterification solution was prepared using dichloromethane (45 mL, Sigma-Aldrich), 4-(dimethylamino)pyridine (56 mg, Acros Organics), pentynoic acid (111.6 mg, Acros Organics), and of N,N'-diisopropylcarbodiimine (180 µL, Acros Organics), in continuous stirring for 4 h at RT. Ultimately, SH patterns with specific geometries were obtained by applying 5% v/v solution of 1H,1H,2H,2H-perfluorodecanethiol (PFDT, Sigma-Aldrich) in acetone onto the polymer surface, followed by UV irradiation (264 nm) through a quartz photomask at 12 mW/cm^2 for 1 min. The remaining alkyne groups were subjected to a thiol-yne reaction with 2-mercaptoethanol (10 % v/v, Alfa Aesar) under 264 nm of UV radiation for 15 min and with 12 $mW \cdot cm^2$ of intensity, originating the formation of SL areas.

2.2. Synthesis and Characterization of Magnetic Nanoparticles

Magnetite nanoparticles (MNPs) were synthesized as previously reported.[17] Briefly, Fe_3O_4 MNPs nanoparticles were synthesized by the co-precipitation reaction of ferrous ($FeCl_2.4H_2O$) and ferric ($FeCl_3 .6H_2O$) salts in the presence of ammonium hydroxide (NH_4OH), at 60°C and under a nitrogen atmosphere. Then, MNPs surface was modified with APTES through a silanization procedure. After washing with deionized water and ethanol, Fe_3O_4-APTES MNPs were conjugated with rhodamine B isothiocyanate (RhodB) as before established.[17,47] Fe_3O_4 –APTES MNPs were previously dispersed in ethanol (5 mg/mL) and then incubated with RhodB (2.5 mg/mL) at RT, overnight. Lastly, Fe_3O_4–APTES RhodB MNPs were washed until no RhodB was detected and freeze dried.

2.3. Cell isolation and Culture

The collected tissues were obtained under a cooperation agreement between CICECO - Aveiro Institute of Materials, University of Aveiro and Hospital da Luz (Aveiro, Portugal), after approval of the Competent Ethics Committee (CEC). The human tissues received were handled in accordance with the guidelines approved by the CEC. Informed consent was obtained from all subjects. Subcutaneous adipose tissue from liposuction procedures was used to isolate human adipose stem cells (hASCs). Briefly, samples were transported in PBS supplemented with 10% (v/v) penicillin-streptomycin and kept at 4 °C. The lipoaspirates were washed with PBS and incubated with collagenase type II A (0.05% w/v) for 45 min at 37 °C in a shaking water bath. The digested samples were filtered (200µm) and centrifuged at 800 g for 10 min at 4 °C. The obtained stromal vascular fraction (SVF) was resuspended in erythrocyte lysis buffer at pH 7.4 containing ammonium chloride (155mM), potassium bicarbonate (5.7mM), and ethylenediaminetetraacetic acid (0.1M, EDTA) in distilled water. After 10 min of incubation at room temperature (RT), the mixture was centrifuged at 300 g for 5 minutes. To isolate the hASCs the red blood cell-free SVF was resuspended in α-MEM medium (Invitrogen) supplemented with fetal bovine serum (10%, FBS, Invitrogen) and penicillin-streptomycin (1% v/v). Culture medium was changed 48h after initial plating and then every 3-4 days.

2.4. Development of freestanding microtissues through magnetic CS engineering

Initially, hASCs were seeded at cell density of $2.4 \times 10^6/cm^2$ and incubated during 24 h at 37 °C and 5% CO_2 in a humidified atmosphere. Then, the cells were incubated with MNPs (1 mg/mL) for 4 h. Afterwards, cells were detached by adding trypLE Express during 5 min at 37 °C. After the centrifugation of the cells at 300 g, the magnetically labelled cells were transferred to the wettable SL domains of the SH surfaces, previously treated with 2% (w/v) alginate solution during 30 min at 37 °C to produce the magnetic microtissues. For the purpose, commercial neodymium block magnets 40 x 20 x 5 mm (strength of 137N and standard N42 magnetization, Supermagnet) were placed at the bottom of the micropatterned surfaces to provide magnetic force. To access the ability to produce hierarchical structures, hASCs were incubated the lipophilic dyes 3,3-dioctadecyloxacarbocyanine perchlorate (DIO, green) and 1,1-Dioctadecyl-3,3,3,3-Tetramethylindodicarbocyanine (DID, purple) (1 mL, 2 µM per 1×10^6 cells) during 300 min at 37°C, prior to cell seeding. Then, the freestanding microtissues were fabricated following a similar procedure. Hierarchical structures were obtained through the stacking of previously formed magnetic microtissues, aided by a neodymium magnet.

2.5. Characterization of the produced magnetic microtissues

After 7 days of culture, the microtissues with different geometries were fixed in formalin 10% (v/v) during 15 minutes at RT. Then, the samples were permeabilized with 0.1 % (v/v) Triton X for 5 minutes at RT and then immersed in 5 % (v/v) FBS/dPBS for 1h. To visualize the shaped structure, the microtissues were incubated with Flash Phalloidin Red 594 (1:50 in dPBS) during 45 min at RT and then counterstained with DAPI (1:1000 in dPBS) for 5 min at RT. The morphology of the freestanding magnetic microtissues with both circle and square-like shape was also accessed by Scanning Electron Microscopy (SEM). For the purpose, samples were washed with PBS and fixed at RT in formalin (10% v/v) for 15 min. After 1 h, samples were dehydrated in an increasing gradient series of ethanol for 10 min each. The samples were gold sputter-coated using an accelerating voltage of 15 kV and visualized by SEM (S4100, Hitachi, Japan).

The microtissues morphology – size and shape fidelity - was accessed by ImageJ software prior and after the magnetic harvesting. For the circle geometry, the shape fidelity was determined by accessing the roundness and circularity through the following equations (Equation 1 and 2), where a perfect circle will exhibit a roundness and circularity of 1.

$$Roundness = \frac{Perimeter}{\sqrt{4\pi \times Area}} \quad (1)$$

$$Circularity = \frac{4\pi \times Area}{Perimeter^2} \quad (2)$$

The shape fidelity of the microtissues with square geometry was determined by accessing the interior angle and the rectangularity by the following equation, where a perfect square will exhibit the typical four interior angle of 90°. Higher rectangularity values also implies a more rectangularity morphology.[48]

$$Rectangularity = \frac{Area}{Lenght \times Widht} \quad (3)$$

To attest the presence of cell-cell and cell-matrix junctions, the magnetic microtissues were incubated with anti-rabbit human vinculin antibody (1:50 in 5% FBS/dPBS, Invitrogen) for 3 h at RT. After samples washing with PBS, the microtissues were incubated with the secondary antibody donkey anti-rabbit AlexaFluor 594 (1:400 in 5% FBS/dPBS). To corroborate these results, a similar immunofluorescence procedure was performed with the addition of the anti-human CD324 - Alexa 488 (E-cadherin, 1:50 in 5% FBS/dPBS, Alfagene). Ultimately, the samples were incubated with Flash Phalloidin Green

488 (1:100 in dPBS) at RT during 45 min and then counterstaining with DAPI (1:1000 in dPBS) for 5 min at RT. Lastly, the samples were visualized by fluorescence microscopy (Axio Imager 2, Zeiss).
The immunofluorescence staining in histological sections was also performed in microtissues after 7 days of culture. The samples previously fixed in 10% (v/v) of formalin were routinely processed in an automated system and embedded in paraffin. The integrity of the produced microtissues was investigated in the histological cross-sections. Sequential sections of 5 µm thickness were produced in adhesive slides to the Haematoxylin & Eosin (H&E) and Masson Trichrome staining.

2.6. Assessment of the morphology of the freestanding microtissues and cell viability

Magnetic microtissues with non-conventional geometry (square-like shapes) were cultured in the micropatterned surfaces during 2 and 7 days - short culturing time and long culturing time, respectively. After such culturing periods, the freestanding magnetic microtissues were peel-off from the surface and cultured in non-adherent plates for 7 days in α-MEM medium. For both culturing times, the microtissues morphology – size and shape fidelity were accessed by ImageJ software. As mentioned above, the shape fidelity of a square geometry can be determined by evaluating the interior angle and the rectangularity.[48]
The survival of the developed freestanding microtissues was accessed after 1, 3 and 7 days through a live-dead fluorescence assay according to the manufacturer's recommendation (ThermoFisher Scientific). Briefly, the samples were washed with dPBS and then stained with the kit components at 37 °C for 20 min. Lastly, samples were visualized by fluorescence microscopy (Axio Imager 2, Zeiss).

2.7. Mitochondrial metabolic activity

Mitochondrial metabolic activity was also determined using an MTS colorimetric assay (CellTiter96® AQueous one solution cell proliferation assay, Promega) as described by the manufacture. Freestanding microtissues (n=3) were incubated with the reagent kit (120 µl per well) during 4 h at 37 °C, protected from light. Finally, the absorbance was read at 490 nm using a microplate reader (Synergy HTX, BioTek Intruments, USA).

2.8. Cell proliferation quantification

The cell proliferation was accessed through the quantification of total DNA of microtissues (Quant-iT™ PicoGreen™ dsDNA Assay Kit, Invitrogen™), previously cultured during 1, 3 and 7 days. Firstly, the samples (n=3) were incubated with 2 % (v/v) Triton 100X (in ultra-pure sterile water) during 1h at 37°C and then, the samples were frozen at −80 °C and stored until use. In order to guarantee that only DNA content would be selected for the quantification assay, MNPs were firstly segregated using a

neodymium magnet. After 10 min of incubation at RT, fluorescence was read at an excitation wavelength of 485/20nm and 528/20nm of emission using a microplate reader. A standard curve for DNA analysis was generated with the provided DNA standard from the DNA assay kit (Synergy HTX, BioTek Intruments, USA).

2.9. Evaluation of tissue invasion ability of the magnetic microtissues

The ability of the freestanding microtissues to invade *in vitro* tissue models was analysed in methacrylated laminarin (LAM) and methacrylated platelet lysates (PLMA) hydrogels, previously synthetized by well-established protocols of the group.[30,31] Briefly, lyophilized LAM (degree of modification - 60%) and PLMA (degree of modification - 25%) were dissolved in a solution of 0.5% w/v 2-hydroxy-4'-(2-hydroxyethoxy)-2-methylpropiophenone (in dPBS) to final concentration of 10% and 15%, respectively. Hydrogels were obtained by pipetting each polymer solution to polydimethylsiloxane (Dow Corning, USA) molds with 6 mm diameter followed by UV irradiation during 60 s at 1.2 W/cm^2 and 0.95 W/cm^2 for LAM and PLMA, respectively. Each microtissue was incorporated in-between two layers of hydrogel. Then, such constructs were cultured in α-MEM medium during 7, 14 and 21 days in both static and dynamic conditions. To attain the dynamic environment, the samples were placed in a stirrer plate with stirrer controller (Biomodul 40B Controller, voltage 115V) at 50 rpm.

2.9.1. Assessment of cell viability of CSs in the tissue models

The survival of the developed microtissues in the tissue models was accessed after 7, 4 and 21 days for both conditions through a live-dead fluorescence assay, following the manufacturer's specifications (ThermoFisher Scientific). Briefly, the samples were washed with dPBS and then stained with the kit components at 37 °C for 45 min. Lastly, samples were visualized by fluorescence microscopy (Axio Imager 2, Zeiss).

2.9.2. Evaluation of the invasion ability

The invasion ability of the freestanding microtissues was evaluated after 7, 14 and 21 days, by collecting brightfield images (Zeiss microscope). The image analysis of the invasion area was conducted by ImageJ software. The constructs (microtissue within hydrogel) were fixed after in formalin 10% (v/v) during 2h at RT. To visualize the invasion within the hydrogel, the aforementioned immunofluorescence staining was also performed in histological sections of the constructs. The samples previously fixed were routinely processed in an automated system and embedded in paraffin. Afterwards, sequential sections of 5 µm thickness were made in adhesive slides. The samples were treated with TE buffer (10 mM Tris/1 mM EDTA, pH 9) for 35 min at 95–98 °C for antigen retrieval.

Then, the samples were incubated 45 min with Flash Phalloidin Red 594 (1:50 in dPBS). All sections were counterstained with DAPI (1:500 in dPBS, Sigma). Control sections for each immunolabelling excluded primary antibody staining were performed. Images were also obtained using fluorescence microscopy (Axio Imager 2, Zeiss).

2.9.3. ELISA immunoassay quantification of cytokines

The expression of vascular endothelial growth factor (VEGF), osteopontin, hepatocyte growth factor (HGF) and interleukin 6 (IL-6) was accessed in the constructs through Elisa Kits (Abcam) according to manufacturer's specifications. For all conditions, the culture media was collected and stored at -80°C until further use. Finally, the absorbance was read at 450 nm using a microplate reader (Synergy HTX, BioTek Intruments, USA).

2.9.4. In vitro biomineralization analysis

After 21 days of culture, the *in vitro* mineralization of the microtissues in LAM and PLMA hydrogels was accessed for both static and dynamic conditions. For this purpose, the deposition of hydroxyapatite nodules was visualized by SEM ((SU-70, Hitachi). Briefly, the microtissues were carbon-coated and analysed by Energy dispersive X-ray spectroscopy (EDS) (QUANTAX 400, Bruker) at an electron voltage of 15 kV.

2.10. Statistics

Statistical analysis was performed using t-test (GraphPad Prism 6.0) with a significance level set at $P < 0.05$. All results were stated as mean ± standard error.

3. Results and Discussion

3.1. Fabrication of the freestanding magnetic tissues

Firstly, magnetic nanoparticles were incubated with cells to allow cellular internalization. Thereafter, the magnetic cells were exposed to an external magnetic field, allowing their controlled manipulation.[13,18] As a platform to produce these small units, we used superhydrophobic surfaces (SH) patterned with wettable shaped domains (SL), where suspensions of cells could be dispersed and microsize CSs could be produced using Mag-TE principles. The dimension and shape of the cellular construct were both controlled by the photomask design. Such platforms were already explored in the fabrication of freestanding biomaterials at the micro scale with high fidelity of shape and dimension by following scaffold-based principles.[19,20] In this work, we intend to widen these promising high-

throughput platforms to engineer entirely living and robust micro-objects with highly tuned geometrical control.

The preparation of the micropatterned surfaces with wettable domains was based on the procedure described before.[19] After the successful isolation of human adipose-derived stem cells (hASCs) from adipose tissue and characterization by flow cytometry (**Figure S1**), the magnetized cells were obtained by the incorporation of magnetic nanoparticles (MNPs) within cells environment, as previously reported by the group.[17] The produced surfaces enabled the deposition of the magnetized cells in the

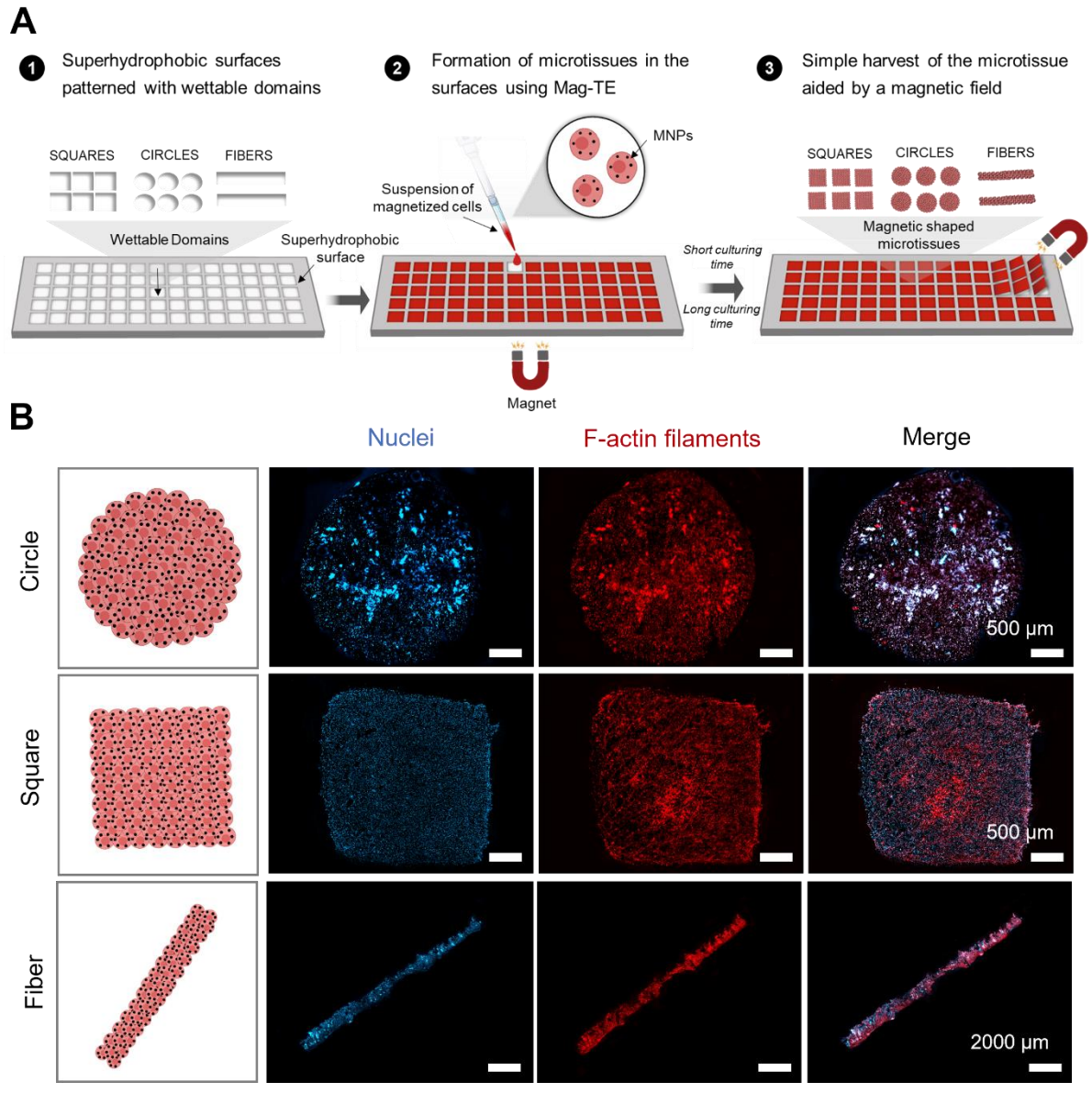

Figure VI.1: A. Schematic illustration of the fabrication of freestanding microtissues composed by hASCs, via Mag-TE. For the purpose, we used superhydrophobic surfaces patterned with wettable domains composed of diverse geometries, including circle, square and fiber-like shapes. The harvest and manipulation of such constructs was carried out with the aid of a magnetic field. **B**. Fluorescence images of the produced freestanding stamp-like microtissues with circle, square and fiber shapes after the harvesting process, previously cultured for 7 days. These images revealed a preserved structure with the presence of F-actin filaments (red) and nuclei (blue).

wettable spots of geometrically defined patterns - namely circle, square and fiber-like shape. Then, the magnet was placed under the surface, forcing the magnetized cells to occupy the bottom of the patterned spots (**Figure VI.1A**). After 7 days of culture in the microplatforms, very stable microtissues were formed. Since the wettable domains did not present adherent domains, the formed microtissues were easily recovered from the surface by magnetic activation on the top of the surface or even by simple agitation.

As displayed in **Figure VI.S2A**, the wettable domains were completely filled with microdroplets of magnetic-labelled cells with high geometric precision. Of note, freestanding magnetic microtissues with preserved geometries, namely circle, square and fiber-like shapes, were also recovered from the micropatterned surface after 7 days, as demonstrated in **Figure VI.1B**. For therapeutic use, it is highly favored that the tissue grafts mimic the anatomical shape of native tissue architecture or the geometry of a defect.

3.2. Morphological characterization of the produced magnetic microtissues

The cohesion of the newly formed stamp-like microtissues was attested through the presence of the red F-actin staining (**Figure VI.1B**). Further morphological characterizations corroborating the integrity of both circular and square microtissues were also performed on-surface, through quantitative fidelity measurements, and on the freestanding shapes, by using scanning electronic microscopy (SEM), hematoxylin & eosin (H&E) and Masson trichrome staining, and the immunostaining of collagen I and the adhesion proteins vinculin and e-cadherin.

For the purpose of quantitively assess the fidelity of cell seeding on patterned domains, thus evaluating the precision and accuracy in recovering the microtissues from the surface with the aid of the magnetic field, two different methodologies were employed: i) measurement of the size of the microtissues; and ii) measurement of the shape – roundness and circularity for circles, and rectangularity and interior angle for squares – **Figure VI.2A**. Pre-harvested microtissues showed over 98% size fidelity for both

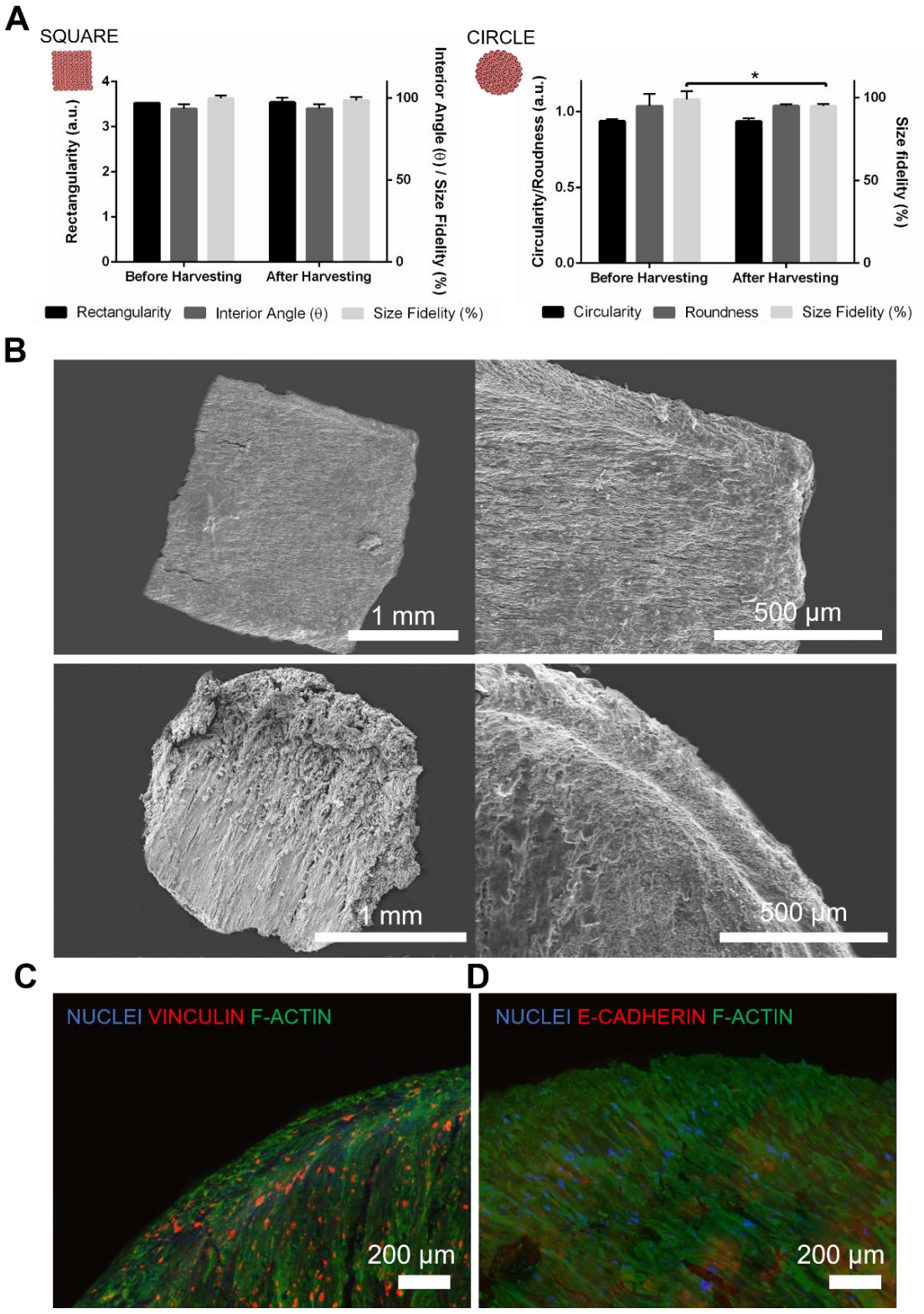

Figure VI.2: Morphological analysis of the freestanding magnetic cell-based microtissues with circle and square geometry. **A**. Assessment of size and shape fidelity of the produced microtissues prior and after the magnetic harvesting; **B**. SEM micrographs of the fabricated magnetic tissues with both geometries; **C**. Freestanding microtissues after 7 days of culture. The cell-cell interactions were visualized by the presence of the vinculin (in red) in F-actin filaments (in green). Cell nuclei are depicted in blue (DAPI); **D**. Cell-cell contact was evidenced through the presence of E-cadherin (in red).

circle and squares, which indicates the highly accurate recreation of the pattern by the magnetized cells. In turn, the size fidelity of the freestanding microtissues remains above the 96%. Similarly, microtissues with circle-shape did not show statistical differences in circularity and roundness after the magnetic harvesting. Analogous behaviour was found for the square microtissues, that did not show changes in the rectangularity and interior angle in the freestanding manner. These results substantiate the efficiency of this approach in the creation of small microtissues with very precise shapes.

The SEM images evidenced in **Figure VI.2B** corroborate the well-defined geometry of these microtissues merely composed by magnetized cells. High cell dense constructs were obtained as exemplified in **Figure VI.S3A**, exhibiting a thickness of approximately of 48.7 ± 5.7 μm (**Figure VI.S3B**). The integrity and robustness of such typical scaffold-free systems are normally associated with their natural self-assembly tendency and the generation of their own ECM.[21] Hence, after confirming the integrity of the microtissues with the H&E staining (**Figure VI.S3C**), we also verified the presence of cell-adhesive proteins such as collagen, that supports and anchors individual cells and the vascular network, exhibiting bioactive roles on morphogenesis and regeneration processes.[22] As displayed in **Figure VI.S3C**, a rich collagen matrix was evidenced in the developed microtissues after 7 days of culture, confirming the correct deposition of ECM within the engineered microtissues. The fabrication of robust tissue-like constructs requires strong cell-cell binding, involving integrin family proteins such as vinculin, that act as receptors for a wide range of ECM components being connected to the actin cytoskeleton.[23] The presence of vinculin in the produced microtissues revealed the high density of cell-cell interactions within the structure (**Figure VI.2C**), validating the robustness of the microtissues. Additionally, the existence of E-cadherin, a key member of the cadherin family that is primarily responsible for tight junctions of cell–cell interactions,[21] was also investigated in the freestanding microtissues and its wide representation can be depicted in **Figure VI.2D**. Activation of E-cadherin in association with cell-cell interactions during the formation of such scaffold-free structures ensures that fully compacted cells have access to putative critical autocrine signals by promoting the cell–cell exchange of signals.[21] Thus, we can assure that our microtissues present a compact construct with the formation of tight junctions along the structure, supporting the high robustness of magnetic tissue-like constructs.

3.3. Assessment of microtissues' architecture along the time

As previously mentioned, during the design of cell-based tissues *in vitro*, the constructs tend to compact along the time and normally, complex tissues are deformed losing their initial shape.[24] Hence, in a second step, we explored the maintenance of the microtissues' architecture without the presence of the magnetic field. To further understand the effect of the time of culture on the fidelity of

microtissues architecture, they were cultured for short (2 days) and long (7 days) periods. After that period (2 or 7 days) the magnetic microtissues were magnetically peeled-off from the surface and placed in non-adherent plates. The size and shape of the constructs were then evaluated for 7 days (**Figure VI.3A**). For the long culturing time, the freestanding magnetic microtissues showed a preserved structure up to 7 days of culture. The morphological analysis of the squares revealed a size fidelity of 97.9 ± 2.1 %. Non-significance differences were obtained after 7 days for rectangularity and interior angle. For the short culturing time (2 days), the microtissues partially lost their geometry, followed by the compaction of the tissue along the time. For this condition, the size fidelity decreased for 87.9 ± 4.2%, accompanied by the diminishing of the rectangularity and the typical interior angle of 90° of square geometries (**Figure VI.3B**).

3.4. Cell survival and proliferation of the freestanding magnetic microtissues

The live-dead assay showed that up to 7 days of culture, most of the cells remained viable for all formulations/culturing conditions (**Figure VI.S4** and **Figure VI.S5**). Since freestanding microtissues with long culturing time showed well-preserved architecture, we also accessed the cell proliferation for this condition, demonstrating an enhanced metabolic activity (**Figure VI.3C**) and DNA content (**Figure VI.3D**) along the time. It has been reported that in CS conformation, high cell dense tissues with 100-200 µm are not able to survive without adequate vascularization due to the lack of oxygen and essential nutrients.[25] Such evidence could explain the absence of proliferation in certain cell aggregates, according to literature findings. In this work, small tissue constructs were produced with the thickness of approximately 50 µm, guarantying the nutrition and oxygen suppling of the microtissues and consequently, prompting the proliferation of the tissues along the time. Thick magnetic tissues could be obtained by increasing the cell density.[16] Moreover, structures with higher dimension can also be fabricated by changing the photomask of the micropatterned platform. For larger tissue constructs, pre-vascularization strategies can be explored to accelerate the perfusion of oxygen and nutrients, prompting the fabrication of functional thick tissues by CS engineering.[17,25]
Microtissues cultured for the longest period (7 days) preserved their initial shape, remained viable and proliferated along the time, emphasizing the capacity of the mature microtissues to survive without requiring the presence of an adherent-substrate or the magnetic field. Such results are most likely related to the robustness of magnetic microtissues cultured during 7 days on the micropatterned surfaces. Notably, magnetic CSs demonstrated remarkable robustness even at microscale, overcoming the contractibility issues of scaffold-free strategies.

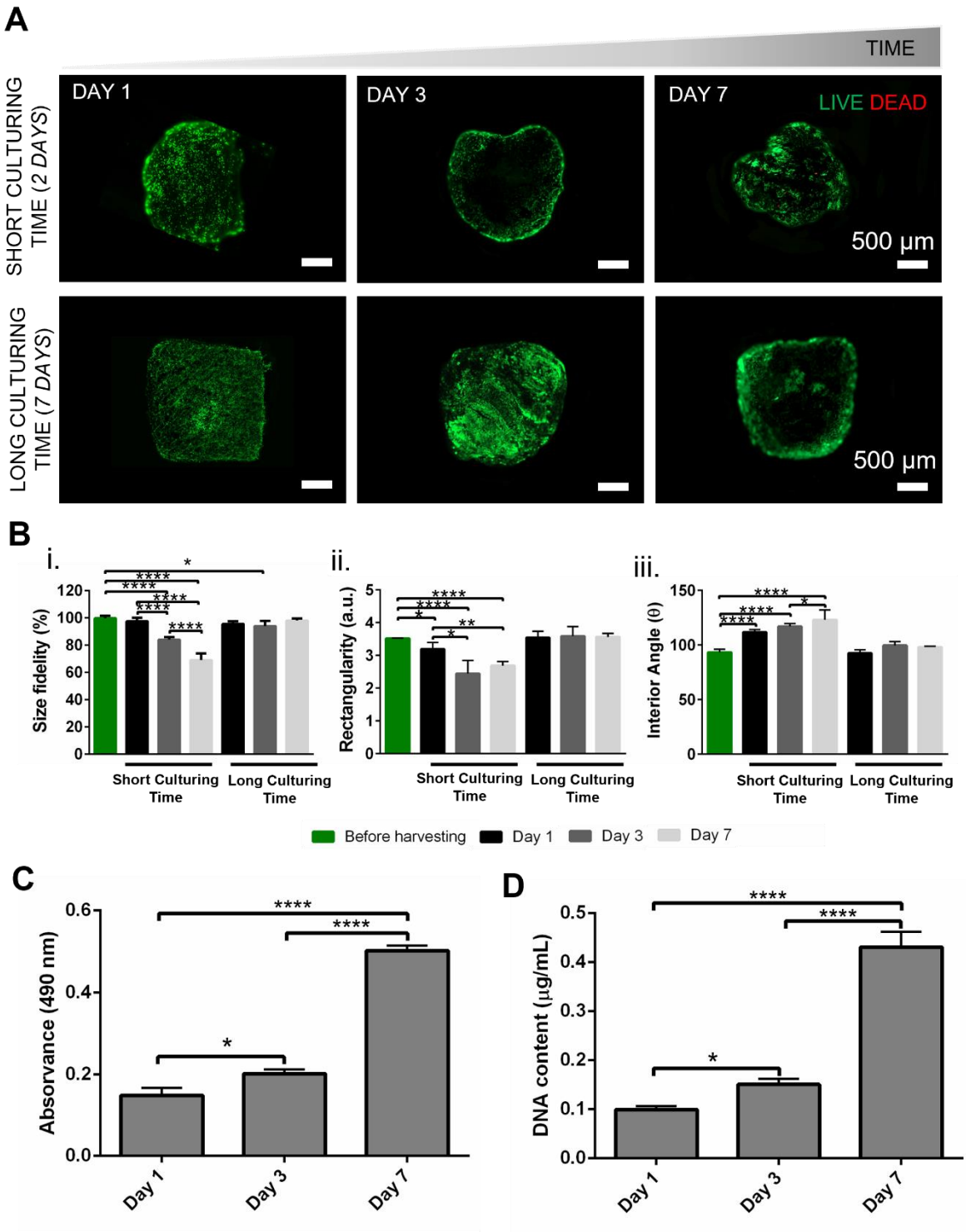

Figure VI.3: A. Live-dead fluorescence assay at days 1, 3 and 7 of culture of freestanding microtissues after short (2 days) and long culturing time (7 days). Living cells were stained with calcein (green) and dead cells by propidium iodide (red); **B**. Morphometric characterization of the freestanding microtissues - i) Size fidelity, ii) Rectangularity and iii) Interior Angle; **C**. Cell metabolic activity determined by MTS colorimetric assay; **D**. Cell proliferation by DNA quantification. $p < 0.05$: *$p < 0.05$; **$p < 0.01$; ***$p < 0.001$; ****$p < 0.0001$.

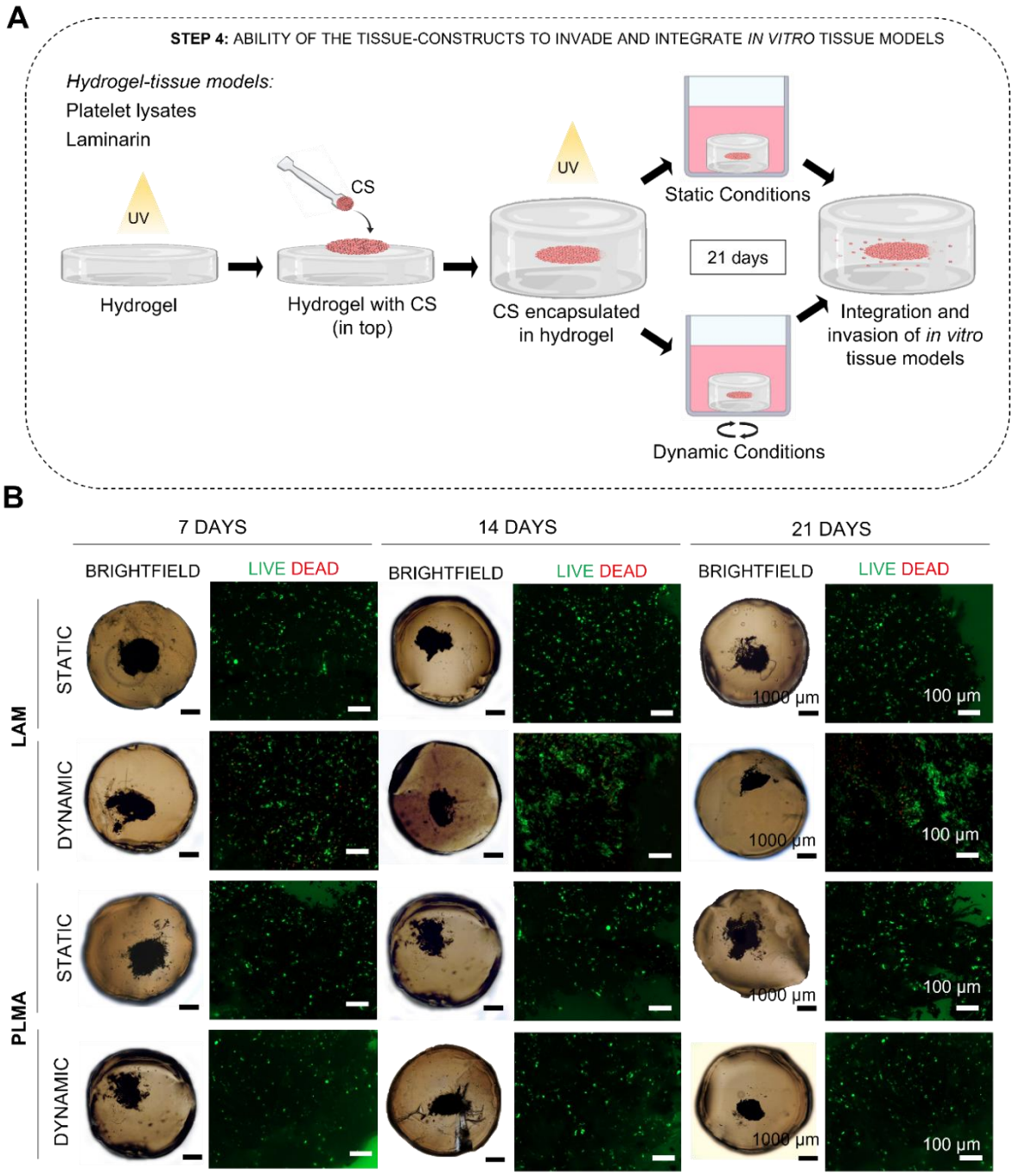

Figure VI.4: A. Schematic representation of freestanding magnetic microtissues ability to fill defects using LAM and PLMA hydrogels as *in vitro* tissue models, in static and dynamic conditions; **B.** Evaluation of the invasion of the freestanding microtissues in the *in vitro* tissue models after 7, 14 and 21 days. For each condition, the brightfield image of the construct (microtissue and hydrogel) is displayed in left panel. The cell survival in the hydrogels was also evaluated along the time for all conditions (in right panel). Living cells were stained by calcein (green) and dead cells by propidium iodide (red).

3.5. Determination of the invasion ability of the proposed freestanding magnetic microtissues

It is anticipated that such cell-based structures could be used to treat conditions requiring surgery or organ replacement, reconstituting the injury with cells capable of performing the function of the tissue

while providing trophic factors for native cells.[26,27] Hence, aiming a correct tissue implantation and regeneration, it is mandatory the integration of the biological constructs with the surrounding tissue.[26] In this sense, *in vitro* tissue models have been explored to attest the capability of tissue constructs in integrating within the host. Hydrogels are one of the most exploited models by allowing to mimic the native ECM.[28] Biopolymer-based scaffolds, mostly natural ones, have been receiving careful attention due to their ability to provide an appropriate environment to support cell functions and ultimately, tissue regeneration.[29] In the present study, two distinct natural-based scaffolds – methacryloyl laminarin (LAM) and methacryloyl platelet lysates (PLMA) hydrogels were used as *in vitro* tissue models to evaluated the invasion ability of the proposed freestanding microtissues.[30,31] Contrary to LAM hydrogels, which lack of cell adhesive domains, PLMA hydrogels display a rich environment in adhesive proteins and growth factors that support the cell growth and invasion.[32] Moreover, in an *in vivo* environment, cells are continuously subjected to physical stimuli, such as the mechanical one that truly influences the cell function and development. In fact, it is reported that the mechanical stimulus can enhance the activity of specific cells cultured *in vitro*, similarity to the *in vivo* scenario.[33] In this sense, we evaluated the ability of the freestanding microtissues in invading both tissue matrix models in both static and dynamic conditions. For this purpose, the microtissues were poured in-between two layers of the hydrogels (**Figure VI.4A**). The integrity and invasion area of the microtissues were then analyzed (**Figure VI.S6**). Initially, the cell viability of microtissues in the hydrogel tissue-models was demonstrated along the time for all conditions (**Figure VI.4B**). Then, the invasion of the developed microtissues within the tissue models was shown over 7 days - **Figure VI.4** and **VI.5**. More pronounced effects were visualized over 21 days in static conditions for both tissue models with higher invasion aeras. As expected, the mechanical stimulation induced the remodeling of ECM related with contraction and compaction phenomenon to produce a denser and more compact ECM.[34] Therefore, the dynamic condition boosted the cell-cell interactions, increasing the compaction of the microtissues along the time, diminishing the invasion area in the hydrogel tissue models (**Figure VI.5A** and **VI.5B**). Still, a greater invasion ability was anticipated and substantiated for PLMA hydrogels due to the rich environment in allogenic fibrous and adhesive proteins, growth factors and other bioactive factors.[32] When compared to the LAM hydrogels without adhesive domains, microtissues exhibited greater capacity to sprout and invade the structure in PLMA for the static condition.

3.5.1. Cytokines detection

Several works reported that stem cells could mediate organ-protective effects by enhancing the neovascularization at the injury sites and the production of local factors. The hASCs have recently shown that they can not only be used in either autologous or allogeneic cell transplants, but simultaneously act as modulators of the immune system.[35] In tissue defects, hASCs prompted the

tissue regeneration by paracrine activation of host cells through secretion of growth factors, autocrine signaling, or through direct cell–cell interactions.[36] The hASCs secrete angiogenic and antiapoptotic growth factors, such as vascular endothelial growth factor (VEGF) and hepatocyte Growth Factor (HGF) that lead to cell growth and suppress cell apoptosis. Results showed a decreased level of VEGF in the presence of dynamic environment for both hydrogel tissue models, with an enhanced effect on the PLMA hydrogel (**Figure VI.5C-i**). As reported in literature, VEGF is a strong angiogenic factor that plays a major role in blood vessel invasion and in the secretion of growth factors to stimulate osteogenesis.[37] Moreover, the down-regulation of VEGF is normally associated with cell differentiation, losing the ability to promote angiogenesis.[38] The multipotency of hASCs has generated interest due to their potential therapeutic value for regenerative medicine. By adding specific cocktails of chemical inducers, cytokines or external force, the differentiation of these cells can be directed.[39] Moreover, the biological similarity between the adipose-derived stem cells and bone-marrow stem cells has been encouraging their application for bone TE. Hence, the expression of osteopontin, a late osteogenic marker, was herein accessed and a higher level of this marker was found for the dynamic conditions (**Figure VI.5C-ii**), corroborating the osteogenic differentiation of the adipose-derived stem cells. We can therefore conclude that the mechanical stimulation prompted the osteogenic differentiation of our microtissues, as already well-documented in the literature.[40] In fact, the presence of shear stress affects the stem cells behavior, stimulating their osteogenic differentiation by enhancing the expression of several osteogenic factors like osteopontin.[40,41] Moreover, PLMA is composed by vitronectin,[31] an abundant multifunctional glycoprotein found in bone, capable of inducing differentiation in the absence of soluble osteoinductive factors.[42] To even substantiate the osteogenic potential of such microconstructs, we also investigated the mineralization of the microtissues after 21 days post-encapsulation in the hydrogels by energy dispersive spectroscopy (EDS). As anticipated, higher content of calcium (Ca) and phosphorus (P) was found to be more prominent for the dynamic conditions (**Figure VI.5D**). While the PLMA hydrogels exhibited the presence of these elements under both conditions (**Figure VI.5D-i**), with enhanced values in dynamic environment, the LAM hydrogels only show deposits of Ca and P under shear stress (**Figure VI.5D-ii**). The overlapping between Ca and P is represented in yellow (**Figure VI.5D-iii**), showing larger deposits of Ca/P for PLMA hydrogels in dynamic condition.

We anticipate that the higher expression of osteogenic markers found for the PLMA hydrogels under dynamic stimulation could be explained by the exposure of the encapsulated microtissues to a double stimulus: shear stress and the presence of osteoinductors like vitronectin.

We also prospected about the ability of the microtissues inserted on tissue models to act as providers of proinflammatory factors, key elements in response to a tissue injury.[43,44] After 21 days post-encapsulation, an increased level of HGF was attained for LAM hydrogels under dynamic environment

(**Figure VI.5E**). Higher levels of interleukin 6 (IL-6) (o proinflammatory cytokine that controls the propagation of the inflammation and accelerates the tissue repair) and HGF were achieved for PLMA hydrogels, with a more pronounced effect in the dynamic condition. In fact, the presence of cytokines like IL-6 and HGF was also implicated in bone tissue formation, being involved in the osteogenic differentiation of stem cells.[45] Such results corroborate the hypothesis that PLMA hydrogels under

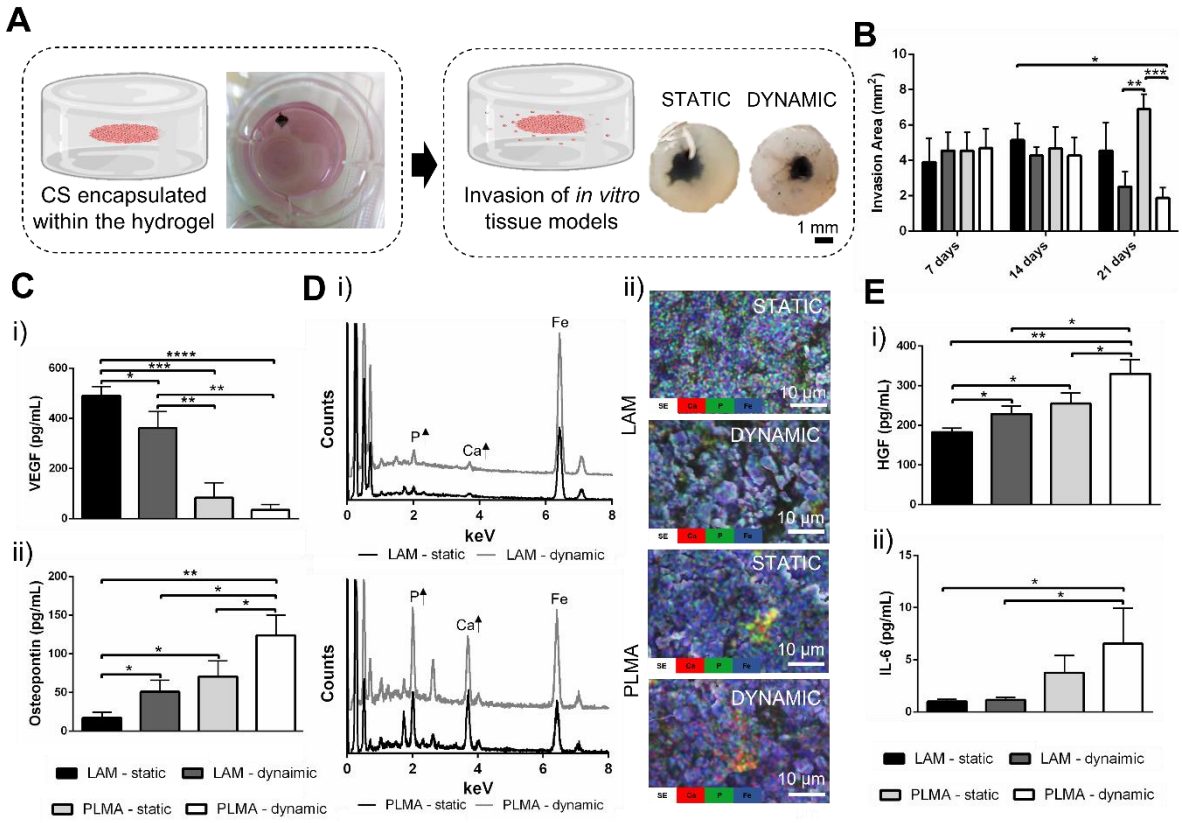

Figure VI.5: Evaluation of the microtissues invasion and their secretory profile in LAM and PLMA hydrogels for both static and dynamic conditions. **A**. Representative illustration of the ability of the CSs encapsulated within the hydrogels to invade and integrate the tissue models; **B**. Quantification of the invasion area of the freestanding magnetic microtissues; **C**. Evaluation of the angiogenic and osteogenic potential of the microtissues after 21 days in hydrogel through the expression of VEGF and osteopontin, respectively; **D**. Assessment of the *in* vitro biomineralization; i) Analysis of the mineral deposition within the magnetic microtissues by Energy dispersive X-ray spectroscopy (EDS); ii) Elemental analysis by chemical mapping of phosphorous (P, red), calcium (Ca, green) and ferrous (Fe, blue); **E**. Proinflammatory profile of microtissues encapsulated in the hydrogels after 21 days of culture: HGF and IL-6. $p < 0.05$: *$p < 0.05$; **$p < 0.01$; ***$p < 0.001$; ****$p < 0.0001$.

dynamic stimulation prompted the osteogenic differentiation of the encapsulated microtissues.

Such freestanding microtissues revealed the ability to provide trophic and immunomodulatory factors namely VEGF, HGF, IL-6 and osteopontin, essential to the proper regeneration of injured tissues. Moreover, the high permanence of cells in the *in vitro* models with decompaction occurring along the time, suggest that such tissue-like constructs may be promising candidates for localized delivery of

therapeutic stem cells, improving the repair of the injury and promoting the formation of healthy neotissues. By adapting the cell phenotype, we envision that these small building blocks can be extended to a wide variety of tissues.

3.6. Prospective application of the magnetic microtissues for tissue regeneration

Regardless of the potential of using such miniaturized tissues individually for TE purposes or simply biological/disease models, we foresee that such small microtissues can be also extended to the engineering of heterogenous tissues constructs by modular TE. **Figure S7** exemplifies that these small tissue units can be magnetic assembled into greater tissue constructs with high complexity. Nevertheless, in an idyllic scenario, the tissue engineering field aspires a total scaffold- and biomaterial-free tissue construct, while guarantying the remarkable properties, functionality, and feasibility of the *in vitro* structures heretofore fabricated. Hence, the next steps of magnetic tissue engineering will surely encompass the introduction of novel strategies for the fabrication of completely material-free tissues constructs, while ensuring the incredible features of the magnetic field in the development of such tissue structures. Magnetic-controllable devices able to capture and release cells were already reported in literature, by using MNPs modified with specific antibodies for the targeted cells.[46] Analogous strategies could be employed to produce material-free tissue constructs by the promising field of magnetic tissue engineering.

4. Conclusion

Overall, this work proposes the high-throughput fabrication of a cell-based microtissue construct, encompassing an array of geometries with high precision and definition, using a straightforward and scalable method. We anticipate that the versatility of the technology could be employed to develop stamp-like living microtissues with injectability, to be incorporated in bioprinting processes, or used individually as disease models or for basic biology studies. Moreover, such small tissue units can be used as building blocks to fabricate larger, modular and heterogenous tissue constructs, where each component can be easily adapted to fulfil the requirement of complex and hierarchical tissues. We hypothesize that such platform could endorse the engineering of tissues for regenerative-based therapies with high complexity and heterogeneity or *in vitro* platforms for disease modelling and drug screening.

Acknowledgements

We acknowledge the project CICECO-Aveiro Institute of Materials, UIDB/50011/2020 & UIDP/50011/2020, financed by national funds through the FCT/MEC and when appropriate co-financed by FEDER under the PT2020 Partnership Agreement and PROMENADE (Ref. PTDC/BTM-

MAT/29830/2017). This work was also supported by the project ATLAS (ref.ERC-2014-ADG-669858). The authors also acknowledge financial support by FCT through a Ph.D. grant (SFRH/BD/141523/2018, Lúcia F. Santos) and through individual contracts (CEECIND/00366/2020, Sónia G. Patrício), (CEECIND/2020.04344, A. Sofia. Silva).

References

1. S. M. Oliveira, R. L. Reis & J. F. Mano. Towards the design of 3D multiscale instructive tissue engineering constructs: Current approaches and trends. *Biotechnol. Adv.* **33,** 842-855 (2015).
2. S. Guven, P. Chen, F. Inci, S. Tasoglu, B. Erkmen & U. Demirci. Multiscale assembly for tissue engineering and regenerative medicine. *Trends Biotechnol.* **33,** 269-279 (2015).
3. V. M. Gaspar, P. Lavrador, J. Borges, M. B. Oliveira & J. F. Mano. Advanced bottom‐up engineering of living architectures. *Adv. Mater.* ***6,*** 1903975 (2019).
4. D. L. Elbert. Bottom-up tissue engineering. *Curr. Opin. Biotechnol.* **22,** 674-680 (2011).
5. C. R. Correia, S. Nadine & J. F. Mano. Cell encapsulation systems toward modular tissue regeneration: from immunoisolation to multifunctional devices. *Adv. Funct. Mater.* ***30,*** 1908061 (2020).
6. C. R. Correia, I. M. Bjørge, S. Nadine & J. F. Mano. Minimalist Tissue Engineering Approaches Using Low Material‐Based Bioengineered Systems. *Adv. Healthc. Mater.* **10,** 2002110 (2021).
7. A. Ovsianikov, A. Khademhosseini & V. Mironov. The synergy of scaffold-based and scaffold-free tissue engineering strategies *Trends Biotechnol.* **36,** 348-357 (2018).
8. C. Norotte, F. S. Marga, L. E. Niklason & G. Forgacs. Scaffold-free vascular tissue engineering using bioprinting. *Biomaterials* **30,** 5910-5917 (2009).
9. J. Yang, M. Yamato, C. Kohno, A. Nishimoto, H. Sekine, F. Fukai & T. Okano. Cell sheet engineering: recreating tissues without biodegradable scaffolds. *Biomaterials* **26,** 6415-6422 (2005).
10. R. M. P. da Silva, J. F. Mano & R. L. Reis. Smart thermoresponsive coatings and surfaces for tissue engineering: switching cell-material boundaries. *Trends Biotechnol.* **25,** 577-583 (2007).
11. I. Y. Kim, R. Iwatsuki, K. Kikuta, Y. Morita, T. Miyazaki & C. Ohtsuki. Thermoreversible behavior of κ-carrageenan and its apatite-forming ability in simulated body fluid. *Mater. Sci. Eng. C* **31,** 1472-1476 (2011).
12. A. Ito, H. Jitsunobu, Y. Kawabe & M. Kamihira. Construction of heterotypic cell sheets by magnetic force-based 3-D coculture of HepG2 and NIH3T3 cells. *J. Biosci. Bioeng.* **104,** 371-378 (2007).
13. A. Ito, Y. Takizawa, H. Honda, K. Hata, H. Kagami, M. Ueda & T. Kobayashi. Tissue engineering using magnetite nanoparticles and magnetic force: heterotypic layers of cocultured hepatocytes and endothelial cells *Tissue Eng.* **10,** 833-840 (2004).
14. E. Castro & J. F. Mano. Magnetic force-based tissue engineering and regenerative medicine. *J. Biomed. Nanotechnol.* **9,** 1129 (2013).
15. F. Xu, C. A. M. Wu, V. Rengarajan, T. D. Finley, H. O. Keles, Y. Sung, B. Li, U. A. Gurkan & U. Demirci. Three‐dimensional magnetic assembly of microscale hydrogels. *Adv. Mater.* **23,** 4254-4260 (2011).
16. L. F. Santos, A. Sofia Silva & J. F. Mano. Complex-shaped magnetic 3D cell-based structures for tissue engineering *Acta Biomater.* **118,** 18-31 (2020).
17. A. S. Silva, L. F. Santos, M. C. Mendes & J. F. Mano. Multi-layer pre-vascularized magnetic cell sheets for bone regeneration. *Biomaterials* **231,** 119664 (2020).
18. J. Dobson. Remote control of cellular behaviour with magnetic nanoparticles. *Nat. Nanotechnol.* **3,** 139-143 (2008)
19. A. I. Neto, K. Demir, A. A. Popova, M. B. Oliveira, J. F. Mano & P. A. Levkin. Fabrication of Hydrogel Particles of Defined Shapes Using Superhydrophobic‐Hydrophilic Micropatterns. *Adv. Mater.* **28,** 7613-7619 (2016).

20. S. Nadine, S. G. Patrício, C. C. Barrias, I. S. Choi, M. Matsusaki, C. R. Correia & J. F. Mano. Geometrically controlled liquefied capsules for modular tissue engineering strategies. *Adv. Biosyst.* **4,** 2000127 (2020).
21. S. Zhang, P. Liu, L. Chen, Y. Wang, Z. Wang & B. Zhang. The effects of spheroid formation of adipose-derived stem cells in a microgravity bioreactor on stemness properties and therapeutic potential. *Biomaterials* **41,** 15-25 (2015).
22. K. Hyldig, S. Riis, C. P. Pennisi, V. Zachar & T. Fink. Implications of extracellular matrix production by adipose tissue-derived stem cells for development of wound healing therapies. *Int. J. Mol. Sci.* **18,** 1167 (2017).
23. M. Bailly. Connecting cell adhesion to the actin polymerization machinery: vinculin as the missing link? *Trends Cell Biol.* **13,** 163-165 (2003).
24. E. Vrij, J. Rouwkema, V. Lapointe, C. Van Blitterswijk, R. Truckenmüller& N. Rivron. Directed assembly and development of material‐free tissues with complex architectures. *Adv. Mater.* **28,** 4032-4039 (2016).
25. K. Moschouris, N. Firoozi & Y. Kang. The application of cell sheet engineering in the vascularization of tissue regeneration. *Regen. Med.* **11,** 559-570 (2016).
26. D. Simpson, H. Liu, T.-H. M. Fan, R. Nerem & S. C. Dudley. A tissue engineering approach to progenitor cell delivery results in significant cell engraftment and improved myocardial remodeling. *Stem Cells* **25,** 2350-2357 (2007).
27. D. Howard, L. D. Buttery, K. M. Shakesheff & S. J. Roberts. Tissue engineering: strategies, stem cells and scaffolds. *J. Anat.* **213,** 66-72 (2008).
28. A. S. Hoffman. Hydrogels for biomedical applications. *Adv. Drug Deliv. Rev.* **64,** 18-23 (2012).
29. M. Zargarzadeh, A. J. R. Amaral, C. A. Custódio & J. F. Mano. Biomedical applications of laminarin. *Carbohydr. Polym.* **232,** 115774 (2020).
30. C. A. Custódio, R. L. Reis & J. F. Mano. Photo-cross-linked laminarin-based hydrogels for biomedical applications. *Biomacromolecules* **17,** 1602-1609 (2016).
31. S. C. Santos, C. A. Custódio & J. F. Mano. Photopolymerizable Platelet Lysate Hydrogels for Customizable 3D Cell Culture Platforms. *Adv. Healthc. Mater.* **7,** 1800849 (2018).
32. C. F. Monteiro, S. C. Santos, C. A. Custódio & J. F. Mano. Human platelet lysates‐based hydrogels: a novel personalized 3D platform for spheroid invasion assessment. *Adv. Sci.* **7,** 1902398 (2020).
33. C. Ribeiro, J. Pärssinen, V. Sencadas, V. Correia, S. Miettinen, V. P. Hytönen & S. Lanceros-Méndez. Dynamic piezoelectric stimulation enhances osteogenic differentiation of human adipose stem cells. *J. Biomed. Mater. Res. Part A* **103,** 2172-2175 (2015).
34. R. Gauvin, R. Parenteau-Bareil, D. Larouche, H. Marcoux, F. Bisson, A. Bonnet, F. A. Auger, S. Bolduc & L. Germain. Dynamic mechanical stimulations induce anisotropy and improve the tensile properties of engineered tissues produced without exogenous scaffolding. *Acta Biomater.* **7,** 3294-3301 (2011).
35. A. J. Braga Osorio Gomes Salgado, R. L. Goncalves Reis, N. Jorge Carvalho Sousa, J. M. Gimble, A. J. Salgado, R. L. Reis & N. Sousa. Adipose tissue derived stem cells secretome: soluble factors and their roles in regenerative medicine. *Curr. Stem Cell Res. Ther.* **5,** 103-110 (2010).
36. S. Natesan, D. G. Baer, T. J. Walters, M. Babu & R. J. Christy. Adipose-derived stem cell delivery into collagen gels using chitosan microspheres. *Tissue Eng. - Part A* **16,** 1369-1384 (2010).
37. K. Hu & B. R. Olsen. The roles of vascular endothelial growth factor in bone repair and regeneration. *Bone* **91,** 30-38 (2017).
38. C. R. Correia, R. P. Pirraco, M. T. Cerqueira, A. P. Marques, R. L. Reis & J. F. Mano. Semipermeable capsules wrapping a multifunctional and self-regulated co-culture microenvironment for osteogenic differentiation. *Sci. Rep.* **6,** 21883 (2016).
39. B. A. Bunnell, M. Flaat, C. Gagliardi, B. Patel & C. Ripoll. Adipose-derived stem cells: isolation, expansion and differentiation. *Methods* **45,** 115-120 (2008).
40. D. A. Hoey, S. Tormey, S. Ramcharan, F. J. O'Brien & C. R. Jacobs. Primary cilia-mediated mechanotransduction in human mesenchymal stem cells. *Stem Cells* **30,** 2561-2570 (2012).

41. S. Nadine, S. G. Patrício, C. R. Correia & J. F. Mano. Dynamic microfactories co-encapsulating osteoblastic and adipose-derived stromal cells for the biofabrication of bone units. *Biofabrication* **12,** 015005 (2020).
42. A. K. Kundu & A. J. Putnam. Vitronectin and collagen I differentially regulate osteogenesis in mesenchymal stem cells. *Biochem. Biophys. Res. Commun.* **347,** 347-357 (2006).
43. M. L. Novak & T. J. Koh. Macrophage phenotypes during tissue repair. *J. Leukoc. Biol.* **93,** 875-881 (2013).
44. G. M. Coudriet, J. He, M. Trucco, W. M. Mars & J. D. Piganelli. Hepatocyte growth factor modulates interleukin-6 production in bone marrow derived macrophages: implications for inflammatory mediated diseases. *PLoS One* **5,** e15384 (2010).
45. S. Deshpande, A. W. James, J. Blough, A. Donneys, S. C. Wang, P. S. Cederna, S. R. Buchman & B. Levi. Reconciling the effects of inflammatory cytokines on mesenchymal cell osteogenic differentiation. *J. Surg. Res.* **185,** 278-285 (2013).
46. X. Yu, R. He, S. Li, B. Cai, L. Zhao, L. Liao, W. Liu, Q. Zeng, H. Wang, S.-S. Guo & X.-Z. Zhao. Magneto‐controllable capture and release of cancer cells by using a micropillar device decorated with graphite oxide‐coated magnetic nanoparticles. *Small* **9,** 3895-3901 (2013).
47. S. Gil, C. R. Correia & J. F. Mano. Magnetically labeled cells with surface-modified Fe_3O_4 spherical and rod-shaped magnetic nanoparticles for tissue engineering applications. *Adv. Healthc. Mater.* **4,** 883-891 (2015).
48. H. Yu, K. P. Lim, S. Xiong, L. P. Tan & W. Shim. Functional morphometric analysis in cellular behaviors: shape and size matter. *Adv. Healthc. Mater.* **2,** 1188-1197 (2013).

Supporting Information

The successful isolation of hACSs from adipose tissue was determined by flow cytometry (Fig. S1). More than 87% of hACSs were found to be positive for mesenchymal stem cell markers CD105, CD90 and CD73 (hASCs).

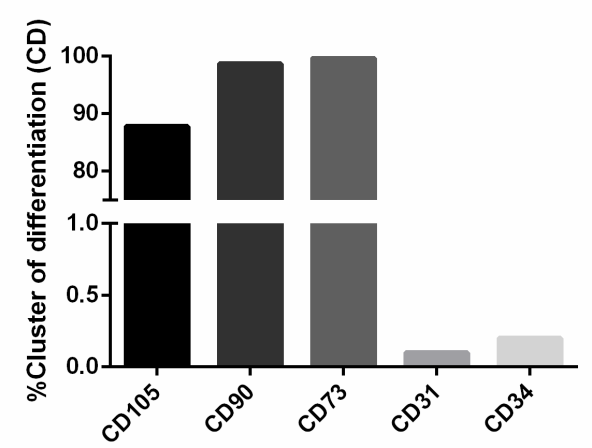

Figure VI.S1: Flow cytometry analysis of surface markers expression of hASCs.

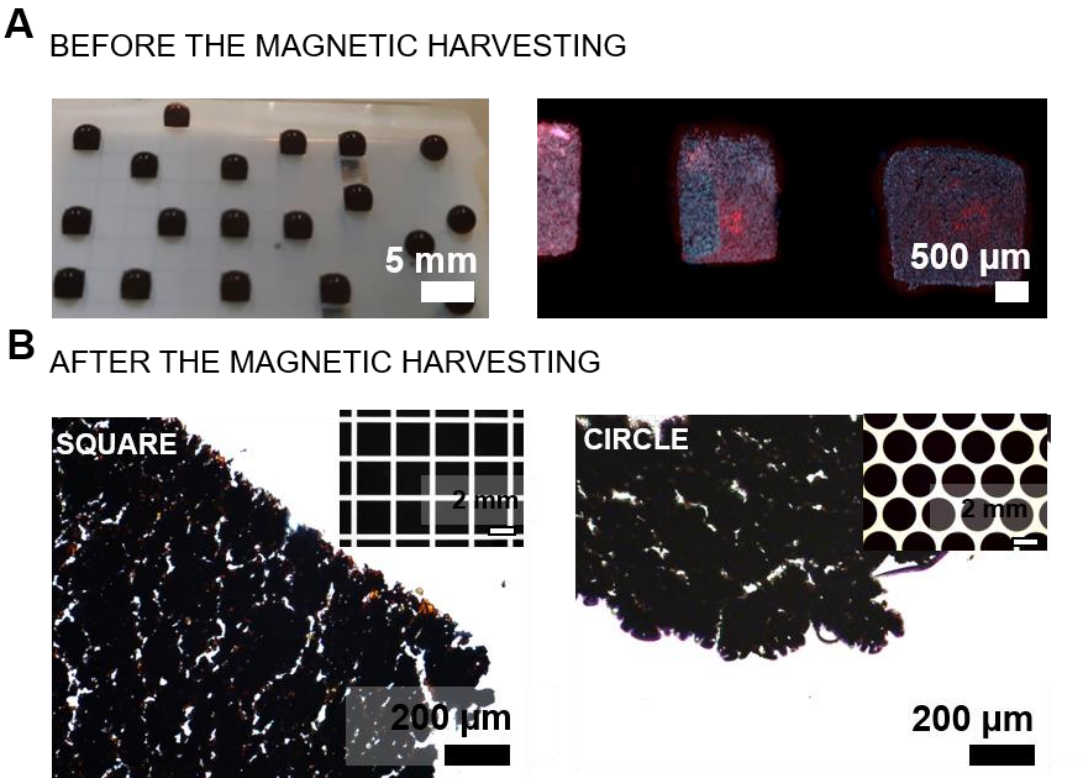

Figure VI.S2: Magnetic microtissues prior and after the magnetic harvesting. **A.** Superhydrophobic surfaces with the fabricated magnetic microtissues prior to the harvesting process. Brightfield images of the microtissues with well-defined geometries (in the left); Fluorescence images of the produced microtissues after 7 days of culture: cells' nuclei (in blue) and F-actin filaments (in red) – in the right; **B.** Brightfield images of the fabricated freestanding microtissues with the geometry of the micropatterned surface after the magnetic harvesting, namely square (in the left) and circle (in the right) like shapes.

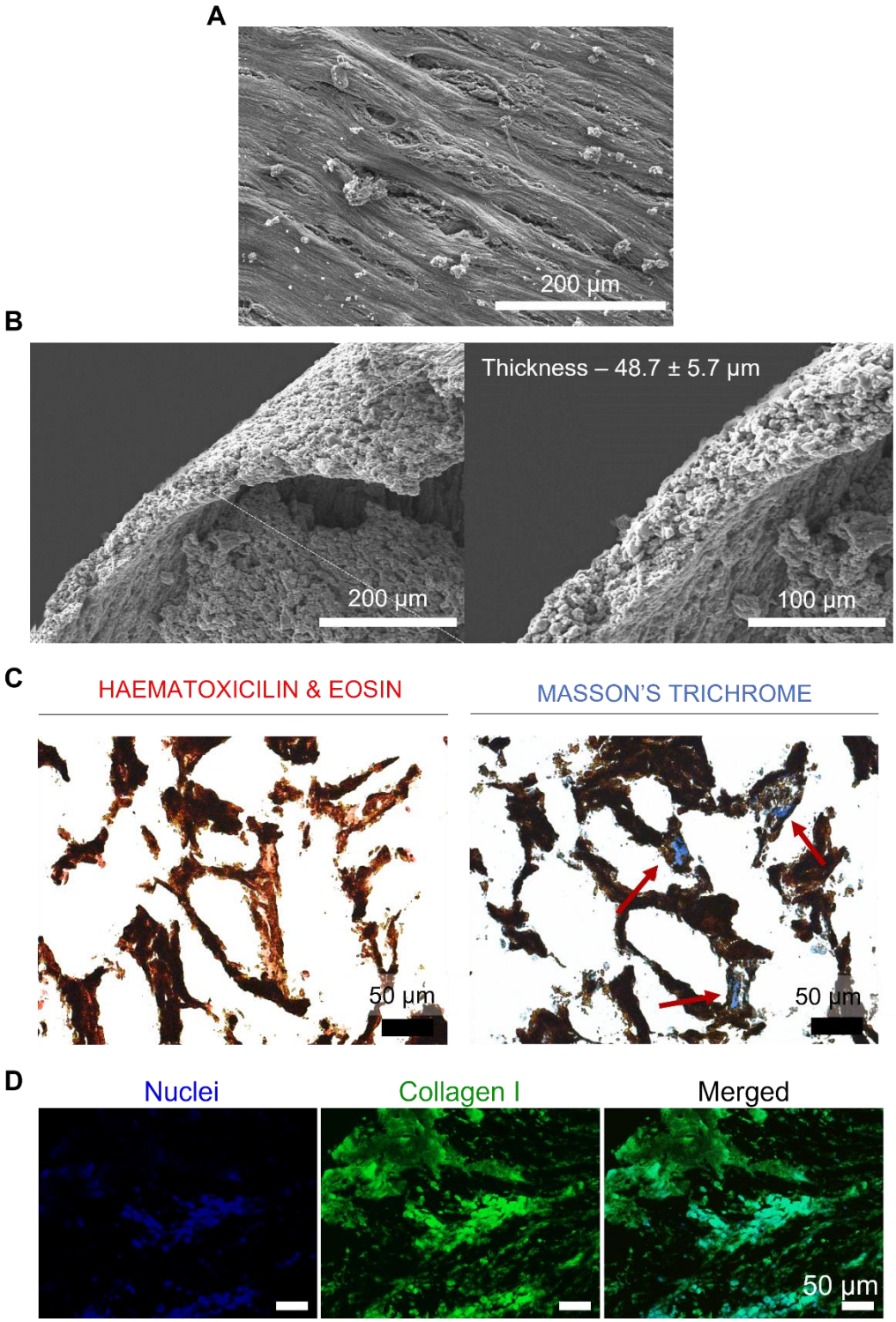

Figure VI.S3: Characterization of the fabricated microtissues. SEM micrographs of the freestanding microtissues after 7 days of culture, revealing a high cell dense structure (**A**) with a thickness of 48.7 ± 5.7 µm (**B**). The microtissues' integrity was also attested by Haematoxylin & Eosin and Masson's Trichrome staining of paraffin-embedded microtissues, displaying the collagenous connective tissue fibers (**C**). **D.** The presence of collagen matrix was also accessed by the immunostaining of collagen I (in green). The cell nuclei are in blue (DAPI).

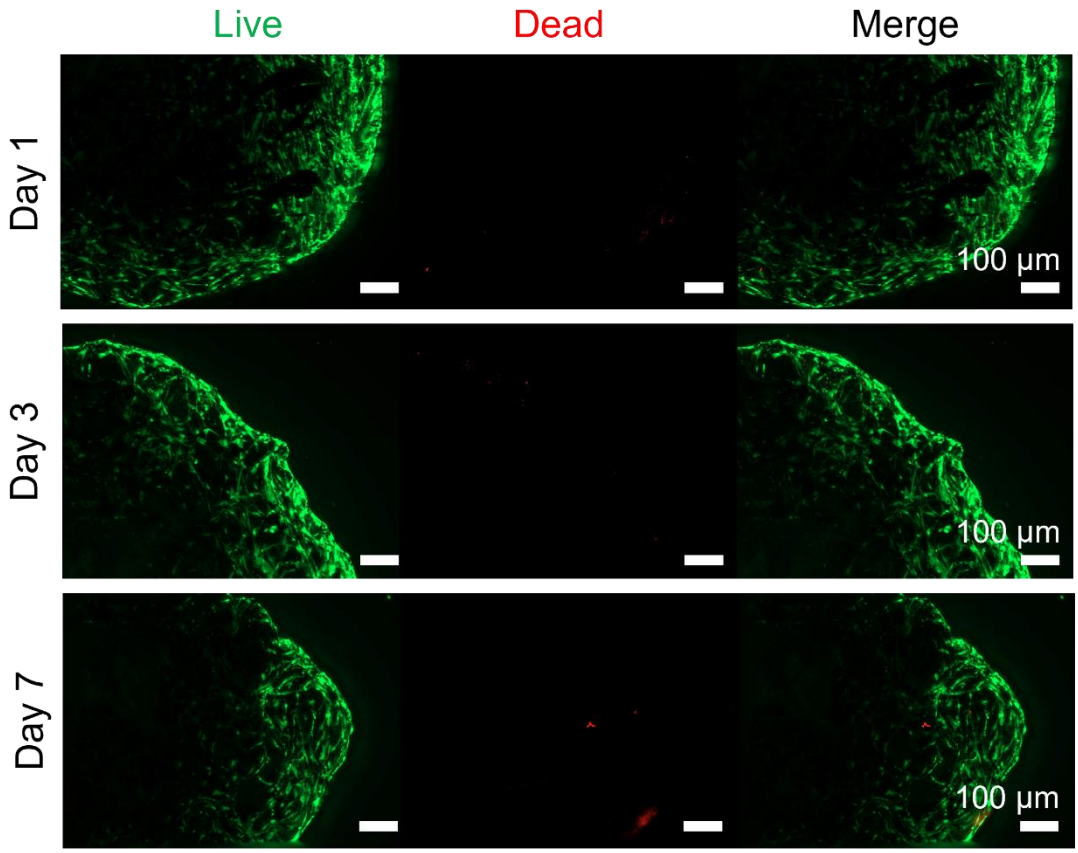

Figure VI.S4: Live-dead fluorescence assay of the freestanding magnetic microtissues after 1, 3 and 7 days of culture. Living cells were stained with calcein (green) and dead cells with propidium iodide (red).

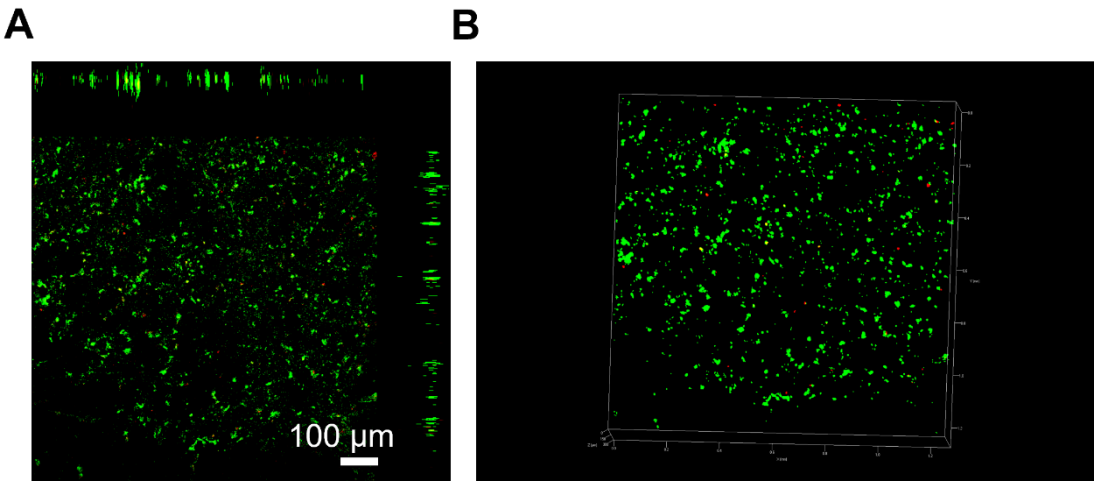

Figure VI.S5: A. Confocal images and side sections of magnetic microtissues after 7 days of culture, showing the living cells (calcein, in green) and the dead cells (PI, in red); **B.** 3D reconstruction of A.

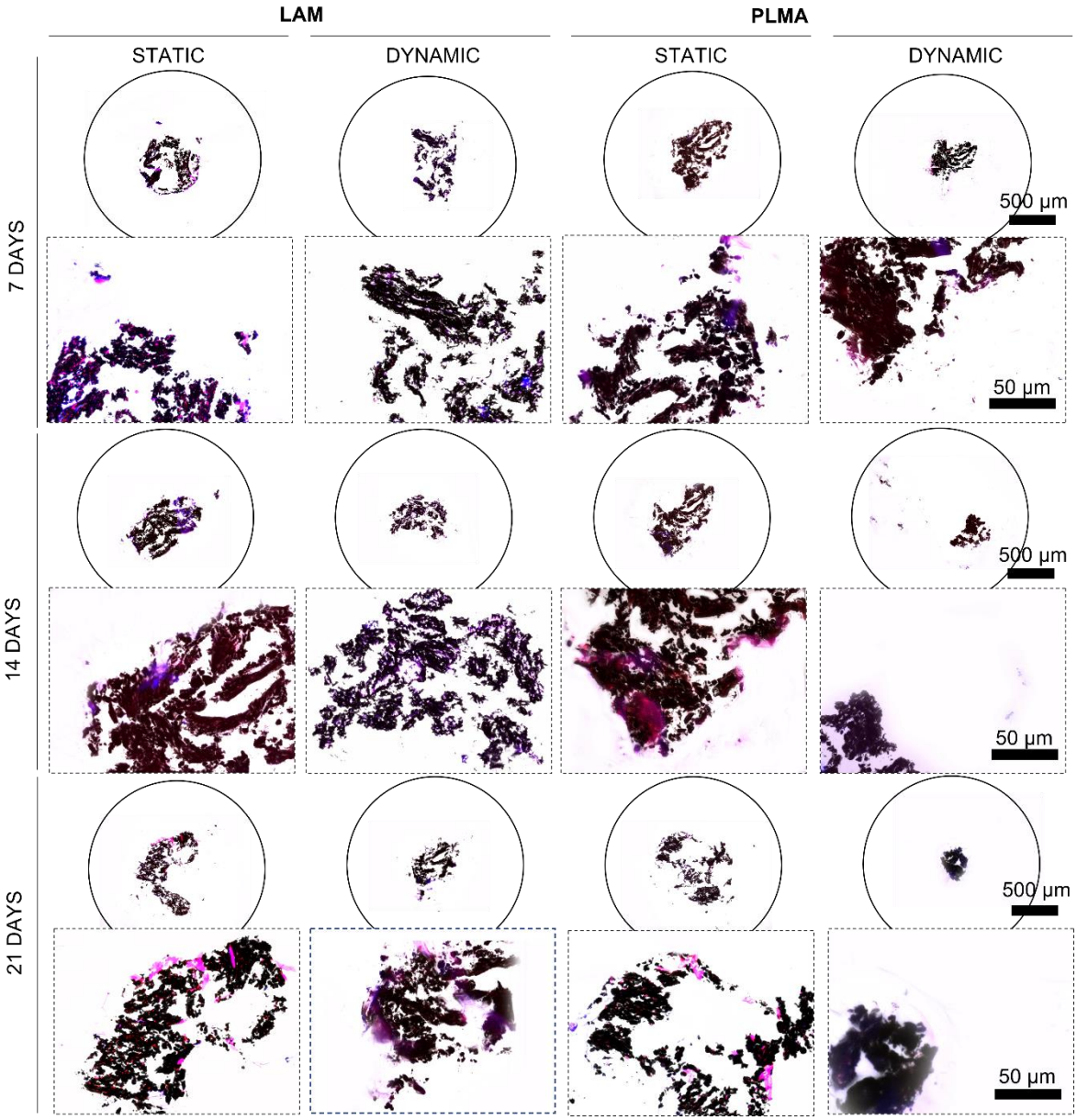

Figure VI.S6: Immunofluorescence staining of histological sections of the magnetic microtissues encapsulated in the hydrogels. F-actin filaments (in red) and nuclei (in blue) are displayed in the brightfield images.

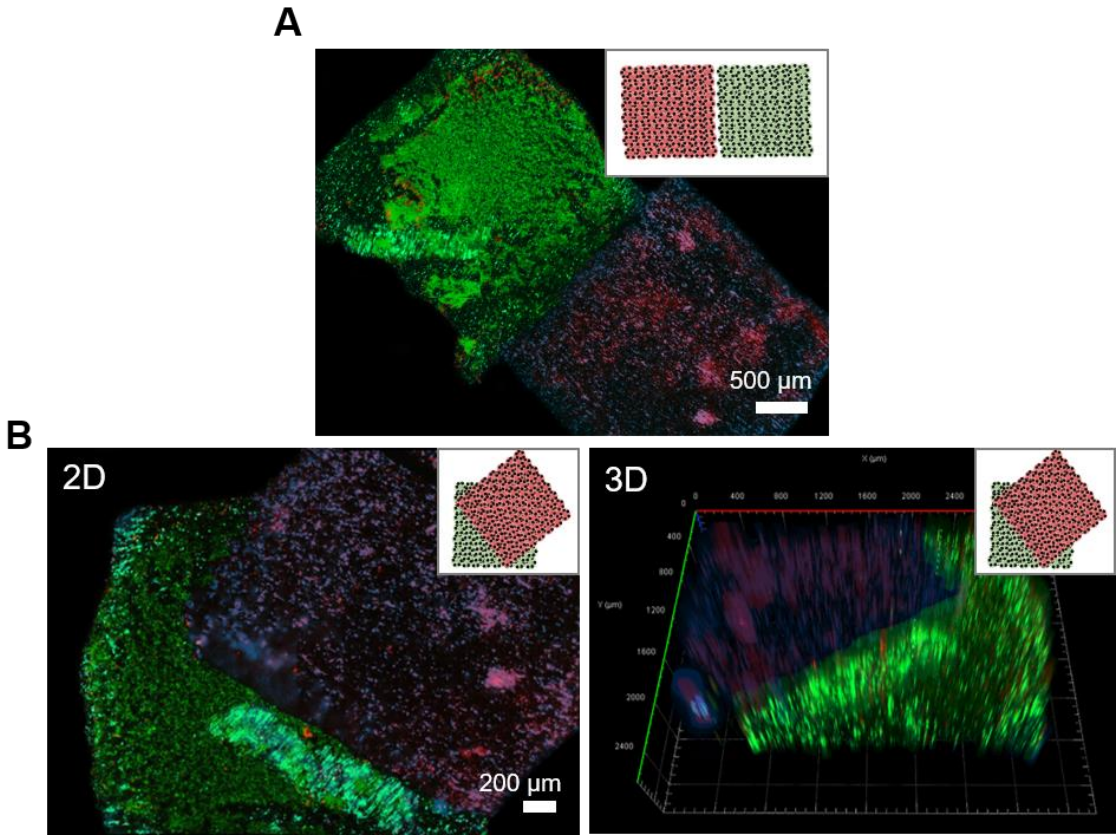

Figure VI.S7: Magnetic assembling of the freestanding magnetic microtissues– hASCs are depicted in green (DiO) or red (DiD) and cell nuclei in blue (DAPI); **A**. modular structure composed by two small building blocks with square-like shape. the ability to create stratified structures is exemplified in **B**).

Chapter VII - A novel therapeutic strategy for *in situ* bone regeneration powered by wireless magnetic stimulation[5]

Abstract

The physiological and functional outcomes of tissues and cells are greatly impacted by the physical microenvironment they inhabit. This microenvironment activates a variety of signaling pathways via mechanostransduction mechanisms, playing an essential role in organogenesis, homeostasis, and cellular functions. Particularly, magnetic fields have been applied to manipulate cellular surroundings, exhibiting encouraging outcomes in the field of tissue engineering (TE). Indeed, internalized magnetic nanoparticles (MNPs) can remotely manipulate receptors at the cell surface, thereby activating critical signaling pathways within tissues.

Building on this knowledge, we propose a novel therapeutic strategy that utilizes magnetic tissue implants with an architecture similar to native tissues to ensure proper tissue integration, while utilizing the superior external trigger of a magnetic field to regulate cell fate in situ.

In this study, we investigated the efficacy of a cyclic magnetic field (CMF) in stimulating magnetized tissues composed of human adipose-derived stem cells (hASCs). After 21 days of CMF exposure, in vitro osteogenic differentiation of the tissues was observed, as evidenced by the presence of key osteogenic indicators such as an enhanced collagen matrix, osteopontin, and hydroxyapatite nodules. The potential of this new therapeutic approach for clinical applications was validated in vivo using mice models. In these trials, the magnetic field accelerated the implant's integration into the host tissue, while triggering its osteogenic differentiation with minimal local tissue inflammation. Our findings suggest that this wireless magnetic stimulation can be a promising approach for in situ bone regeneration, highlighting the potential of magnetic tissue engineering for clinical applications.

[5]Baseed on the publication: Lúcia F. Santos, Maria C. Mendes, Isabel Dias, Carlos Viegas, Carlos O. Amorim, João S. Amaral, Håvard J. Haugen, A. Sofia Silva, João F. Mano. A novel therapeutic strategy for in situ bone regeneration powered by wireless magnetic stimulation. *In preparation*

1. Introduction

In multicellular tissues, cells are exposed to a myriad of forces, including compression, tension fluid shear stress and hydrostatic pressure, playing a key role in the development and maintenance of tissues as a whole.[1] The way cells interact with these forces and consequently, with their adjacent cells and extracellular matrix (ECM), is responsible for the tissue function. Among them, stem cells have aroused the interest of molecular biology in identifying which processes can regulate the cells fate. Their highly dynamic environment is responsible for modulating stem cells behavior, including cell adhesion, migration, proliferation/apoptosis, and differentiation.[2],[3] By identifying these mechanisms, stem cells can be guided into predesigned cell lineages for desired tissue function, based on their surroundings. Therefore, stem cells are considered as promising candidates for TE, being conducive for repairing injured tissues. Several studies have evidenced the role of biochemical and biophysical cues in regulate cells' behavior and directly determine the stem cells fate.[4]

So far, TE field has been mainly focused on the development of biomaterials with immobilized growth factors or with chemical modifications on their surface, in a straightforward strategy for providing biochemical cues.[5] In contrast, the significance of the biophysical properties including stiffness, topography, external forces and physical stimuli in stem cell manipulation have been underestimated. Besides the low cost and the easy application, biophysical stimulation is characterized by its high efficiency on triggering cell differentiation[6] Thus, the potential of biophysical factors in TE and regenerative medicine arose as a matter of research in the past years. Particularly, the extrinsic and intrinsic mechanical signals have shown a dramatic role on directing stem cells' fate.[7]

Mechanotransduction processes are responsible for translating these mechanical events into global changes in cellular function, where a set of cells' sensory elements and mechanisms can probe and detected the external forces.[8] This force-sensing can occur through force-induced conformational or organizational changes in cellular molecules or structures, such as stretch-sensitive ion channels, cadherin complexes, integrins and others cell adhesion receptors. Once the mechanical cue is perceived, the signal is amplified and propagated through a series of force-dependent biochemical reactions.[9]

From the biophysical stimuli, the magnetic manipulation of cells is becoming an attractive research area in mechanotransduction with important biomedical implications.[10] By changing the mechanical environment, MNPs can remotely regulate the receptors on the surface of stem cells to

activate proliferation or differentiation signaling pathways for regenerative medicine purposes. Comparing to the other external stimuli, magnetic field provides a superior external trigger for cell fate regulation, with adjustable field strength and low attenuation in biological organisms.[8] Hence, magnetic-mechanotransduction has become a relevant approach to noninvasively and precisely control the forces applied to the cells.

So far, magneto-therapies have been directed by continuous or pulsed magnetic fields. In fact, large effects on cellular microenvironment were observed in the presence of pulsed magnetic fields.[11],[12] Physiological alterations in proliferation, secretion of growth factors and gene transcription were already reported in several studies.[13] The extension of these effects are determined by key parameters like the strength and frequency of the magnetic field.

Regardless of the impacts of pulsed magnetic field on regenerating several tissues, the potential of this stimulus has been highlighted for bone tissue regeneration. The combination of MNPs and magnetic stimulus triggered several osteogenic enhancements in bone regeneration, [14] by prompting the healing process, the proliferation of osteoblasts and osteoclasts, and the deposition of mineral components.[15] Still, the major achievements resided on accelerating the healing process of bone tissues. More advanced strategies on guiding the cell behavior still restricted to isolated cells or 2D cell cultures. Therefore, the whole potential behind the magnetic stimuli for bone TE is still poorly explored.

Directing to TE strategies, magnetic force-based tissue engineering (Mag-TE) has been explored for the fabrication of functional tissue replacements, as alternative to conventional TE approaches. The inherent magnetic features empower the engineering of tissue constructs with high control of size, architecture and extremely tissue guided-assembling.[16],[17] Upon implantation, the tissue substitutes can be effortlessly tracked and monitored along the time.

In the last years, our group has been focused on engineering functional and robust tissues through Mag-TE. Using magnetized cells as basic building units, versatile heterotypic tissues were already fabricated, with enhanced mechanical performance and ability to stimulate new blood vessels formation, while integrating neighboring tissues.[18]–[20] Nevertheless, we anticipate that Mag-TE principles could be further explored for directing cells' fate into bone tissue formation. Led by the magnetic stimulus, we intend to investigate the power of CMF in regulating the *in situ* osteogenic differentiation of the magnetized tissues composed by hASCs.

We hypothesize that the magnetized cells can act as *in vivo* bioreactors and orchestrate the right signals towards new bone formation under a wireless CMF, without requiring further biochemical supplementation. We envisioned that this new strategy could boost the healing process of bone

fractures and accelerate the bone tissue formation, while guarantying the remote control over the tissue implant and its monitorization along the regeneration process.

2. Materials and Methods

All chemicals were purchased from Sigma-Aldrich and used as received, unless otherwise specified.

2.1. Synthesis and Characterization of Magnetic Nanoparticles

MNPs were synthesized and characterized as previously described by the group.[18],[20] Briefly, ferrous magnetite Fe_3O_4 MNPs nanoparticles were synthesized by the co-precipitation reaction of ferrous ($FeCl_2.4H_2O$) and ferric ($FeCl_3.6H_2O$) salts in the presence of ammonium hydroxide (NH_4OH), at 60 °C and under a nitrogen atmosphere. Then, MNPs surface was modified with (3-aminopropyl)triethoxysilane (APTES) through a silanization procedure.[18] For that, APTES solution was added to MNPs, previously dispersed in a mixture of water and absolute ethanol, at RT and nitrogen atmosphere. After 2 h, the APTES-MNPs were washed 3 times with water. Lastly, MNPs-APTES were visualized by TEM (20 kV, HR-TEM20-SE, JEOL), which were previously added dropwise to a carbon film copper grid.

2.2. Cell Isolation and Culture

The collected tissues were obtained under a cooperation agreement between CICECO–Aveiro Institute of Materials, University of Aveiro and Hospital da Luz (Aveiro, Portugal), after approval of the Competent Ethics Committee (CEC). The human tissues received were handled in accordance with the guidelines approved by the CEC and informed consent was obtained from all studies. Aiming the isolation of hASCs, subcutaneous adipose tissue from liposuction was collected. The tissues were transported in PBS supplemented with 10% (v/v) penicillin-streptomycin and kept at 4 °C. After washing with PBS, the lipoaspirates were incubated with collagenase type II A (0.05% w/v) during 45 min at 37 °C. Then, the samples were filtered (200 µm) and centrifuged at 800 g at 4 °C during 10 min. The obtained stromal vascular fraction (SVF) was resuspended in erythrocyte lysis buffer at pH 7.4 containing ammonium chloride (155×10^{-3} M), potassium bicarbonate (5.7×10^{-3} M), and ethylenediaminetetraacetic acid (0.1 M, EDTA) during 10 min at RT. To isolate the hASCs the red blood cell-free SVF was resuspended in α-MEM medium (Invitrogen) supplemented with fetal bovine serum (10%, FBS, Invitrogen) and penicillin-streptomycin (1% v/v). Culture medium was changed 48 h after initial plating and then every 3–4 days.

2.3. Fabrication of magnetic tissue constructs

Firstly, hASCs were seeded at cell density of 2.4×10^6 cm^{-2} and cultured for 24 h at 37 °C and 5% CO_2 in a humidified atmosphere. To obtain magnetized cells, the cells were incubated with MNPs (1 mg mL^{-1}) for 4 h and then, the cells were detached by adding trypLE Express during 5 min at 37 °C. Later, the magnetized cells were transferred to ultralow-attachment 96-well plates (previously treated with 2% w/v alginate solution during 30 min). To produce the magnetized tissues, commercial neodymium rod magnets Ø 10 mm, height 40 mm (strength of 108 N and standard N41 magnetization) (Supermagnet) were placed at the bottom of the reverse side of the ultra-low attachment plate. The magnetic tissues were cultured during 7 days in α-MEM medium, supplemented with 10% (v/v) fetal bovine serum and 1% (v/v) penicillin-streptomycin.

2.4. Magnetic stimulation of the produced tissue constructs

After 7 days of culture, the produced magnetic tissues were collected from the 96-well ultralow-attachment plates with the aid of a magnet and transferred to a PDMS mold containing the same culture medium volume. Then, the magnetic stimulus was generated by a lab-made apparatus (**Figure S1**) composed of two neodymium rod magnets Ø 10 mm, height 40 mm (strength of 108 N and standard N41 magnetization) (Supermagnet) placed on opposite sides of a PVA plastic bar with 28 cm, on top of a rotary motor. Briefly, the oscillation of the magnet position caused by the rotary motor induced changes on the magnetic field strength applied to the samples, acting as CMF. For each position, the generated magnetic field was determined using a gaussmeter (Tesla Meter). Along this work, samples under CMF are referred as dynamic condition.

For *in vitro* experiments, the position of the magnetic setup was adjusted for 3.5 cm of distance from the plates, with a magnetic field intensity of 13 mT and the frequency of 71 mHz – dynamic condition. For the control samples, the magnets were removed from the 96-well ultralow-attachment plates. All samples were cultured in basal α-MEM medium during 7, 14 and 21 days.

Similar experimental setup was used for the *in vivo* tests. Concisely, the lab-made apparatus was placed on the side of the mice cages, also at a distance of 3.5 cm.with a magnetic field around 13 mT and the frequency of 71 mHz. In the control condition, the mice cages were moved to the opposite side of the room, to guarantee the complete absence of the magnetic field.

After the determination of the magnetostatic field for each position, the computer simulation of the magnetic fields generated by the lab-made setup was performed using the pcolormesh() function in pyplot module of matplotlib library for both *in vitro* and *in vivo* scenarios.

2.5. Determination of total iron on the produced tissues

The total iron mass in magnetic tissues was determined for both conditions after 7, 14 and 21 days by Inductively Coupled Plasma Optical Emission Spectrometry (ICP-OES) (Activa M, Horiba Jobin Yvon). For each measurement, the magnetic tissues (10 mg) were dried at 37°C, overnight. Then, 1 mL of nitric acid (HNO_3) was added to each sample for the microwave acid digestion.

2.6. Magnetization of the produced tissues

The magnetic characterization of the produced magnetic tissues was performed using a Quantum Design MPMS3 SQUID magnetometer.[21] Magnetizations versus applied magnetic field curves were obtained at 300K. The magnetic moment measurements were performed using a 1 mm SQUID-VSM amplitude and a 30 mm DC-scan length. For this purpose, magnetic tissues were dried at 37 °C during 24 h and then, the dried materials were used for each measurement, normalizing the obtained magnetization values by the mass of the magnetic tissues.

2.7. *In vitro* analysis of the magnetic stimulation of the produced tissues

2.7.1. Characterization of the magnetic microtissues

After 21 days, the samples were fixed in formalin 10% (v/v) during 15 min at RT. Then, the samples were permeabilized with 0.1% (v/v) Triton-X for 5 min at RT and then immersed in 5% (v/v) FBS/dPBS for 1 h. To access the tissue morphology, the samples were incubated with Flash Phalloidin Red 594 (1:50 in dPBS) during 45 min at RT and then counterstained with DAPI (1:500 in dPBS) for 5 min at RT. The morphology was also investigated by scanning electron microscope (SEM). For this, the samples previously fixed in formalin were dehydrated in increasing gradient series of ethanol (70, 80, 90 and 100 % v/v) for 10 min each. Then, the samples were gold sputter-coated using an accelerating voltage of 15 kV and visualized by SEM (S4100, Hitachi, Japan). The robustness of the magnetic tissues was evaluated by accessing the presence of vinculin and collagen I. After the incubation with Triton-X and FBS/dPBS as previously described, the tissues were incubated with anti-rabbit human vinculin antibody (1:50 in 5% FBS/dPBS, Invitrogen) and anti-mouse human collagen I (1:50 in 5% FBS/dPBS, Novusbio) for 3 h at RT. After washing the samples with PBS, the magnetic tissues were incubated with the secondary antibody chicken anti-rabbit AlexaFluor 647 (1:400 in 5% FBS/dPBS, Thermofisher) and goat anti-mouse AlexaFluor 647 (1:400 in 5% FBS/dPBS, Thermofisher). Then, all the samples were incubated with Flash Phalloidin Green

488 (1:50 in dPBS, Biolegend) during 45 min at RT and then counterstained with DAPI (1:500 in dPBS, Thermofisher) for 5 min at RT.

2.7.2. Microtomography

Microtomography (microCT) was performed in the magnetic tissues after 21 days of culture (Bruker Skyscan 1172, Bruker micro-CT, Kontich, Belgium). Firstly, the samples were fixed in 4% w/v formaldehyde solution for 1 h. Then, scans were performed with the acquisition parameters set to 70 kV of accelerating voltage, 210 µA of current, 0.125 mm aluminum filter, rotation step of 0.29° over 360°, exposure time of 0.650 ms per projection and a frame-averaging of 2. The reconstruction of the virtual slices was performed with NRecon software with a final voxel size of 0.7 µm. The 3D images were rendered using Dragonfly software.

2.7.3. Assessment of metabolic activity, cell viability and proliferation

The cell survival of the produced tissues was accessed after 7, 14 and 21 days through a live-dead fluorescence assay, according to the manufacturer's descriptions (ThermoFisher Scientific). Concisely, the samples were washed with dPBS and then stained with the kit components at 37 °C for 45 min. Finally, samples were visualized by fluorescence microscopy (Axio Imager 2, Zeiss). The metabolic activity was also quantified by using an MTS colorimetric assay (CellTiter96 AQueous one solution cell proliferation assay, Promega) by following the manufacturer's specifications. The tissues (n=3) were incubated with the reagent kit (120 µL per well) at 37 °C for 4 h, protected from the light. At the end, the absorbance was read at 490 nm u sing a microplate reader (Synergy HTX, BioTek Instruments, USA). Furthermore, the cell proliferation was determined by quantifying the total DNA of the produced magnetic tissues. For this purpose, the samples (n=3) were incubated with 2% (v/v) Triton 100× (in ultra-pure sterile water) during 1 h at 37 °C and then, the samples were frozen at −80 °C and defrost several times to promote the ECM disruption. Firstly, the MNPs were segregated using a neodymium magnet. Then, the samples and the kit components were incubated for 10 min, at RT and finally, the fluorescence was read at an excitation wavelength of 485/20 nm and emission wavelength 528/20 nm using a microplate reader. A standard curve for DNA analysis was generated with the provided DNA standard from the DNA assay kit (Synergy HTX, BioTek Intruments, USA).

2.8. Assessment of the role of magnetic stimulation on osteogenic differentiation

2.8.1. Analysis of tissue stemness after magnetic stimulation

The stemness of the tissues composed by hASCs was accessed after 7, 14 and 21 days of magnetic stimulation. The samples were fixed at RT in formalin (10% v/v) for 15 min. After the permeabilization with 0.1% (v/v) Triton-X for 5 min at RT, the samples were incubated with 5% (v/v) FBS/dPBS during 1 h. Afterwards, the tissues were stained with the anti-mouse human CD105 conjugated with FITC (1:50 in 5% FBS/dPBS, Biolegend) during 3h at RT. At the end, all the samples were stained with Flash Phalloidin Red 594 (1:50 in dPBS) during 45 min at RT and then counterstained with DAPI (1:500 in dPBS) for 5 min at RT. To quantify this CD105 expression, the tissues were immunostained with anti-mouse human CD105 conjugated with FITC (1:50 in 5% FBS/dPBS, Biolegend) - 5 µL of antibody per 1×10^6 of cells, during 45 min at 4 °C and in the dark. Both samples were washed with a staining washing buffer (2% w/v BSA, 0.1% w/v sodium citrate in PBS) and centrifuged at 500 g for 5 min, followed by a resuspension in the acquisition buffer (1% v/v formaldehyde and 0.1% w/v sodium azide in PBS). Finally, the samples were acquired on a BD Accuri C6 Plus flow cytometer (BD Biosciences). All data were analyzed using FlowJo Software (version 10, Ashland).

2.8.2. ELISA Immunoassay Quantification of Cytokines

The expression of vascular endothelial growth factor (VEGF) (Abcam), osteopontin (Abcam), extracellular signaling-regulated kinase 1/2 (ERK1/2) (Abcam) and phosphorylated focal adhesion kinases [pY397]FAK (Invitrogen) was accessed in the magnetic tissues after 7, 14 and 21 days through Elisa Kits according to manufacturer's specifications. The levels of ERK1/2 was normalized by the total protein content, previously quantified by Micro BCA protein assay kit (Thermo Fisher Scientific). The expression of [pY397]FAK was normalized by the FAK (total), determined by a Elisa Kit (Abcam).

For all conditions, the culture media was collected and stored at −80 °C until further use. Finally, the absorbance was read at 450 nm using a microplate reader (Synergy HTX, BioTek Intruments, USA).

2.8.3. RNA extraction and cDNA Production

The isolation of total RNA was performed using a column-based kit (PureLink RNA Mini Kit, ThermoFisher Scientific) according to the manufacturer's specifications. After 21 days, magnetic

tissues (n=3) were lysed with a Lysis Buffer containing 1% of 2-mercaptoethanol and a homogenized with potter elvehjem tissue homogenizer. One volume of 100 % (v/v) of ethanol was added to each volume of cell homogenate, and then, the mix was entirely transferred to a spin cartridge. After several washes, the membrane-bounded RNA was eluted in RNase-free water and collected in single tubes. RNA quantity and purity were determined in a nanodrop spectrophotometer (NanoDrop ND-1000, ThermoFisher Scientific). Samples with a 260/280 purity ratio higher than ≈2.0 were used for cDNA synthesis. The cDNA synthesis was performed using a SuperScript IV VILO Master Mix kit (ThermoFisher Scientific) and the ProFlex 2 × 96-well PCR System (ThermoFisher Scientific). All samples were normalized (1 ng of RNA per µL of RNase-free water).

2.8.4. Quantitative Real-Time Polymerase Chain Reaction (qRT-PCR)

The expression of adipogenic and osteogenic genes were quantified in the cDNA samples using a qRT-PCR reaction, namely peroxisome proliferator-activated receptor (PPARG), collagen I (COL1A1), runt-related transcription factor 2 (RUNX2) and VEGF. The qRT-PCR was performed on a QuantStudio 3 Real-Time PCR system with the TaqMan Fast Advanced Master Mix (ThermoFisher Scientific) and using TaqMan gene expression assays (ThermoFisher Scientific), namely Hs00164004_m1 (COL1A1), Hs01115513_m1 (PPARG), Hs00231692_m1 (RUNX2), and Hs00900055_m1 (VEGF). Glyceraldehyde 3-phosphate dehydrogenase (GAPDH) (Hs99999905_m1, ThermoFisher Scientific) was used as the endogenous housekeeping control. Amplification profiles were analyzed with QuantStudio Design and Analysis Software v1.5.1 (ThermoFisher Scientific). The relative expression levels of each gene in cells were normalized to the GAPDH gene using the 2–ΔΔCt method (Perkin-Elmer). Three independent experiments were performed.

2.9. *In Vitro* Biomineralization Analysis

The *in vitro* mineralization of magnetic tissues was accessed along the time for control and dynamic conditions. Firstly, the samples were fixed at RT in formalin (10% v/v) for 15 min. Posteriorly the OsteoImage™ Assay was used to visualize the hydroxyapatite portion of bone-like nodules deposited by cells. The OsteoImage™ Staining reagent (1:100 v/v) was added to the previously fixed magnetic tissues and incubated for 30 min. After this, the samples were washed 3 times and visualized under fluorescence microscope. The mineral formation was also accessed by SEM. Energy dispersive X-ray spectroscopy (EDS) (QUANTAX 400, Bruker) was used to examine the chemical composition of the minerals' deposits within the fabricated magnetic tissues. The samples were carbon-coated and imaged at an electron intensity of 15 kV (SU-70, Hitachi).

2.10. *In vivo* animal studies

All animal handling practices followed the Directive 2010/63/EU of the European Parliament and the Council on the protection of animals used for scientific purposes. The conduct of the *in vivo* study was approved by the national authority that oversees experimental animal studies – DGAV Of. n° 0421/000/000/2022, Portugal.

Twenty-four 10 weeks nude male mice (Crl:NU(NCr)-Foxn1NU from Charles River Laboratories France), were used in this *in vivo* study. The mice were divided in two groups: i) the control group and ii) the one subjected to a CMF.

For implantation purposes, the nude mice were anesthetized and maintained with inhalant isoflurane. The dorsal skin was cleaned with chlorhexidine and 70% ethanol and sprayed with bupivicaine/lidocaine at the surgical site. A skin incision was produced on the back of each mouse, between its shoulders, and one subcutaneous (SC) pouch was performed. One magnetic tissue was implanted in each SC pouches. To close the skin incision, two sutures were performed – a continuous one in the SC tissue (gluconate synthetic absorbable monofilament suture 5-0) and a simple interrupted skin suture (silk 5-0). Half of the nude mice were maintained under a CMF and the other half under normal conditions, away from the effect of the magnetic field. After 4 and 6 weeks, the nude mice were anesthetized with inhalant isoflurane to obtain a blood sample from the infraorbital sinus and euthanized immediately after this procedure by an intraperitoneal injection of pentobarbital sodium. The implants were resected and photographed to determine the changes in implant morphology and dimensions.

2.10.1. Biosafety analysis of the magnetic stimulation

At each time-point, the potential toxicity of the magnetic stimulation in both animal groups was analyzed. Blood biochemistry of liver and kidney panels was analyzed by CEDIVET Laboratories. Subsequently, the magnetic tissues were explanted by cutting the animal tissues surrounding the implant. The cell viability of the magnetic tissues *in vivo* was accessed by a live/dead assay, through the incubation of the samples with calcein/PI stains, as described in *section 5.3.*

2.10.2. Histological analysis of the magnetic tissue and surrounding environment

Initially, the samples were collected by cutting the area around the magnetic tissue implant in order to obtain samples containing both the host tissues and the magnetic tissue. After fixing the tissue blocks with 4% formaldehyde (overnight), the samples were embedded in paraffin. Then, sequential

sections of 5 µm thickness were produced in adhesive slides for Hematoxylin–Eosin staining (H&E), Masson Trichrome and immunohistochemical analysis such as CD105, osteopontin and Osteoimage™.

For immunohistochemical purposes, the samples were treated with sodium citrate buffer (10 mM sodium citrate, 0.05% v/v Tween-20, pH 6) for 35 min at 95–98°C for antigen retrieval. Then, the histological sections were incubated during 3 h with primary mouse anti-human osteopontin SPP1 antibody (1:100 in 5% FBS/dPBS, Biolegend) and conjugated anti-mouse APC - CD45 (1:100 in 5% FBS/dPBS, Biolegend), anti-mouse CD68 - Alexa Fluor 647 (1:100 in 5% FBS/dPBS, Biolegend), anti-mouse CD105 – FITC (1:50 in 5% FBS/dPBS, Biolegend). Later, the samples were incubated with the secondary anti-mouse Alexa Fluor 647 antibody (1:400 in 5 % FBS/dPBS) for 1 h in the dark at RT. Lastly, all the samples were stained with Flash Phalloidin Red 594 (1:50 in dPBS) during 45 min at RT and counterstained with DAPI (1:500 in dPBS) for 5 min at RT. The presence of hydroxyapatite nodules was also accessed by OsteoImage™ Assay. The OsteoImage™ Staining reagent (1:100 v/v) was added to the previously fixed samples and incubated for 30 min. After this, the samples were washed 3 times and visualized under fluorescence microscope. At the end, the cross-sections were visualized using a fluorescence inverted microscope (AxioImager Z1, Zeiss).

2.10.3. Gene Expression

The profile of osteogenic gene expression was determined after 6 weeks of implantation. To compare *in vitro* and *in vivo* environments, the gene expression was analyzed by the methodology presented in *section 5.3.5 and 5.3.6*. with some modifications. For RNA extraction, the implant was firstly frozen in liquid nitrogen and then, mechanically destroyed. After that, RNA extraction was performed using a tissue homogenizer and the TRIzol® Plus RNA Purification Kit, as previously described. At the end, the expression of RUNX2 (Hs00231692_m1) and COL1A1 (Hs00164004_m1) was determined using the TaqMan® gene expression assays.

2.10.4. Nanotomography

The morphological analysis of the implants was performed by NanoCT system (Bruker Skyscan 2211, Bruker micro-CT, Kontich, Belgium) after 6 weeks for control and dynamic conditions. Firstly, the implant and surrounding tissue were cut and fixed in 4% formaldehyde (overnight, RT). Then, the images were acquired at a final isotropic resolution of 5.5 µm per pixel, at camera binning = 1×1, at 70 kV accelerating voltage, 210 µA of current, and with a 0.125 mm aluminum filter placed in front of the camera. The samples were rotated 360° about their vertical axis using a step size of 0.37°,

and the exposure time was set to 1100 ms per projection. For visualization, Dragonfly software version 3.6 was used.

2.11. Statistics

Statistical analysis was performed using t-test or two-way ANOVA (GraphPad Prism 6.0) with a significance level set at $p < 0.05$. All results were stated as mean ± standard error.

3. Results

3.1. Fabrication of magnetic tissues

Firstly, hASCs were successfully isolated from adipose tissue and characterized by flow cytometry (**Figure VII.S2**). Then, MNPs were incorporated within cells environment to obtain magnetized cells using well-described methodologies.[18],[20] The magnetized cells were transferred to a non-adherent plate and, by placing a magnet below, magnetic sheets of cells started to be formed at the bottom of the plate. After 7 days of culture, magnetic living tissues with high stability and robustness were formed. Later, the magnetic cell sheets were divided into two distinct groups. In the control group, the magnets were removed from the plates after 7 days. For the dynamic condition, the tissues were recovered from the plates by magnetic activation and transferred to PDMS molds containing basal culture medium.

3.2. *In vitro* performance of magnetic tissues under magnetic stimulation

To generate the magnetic stimulus, a lab-made apparatus was developed by the group and was composed of two permanent magnets located on opposite sides of a PVA plastic bar (at 28 cm of distance from each other), all placed on top of a rotary motor, generating a CMF, also referred as the dynamic condition (**Figure VII.1A** and **VII.1B**). After 7, 14 and 21 days under magnetic stimulation, the tissues were magnetically characterized and compared to MNPs (**Figure VII.1C** and **VII.1D**). As shown in **Figure VII.1D**, the iron (Fe) content of tissues had a slightly decreased along the time. As anticipated, for the magnetized tissues, the saturation magnetization values also decreased along the time (**Figure VII.1C**). Nevertheless, the saturation magnetization values normalized per DNA content remained constant along the time. But most importantly, all the magnetic tissues demonstrated a superparamagnetic behavior with remanent magnetizations and coercive fields close to zero (**Figure VII.S3**). Thus, we herein demonstrated the ability to produce superparamagnetic living materials with long-term stability in culture. The correct synthesis of the

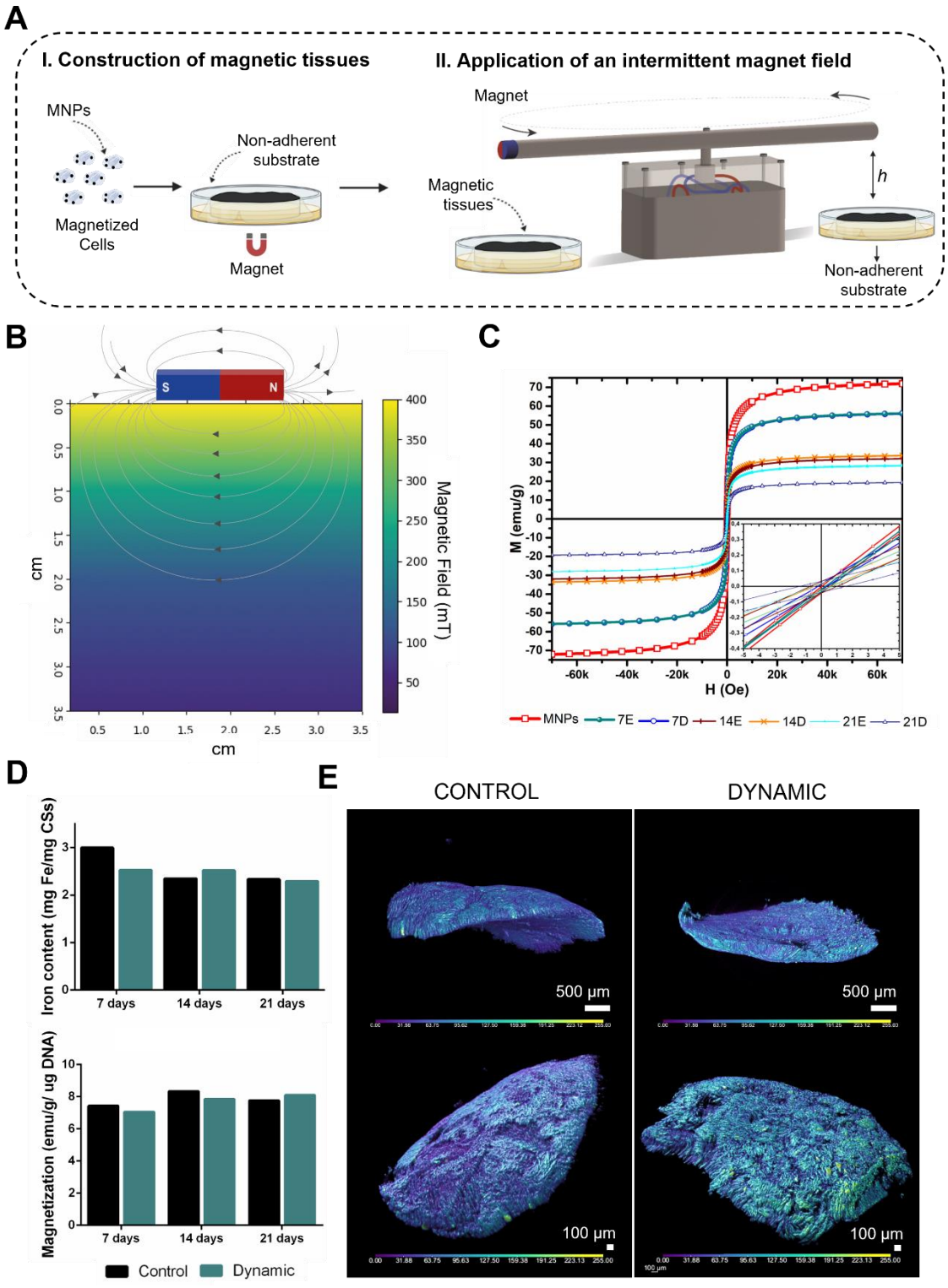

Figure VII.1: Stimulation of magnetic tissues using a CMF. **A.** Illustration of the experimental methodology. Magnetic tissues were formed by Mag-TE principles. After 7 days, the magnetic tissues were subjected to a CMF using a lab-made magnetic apparatus. **B.** Mapping of the magnetic field produced by the lab-made magnetic apparatus. **C.** Magnetization profile of the magnetized tissues along the time. MNPs were used as positive control. **D.** The total iron content was determined by ICP and the magnetization of the produced tissues was normalized by the DNA content. **E.** 3D reconstruction of MicroCT images of the magnetized tissues after 21 days of experiment. .

MNPs was also confirmed by the saturation magnetization values similar to bulk magnetite (75 emu/g).[22]

The effect of the CMF on tissue integrity was also analyzed after 21 days. According to **Figure VII.1E**, the structure remains intact and morphological alterations can be observed in the samples subject to the stimulus. In fact, the magnetic field prompt the compaction of the tissue and a certain alignment of the magnetized cells.

3.3. Cell survival and proliferation of the magnetic tissues

After confirming the integrity of the tissues (**Figure VII.2A**), we also investigated the role of the CMF on the tissues' viability. The live/dead assay showed that up to 21 days of culture, most of the cells remained viable for all the culturing conditions (**Figure VII.2B**). Additionally, the metabolic activity and DNA content also increased along the time (**Figure VII.2C**), evidencing the ability for long-term cell survival even in the presence of an external stimulus such as the CMF.

3.4. Assessment of the role of magnetic stimulation on tissues composed by stem cells

As previously stated in literature, the presence of a magnetic field could potentially guide stem cells for osteogenic lineages, using isolated cells or under 2D cell culture.[15] In this work, we intend to explore the role of a CMF on guiding the cell fate of magnetized tissues previously produced *in vitro*.

3.4.1. Assessment of the magnetic role on osteogenic differentiation

Firstly, we investigated the effects of CMF on tissues' stemness. By accessing the expression of CD105 by flow cytometry (**Figure VII.S4**), we identified a pronounced decrease of such stemness marker in the dynamic condition. It is well established in the literature that stem cells, after being

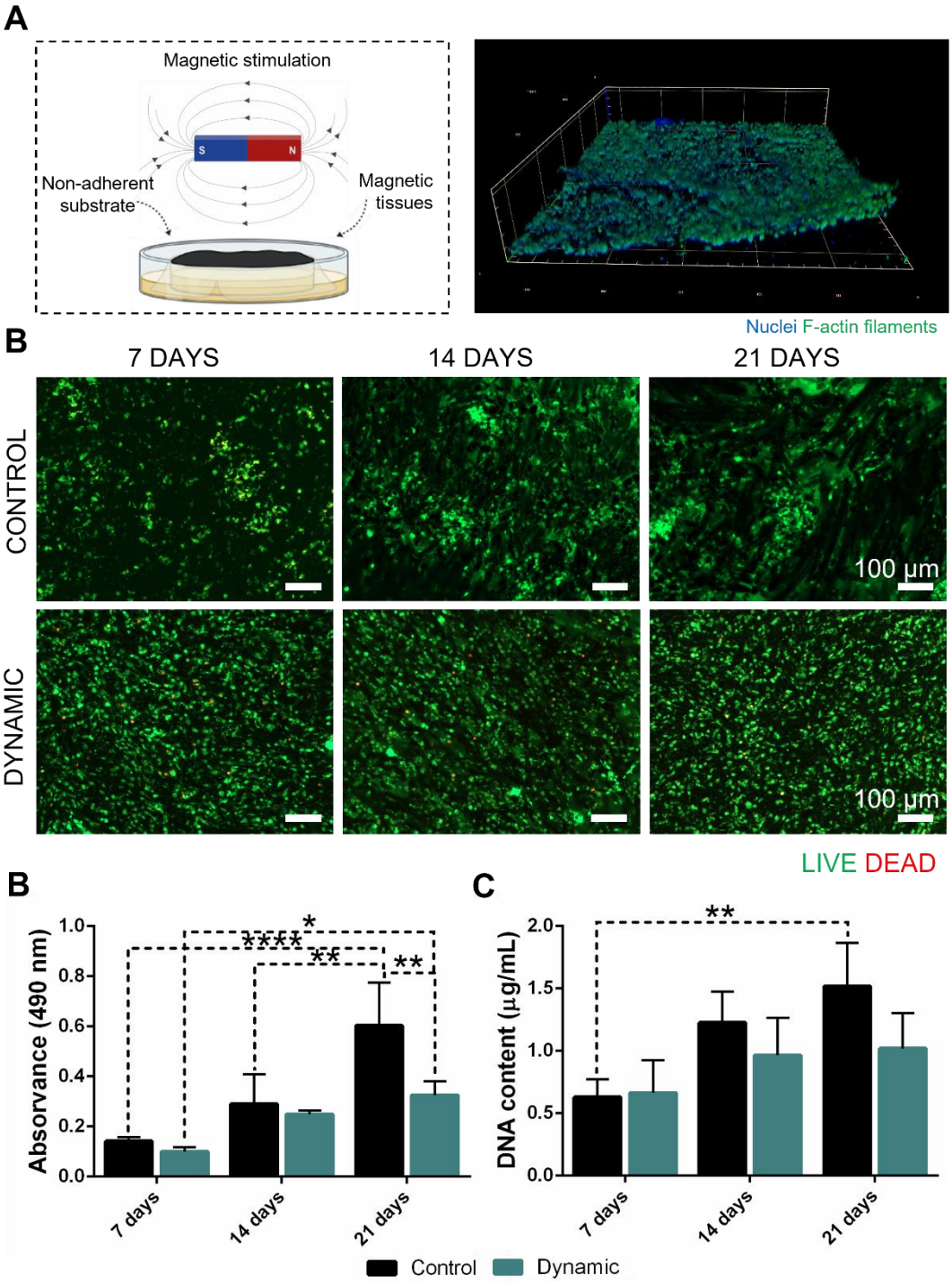

Figure VII.2: Characterization of the magnetic tissues after magnetic stimulation. **A.** The cohesive tissue structure was attested by the enriched presence of the actin-filaments (in green). DAPI stained all nuclei (in blue). **B.** The cell survival was determined for magnetic tissues in control and dynamic conditions by a live-dead assay, where calcein stained live cells (in green) and PI stained dead cells (in red). These results were corroborated by the metabolic activity quantified by MTS assay (**C**) and DNA content (**D**).

differentiated lose their ability to express stemness markers such as CD105.[23] Encouraged by these findings, we explored the ability of CMF on inducing the differentiation of stem cells (**Figure VII.3A**).

Cytokines detection

The release profile of osteopontin and VEGF from the magnetic tissues is disclosed in **Figure VII.3B**. In the absence of the CMF, the release of VEGF remained constant up to 21 days. For the dynamic condition, a decreased level of VEGF was verified as the culture time increased. Several studies report that hASCs stimulate blood vessel growth due to the secretion of many angiogenic and anti-apoptotic growth factors, such as VEGF.[24] Moreover, the release of VEGF and the osteogenic stage of differentiation of the hASCs are intrinsically correlated, where osteogenic differentiated hASCs have a decreased ability to enhance angiogenesis by diminishing the VEGF release.[18],[25] Concerning the decreased expression of VEGF in the dynamic environment, we investigated the osteogenic differentiation of the magnetic tissues in the presence of the CMF. According to **Figure VII.3B**, the dynamic environment promoted the expression of osteopontin, an important osteogenic marker.[26] Residual values were observed for the control condition. In the end, the presence of an CMF lead to the osteogenic differentiation of the magnetic tissues by diminishing the VEGF release and endorsing the osteopontin expression.

The presence of a biophysical stimuli triggers the cytoplasmic signaling pathways, leading to an up-regulation of osteogenic factors such as osteopontin. Mitogen-activated protein kinase (MADK) has already demonstrated an important role in the mechanotransduction signaling of osteoblasts.[27] Briefly, upon a mechanical stimulus, several signaling intermediates are regulated due to the cytoskeletal arrangements in the presence of a physical force. Then, FAK and integrins are activated and initiate a complex cascade of intracellular signals, involving the MADK. Among the MADPK family, ERK1/2 is the member with relevant function on biophysical environments, being also dependent on the FAK's activation.[28] Based on this knowledge, we evaluated the expression of ERK1/2 and FAK phosphorylation. As anticipated, increased levels of these two members of MADK family were verified in the presence of the CMF – **Figure VII.3C**.

Gene expression

According to previous studies, the up-regulation of these signaling kinases lead to the expression of important genes for the proliferation and differentiation of mesenchymal stem cells, previously implicated on tissue osteogenesis.[29],[30] After confirming the expression of

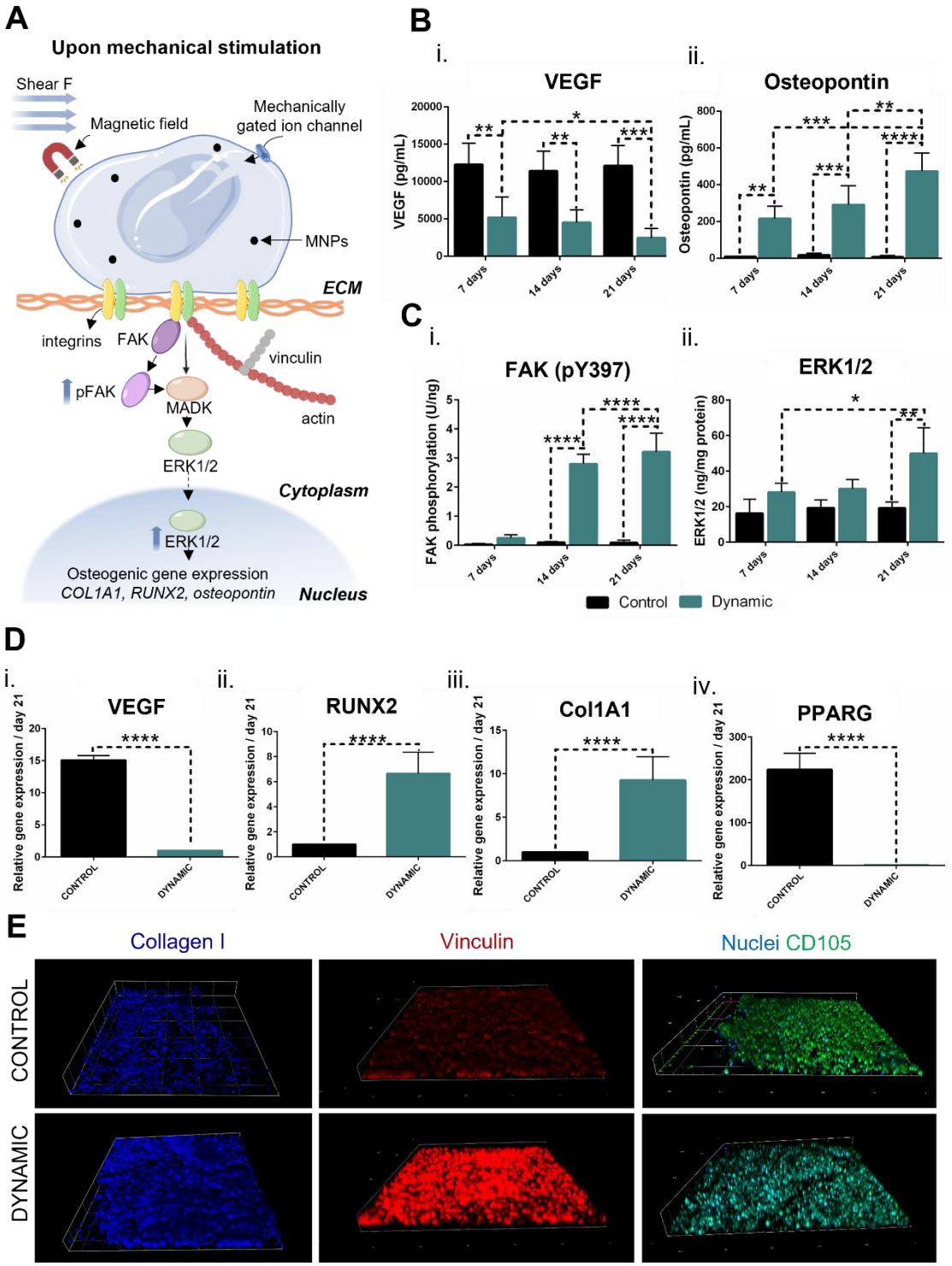

Figure VII.3: The role of the CMF on magnetic tissues. **A.** Upon stimulation, the key signaling pathways for cell differentiation were investigated, being the MADK complex the pivot. **B.** The release of VEGF and osteopontin was accessed by ELISA assays for control and dynamic conditions. **C.** The expression of two major members of MADK family – ERK1/2 and phosphorylated FAK was also verified along the time. **D.** To corroborate these findings, the relative expression of key adipogenic and osteogenic genes was determined after 21 days, including VEGF, RUNX2, Col1A1 and PPARG. **E.** Immunostaining images of important cytoskeletal proteins namely collagen I and vinculin. The expression of CD105 marker was also clarified by immunostaining.

osteopontin and VEGF by ELISA kits, we investigated the expression of important bone forming genes namely collagen I, RUNX2 and VEGF. As displayed in **Figure VII.3Di,** the gene expression profile for VEGF was similar to the cytokine release (**Figure VII.3C**). Moreover, the expression of RUNX2 (**Figure VII.3Dii**) and collagen I (**Figure VII.3Diii**), relevant in bone tissue formation, was enhanced by the presence of the magnetic field. Owing to the natural source of hASCs, and to guarantee that the CMF is specifically guiding the stem cells differentiation towards the osteogenic linage, we also investigated the expression of PPARG (**Figure VII.3Div**), an adipogenic gene . Interestingly, in the dynamic environment, no PPARG expression was detected.

Expression of cytoskeletal protein

Considering the results of collagen I gene expression, we hypothesized that the magnetic stimulus prompt the cell-cell and cell-matrix interactions, forming a more compact and robust structure. Moreover, cytoskeletal proteins like collagen I and vinculin are also reported in literature as major contributes for MADK signaling pathway.[31] The immunostaining of collagen I and vinculin corroborated the gene expression results, with enhanced deposition of these proteins after the tissue stimulation by the CMF (**Figure VII.3E**).

Biomineralization of produced tissues

The *in vitro* mineralization of the produced magnetic tissues was evidenced by EDS and Osteoimage™, supporting the previous findings. Hydroxyapatite crystals were visualized after 14 days under dynamic environment. In the control condition, the deposition of calcium (Ca) / phosphate (P) was not verified along the time (**Figure VII.4A**). Considering the dynamic condition, the chemical analysis of the minerals by EDS displayed Ca and P peaks increasing over time, with a higher Ca/P ratio attained after 21 days – see **Figure VII.4B**. In the end, the presence of the CMF resulted in an enhanced newly deposited mineralized ECM, without requiring the presence of any osteogenic induction factor.

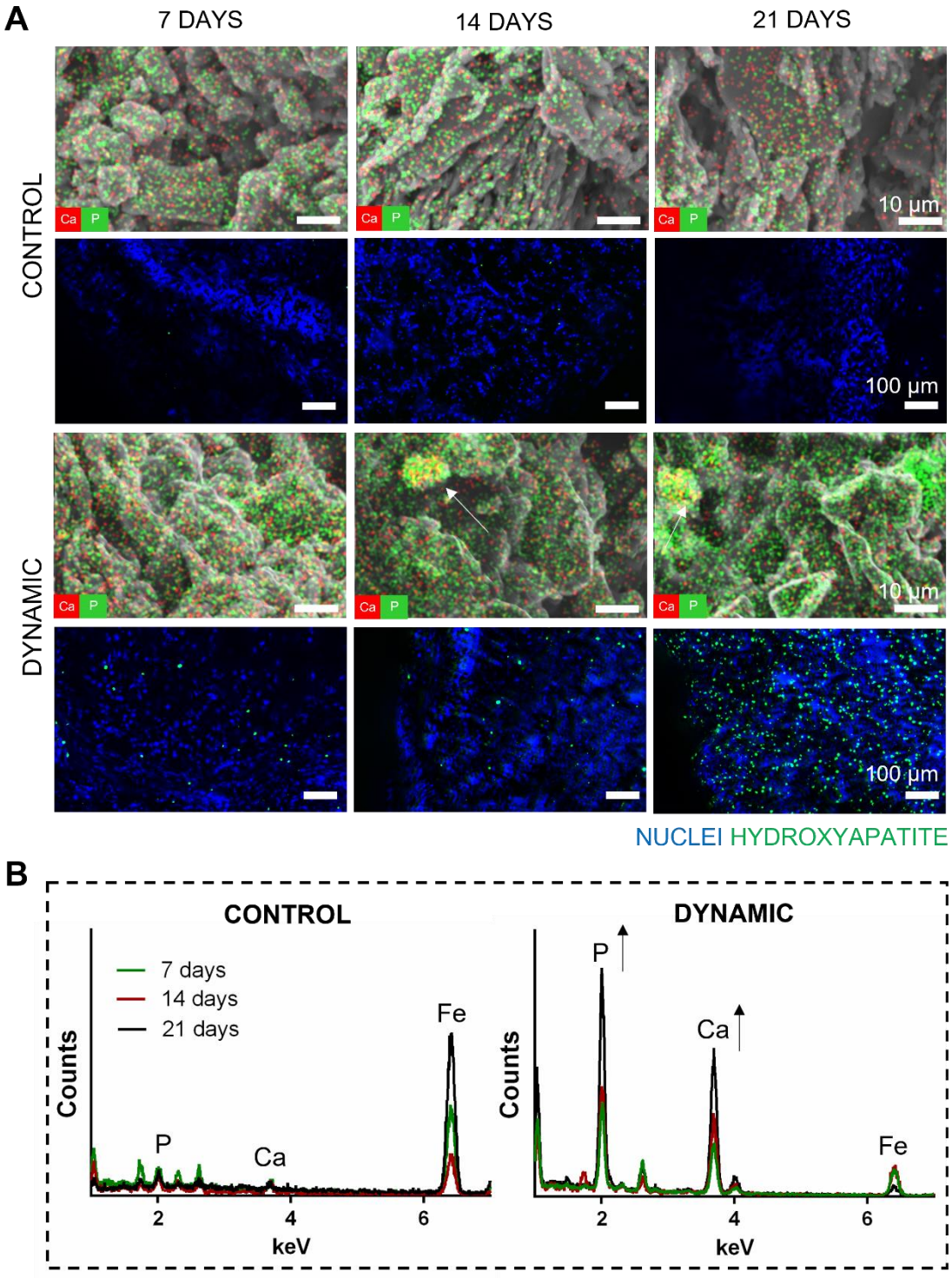

Figure VII.4: The *in vitro* mineralization of the magnetic tissues was accessed along the time **A.** The deposition of hydroxyapatite nodules was visualized through fluorescent OsteoImage™ Mineralization Assay: cell nucleus - DAPI (blue) and hydroxyapatite (green). SEM micrographs displaying calcium deposits are depicted in the right panel. **B.** Energy dispersive X-ray spectroscopy (EDS) spectra of minerals formed within the magnetic tissue.

3.5. *In situ* stimulation of magnetic tissue implants using a *in vivo* mice model

Similar to *in vitro* assays, magnetic tissues were formed for 7 days, prior to the *in vivo* implantation. Then, each magnetized tissue was implanted subcutaneously in a mice model. Same lab-made magnetic apparatus was used to magnetically stimulate the tissue implants, during 4 and 6-weeks (**Figure VII.5A**). As evidenced in **Figure VII.5B**, all mice survived without malignancy, infections, or abscesses at implantation sites. Blood and tissue samples were collected 4 and 6-weeks post-implantation. After total blood count, the host inflammatory response was evaluated by white blood counting including white blood cells, lymphocytes, monocytes and neutrophiles. The parameters were within the normal range for control and dynamic conditions. Full hemogram can be consulted in **Figure VII.S5** and **VII.S6**. The satisfactory results of red blood cells and hemoglobin also attested the biocompatibility of the magnetic implants and the magnetic stimulation, with no signals of hemolysis or anemia. In addition, serum biochemistry analyses were performed 6 weeks post implantation by CEDIVET laboratories. Comparing to the reference range, no sign of liver and kidney damages were observed (**Figure VII.S7**), suggesting the low toxicity of magnetic field on living organisms at the applied strength and frequency. Such results were also corroborated by the immunostaining of lymphocytes (CD45) and macrophages (CD68). Similar profile was visualized for both conditions, displaying low levels of these immunoinflammatory markers - **Figure VII.S8** and **VII.S9**.

Additionally,, the cell survival of tissue implants was also accessed by a live-dead assay. As expected, the *in vivo* scenario and the influence of the CMF did not interfere with cell survival (**Figure VII.5C**).

3.5.1. Characterization of the magnetic implant upon stimulation

Histological analysis of the explanted samples, namely H&E, showed that CMF favored the implant integration in the mice model – **Figure VII.S10**. Even though 4 weeks post implantation the magnetic tissue constructs from both populations (dynamic and control) were integrated within the host, a small tissue invasion could be perceived for the dynamic condition (represented by the black arrows). Nevertheless, when compared to the control condition, after 6 weeks the magnetic tissues under the CMF were able to invade an extended area of the surrounding host tissue. A 3D reconstruction of the tissue implant was performed by nanoCT (**Figure VII.6A)**, allowing the mapping of the magnetic implant along the host tissue. As displayed, in the control population, the magnetic tissues remained in bulk conformation with the spreading of limited number of cell

aggregates along the implantation zone. The magnetically stimulated implants were able to invade the adjacent tissue, confirming the H&E results.

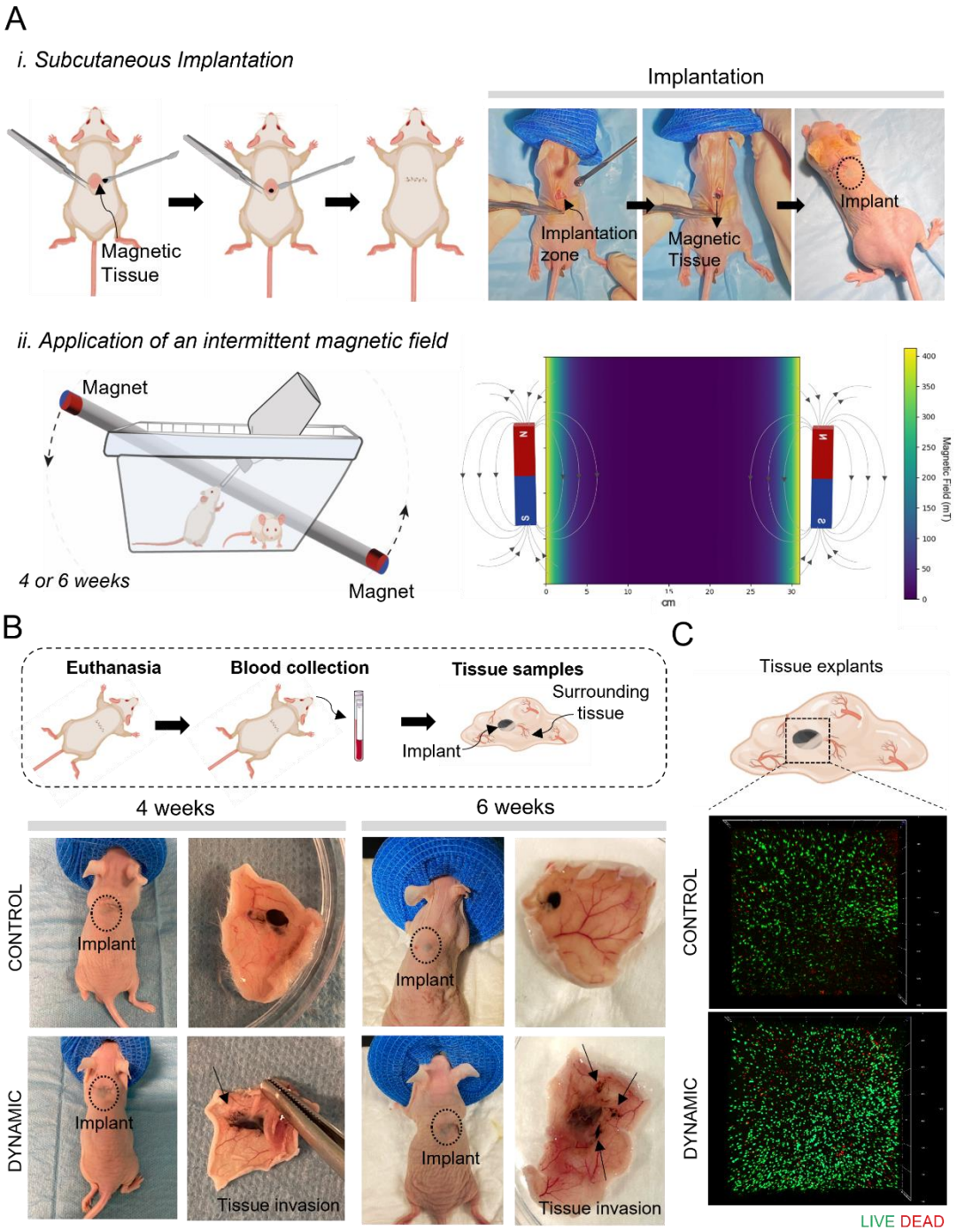

Figure VII.5: Magnetic stimulation of the magnetic tissues using an *in vivo* mice model. **A.** Schematic representation of the *in vivo* experimental design; i) Surgical procedure for implanting one magnetic tissue per mouse; ii) Representative illustration of the setup for magnetic stimulation (in left) and the mapping of the magnetic field (in right). **B.** 4 and 6 weeks post-implantation, blood and tissue samples were collected. Photographs of the animals and the tissue samples composed of the implant and the surrounding tissue. **C.** The cell viability on tissue implants was demonstrated by a live-dead assay after 6 weeks for control and dynamic conditions.

The morphology of the implants was also investigated by assessing the presence of collagen by Masson's Trichrome staining. The presence of collagen (blue staining) was evidenced for all conditions - **Figure VII.6B**. Notably, enhanced deposition of collagen around the implant and within the magnetic tissues was visualized upon the CMF. Concerning the implant integration, Masson's Trichrome staining corroborated the H&E results. After 4 weeks, we can be visualized a greater tissue integration for implants subjected to the magnetic field. Additionally, after 6 weeks the implants were integrated within the muscle tissues, stained with red.

3.5.2. Osteogenesis evaluation of the tissue implant upon magnetic stimulus

Evaluation of the tissue stemness and expression of osteopontin

Upon the magnetic stimulation, we evaluated the cell differentiation on the magnetized tissue implant. For this purpose, we assessed the stemness of the tissue implant and the expression of one key osteogenic factor – osteopontin. Similarly to the *in vitro* environment, after 4 weeks the expression of CD105 decreased in the presence of the magnetic stimulation (**Figure VII.6C**). In contrast, the level of osteopontin in tissue implants increased upon magnetic stimulation. As displayed in **Figure VII.7A**, the presence of osteopontin was only visualized on tissue implants under the dynamic environment.

Gene expression and biomeralization assessment

Similar to the *in vitro* model, the expression of the osteogenic genes such as collagen I and RUNX2 were also evaluated. The results were in accordance with the osteopontin staining, where the expression of these two osteogenic genes was verified for the dynamic environment, with more pronounced effect after 6 weeks – see **Figure VII.7B**. Lastly, the presence of Ca/P deposits was investigated after 4 and 6 weeks. According to the **Figure VII.7C** and **Figure VII.S11**, the biomineralization of the tissue implants occurred after 4 weeks of magnetic stimulation.

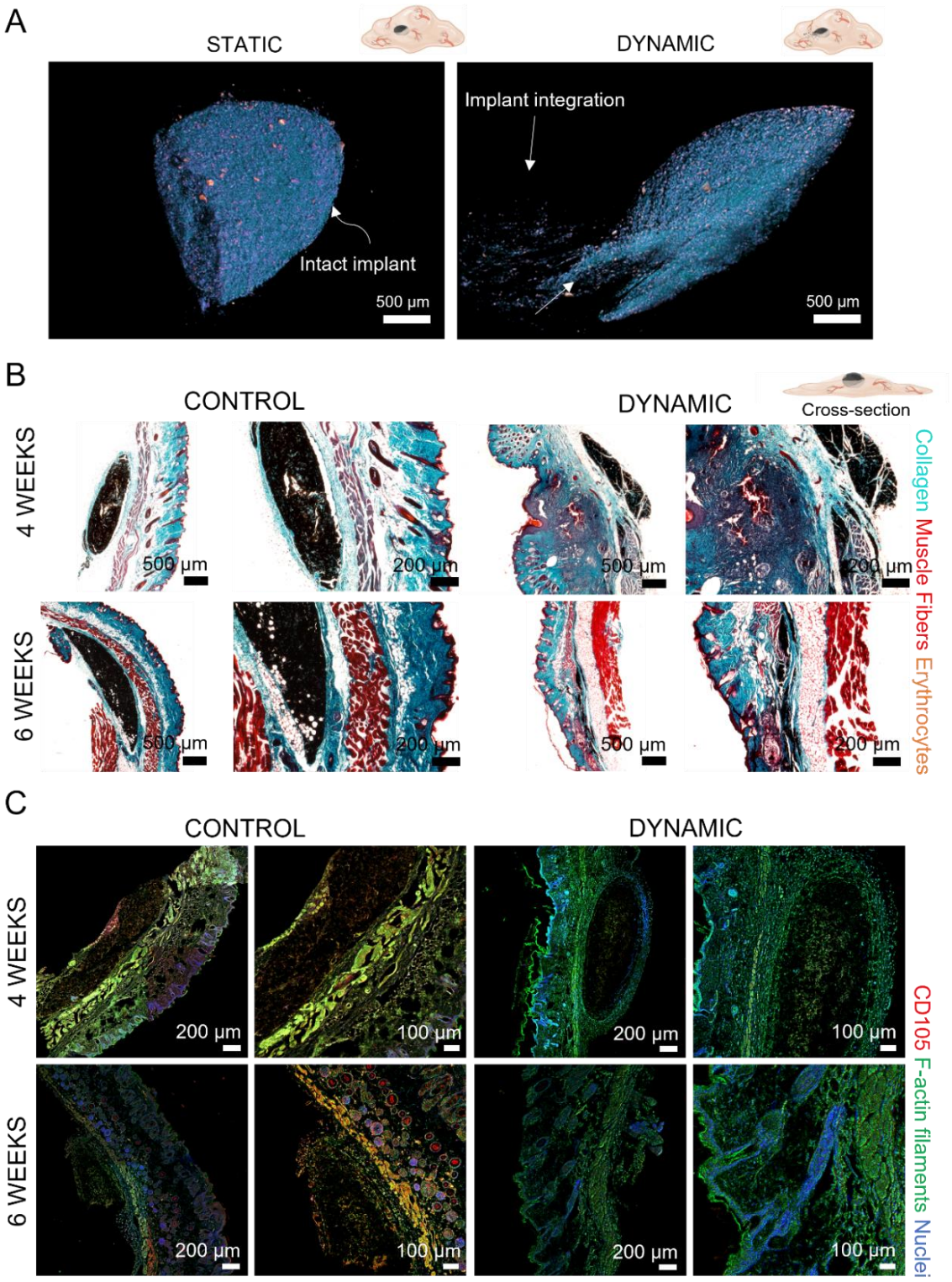

Figure VII.6: Characterization of the tissue implants after 4 and 6 weeks. **A.** 3D reconstruction of the magnetic tissue through nanoCT, 6-weeks post-implantation. **B.** Collagenous connective tissue fibers identified by Trichrome Masson staining (in blue) on histological sections. **C.** The stemness of the tissue implant was evaluated by accessing the presence of the stemness marker CD105 (in red). F-actin filaments are stained in green, and all the nuclei are stained in blue.

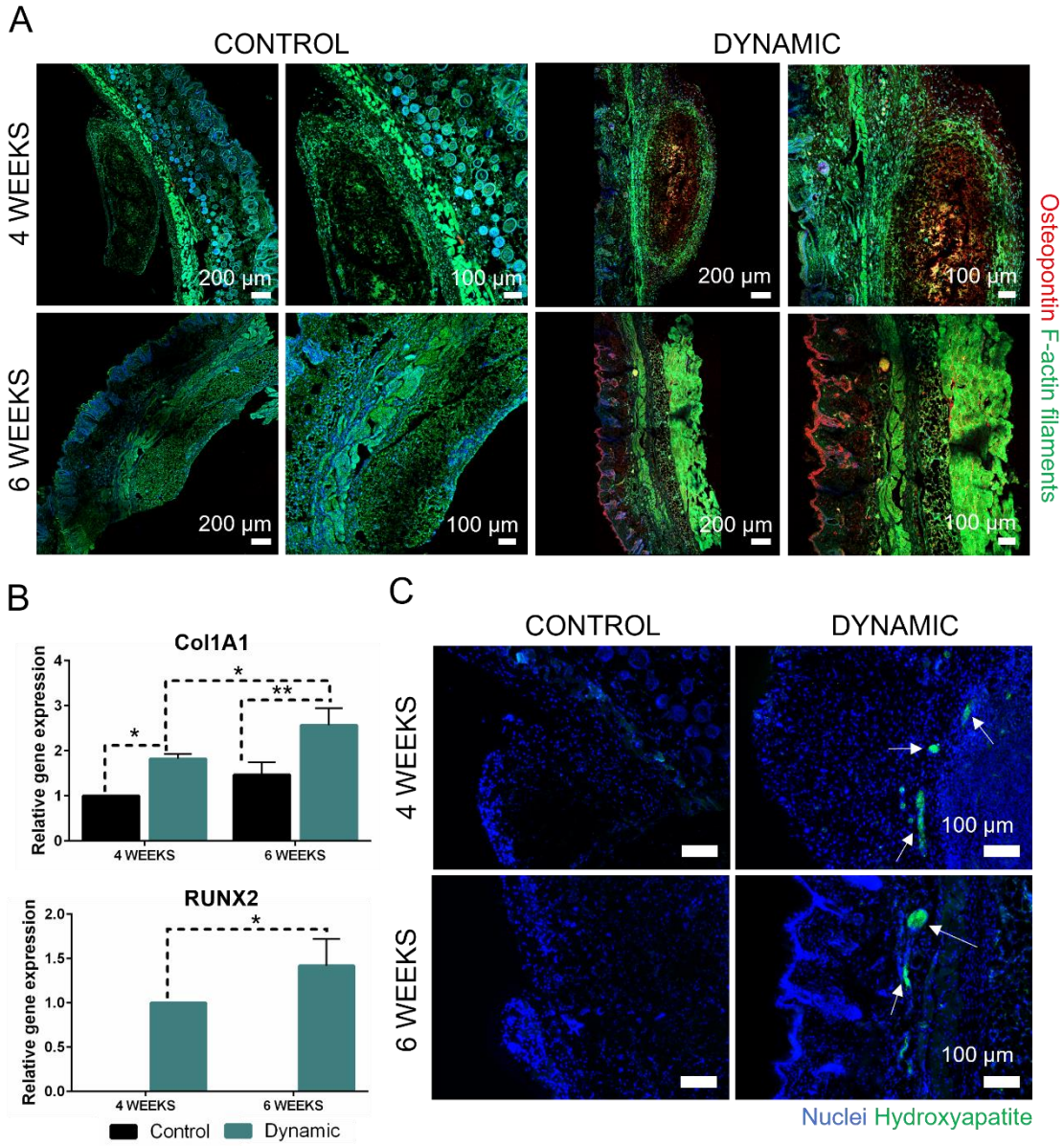

Figure VII.7: The power of the CMF on stimulating the osteogenic differentiation of the magnetic tissue implants. **A.** The presence of osteopontin (in red), an important osteogenic marker, was accessed 4 and 6 weeks post implantation. F-actin filaments are stained in green and all the nuclei are stained in blue. **B.** Relative expression of important osteogenic genes namely collagen I (col1A1) and RUNX2. **C.** Mineralization of the tissue implants upon magnetic stimulation. The hydroxyapatite portion of bone-like nodules deposited by cells was visualized through fluorescent OsteoImage™ Mineralization Assay: cell nucleus - DAPI (blue) and hydroxyapatite (green).

4. Discussion

Biological organisms are daily subject to environmental pressures and interestingly, the inherent forces of cellular microenvironment are known to regulate several tissue functions.[32] Therefore,

the scientific community has been investigating how biophysical cues are integrated in tissues, and how they can regulate cell behavior throughout the tissue development [4]

Stem cells are considered attractive candidates for clinical applications due to the high differentiation potential and self-renewal ability. Mechanobiology has been implicated on the control of stem cells fate, including cell adhesion, proliferation and differentiation.[33] Thus, several biophysical cues have been investigated for guiding stem cells into specific tissue functions. Contrary to biological and chemical signals, physical cues have adjustable properties and can be used in a timely and localized manner, being a trending topic of research in the fields of biomaterials, TE and cell biology. Physical stimuli can be classified into six categories: mechanical, light, thermal, electrical, acoustic and magnetic.[34] Generally, physical fields at the macroscale cannot modulate stem cells fate. Only localized physical signals are sensed by the surface of cell receptors via functional nanostructures. Following this rational, functional materials at the nanoscale have been engineered for releasing localized energy through their nanostructures.[17]

The advances on nanofabrication during the last decades have enabled the production of nanoparticles with structural and compositional accuracy. At the forefront of nanotechnology, MNPs have been extensively investigated owing to their promising potentials in biomedical applications that take advantage of their inherent properties such biocompatibility and rapid response to magnetic field remotely.[35] Tremendous progress has been achieved using MNPs, with ones being included in cells and scaffolds, and/or acting as magnetic carriers for drugs and biomolecules. Additionally, MNPs can regulate the receptors at the cell surface and then activate key signaling pathways. Thus, the magnetic biophysical stimulus can potentially control the forces applied to the cell environment, in an extremely precise, remote and noninvasively manner. [36] By adjusting the strength and exposure time, the magnetic field allows a unique guidance of cell fate. When applied to stem cells, several physiological alterations on the cellular microenvironment (such as cell proliferation, secretion of growth factors and gene transcription), are already disclosed in the literature.[37] Particularly, the dynamic magnetic stimuli, including pulsed, alternating and rotating magnetic fields, have already been implicated on bone tissue formation by boosting the healing process or by directing the osteointegration of bone implants.[38]–[40] Additionally, under a dynamic magnetic field, the generated electric field changes the permeability of the cells' membrane changes, thereby altering the activities of the cyclic guanosine monophosphate and adenosine monophosphate, promoting the osteogenic differentiation.[41] This strategy was already

disclosed for isolated cells and 2D cell cultures. Nevertheless, aiming for bone TE, such approach has been explored using biochemical inductors or pre-targeted tissue cells.

Mag-TE has been widely explored in our group for the fabrication of vascularized and robust tissue constructs with complex and well-defined architecture, achieving encouraging outcomes in host tissue integration.[18],[20] We now hypothesized that the magnetic actuation could prompt bone tissue formation in magnetized tissues. For the purpose we evaluated, for the first time, the ability to guide *in situ* bone tissue formation, by applying a CMF to stimulate the osteogenic differentiation of the magnetized tissues, previously developed *in vitro.*

In this sense, we started by fabricating magnetized tissues *in vitro* composed by hASCs, following the previous and well-defined methodologies of the group. After 7 days, the magnetic constructs were placed under a CMF and cultured without any osteogenic supplementation. For the control condition, the magnets were removed from the tissues, and strategically re-located to avoid any magnetic actuation.

The success of this novel concept truly relies on the magnetic power of the produced tissues. However, literature reports that in biological environments certain magnetic nanomaterials tend to rapidly oxidized, creating species that are nonmagnetic or weakly magnetic.[42] Therefore, to recognize the potential of magnetic field on our magnetized tissues, an adequate magnetic characterization along the time is essential. Both iron content and magnetization character showed decreased values along the time. Nevertheless, this phenomenon can be easily explained by the cell proliferation within the tissues, where the newly formed cells are not magnetized. By normalizing the magnetization character per DNA content, we verified that the magnetic power of the tissues remained constant even after 21 days. But most importantly, our magnetized tissues demonstrated superparamagnetic behavior that favor their application in TE. Briefly, when the magnetic field is removed, the magnetic tissues do not retain any magnetic moment, avoiding the formation of aggregates and by guarantying their elimination when they are no longer submitted to the magnetic field.[43]

Moreover, we also speculated about the influence of the magnetic field on the tissue structure. As displayed in **Figure VII.1E** and **Figure VII.2A**, the magnetized tissues remained intact after 21 days, for both conditions. By looking for tissue morphology, some morphological and structural alterations were denoted on the magnetized tissues after magnetic stimulation. The impacts of these structural alternations on cell behavior were then investigated. Firstly, we evidenced that cell viability was not influenced by the CMF Then, we observed the stagnation of metabolic activity and

DNA content. As well-reported in the literature, such data can be a marker of cells differentiation.[18],[25] Herein, we postulate that CMF could trigger the differentiation of hASCs.

As well-documented in the literature, upon magnetic stimulation, the cells' integrins are actively involved in outside-in and inside-out signaling mediated by polymerization and contraction of the cytoskeleton known to control cellular mechanotransduction pathways. Therefore, a changed physical microenvironment can be detected by the integrin–ECM interaction. In fact, the integrin-ECM complex is considered the primary target of MNPs for controlling cells' behavior.[27] In response to such alterations in cytoskeleton, FAK is recruited and activated by autophosphorylation. This mechanism leads to the intracellular mechanotransduction, by activating downstream mechanotransducers within the cytoplasm. The interplay between FAK and the contractile cytoskeletal network is tightly controlled in the cell for regulating the force transmitted to the nucleus.[44] Vinculin transmits these forces by increasing ECM-bound integrin–talin complexes, essential to propagate this force to the actin cytoskeleton. From the MADK signaling cascades, ERK1/2 has the key role on mediating the gene expression. In fact, FAK-ERK complex was already implicated in the phosphorylation of RUNX2 transcription factor that controls the osteogenic gene expression.[45],[46] Hence, concerning the mechanism behind magnetic stimuli, we investigated the expression of key signaling markers namely FAK phosphorylation, ERK1/2 and vinculin in magnetized tissues after the magnetic stimulation. The impact of the CMF can be depicted in **Figure VII.3C**. Upon magnetic stimulation, the FAK complex was stimulated and triggered the expression of ERK1/2. After 14 days, we visualized an increased level of FAK phosphorylation. Since the activation of ERK1/2 is dependent on FAK's phosphorylation, we only observed an increased expression of ERK1/2 after 21 days. Of note, the levels of the complex FAK-ERK remained constant along the time for the control condition. We can therefore conclude that the mechanotransductions pathways were activated in magnetized tissues in the presence of the magnetic field. Thus, we investigated the impact on cell differentiation by analyzing the stemness of the tissue and the established osteogenic indicators. As demonstrated by flow cytometry and immunostaining, the stemness marker CD105, decreased along the time for the dynamic *in vitro* environment.[47] Additionally, VEGF, which is secreted by hASCs, appeared to be downregulated after 7 days in the magnetized tissues subjected to the CMF, substantiating the differentiation of stem cells along the time in the dynamic condition.

By analyzing the osteopontin expression profile, we attested that the CMF prompted the osteogenic differentiation of the magnetized tissues composed by hASCs. Such findings were corroborated by the gene expression data. Dynamic stimulus triggered the expression of important genes for bone

tissue formation, including RUNX2 and collagen I. Moreover, the level of VEGF and PPARG genes also corroborated that hASCs lost their adipogenic markers.

Aspiring the bone tissue formation, the mineralized inorganic component is crucial for proper tissue function. Bone tissue is composed by apatite minerals, a crystalline complex of calcium and phosphate commonly denominated hydroxyapatite.[48] Hence, we investigated the impact of the dynamic stimulus on the mineral composition of the magnetized tissues. Such results were in accordance with the cytokines and gene expression data, where the presence of hydroxyapatite was only visualized in tissues magnetically stimulated.

Nevertheless, the power of magnetism on cell differentiation could be dramatically affected when translated to complex living organisms. For that reason, as proof-of-concept study, magnetized tissues were formed *in vitro* and implanted subcutaneously in a mice model after 7 days. Then, the animals were subjected to the CMF for a period of 6 weeks. following implantation, the tissue substitute could face several challenges. At the top, implant viability and correct tissue integration are the major concerns. In this sense, we started by confirming the cell viability of the magnetized tissues after 6 weeks. Concerning the tissue integration, we visualized that the magnetic stimulus accelerated the tissue integration. After 4 weeks, tissues of the control population remained in the implantation zone but without integrating the surrounding tissue. In contrast, magnetized tissues subjected to the dynamic environment for the same time were able to integrate within the host tissue and started to invade the neighboring tissue. Upon implantation, the inserted construct is responsible for initiating the remodeling process by partially degrading the matrix and by secreting molecular signals for attraction and differentiation of other cell types, such as fibroblasts, that build up new ECM.[49] Moreover, since our magnetized tissues are fully composed of hASCs, the initial release of VEGF stimulates a localized neovascularization feeding the graft surroundings, and consequently reducing fibrosis and scar tissue formation while facilitating osteogenesis.[50] It is well-established that the osteogenesis and healing processes occur simultaneously. By promoting the tissue invasion and integration, the CMF triggers the healing process and the osteogenic differentiation. To corroborate these findings, we evaluated the osteogenic markers previously stated in the *in vitro* scenario. Masson Trichrome staining attested not only the integration of the magnetized tissues within the surrounding tissue, but also an enhanced deposition of collagen. Even with all the *in vivo* constrains, that include the tissue surrounding the implant and the daily routine of the animals, the magnetic stimulation triggered the osteogenic differentiation of the magnetized tissues. In fact, tissues under the CMF exhibited the expression of key osteogenic markers such as osteopontin, deposition of hydroxyapatite nodules, and the expression of crucial

osteogenic genes like RUNX2 and collagen I. Aspiring the application of this new therapeutic approach for clinical practice, the safety concerns regarding the use of MNPs and magnetic field must be well-clarified.[51] In this particular work, the presence of MNPs and the magnetic field showed no adverse effects on the animals. Throughout the study, there were no cases of mice exhibiting any pain behavior and none of the mice displayed visible inflammation or infection. By blood test analyses, we verified that all parameters were within the normal range with no signals of hemolysis or anemia (**Figure VII.S5** and **VII.S6**). The serum biochemistry panel (**Figure VII.S7**) also did not display any signal of liver or kidney damage. We can conclude that the application of a CMF at this range of frequency and strength does not appear to be toxic for living organisms.

Local tissue response to the implanted magnetic tissue construct was characterized by the presence of macrophages (CD68) and lymphocytes (CD45), the key cells of immune system involved in host defense. For all the conditions, low immunoreactivity was observed (**Figure VII.S9** and **Figure VII.S10**). In fact, a study developed by Gujjalapudi and colleagues also showed no impacts on humans treated under the influence of the magnetic field. In this study, the magnetic field accelerated the healing process after the placement of a titanium dental implant, leading to a faster osteointegration.[41]

Previous preliminary studies indicate that besides the physical modifications of MNPs along the time and its degradation at atomic scale, no toxic effects were observed in living organisms. According to Claire Wilhelm and co-workers, cells could timely orchestrate the redistribution of a nanoparticle from a dense assembly in early endosomes to a more dispersed and exposed state into lysosomal compartments.[52] This mechanism might be activated to retard the release of free cytotoxic iron ions only to the lysosome, where ferritin proteins can store the released iron in a safe form. Nevertheless, the MNPs degradation mechanism under *in vivo* scenarios is still poorly explored, leading to an apprehensive use of MNPs in biomedicine. Hence, we believe that the use of MNPs still needs further translational studies to attest their efficacy and safety for TE and regenerative medicine purposes.

After this proof-of-concept study using subcutaneous implantations, we envision that this strategy can be extended for bone tissue regeneration using bone defect models. For the purpose, a synergetic strategy encompassing scaffold free and scaffold-based approaches could represent an added value for the development of mechanically resistant living materials to further potentiate the bone healing process. Also, as the interplay between inflammatory cues, cellular components and vascular networks is a complex spatiotemporal process essential in bone tissue repair, the use

of pre-vascularized magnetic tissues could further accelerate a proper tissue formation while guaranteeing cellular gaseous exchange, nutrient supply, and waste product removal.

5. Conclusion

Within biological organisms, the tissue functions are determined by its surrounding environment. Hence, by recapitulating the physical and/or biochemical features, cell behavior can be modulated. Over the past decades, mechanical stimuli showed outstanding results on directing stem cells fate in 2D cell cultures. In our group, Mag-TE has been applied to create improved tissue substitutes with intricate hierarchy and geometries for tissue regeneration and disease modeling purposes. Herein, we hypothesized that remote magnetic stimulation could be further use to direct stem cells' fate on a magnetic living construct, prompting *in situ* tissue formation. By acting as living bioreactors, magnetic tissues composed by hASCs were remotely stimulated by a CMF, both *in vitro* and *in vivo*, triggering the osteogenic differentiation of the tissue constructs. Following *in vivo* implantation, the closely cell-to-cell interactions of the magnetized tissues and the secretory profile of hASCs also led to an enhanced tissue integration and remodeling with improved osteogenic expression, offering new prospects for advanced cell transplantation methodologies.

Altogether, we hypothesize that this novel therapeutic strategy could prompt the bone tissue formation in an extremely guided and wireless manner, while favoring a fast and adequate tissue integration. Even though this study focused on bone regeneration, we also anticipate that by adjusting the initial cell phenotype and the target organ, this approach could be further extended for the regeneration and repair of a plethora of tissues.

Acknowledgements

We acknowledge the project CICECO-Aveiro Institute of Materials, UIDB/50011/2020, UIDP/50011/2020 & LA/P/0006/2020, financed by national funds through the FCT/MCTES (PIDDAC). The authors also acknowledge financial support by FCT through a Ph.D. grant (SFRH/BD/141523/2018, Lúcia F. Santos) and through the individual contract (CEECIND/2021.02196, A. Sofia Silva).

References

1. Jaalouk, D. E. & Lammerding, J. Mechanotransduction gone awry. *Nature Reviews Molecular Cell Biology 2009 10:1* **10,** 63–73 (2009).
2. Wan, X., Liu, Z. & Li, L. Manipulation of Stem Cells Fates: The Master and Multifaceted Roles of Biophysical Cues of Biomaterials. *Adv Funct Mater* **31,** 2010626 (2021).

3. Hamouda, M. S., Labouesse, C. & Chalut, K. J. Nuclear mechanotransduction in stem cells. *Curr Opin Cell Biol* **64,** 97–104 (2020).
4. Dufort, C. C., Paszek, M. J. & Weaver, V. M. Balancing forces: architectural control of mechanotransduction. *Nature Reviews Molecular Cell Biology 2011 12:5* **12,** 308–319 (2011).
5. Ding, S. *et al.* Synthetic small molecules that control stem cell fate. *Proc Natl Acad Sci U S A* **100,** 7632–7637 (2003).
6. McMurray, R. J., Dalby, M. J. & Tsimbouri, P. M. Using biomaterials to study stem cell mechanotransduction, growth and differentiation. *J Tissue Eng Regen Med* **9,** 528–539 (2015).
7. Na, S. *et al.* Rapid signal transduction in living cells is a unique feature of mechanotransduction. *Proc Natl Acad Sci U S A* **105,** 6626–6631 (2008).
8. Wu, C. *et al.* Recent Advances in Magnetic-Nanomaterial-Based Mechanotransduction for Cell Fate Regulation. *Advanced Materials* 1705673 (2018). doi:10.1002/adma.201705673
9. Vining, K. H. & Mooney, D. J. Mechanical forces direct stem cell behaviour in development and regeneration. *Nature Reviews Molecular Cell Biology 2017 18:12* **18,** 728–742 (2017).
10. Holle, A. W. *et al.* In situ mechanotransduction via vinculin regulates stem cell differentiation . *Stem Cells* **31,** 2467–2477 (2013).
11. Peng, L. *et al.* The Effect of Pulsed Electromagnetic Fields on Angiogenesis. *Bioelectromagnetics* **42,** 250–258 (2021).
12. de Mattei, M. *et al.* Effects of Pulsed Electromagnetic Fields on Human Articular Chondrocyte Proliferation. *Connect Tissue Res* **42,** 269–279 (2009).
13. Sun, L. Y. *et al.* Effect of pulsed electromagnetic field on the proliferation and differentiation potential of human bone marrow mesenchymal stem cells. *Bioelectromagnetics* **30,** 251–260 (2009).
14. Noriega-Luna, B., Sabanero, M., Sosa, M. & Avila-Rodriguez, M. Influence of pulsed magnetic fields on the morphology of bone cells in early stages of growth. *Micron* **42,** 600–607 (2011).
15. Xia, Y. *et al.* Magnetic field and nano-scaffolds with stem cells to enhance bone regeneration. *Biomaterials* **183,** 151–170 (2018).
16. Dobson, J. Remote control of cellular behaviour with magnetic nanoparticles. *Nat Nanotechnol* **3,** 139–143 (2008).
17. Pankhurst, Q. A., Connolly, J., Jones, S. K. & Dobson, J. Applications of magnetic nanoparticles in biomedicine. *J Phys D Appl Phys* **36,** R167 (2003).
18. Silva, A. S., Santos, L. F., Mendes, M. C. & Mano, J. F. Multi-layer pre-vascularized magnetic cell sheets for bone regeneration. *Biomaterials* **231,** 119664 (2020).
19. Santos, L. F., Sofia Silva, A. & Mano, J. F. Complex-shaped magnetic 3D cell-based structures for tissue engineering. *Acta Biomater* **118,** 18–31 (2020).
20. Santos, L. F., Patrício, S. G., Silva, A. S. & Mano, J. F. Freestanding Magnetic Microtissues for Tissue Engineering Applications. *Adv Healthc Mater* 2101532 (2022). doi:10.1002/ADHM.202101532
21. Gyu Kang, H. *et al.* A geometry-independent moment correction method for the MPMS3 SQUID-based magnetometer . *Measurement Science and Technology* **32,** 105602 (2021).
22. Hu, P. *et al.* High saturation magnetization Fe3O4 nanoparticles prepared by one-step reduction method in autoclave. *J Alloys Compd* **728,** 88–92 (2017).
23. Jin, H. J. *et al.* Down-regulation of CD105 is associated with multi-lineage differentiation in human umbilical cord blood-derived mesenchymal stem cells. *Biochem Biophys Res Commun* **381,** 676–681 (2009).
24. Barati, D. *et al.* Spatiotemporal release of BMP-2 and VEGF enhances osteogenic and vasculogenic differentiation of human mesenchymal stem cells and endothelial colony-forming cells co-encapsulated in a patterned hydroge. *Journal of Controlled Release* **223,** 126–136 (2017).
25. Correia, C. R. *et al.* Semipermeable Capsules Wrapping a Multifunctional and Self-regulated Co-culture Microenvironment for Osteogenic Differentiation. *Sci Rep* **6,** 21883 (2016).

26. Atkins, G. J., Findlay, D. M., Anderson, P. H. & Morris, H. A. Target Genes: Bone Proteins. *Vitamin D* **23,** 411–424 (2011).
27. Martino, F., Perestrelo, A. R., Vinarský, V., Pagliari, S. & Forte, G. Cellular mechanotransduction: From tension to function. *Front Physiol* **9,** 824 (2018).
28. Ramage, L., Nuki, G. & Salter, D. M. Signalling cascades in mechanotransduction: cell–matrix interactions and mechanical loading. *Scand J Med Sci Sports* **19,** 457–469 (2009).
29. Chandran, S. V., Vairamani, M. & Selvamurugan, N. Osteostimulatory effect of biocomposite scaffold containing phytomolecule diosmin by Integrin/FAK/ERK signaling pathway in mouse mesenchymal stem cells. *Scientific Reports 2019 9:1* **9,** 1–13 (2019).
30. Salasznyk, R. M., Klees, R. F., Williams, W. A., Boskey, A. & Plopper, G. E. Focal adhesion kinase signaling pathways regulate the osteogenic differentiation of human mesenchymal stem cells. *Exp Cell Res* **313,** 22–37 (2007).
31. Chen, T. J., Wu, C. C., Tang, M. J., Huang, J. S. & Su, F. C. Complexity of the Tensegrity Structure for Dynamic Energy and Force Distribution of Cytoskeleton during Cell Spreading. *PLoS One* **5,** e14392 (2010).
32. Hamill, O. P. & Martinac, B. Molecular basis of mechanotransduction in living cells. *Physiol Rev* **81,** 685–740 (2001).
33. Han, S.-B. *et al.* Mechanical Properties of Materials for Stem Cell Differentiation. *Adv Biosyst* **4,** 2000247 (2020).
34. Kong, Y. *et al.* Regulation of stem cell fate using nanostructure-mediated physical signals. *Chem Soc Rev* **50,** 12828–12872 (2021).
35. Pankhurst, Q. A., Thanh, N. T. K., Jones, S. K. & Dobson, J. Progress in applications of magnetic nanoparticles in biomedicine. *J Phys D Appl Phys* **42,** 224001 (2009).
36. Pardo, A. *et al.* Magnetic Nanocomposite Hydrogels for Tissue Engineering: Design Concepts and Remote Actuation Strategies to Control Cell Fate. *ACS Nano* **15,** 175–209 (2021).
37. Sniadecki, N. J. Minireview: A Tiny Touch: Activation of Cell Signaling Pathways with Magnetic Nanoparticles. *Endocrinology* **151,** 451–457 (2010).
38. Sikavitsas, V. I., Bancroft, G. N., Holtorf, H. L., Jansen, J. A. & Mikos, A. G. Mineralized matrix deposition by marrow stromal osteoblasts in 3D perfusion culture increases with increasing fluid shear forces. *Proceedings of the National Academy of Sciences* **100,** 14683–14688 (2003).
39. di Bartolomeo, M. *et al.* Pulsed Electro-Magnetic Field (PEMF) Effect on Bone Healing in Animal Models: A Review of Its Efficacy Related to Different Type of Damage. *Biology 2022, Vol. 11, Page 402* **11,** 402 (2022).
40. Naomi M Shupak, FrankS. P. Therapeutic Uses of Pulsed Magnetic-Field Exposure: A Review. *URSI Radio Science Bulletin* **307,** 9–32 (2003).
41. Gujjalapudi, M. *et al.* Effect of Magnetic Field on Bone Healing around Endosseous Implants – An In-vivo Study. *J Clin Diagn Res* **10,** ZF01 (2016).
42. Frimpong, R. A. & Hilt, J. Z. Magnetic nanoparticles in biomedicine: synthesis, functionalization and applications. *Nanomedicine* **5,** 1401–1414 (2010).
43. Miguel, M. G., Lourenço, J. P. & Faleiro, M. L. Superparamagnetic Iron Oxide Nanoparticles and Essential Oils: A New Tool for Biological Applications. *International Journal of Molecular Sciences 2020, Vol. 21, Page 6633* **21,** 6633 (2020).
44. Galbraith, C. G., Yamada, K. M. & Sheetz, M. P. The relationship between force and focal complex development. *Journal of Cell Biology* **159,** 695–705 (2002).
45. Tang, B. *et al.* Harnessing Cell Dynamic Responses on Magnetoelectric Nanocomposite Films to Promote Osteogenic Differentiation. *ACS Appl Mater Interfaces* **10,** 7841–7851 (2018).
46. Salasznyk, R. M., Klees, R. F., Boskey, A. & Plopper, G. E. Activation of FAK is necessary for the osteogenic differentiation of human mesenchymal stem cells on laminin-5. *J Cell Biochem* **100,** 499–514 (2007).
47. Hu, K. & Olsen, B. R. The roles of vascular endothelial growth factor in bone repair and regeneration. *Bone* **91,** 30–38 (2017).

48. Grünewald, T. A. *et al.* Magnesium from bioresorbable implants: Distribution and impact on the nano- and mineral structure of bone. *Biomaterials* **76,** 250–260 (2016).
49. Lutolf, M. P. *et al.* Synthetic matrix metalloproteinase-sensitive hydrogels for the conduction of tissue regeneration: Engineering cell-invasion characteristics. *PNAS April* **29,** 5413–5418 (2003).
50. Hao, S. *et al.* Integration of a Superparamagnetic Scaffold and Magnetic Field to Enhance the Wound-Healing Phenotype of Fibroblasts. *ACS Appl Mater Interfaces* **10,** 22913–22923 (2018).
51. Silva, A. K. A., Silva, É. L., Egito, E. S. T. & Carriço, A. S. Safety concerns related to magnetic field exposure. *Radiat Environ Biophys* **45,** 245–252 (2006).
52. Lartigue, L. *et al.* Biodegradation of iron oxide nanocubes: High-resolution in situ monitoring. *ACS Nano* **7,** 3939–3952 (2013).

Supporting Information

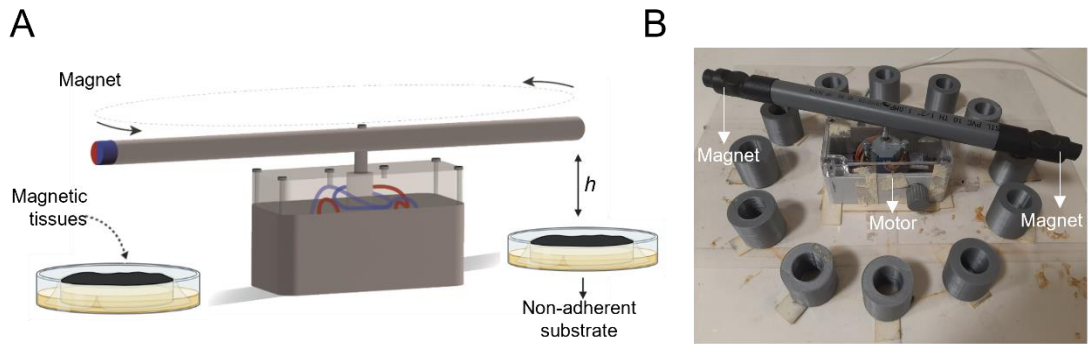

Figure VII.S1: Lab-made magnetic apparatus developed by group, composed by magnets in opposite sides and a rotating motor. **A.** Schematic representation of the equipment; **B.** Photograph of the magnetic apparatus that allowed the production of a cyclic magnetic field.

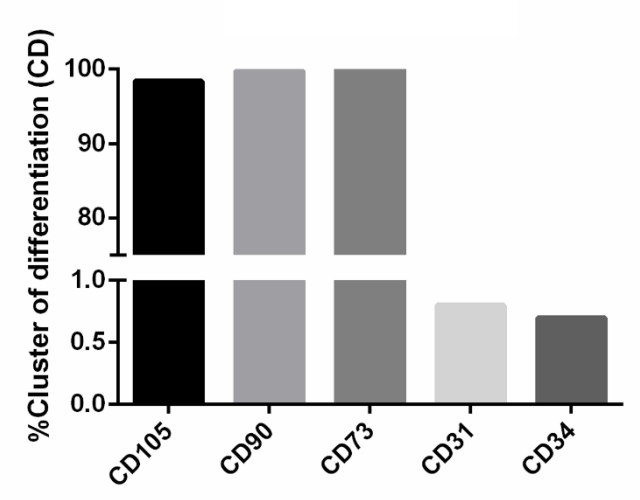

Figure VII.S2: The successfully isolation of hASCs from adipose tissues was confirmed by flow cytometry. Positive markers – CD105, CD90 and CD73. Negative markers – CD31 and CD34.

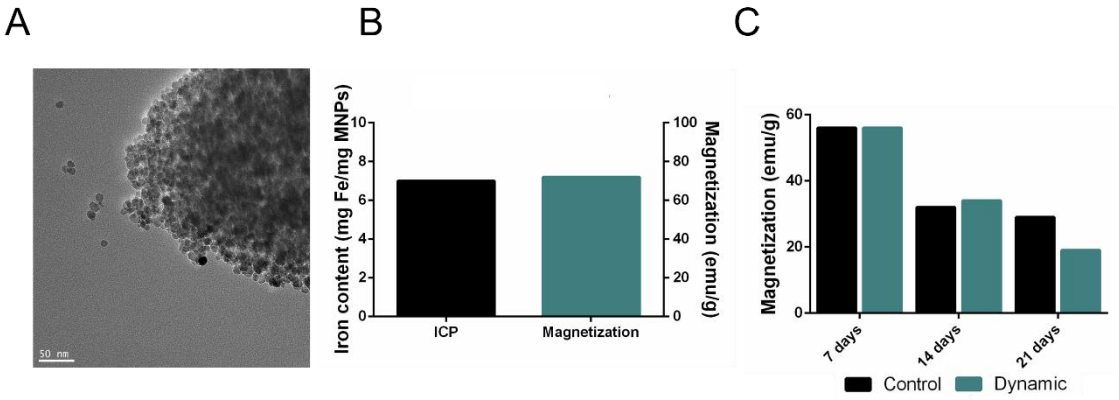

D

Sample	Msat (emu/g)	ΔMsat (emu/g)	-Hc (Oe)	Δ[-Hc] (Oe)	+Hc (Oe)	Δ[+Hc] (Oe)	+Mr (emu/g)	Δ[+Mr] (emu/g)	-Mr (emu/g)	Δ[-Mr] (emu/g)
7d Dyn	56	2	0	1	0	1	0.02	0.06	-0.02	0.06
7d Cont	56	1	1	1	0	1	0.02	0.07	-0.02	0.07
14d Dyn	34	2	0	1	1	1	0.02	0.04	-0.02	0.04
14d Cont	32	2	-1	1	1	1	0.03	0.05	-0.04	0.04
21d Dyn	19	1	-1	1	2	1	0.03	0.02	-0.04	0.02
21d Cont	29	1	-1	1	1	1	0.02	0.04	-0.03	0.04
MNPs	72	6	0	1	1	1	0.00	0.08	-0.04	0.08

Figure VII.S3: Magnetic characterization of the MNPs and the magnetized tissues. **A.** TEM images of the MNPs; **B.** Magnetic characterization of the MNPs, namely the magnetization and the iron content determined by ICP; **C.** Magnetization of the magnetic tissues along the time – control and dynamic conditions; **D.** Detailed information of magnetization features of MNPs and magnetic tissues.

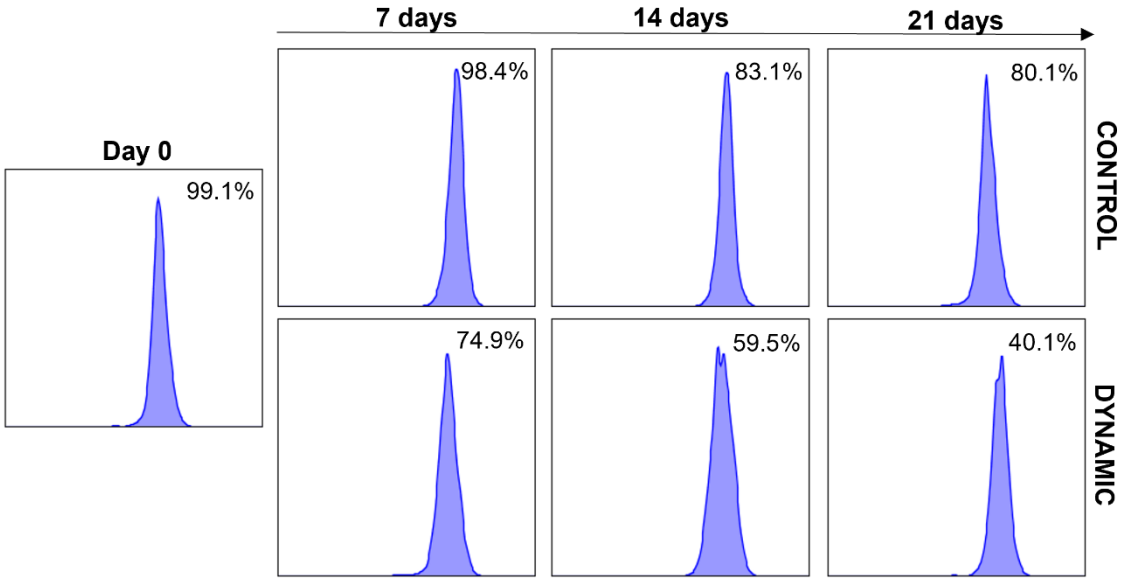

Figure VII.S4: The stemness of the magnetic tissues composed by hASCs was determined by analyzing the CD105 stemness marker through flow citometry

Parameters	Reference Range	Control	Dynamic
Erythrocytes (10^{12}/L)	4.2 – 6.7	8.2 ± 0.3	8.4 ± 0.6
Hemoglobin (g/dL)	9.5 – 14.5	14.5 ± 0.8	14.2 ± 0.7
Hematocrit (%)	27.2 – 45.9	41.0 ± 2.3	39.9 ± 2.2
MCHC (g/dL)	31.0 – 34.9	35.0 ± 0.2	35.6 ± 0.8
MVC (fL)	59.1 – 75.4	59.0 ± 1.9	59.3 ± 2.1
Neutrophiles (10^9/L)	0.8 – 2.9	1.0 ± 1.4	1.0 ± 0.3
Lymphocytes (10^9/L)	2.2 – 5.3	2.2 ± 0.4	2.0 ± 0.2
Monocytes (10^9/L)	< 0.4	0	0
Eosinophiles (10^9/L)	< 0.4	0.05 ± 0.05	0.10 ± 0.05
Basophiles (10^9/L)	< 0.6	0	0
Platelets (10^9/L)	136.6 – 558.4	730 ± 331	353 ± 205

Figure VII.S5: Hematological analysis of the animals after 4 weeks post implantation. Values expressed by means ± SEM.

Parameters	Reference Range	Control	Dynamic
Erythrocytes	4.2 – 6.7	8.2 ± 0.3	7.8 ± 0.1
Hemoglobin	9.5 – 14.5	13.8 ± 0.5	12.8 ± 0.6
Hematocrit	27.2 – 45.9	40.4 ± 1.0	37.9 ± 2.2
MCHC	31.0 – 34.9	34.2 ± 0.3	33.7 ± 0.3
MVC	59.1 – 75.4	59.9 ± 12.2	58.7 ± 2.0
Neutrophiles	0.8 – 2.9	1.2 ± 0.3	0.8 ± 0.3
Lymphocytes	2.2 – 5.3	2.6 ± 0.3	2.4 ± 0.1
Monocytes	< 0.4	0.10 ± 0.05	0
Eosinophiles	< 0.4	0.10 ± 0.10	0
Basophiles	< 0.6	0	0
Platelets	136.6 – 558.4	548 ± 207	485 ± 112

Figure VII.S6: Hematological analysis of the animals after 6 weeks post implantation. Values expressed by means ± SEM.

	ALT (UI/L)	ALP (UI/L)	GLUCOSE (mg/dL)	ALBUMINE (g/dL)
Reference Range	14 – 80	12 - 96	65 - 278	2.4 – 2.7
Control	70 ± 18	58 ± 41	116 ± 11	2.7 ± 0.1
Dynamic	66 ± 40	75 ± 12	84 ± 31	2.5 ± 0.2

Figure VII.S7: Blood serum analysis of the animals, 6 weeks post implantation. Values expressed by means ± SEM.

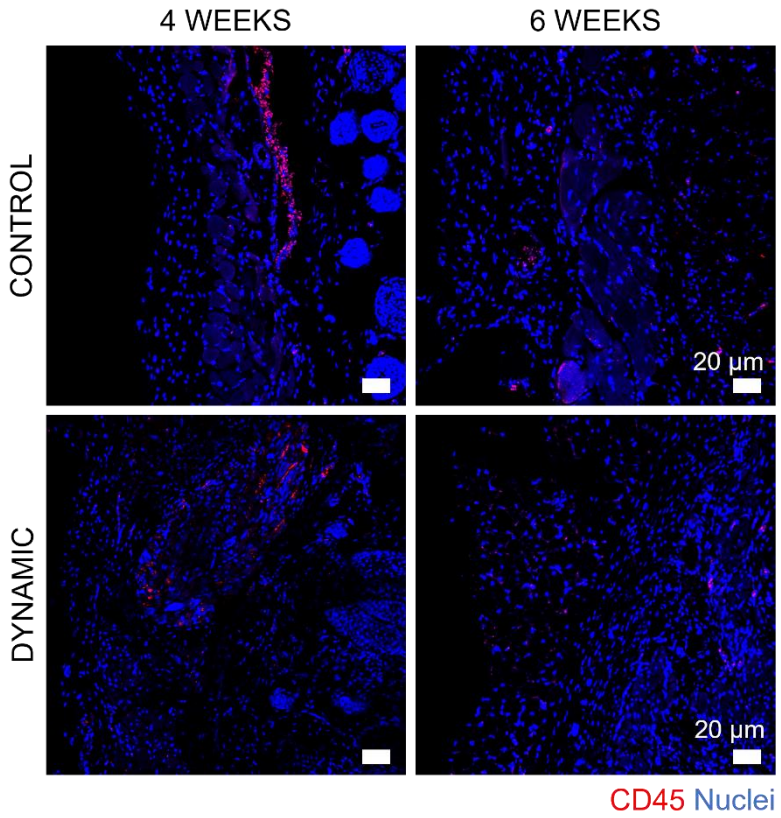

Figure VII.S8: The presence of lymphocytes was investigated in implant and neighbored tissue by analysis the CD45 marker for both control and dynamic condition after 4 and 6 weeks.

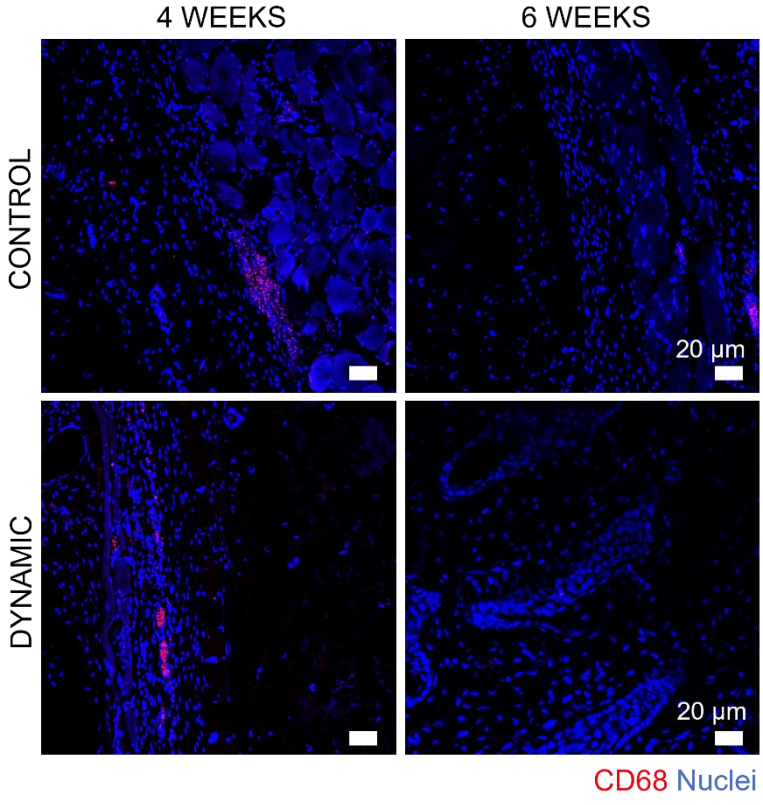

Figure VII.S9: The presence of macrophages was investigated in implant and neighbored tissue by analysis the CD68 marker for both control and dynamic condition after 4 and 6 weeks.

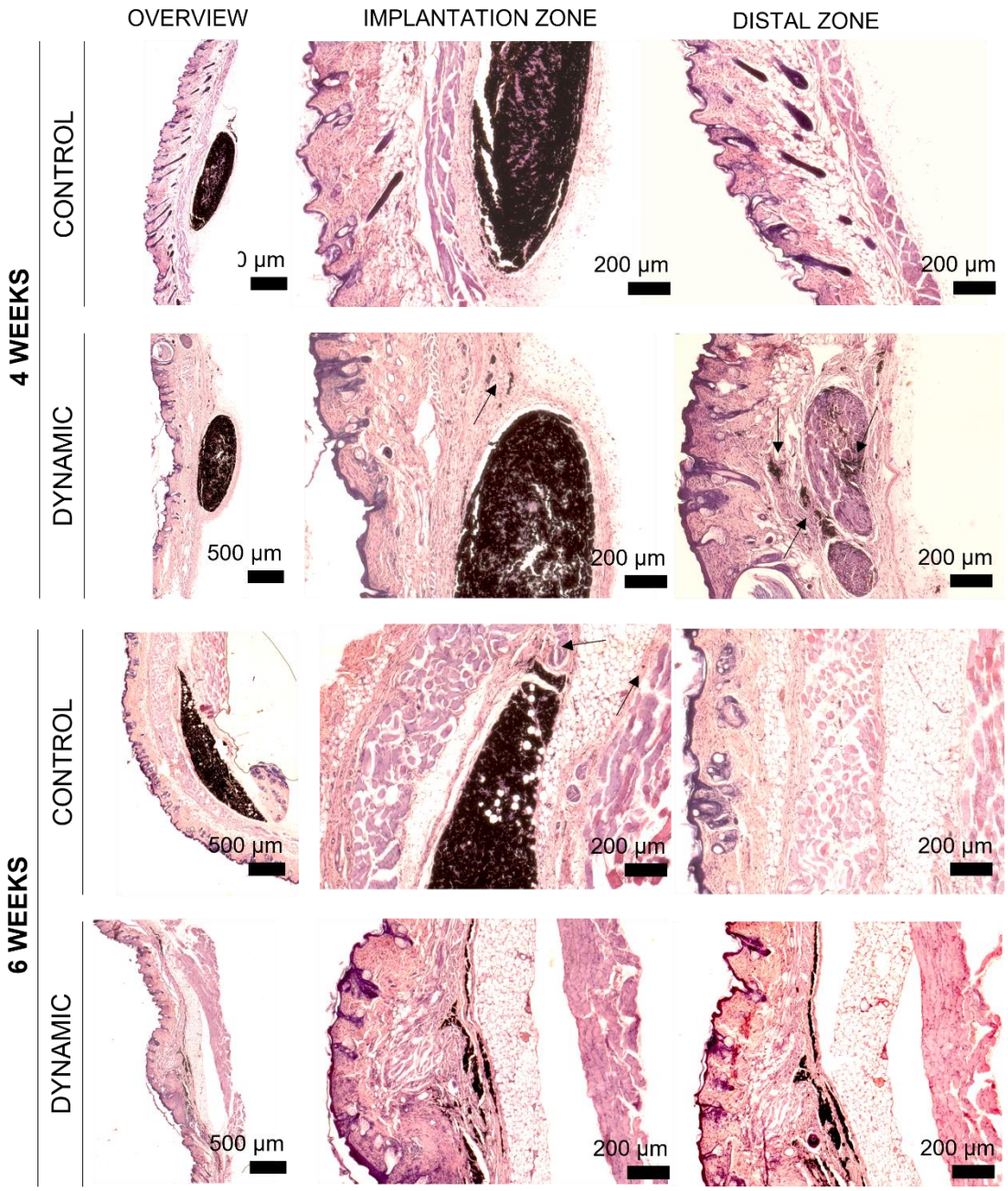

Figure VII.S10: H&E staining of paraffin-embedded magnetized tissues under control and dynamic conditions, 4 and 6 weeks post implantation.

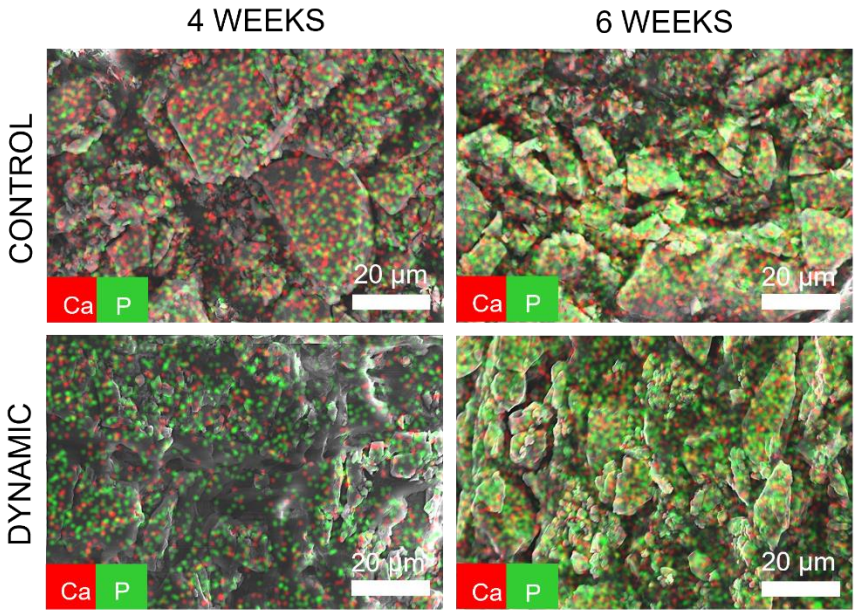

Figure VII.S11: Analysis of the mineral deposition within the magnetic implant by EDS. The hydroxyapatite nodules can be identified in yellow, by the overlapping of calcium (in red) and phosphorus (in green).

4

Conclusion

Chapter VIII

Conclusions and Future Perspectives

Chapter VIII - Conclusions and Future Perspectives

Tissue Engineering (TE) aims to fabricated tissue substitutes to replace, repair or regenerate lost tissue function. Despite of the incredible efforts of TE in last years, the translation to clinical practices remains a challenge. A feasible justification relies on the lack of tissue engineered constructs with appropriate functional and morphological features. During the design of tissues, the key functional aspects of tissue microenvironment must be recapitulated. Therefore, in the last years, TE has been focused on the development of a new class of biomimetic materials closely mimicking the critical aspects of natural tissue regarding its physical and chemical properties. To face this challenge, scaffold-free TE has emerged as a powerful strategy using multicellular building blocks, including spheroids, tissue strands and CSs to fabricate large cohesive tissue constructs and produce ECM, essential for naturally developing their tissue architecture. Particularly, CS engineering was already implicated on the fabrication of functional, complex and robust living structures. Nevertheless, the recapitulation of the complex, well-organized and hierarchical architecture of tissues and organs is still not fulfilled by traditional approaches. Therefore, in this PhD project we established a novel strategy for the fabrication of improved functional tissue substitutes through the combination of magnetic force-based TE with CS technology. Using magnetized cells as basic living units, we conceived tissues akin to biological organism with precise control over the positioning of cells and tissue assembly.

In **Chapter IV**, we started by recapitulating the complexity, strength and longevity of natural tissues. Magnetic tissues with complex architectures and enhanced mechanical behaviour were fabricated using a simple, time-saving and cost-effective strategy. A plethora of shaped microtissues were created by simply relying on the designs of the substrate and the magnet, cell density and magnet strength. Herewith, we attested the ability of designing cell-based constructs resembling the complex environment of native tissues with enhanced mechanical performance, offering potential applications for the development of *in vitro* disease models or implantable structures for tissue regeneration purposes.

Ambitioning the implantation of such cell-dense tissue constructs, the proper diffusion of nutrients and oxygen must be guaranteed. The lack of effective strategies to produce vascularized transplants *in vitro*, hampers the translational of lab-based engineered tissues to clinical practices. Hence, in **Chapter V** pre-vascularized magnetic tissues were developed by combining ASCs and HUVECs in a stratified conformation. The synergetic effect of such cell phenotypes triggered the osteogenesis of the tissue constructs. Noteworthy, using an *in vivo* CAM assay we verified that our tissues,

composed of a preserved human vascular structure, were able to recruit blood vessels, stimulate angiogenesis and integrate within the chick vasculature. Such results open new prospects for the clinical translation of magnetized tissues.

Hereto, the complexity of the tissues was achieved by the stacking of individual CSs or simple suspensions of magnetized cells (z-direction) in a stratified conformation. Aiming the design of tissues akin to biological organisms, the assembling of the tissue's modules in a puzzle-like manner (x,y-directions) is mandatory for mimicking the native tissue architecture. Thus, in **Chapter VI**, freestanding magnetic microtissues with preserved geometries and tissue integrity were fabricated through the combination of Mag-TE and a superhydrophobic high throughput platform. Such freestanding miniaturized tissues could serve as building blocks for the construction of intricate and hierarchical tissues or be used as *in vitro* platforms for disease modelling and drug screening.

Until here, we demonstrated the potential of Mag-TE on the development of improved tissue substitutes. Magnetic nanoparticles (MNPs), by changing the cell mechanical environment, can also modulate several signalling pathways in tissues upon magnetic stimulation. Taking advantage of the magnetic character of our tissues, in **Chapter VII** we proposed a new therapeutic strategy for bone regeneration, where magnetized cells acted as living bioreactors. After the implantation of the magnetic tissue construct, the osteogenic differentiation was remotely triggered in the presence of a cyclic magnetic field. Moreover, in an *in vivo* mice model, superior integration of these living tissues was verified under the magnetic stimulation. Overall, we envisioned that the wireless magnetic actuation could prompt the *in situ* bone regeneration, empowering the potential of Mag-TE for regenerative medicine and accelerating its translation to the clinical practices.

Besides the promising results of Mag-TE on regenerative medicine, the safety concerns regarding the use of MNPs and the magnetic field on TE have been hampering their translation to clinic practice. In **Chapter VII**, we demonstrated no signs of toxic effects in all animals following 6 weeks of implantations. Nevertheless, for the completely acceptance by the scientific community, we believe that all the benefits and potential drawbacks of Mag-TE must be clarified. With the advances in nanotechnology, new strategies for the fabrication of MNPs arose, permitting the design of MNPs with distinct features namely shape, size, structure, and surface' modifications. The next steps of Mag-TE will surely encompass the selection of the best design of MNPs for biomedical applications. Magnetic field is already part of few clinical trials for monitoring purposes on regenerative medicines. However, the impact of the magnetic field on biological organisms must be also well-investigated, identifying the long-term biological effects.

Pondering on an idyllic scenario for tissue implantation, the tissue implant must closely mimic the physical and biochemical cues of the envisioned tissue or organ. The scientific community believes that the merging of scaffold-based and scaffold-free approaches, previously stated as rivals, into a synergetic TE strategy can be a valuable solution for regenerative medicine. We anticipate that such synergism will accelerate the *in situ* tissue formation by combining the native tissue environment, granted by scaffold-free technology, with the enhanced mechanical performance offered by the scaffold-based expertise. Additional combination with Mag-TE could provide extra control over the tissue formation with tunable tissue size, shape, and architecture, contributing to the development of completely functional tissues. In the future, the introduction of advanced biofabrication technologies namely 3D bioprinting or robotic-assisted deposition of magnetic living blocks will enable the creation of denser tissues with intricate geometries that could better resemble the tissue architecture, opening new insights not only for the regeneration of tissues but also for the development of ameliorated disease models. In fact, such methodologies can also be conjugated with iPSC technology for the development of tissue models that better meet the patient needs.